



POLITECNICO DI MILANO

Doctoral Program in Industrial Chemistry and Chemical Engineering

Department of Chemistry Materials and Chemical Engineering

“Giulio Natta”

Process Systems Engineering for early-stage process development: the case of sustainable bio-derived adipic acid.

Advisor: Prof. Attilio CITTERIO
Tutor: Prof. Massimo MORBIDELLI
Chair of the Ph.D. Program: Prof. Alessio FRASSOLDATI

Doctoral Dissertation of: Alessandro ROSENGART
Identification Number: 10497902

XXX Cycle
Academic Year 2016-2017

Dedicated to my Family

ὡς ὁ κωμικός φησι,
τὰ σῦκα σῦκα, τὴν σκάφην δὲ σκάφην ὀνομάσων,
οὐ μίσει οὐδὲ φιλία τι νέμων οὐδὲ φειδόμενος

*(The writer should be), as the comedian says,
calling the fig fig and the cup cup,
neither parsimonious nor prodigal due to aversion or friendship*

Lucianus Samosatensis

Luc. Hist. Conscr. 41

Abstract

The awareness of the negative impacts of human activity against environment and public health has pushed western governments to support long-term programs aimed at mitigating pollution and reducing resource consumption. In this spirit, both industry and academia are searching for new solutions towards a “green” manufacturing practice, and the concept of “biorefinery” is taking place, as a renewable counterpart of the ill-famed oil industry. Biorefineries are supposed to produce entire classes of chemicals and fuels just as a real refinery, with the great difference that the carbon source is no more fossil, but follows the natural cycle of CO₂, which is captured from atmosphere and fixed into living organisms (plants, algae, bacteria).

This Doctoral Thesis deals with the feasibility evaluation of a drop-in biorefining application for the production of sustainable adipic acid from biomass (2nd generation technology), defining the full-scale process flowsheet, assessing the environmental and economic performances, and identifying the current challenges that R&D should address before industrialization. Some of these challenges have been tackled in this work applying several Process Systems Engineering computational tools, in particular dealing with problems of predictive models development, uncertainty propagation study and parameter regression from experimental data.

The current adipic acid production covers a market of 3.7 million tons per year (with a 4.1% of yearly growth) and, in spite of 70 years of technological maturity, the traditional benzene-based processes still raises serious safety and environmental concerns. For these reasons, both private and public research institutions have pursued alternative bio (and chemical) routes for adipic acid; however, none of these processes has reached industrialization yet, also due to the oil-price fall in 2014. This event evidenced the main weakness of drop-in biorefineries: the need to compete in costs with a well-established and optimized technology. A novel approach to process development is therefore required for the case of bulk bio-derived chemical with low added value. In particular, conceptual design acquires particular importance from the early stage of process development, to produce reliable cost estimates and projections, and to define a strategy for R&D.

Given the extensive and interdisciplinary literature accumulated dealing with green adipic acid, the first activity carried out for this Doctoral study was the collection and systematisation of the available knowledge, identifying the current alternative processing

routes and assessing their actual sustainability with objective green metrics. In the specific, a two step biological-chemical process was considered worth of more detailed investigation for its good yields and sustainability potential. This process consists in a first fermentation to produce an unsaturated intermediate, muconic acid, starting from either glucose (from cellulose) or benzoic acid (from lignin); muconic acid is then catalytically hydrogenated to adipic acid.

A computer aided process synthesis-and-design methodology was therefore applied for the case study of adipic acid from muconic acid, to evaluate systematically the highest number of process alternatives to produce the best flowsheet concept at the state of the art. The method is implemented in a tool belonging to “ICAS software”, practiced during the author’s Ph.D. visiting period at DTU (Denmark Technical University, Copenhagen). This tool, given a number of alternative feedstocks, technologies (intended as unit operations, process conditions), and products, allows building a superstructure, which is translated into a Mixed Integer (Non) Linear Programming optimization problem solved in GAMS[®]. The solution is a processing route that maximizes the objective function (economic potential) providing also the material and energy balances. The plant feasibility was then evaluated for different market scenarios, the process bottlenecks were identified and more detailed green metrics were calculated (e.g. water consumption, energy consumption, CO₂ equivalent). Thus, the process flowsheet concept was achieved avoiding the simplified approaches of order-of-magnitude estimates or the “analogy principle”. Also, the used methodology guarantees in general higher flexibility than a detailed process simulator, as each unit operation is defined by few user-defined parameters, that allow giving some cost/performance estimates even in presence of preliminary, lab-scale data. At the base of this approach there is the Processing-Step-Interval Network representation, according to which any unit operation can be systematically decomposed into basic tasks with cost associated function (mixing, reaction, waste removal, product separation and utilities consumption), modelled in a modular structure. In case of missing information, some assumptions can be made, which become the object of future research if proven determinant in the process economics (SMART objectives definition).

The problem of how the scarce information at early stage of research can affect the trustworthiness of a cost function was addressed in detail for a unit operation which relies much on experimental data, not available for muconic acid fermentation: cross flow microfiltration. In facts, using literature data in analogy with existing plants can be extremely deceptive, as the design and the operating conditions (transmembrane pressure, crossflow velocity, membrane regeneration) are calibrated on the specific properties of a

particular microorganism. A grey-box model was developed on the structure of a Darcy additive resistance equation, to represent the dynamic behaviour of the progressive bacterial fouling of a filtration membrane. The model, a system of algebraic and differential equations, is general and flexible, able to represent different strains in virtue of its adaptive parameters. The parameters “carry” the uncertainties deriving from the experimental error or from the actual representation limits of the model. Further uncertainties are introduced when using the model in a predictive way, i.e. extending the parameters validity to “similar” systems, as performed for the case of the strains for muconic acid production, whose filterability properties have not been measured yet. The uncertainty propagation was therefore studied applying Possibility theory and the Fuzzy Logic of Zadeh. This uncertainty analysis allowed identifying the most likely range of filtration performances of an industrial membrane system, which, in association with a cost function, provided an indication of the error of cost estimates and the risk in the absence of specific R&D.

The final conversion step for the production of green adipic acid, i.e. the catalytic hydrogenation of muconic acid, lacked as well of the sufficient data to perform reliable estimates on the reaction scale up. In this case, an experimental campaign was started, in collaboration with the laboratories of Industrial Chemistry of Università degli Studi di Milano. The purpose was to identify the optimal reaction conditions (low pressure, low temperature, and catalyst recyclability) and identify the hydrogenation mechanism, to develop the first kinetic model for the system. Several models with LHHW structure were used to interpret the experimental values, considering the species adsorption-desorption equilibria of the involved species. A dual-step hydrogenation mechanism was demonstrated, with hydrogen dissociation on the metal (Pt/C 5%). Muconic acid (in its *trans,trans* form) is first hydrogenated to hexenedioic acid (present in its two *cis* and *trans* isomers, in equilibrium) which is then converted to adipic. The model parameter regression was performed with the C++ library BzzMath, characterized by robust minimization algorithms, to tackle the computational challenges related to the use of models with strong collinearity. The models were thus re-parametrized and progressively simplified, obtaining a good representation of the experimental data and providing the first reference values of the species activation energies.

The Thesis is structured as follows. Chapter 1 introduces the general framework of this study, highlights the issues of oil-based production of adipic acid, and presents the main challenges for the establishment of green bulk chemical productions. Chapter 2 provides an overview of the current alternatives for a sustainable adipic acid, giving the first estimates of their “green potential” and selecting the best route. Chapter 3 reports the

application of the process synthesis and design methodology, with a detailed description of the unit operations selection and modelling, and with the analysis of the superstructure optimization results to define a research strategy. Chapter 4 describes the model development and the uncertainty propagation for the cross-flow microfiltration membranes in broth clarification applications. Chapter 5 describes the experimental campaign on muconic acid hydrogenation, and reports the kinetic study performed to achieve the reaction model. Finally, the Conclusions summarize the achievements of three year of investigation and introduce the possible future works.

Sommario

La consapevolezza degli impatti dell'uomo sull'ambiente e sulla salute pubblica ha spinto i governi occidentali a sostenere programmi di riduzione dell'inquinamento e del consumo di risorse. In questo contesto, sia le industrie che le istituzioni accademiche si impegnano a ricercare nuove soluzioni nella direzione di una nuova produzione "verde". Inoltre, nuovi concetti vanno affermandosi nel linguaggio industriale, come la "bioraffineria", intesa come contrapposizione rinnovabile alle mal viste raffinerie tradizionali. Le bioraffinerie dovrebbero produrre prodotti chimici e combustibili esattamente come le raffinerie esistenti, con la differenza che il carbonio non deriva più da petrolio fossile, ma dal ciclo naturale della CO₂, fissata dall'atmosfera agli organismi viventi (piante, alghe, batteri).

Questa Tesi di Dottorato verte principalmente sullo studio di fattibilità di un'applicazione di bioraffineria drop-in per la produzione di acido adipico sostenibile da biomassa (tecnologia di 2° generazione), studio che consiste nella definizione dello schema di processo, nella valutazione delle performance economiche ed ambientali e nell'identificazione delle principali sfide che la ricerca applicata deve ancora affrontare per raggiungere l'industrializzazione. Alcuni di questi aspetti, finora mai studiati in dettaglio, sono stati trattati in questo lavoro applicando metodi computazionali della Process System Engineering, per risolvere problemi legati allo sviluppo di modelli predittivi, alla propagazione dell'incertezza e alla regressione di parametri da dati sperimentali.

Osservando in dettaglio la situazione attuale dell'industria dell'acido adipico, la sua produzione ricopre un fabbisogno di 3.7 milioni di tonnellate annue (con una crescita prevista del 4.1% annuo). Tuttavia, il processo produttivo tradizionale, basato su risorse petrolifere (benzene), solleva ancora grosse preoccupazioni per la sua pericolosità e gli elevati impatti ambientali, nonostante più di 70 anni di maturità tecnologica. Per questo motivo istituti di ricerca sia pubblici che privati hanno ricercato vie produttive alternative (bio e chimiche) per l'acido adipico negli ultimi vent'anni. Ciononostante, nessuno di questi processi ha ancora raggiunto l'industrializzazione, anche a causa del crollo del prezzo del petrolio nel 2014. Questo evento mostrò la principale debolezza delle bioraffinerie di tipo drop-in: la necessità di competere in termini di costo con tecnologie consolidate e altamente ottimizzate. Pertanto, è richiesto un nuovo approccio ingegneristico in fase di sviluppo di processi chimici per prodotti di grande scala bio-derivati ma a basso valore aggiunto. In particolare, il design concettuale di impianto diventa estremamente importante fin dai primi momenti dello sviluppo di processo, in modo da generare stime di

costo e proiezioni fin da subito, così da definire una strategia vincente per la ricerca e sviluppo.

Dato il corpus esteso di contributi scientifici e brevetti accumulati sull'argomento dell'acido adipico "green", la prima delle attività affrontate in questa Tesi è stata la raccolta e l'organizzazione sistematica delle conoscenze disponibili, per identificare le produzioni alternative e valutarne oggettivamente la sostenibilità con metriche green. Nello specifico, è stato ritenuto degno di ulteriori analisi un processo a doppio stadio (biologico e chimico) in virtù delle sue alte rese e della sua potenziale sostenibilità. Tale processo consiste in una prima fermentazione partendo da glucosio (da cellulosa) o da acido benzoico (da lignina) per produrre un intermedio insaturo, l'acido muconico, che poi è convertito per idrogenazione catalitica ad acido adipico.

Si è quindi applicata una metodologia CAPE (computer aided process engineering) per la sintesi e design del processo per acido adipico da acido muconico, in modo da valutare sistematicamente il più alto numero possibile di alternative di processo e generare il migliore flow-sheet allo stato dell'arte della ricerca. Questa metodologia è implementata in uno strumento del software ICAS, appreso dall'autore durante il suo soggiorno all'estero come PhD visiting student presso la DTU (Denmark Technical University, Copenhagen). Il software, in presenza di un set di materie prime, alternative di trasformazione (operazioni unitarie, ma anche condizioni di processo) e possibili prodotti, permette di costruire una sovrastruttura (o network di alternative) che poi è tradotta in un problema di ottimizzazione (MINLP) Mixed Integer Non Linear Programming, risolvibile in ambiente GAMS®. La soluzione è un layout di processo che massimizza la funzione obiettivo (potenziale economico di impianto) e ne fornisce anche i bilanci di materia ed energia.

La fattibilità industriale del processo è stata quindi valutata per scenari di mercato diversi, sono stati identificati i potenziali colli di bottiglia tecnologici e sono state calcolate nuove e più dettagliate metriche green (consumo d'acqua, d'energia, produzione di CO₂ equivalente). La conformazione di processo si è quindi ottenuta evitando gli approcci semplificati come le stime tramite ordine di grandezza o applicando il principio dell'analogia, usati comunemente nelle prime fasi dello sviluppo di processo. Inoltre, la metodologia applicata consente maggiore flessibilità di un simulatore di processo, dal momento che ciascuna operazione unitaria è definita da pochi parametri tecnici, che permettono di avere stime di costo e prestazioni anche in presenza di dati preliminari ottenuti su piccola scala (laboratorio). Alla base di questo approccio semplificato c'è la rappresentazione Processing Step-Interval Network, secondo cui qualsiasi operazione unitaria può essere decomposta in unità basilari con funzioni di costo associate (mix, reazione, rimozione sottoprodotti, separazione prodotti e consumo utility), tutte modellate

con una struttura modulare e universale. In caso di informazioni mancanti, si possono fare delle assunzioni che, se dimostrate determinanti per l'economia di processo, possono diventare l'oggetto delle future campagne di ricerca (definizione di obiettivi SMART).

Il problema di come le scarse informazioni nelle prime fasi di sviluppo di un processo possano influenzare l'affidabilità di una stima di costi è stato affrontato in dettaglio per un'operazione unitaria che dipende molto da studi sperimentali, non disponibili per la fermentazione dell'acido muconico: la filtrazione tangenziale a membrana per la chiarificazione del fermentato. L'utilizzo di dati di letteratura presi per sistemi "simili" a quello in studio può essere estremamente fuorviante, dal momento che il design e le condizioni di processo (pressione transmembrana, velocità del flusso tangenziale e rigenerazione della membrana) sono calibrate sulle proprietà di un particolare microorganismo, e potrebbero non applicarsi in altri casi. Un modello semi-empirico è stato quindi sviluppato sulla struttura dell'equazione di Darcy a resistenza additive, per rappresentare il comportamento dinamico dello sporciamento delle membrane ad opera dei microorganismi. Il modello, un sistema di equazioni algebriche e differenziali, è generico e flessibile, capace di rappresentare diversi tipi di microorganismi grazie ai suoi parametri adattativi: questi portano in sé l'incertezza derivante da errori sperimentali o errori derivanti dai limiti intrinseci del modello. Ulteriori incertezze sono introdotte utilizzando il modello in modo predittivo, cioè estendendo la validità dei parametri per sistemi simili, come effettuato per i microorganismi che producono l'acido muconico, le cui caratteristiche di filtrabilità non sono ancora state investigate. La propagazione dell'incertezza nel modello è stata quindi studiata applicando la Teoria della Possibilità e la Logica Fuzzy di Zadeh. Quest'analisi dell'incertezza ha permesso di identificare gli intervalli più verosimili delle prestazioni dei filtri, che, in associazione con una funzione di costo, hanno permesso di ottenere l'errore delle stime di costo e il rischio legato all'assenza di valori sperimentali diretti.

Il passaggio finale per la produzione di acido adipico, cioè l'idrogenazione catalitica dell'acido muconico, mancava anch'esso dei dati minimi per effettuare stime attendibili sullo scale-up della reazione. In questo caso, è stata avviata una campagna sperimentale in collaborazione con il dipartimento di Chimica Industriale dell'Università degli Studi di Milano. Lo scopo è stato quello di identificare le condizioni di reazione ottimali (bassa pressione e temperatura, riciclabilità del catalizzatore) e di identificare il meccanismo di reazione, per sviluppare il primo modello cinetico della reazione. Diversi modelli con struttura LHHW sono stati testati per interpretare i valori sperimentali, considerando gli equilibri di adsorbimento e desorbimento delle specie coinvolte. È stato dimostrato infine

un meccanismo a doppio stadio con dissociazione dell'idrogeno su metallo (Pt/C 5%). L'acido muconico (nella sua forma *trans,trans*) è idrogenato inizialmente ad acido esendioico (presente nelle sue due forme isomeriche *cis* e *trans* in equilibrio tra loro), che successivamente è convertito ad acido adipico. La regressione dei parametri del modello è stata effettuata con la libreria C++ BzzMath, caratterizzata da algoritmi per la minimizzazione robusta, necessari per superare le difficoltà computazionali legate all'uso di modelli che presentano forti collinearità dei parametri. I modelli sono stati pertanto riparametrizzati e progressivamente semplificati, ottenendo alla fine una buona rappresentazione dei dati sperimentali e fornendo i primi valori di riferimento per le energie di attivazione delle specie.

La struttura della Tesi è la seguente. Il capitolo 1 introduce il contesto generale di questo studio, evidenziando i problemi della produzione tradizionale dell'acido adipico e presentando le sfide principali da affrontare per stabilire produzioni "green" di prodotti chimici su grande scala. Il capitolo 2 fornisce una visione sulle alternative disponibili per un acido adipico green, dando una prima stima della loro potenziale sostenibilità e selezionando quindi la più promettente. Il capitolo 3 descrive l'applicazione della metodologia di sintesi e design di processo, riportando in dettaglio l'attività di selezione e modellazione delle operazioni unitarie, e l'analisi finale dei risultati dell'ottimizzazione della sovrastruttura, definendo una strategia per la ricerca. Il capitolo 4 descrive lo sviluppo di modello e l'analisi della propagazione dell'incertezza per le membrane di microfiltrazione tangenziale per la chiarificazione del fermentato. Il capitolo 5 descrive la campagna sperimentale di idrogenazione dell'acido muconico, riportando lo studio cinetico effettuato per ottenere il modello della reazione. Infine, le conclusioni riassumono i principali traguardi raggiunti in tre anni di ricerca e introducono i possibili sviluppi futuri che possono originare da questo Dottorato.

Aknowledgements

This Ph.D. thesis would have been much shorter without the influence of the Scholars and Scientists I had the luck to come across in these three years. In the following lines I will mention and formally aknowledge the ones who were most important for me. From Politecnico di Milano, I would like to thank prof. Flavio Manenti, who gave me the right hints at the right moment and helped me to build that inter-university network that transformed a “let’s try this way- idea” into a structured and ambitious chemical engineering Ph.D. project. I am thankful to prof. Carlo Pirola from Università degli Studi di Milano, who always believed in this project, and actually opened a research line on the chemical aspects of this thesis. Special thanks go to prof. Rafiqul Gani and John Woodley, from DTU (Denmark Technical University), who taught me the true meaning of optimization and bioprocess engineering, and hosted me in their Copenhagen research group. Thanks also to prof. Piero Baraldi from the Energy department of Politecnico di Milano, for introducing me to fuzzy logic, and thanks to prof. Frank Lipnizki from Lund University (Sweden) for giving me support in my stubborn decision to understand filtration systems. Thanks also to Dr. Stefano Alini, from Radici.spa, who has played the role of the Industrial counterpart of an otherwise merely academic project. I would like to mention in these aknowledgements also prof. Maurizio Galimberti, with whom I had the pleasure to collaborate in some fruitful side-projects.

Many students describe the Ph.D. as a “journey”, but I do not agree completely: travel companions come and go. I would rather prefer to to thank my “Comrades in arms”, who shared with me the though life of the front (academically speaking). First of all my office/nightlife/apartment-mates Enza, Bebo, Jemeng and Chiara P., practically my family at the department. Before only Arianna, Sara and Sepehr were able to stand me for longer periods in my “second office” (and thanks for the Iran trip). Thanks also to my “third office” fellows: Mich (who was my first coach), Dave, Frank, Bax (resisti!), Anisolo and Andrè. In my “fourth office” (Capanno) I met the best colleague ever: Sofia (It has been a pleasure to fight together!). In Capanno I met also Marta, who gave me many more things to think about! I had a “fifth office”, in Copenhagen: there I met Olivia and Xinyen. I am also thankful to the mates of my “sixth honorary office” in Math department of DTU: Giulia and Sebastian (you made my stay there less hygge, luckily)! Special thanks go to Mattia, who gave me faith in younger generations.

Academia is not only made by Academia. Therefore, I have to acknowledge all those friends that stayed at my side out of Academia, listening to me while complaining about Academia. Starting from Milano, thanks to Fabio (THE coinquilino) and Chiaretta, to Ale Porta, Sara (and FinaleLigure). Thanks also to Valentina and Elona and Dramatrà.

Passing through Varese, very big thanks to Bress (THE travel-mate), and heading to Padova, I have to thank Giorgia, Pippo, Elena, and Max, Sere, Colli, CateCampo, and also Giulia DT(!). A rapid stop in SanDonà to thank i “very duri”: Mtt, Gege and Cesco for being always here, there, wherever. And also Mirco, Enrico de Tuoni and Marta from the other side of Piave. I still have to go East a little bit more (to Seoul) to thank AlePace.

Surely I forgot somebody, I’ll pay you a spritz.

My final thanks go to my Family (Enrico, Graziella, Edo) who have always been supporting all my choices, even the most questionable.

Grazie!

Index

ABSTRACT	V
SOMMARIO	IX
AKNOWLEDGEMENTS	XIII
INDEX	XV
LIST OF FIGURES	XIX
LIST OF TABLES	XXV
LIST OF PAPERS	XXIX
PREFACE	XXXI
CHAPTER 1	1
INTRODUCTION	1
1.1 - GREEN CHEMISTRY AND BIOREFINING	2
1.1.1 - <i>Environmental impact mitigation: a paradigm for industry</i>	2
1.1.2 - <i>The concepts of Green process and the Biorefinery</i>	7
1.2 - ADIPIC ACID: OVERVIEW OF A STRATEGIC PLATFORM CHEMICAL	11
1.2.1 - <i>The traditional oil-based processes</i>	11
1.2.2 - <i>General economic considerations</i>	13
1.3 - THE CHALLENGES OF DEVELOPING AN ADIPIC ACID BIOREFINERY	16
1.4 - OBJECTIVES OF THE THESIS AND STRUCTURE	21
1.5 - REFERENCES CHAPTER 1	23
CHAPTER 2	27
GREEN ADIPIC ACID: STATE OF THE ART	27
2.1 - RENEWABLE FEEDSTOCKS, A GREEN CHEMISTRY DEFINITION	28
2.1.1 - <i>Citrus Peel Waste</i>	31
2.1.2 - <i>Dairy waste</i>	34
2.1.3 - <i>Biomass, cellulosic fraction</i>	36
2.1.4 - <i>Biomass, lignin fraction</i>	41
2.1.5 - <i>Spent oil, fat</i>	42

2.1.6 - <i>Best feedstocks selection</i>	44
2.2 - ANALYSIS OF THE ROUTES TO ADIPIC ACID.....	48
2.2.1 - <i>Rivertop nitric acid oxidation of C6 sugars</i>	48
2.2.2 - <i>Rennovia hydrodeoxygenation of aldaric acids</i>	54
2.2.3 - <i>The bio-catalytic routes</i>	56
2.3 - ROUTE SELECTION AND PROJECT MANAGEMENT.....	63
2.4 - CONCLUSIONS	67
2.5 - REFERENCES CHAPTER 2	68
CHAPTER 3	75
EARLY STAGE PROCESS SYNTHESIS AND DESIGN.....	75
3.1 - A COMPUTER AIDED FRAMEWORK FOR PROCESS SYNTHESIS AND DESIGN	76
3.1.1 - <i>Historical perspective on Process Design and Optimization</i>	76
3.1.2 - <i>The generic framework: main concepts and workflow</i>	79
3.1.3 - <i>MILP problem structure</i>	90
3.2 - PROCESS SUPERSTRUCTURE DEVELOPMENT AND ASSUMPTIONS	93
3.2.1 - <i>Raw Materials and Component list (processing step I)</i>	97
3.2.2 - <i>Bioreaction (step II)</i>	99
3.2.3 - <i>Biomass deactivation (step III)</i>	103
3.2.4 - <i>Bacterial Removal 1 (step IV)</i>	105
3.2.5 - <i>Bacterial Removal 2 (step V)</i>	108
3.2.6 - <i>Broth Recovery (step VI)</i>	112
3.2.7 - <i>Colloids removal (step VII)</i>	115
3.2.8 - <i>Impurities removal (step VIII)</i>	116
3.2.9 - <i>Concentration (step IX)</i>	118
3.2.10 - <i>Water separation (step X)</i>	121
3.2.11 - <i>Solvent dissolution (step XI)</i>	126
3.2.12 - <i>Solvent filtration (step XII)</i>	127
3.2.13 - <i>Solvent separation (step XIII)</i>	128
3.2.14 - <i>Intermediate dissolution in water(step XIV)</i>	129
3.2.15 - <i>Hydrogenation (step XV)</i>	130
3.2.16 - <i>Product recovery (step XVI)</i>	133
3.2.17 - <i>Re-dissolution (step XVII)</i>	137
3.2.18 - <i>Rectification (step XVIII)</i>	138
3.2.19 - <i>Product (step XIX)</i>	139
3.2.20 - <i>Economic aspects</i>	139
3.3 - SUPERSTRUCTURE OPTIMIZATION AND RESULTS ANALYSIS	141

3.3.1 - <i>The best process configurations ranking</i>	141
3.3.2 - <i>Sustainability analysis</i>	144
3.3.3 - <i>Sensitivity analysis for the glucose route</i>	149
3.4 - CONCLUSIONS	152
3.5 - REFERENCES CHAPTER 3	153
CHAPTER 4	159
DEVELOPMENT OF A PREDICTIVE MODEL FOR MICROFILTRATION.....	159
4.1 - BROTH CLARIFICATION, A CHALLENGE FOR MODELLING.....	160
4.2 - MANAGE UNCERTAINTY WITH FUZZY LOGIC: POSSIBILITY THEORY	163
4.3 - THEORY OF FILTER FOULING AND MODEL DEVELOPMENT.....	168
4.3.1 - <i>Clean membrane resistance</i>	169
4.3.2 - <i>Adsorption resistance</i>	169
4.3.3 - <i>Polarization resistance</i>	170
4.3.4 - <i>Cake resistance</i>	174
4.3.5 - <i>Model for a filtration unit</i>	178
4.4 - RESULTS AND DISCUSSION	181
4.4.1 - <i>Model validation</i>	181
4.4.2 - <i>Uncertainty propagation</i>	184
4.5 - CONCLUSIONS	189
4.6 - NOMENCLATURE	190
4.7 - REFERENCES CHAPTER 4	191
CHAPTER 5	195
KINETIC STUDY OF MUCONIC ACID HYDROGENATION.....	195
5.1 - MUCONIC ACID HYDROGENATION: STATE OF THE ART	196
5.2 - MATERIALS AND METHODS	199
5.2.1 - <i>Experimental setup</i>	199
5.2.2 - <i>Analytical methods</i>	205
5.2.3 - <i>LHHW models and nonlinear regression</i>	208
5.3 - RESULTS AND DISCUSSION	211
5.3.1 - <i>Hydrogenation to adipic acid in mild conditions</i>	211
5.3.2 - <i>Kinetic modelling</i>	215
5.4 - CONCLUSIONS	226
5.5 - REFERENCES CHAPTER 5	228
GENERAL CONCLUSIONS	231
APPENDIX 1	235

APPENDIX 2	239
APPENDIX 3	247
APPENDIX 4	264

List of Figures

Figure 1.1 - Official logo and slogan of the EU 7 th Environment Action Programme.....	2
Figure 1.2 - GHG emissions by economic sector adapted from ref.4. The acronym AFOLU stands for “agriculture, forestry and other land use”	4
Figure 1.3. - GHG emissions by manufacturing category adapted from ref. 4.....	5
Figure 1.4. Chemical sales growth rates of selected countries between 1997 and 2007....	6
Figure 1.5 - Representation of the effective H/C ratio of bulk and commodity chemicals, with renewable feedstocks and the qualitative degree of processing, adapted from ref. 19. B benzene, BDO 1,4-butanediol, EG ethylene glycol, EO ethylene oxide, GVL γ -valero lactone, PE polyethylene, PG propylene glycol, PP polypropylene, T toluene, X xylenes.	10
Figure 1.6 - Commercial processes for adipic acid, adapted from ref.24.	12
Figure 1.7 - Original picture of the flames generated by the explosion of reactor 5 in Flixborough cyclohexane oxidation plant, 1974. Ref. 26	13
Figure 1.8 - Price trends of benzene FOB in US, for the decade 2006-2015.....	14
Figure 1.9 Adipic acid market share, adapted from ref. 24.....	15
Figure 1.10 Time horizon for the development of a new process following the traditional consecutive step scale up.	19
Figure 1.11 - Steps in the development of a pharmaceutical bioprocess from the product idea to the operating plant, adapted from ref. 39. The arrows point the tasks where conceptual design activity is determinant.....	20
Figure 2.1 - Overview of alternative routes proposed for the production of adipic acid from renewables.....	28
Figure 2.2 – Pectin schematic structure and composition, CP-Kelco® informative material.	32
Figure 2.3 – Chemical structure of lactose with on the left galactose and on the right glucose molecules.	35
Figure 2.4 – General composition of lignocellulosic biomass, adapted from ref. 50.....	38
Figure 2.5 – Cellulose crystalline strands surrounded by amorphous hemicellulose and lignin, adapted from ref.58.....	39
Figure 2.6 – Renmatix process to recover simple fermentable sugars from lignocellulosic biomass, based on supercritical water hydrolysis.	40

Figure 2.7 – Structure of the three primary monomeric building blocks of the 3D amorphous polymer lignin. Adapted from ref.62.....	41
Figure 2.8 – Metabolic pathways of a) the chain reduction of fatty acids and b) ω -oxidation by a Verdezyne genetically modified microorganism. ³⁰	44
Figure 2.9 – Metabolic pathways to muconic acid (adipic acid precursor, adapted from ref.23). Both phenol and benzoic acid can be processed.	47
Figure 2.10 – Chemical structure of glucaric acid (left), and its structural isomer galactaric acid (right, also known as mucic acid). The first is optically active, the second not, being a meso form).	49
Figure 2.11 – Equilibria between glucaric acid and its lactone derivatives, adapted from ref.73.	50
Figure 2.12 – Flowsheet concept base on the Rivertop- DCI facilities.....	51
Figure 2.13 – Nitric acid oxidation (step 1) followed by neutralization (step 2) and back acidification (step 3).....	52
Figure 2.14 – Block flow diagram of the Rennovia process for the production of green adipic acid from glucose.	56
Figure 2.15 – Chemical structure of muconic acid isomers.	57
Figure 2.16 – Muconic acid synthetic pathway for <i>E.coli</i> , adapted from ref.20.	59
Figure 2.17 – Reaction pathways for the maximal conversion of glucose to DAHP, adapted from ref. 95. [G6P, glucose; F6P, fructose; 1,6FDP 1,6-fructose diphosphate; DHAP, dihydroxyacetone phosphate; GAP, glyceraldehyde 3-phosphate; R5P, ribose 5-phosphate, X5P, xylulose 5-phosphate; S7P, sedoheptulose 7-phosphate; PYR, pyruvate]	60
Figure 2.18 – Metabolism from aromatic compounds by ortho-cleavage pathway of catechol. The inhibition of muconate cycloisomerase allows to accumulate muconic acid.	62
Figure 2.19 – Conceptual map of the decisions to be taken when developing the process shape of green adipic acid process.	64
Figure 3.1 - Scheme of the workflow and dataflow for the process synthesis methodology.	81
Figure 3.2 - Processing Step-Interval Network (PSIN) representation. Columns represent processing steps (for example, pretreatment, concentration, purification), boxes represent alternative processing intervals (transformation technologies), and arrows represent feasible connections between intervals.....	82

Figure 3.3 - Processing interval scheme with variables used for modelling: index k refers to the interval “k”, i refers to component “i” in a multi-component flow rate.	83
Figure 3.4 - The feasible region is multiplied by a big factor M so to contain also the polyhedron determined by the active constraint	91
Figure 3.5 - Simplified superstructure for process synthesis and design of a renewable two steps adipic acid process.	96
Figure 3.6 - Solubility curves for the isomers of muconic acid and similarity with adipic acid.....	124
Figure 3.7 – Flowsheet of the best processing route.....	143
Figure 3.8 - Cost breakdown for the optimal processing configuration.....	149
Figure 3.9 - Sensitivity analysis of different variables on the production cost. In green, the points improving the process feasibility, in yellow and red, the ones negatively affecting it.	151
Figure 4.1 - Example of triangular possibility distribution.....	165
Figure 4.2 - Algorithm scheme: each α -cut determines the variation intervals for the uncertain parameters, defining the search space for the min/max optimization algorithm. The results are used to build the possibility distributions for the permeate flux and costs.....	167
Figure 4.3 - Fed batch filtration unit with buffer tanks, simplified scheme.....	169
Figure 4.4 - Measured values for diffusivities of colloidal particles according to ref 36.	172
Figure 4.5 - Possibility distribution of the solidsity ratio.....	174
Figure 4.6 - Possibility distribution of the compressibility index for rod shaped microorganisms.....	176
Figure 4.7 - Possibility distribution of the compressibility index for spheroidal microorganisms.....	176
Figure 4.8 - Possibility distributions of the cake porosity for rod shaped microorganisms.	178
Figure 4.9 - Possibility distributions of the cake porosity for spheroidal microorganisms.	178
Figure 4.10 - Flux reduction profiles for batch <i>L. delbrueckii</i> cross flow ultrafiltration: sensitivity analysis for crossflow velocity variation.	181
Figure 4.11 - Flux reduction profiles for batch <i>L. delbrueckii</i> cross flow ultrafiltration: sensitivity analysis transmembrane pressure.....	182
Figure 4.12 - Flux reduction profiles for batch <i>L. delbrueckii</i> cross flow ultrafiltration: sensitivity analysis for filtrate particle size.....	183

Figure 4.13 - Flux reduction and irreversible clogging.....	184
Figure 4.14 - Flux reduction profiles for batch <i>L. delbrueckii</i> cross flow ultrafiltration: comparison between the measured and calculated values.....	184
Figure 4.15 - Average permeate flux possibility distribution for a full-scale fed-batch ultrafiltration of <i>L. delbrueckii</i> (time step 10s - 20 α -cuts).....	185
Figure 4.16 - Cost possibility distribution for a full-scale biorefinery fed-batch ultrafiltration plant, for the clarification of a <i>L. delbrueckii</i> fermentation broth (time step 10 s – 20 α -cuts).	186
Figure 4.17 - Limit cumulative probability functions, corresponding to the cost possibility distribution of figure 4.16.	187
Figure 4.18 - Limit cumulative probability functions for a full-scale fed-batch ultrafiltration of <i>S. cerevisiae</i> (time step 10s - 20 α -cuts).	188
Figure 4.19 - Limit cumulative probability functions for a full-scale fed-batch ultrafiltration of <i>E. coli</i> (time step 10s - 20 α -cuts).	188
Figure 5.1 – Chemical structure of muconic acid isomers and related equilibria.	199
Figure 5.2 - Reactor scheme adapted from MSc thesis of Giulia Locatelli. Ref.18.....	201
Figure 5.3 - Sodium trans,trans-muconate conversion at 250, 500 and 700 rpm T=60°C, P(H ₂)= 4 bar, reaction time= 60 min, sub/cat= 10 (wt/wt) and [MA]= 7·10 ⁻² M	204
Figure 5.4 - Workflow scheme of the analytical procedure for obtaining the conversion and the selectivity of the hydrogenation.	207
Figure 5.5 - Conversion evaluation at different substrate/catalyst ratio and at 60 °C, stirring=500 rpm, P(H ₂)= 4 bar, [MA]= 7·10 ⁻² M, time 4 h.	212
Figure 5.6 - Sodium trans,trans-muconate conversion at (Δ) 40°C, (\circ) 50°C, (\diamond) 60°C, (\square) 70°C, and (\times) and 40°C with catalyst removal after 60 min by hot filtration. In all samples P(H ₂) = 4 bar, stirring = 500 rpm, sub/ca t=10 (wt/wt), [ttMA] ⁰ = 7·10 ⁻² M.....	212
Figure 5.7 - MA conversion (solid line) and AA selectivity (dashed line) - (\circ) <i>cis,cis</i> -MA in the synthetic salt fermentation broth and (\diamond) in pure water: P(H ₂)= 4bar, T=70 °C, stirring= 500 rpm.	214
Figure 5.8 - Reaction scheme with all the possible monounsaturated intermediate isomers. The species reported are <i>trans,trans</i> -muconic acid (MA), α,β - <i>cis</i> -hexenedioic acid (cHDA), α,β - <i>trans</i> -hexenedioic acid (tHDA), β,γ - <i>cis</i> -hexenedioic acid (cHDA _{bg}), β,γ - <i>trans</i> -hexenedioic acid (tHDA _{bg}), adipic acid (AA). In the simplified mechanism, all the intermediates were considered as a single pseudo- component “IN”.	216

Figure 5.9 - Concentration profiles for the hydrogenation of ttMA on Pt/C 5% catalyst at 4bar hydrogen at 60°C. Results of the preliminary regression with the pseudo intermediate, (left without hydrogen dissociation, right with). The arrows point the systematic overestimation of the intermediate concentration.	217
Figure 5.10 - Hypothesized reaction scheme of model LHHW_17P.....	220
Figure 5.11 - Concentration profiles for the hydrogenation of ttMA on Pt/C 5% catalyst at 4bar hydrogen. Results of the regression with model LHHW_17P.....	223
Figure 5.12 - Sensitivity analysis on the parameters of model LHHW_13P.	224
Figure 5.13 - Concentration profiles for the hydrogenation of ttMA on Pt/C 5% catalyst at 4bar hydrogen. Results of the regression with model LHHW_11P.....	225

List of Tables

Table 1.1 - Overview of the companies investing on the development of alternative routes for adipic acid.....	16
Table 2.1 - List of fundamental references for each of the routes for renewable adipic acid. Symbols: BIO (biocatalytic approach), CHEM (chemical approach), HYB (hybrid chemical-biochemical approach).....	29
Table 2.2 - Composition of the main sources of lactose in the dairy industry.....	36
Table 2.3 - Summary of the green metrics and cost estimates for the considered feedstocks	46
Table 2.4 - Main green indicators for the traditional oxidation-recovery steps, on a scale of ca. 150 grams of product as reported in the Rivertop patent examples.....	53
Table 2.5 - Green metrics on Rennovia process.....	55
Table 2.6 - Overview of the most recent bio-based approaches toward adipic acid.....	58
Table 2.7 - SWOT matrix for the realization of an early stage techno-economic feasibility study.....	65
Table 3.1 - List of the components (RM = raw materials, C component, P product, PC pseudo component)	98
Table 3.2 - Growth support composition for E. coli fermentation.....	99
Table 3.3 - Fermenter mixing ratios.....	101
Table 3.4 - Fermenter cost function [\$(2014)/kg: reference stream f M]	102
Table 3.5 - Fermenter utility consumption ratios.....	103
Table 3.6 - Heat exchanger mixing ratios.....	104
Table 3.7 - Heat exchanger cost function [\$(2014)/kg: reference stream fM].....	104
Table 3.8 - Heat exchanger utility consumption ratios.....	104
Table 3.9 - Centrifuges cost function [\$(2014)/kg: reference stream fM]	106
Table 3.10 - Utility consumption ratios	106
Table 3.11 - Centrifuges cost function [\$(2014)/kg: reference stream fM]	107
Table 3.12 - Centrifuges utility consumption ratios.....	107
Table 3.13 - Deep filter mixing ratios.....	108
Table 3.14 - Deep filter cost function [\$(2014)/kg: reference stream fM].....	108
Table 3.15 - Deep filter utility consumption ratios	109
Table 3.16 - Process conditions for cross flow filtration units implemented in the model.	111

Table 3.17 - Cross-flow filters cost function [\$(2014)/kg: reference stream fM].....	111
Table 3.18 Cross-flow filters utility consumption ratios.....	112
Table 3.19 - Rotary drum filter (microfiltration recovery) cost function [\$(2014)/kg: reference stream fM].....	114
Table 3.20 - Rotary drum filter (microfiltration recovery) utility consumption ratios ...	114
Table 3.21 - Rotary drum filter (centrifuge recovery) cost function [\$(2014)/kg: reference stream fM].....	115
Table 3.22 - Rotary drum filter (centrifuge recovery) utility consumption ratios.....	115
Table 3.23 - Ultrafiltration filters cost function [\$(2014)/kg: reference stream fM]	116
Table 3.24 - Activated carbon treatment mixing ratios.....	118
Table 3.25 - Activated carbon cost function [\$(2014)/kg: reference stream fM]	118
Table 3.26 - Evaporators cost functions [\$(2014)/kg: reference stream fM].....	120
Table 3.27 - Evaporators utility consumption ratio.....	121
Table 3.28 - Solubility points for the isomers of muconic acid available in literature. ..	123
Table 3.29 - Crystallizers mixing ratios.....	125
Table 3.30 - Crystallizers cost function [\$(2014)/kg: reference stream fM].....	125
Table 3.31 - Crystallizers utility consumption ratios	126
Table 3.32 - Ethanol dissolution mixing ratios	127
Table 3.33 - Ethanol dissolution cost function [\$(2014)/kg: reference stream fM].....	127
Table 3.34 - Ethanol dissolution utility consumption ratios	127
Table 3.35 - Solvent ultrafiltration cost function [\$(2014)/kg: reference stream f ^M].....	128
Table 3.36 - Solvent ultrafiltration utility consumption ratios.....	128
Table 3.37 - Crystallizers (ethanol system) cost function [\$(2014)/kg: reference stream fM]	129
Table 3.38 - Crystallizers (ethanol system) utility consumption ratios.....	129
Table 3.39 - Water dissolution mixing ratios.....	130
Table 3.40 - Water dissolution cost function [\$(2014)/kg: reference stream fM].....	130
Table 3.41 - Water dissolution utility consumption ratios	130
Table 3.42 - Hydrogenation reactors mixing ratios.....	132
Table 3.43 - Hydrogenation reactors cost function [\$(2014)/kg: reference stream fM] .	132
Table 3.44 - Hydrogenation reactors utility consumption ratios.....	133
Table 3.45 - Adipic acid crystallizers (broth) mixing ratios.	133
Table 3.46 - Adipic acid crystallizers (broth) cost function [\$(2014)/kg: ref. stream fM]	134
Table 3.47 - Adipic acid crystallizers (broth) utility consumption ratios	134
Table 3.48 - Adipic acid crystallizers (pure water) mixing ratios.....	135
Table 3.49 - Adipic acid crystallizers (pure water) cost function.	135

Table 3.50 - Adipic acid crystallizers (pure water) utility consumption ratios.....	135
Table 3.51 - Adipic acid crystallizers (ethanol) mixing ratios.....	136
Table 3.52 - Adipic acid crystallizers (ethanol) cost function [\$(2014)/kg: ref. stream fM]	136
Table 3.53 - Adipic acid crystallizers (ethanol) utility consumption ratios	136
Table 3.54 - Ethanol re-dissolution mixing ratios.....	137
Table 3.55 - Ethanol re-dissolution cost function [\$(2014)/kg: reference stream fM] ...	137
Table 3.56 - Ethanol re-dissolution utility consumption ratios.....	137
Table 3.57 - Adipic acid re-crystallization mixing ratios.....	138
Table 3.58 - Adipic acid recrystallization cost function [\$(2014)/kg: reference stream fM]	138
Table 3.59 - Adipic acid re-crystallization utility consumption ratios.....	139
Table 3.60 - Utility costs summary.....	140
Table 3.61 - Integer cut analysis, ranking of the best process configurations	142
Table 3.62 – Multiscenario analysis and process profitability.....	145
Table 3.63 - Environmental impact factors, comparison with the traditional oil-based process.....	147
Table 3.64 - WAR algorithm evaluation results for selected solution scenarios. ATP is Aquatic Toxicity Potential; TTP is the Terrestrial Toxicity Potential; and HTPE is the Human Toxicity Potetial by Exposition.	148
Table 4.1 - List of the phenomena influencing the cake formation and flux reduction ..	161
Table 4.2 - Filtration cake properties of selected microorganisms	175
Table 4.3 - Simulated fermentation broth characteristics and membrane properties.	179
Table 4.4 - Cost function composition.....	180
Table 5.1 - Main literature contributions list on muconic acid hydrogenation.	197
Table 5.2 - Parameters required for the evaluation of the mass transfer phenomena	203
Table 5.3 - catalyst recycling tests results at P(H ₂) = 4 bar, stirring= 500 rpm, sub/cat=10 (wt/wt), [MA]= 7·10 ⁻² M	214
Table 5.4 - Generic equations for the simplified mechanism with intermediate pseudo component. Dual site L-H model according to Yang and Hougen tables, n=2 without H ₂ dissociation, n=3 with dissociation.....	217
Table 5.5 - Species concentration in time for the reaction T=60 °C, Pt/C 5 %, P(H ₂)=4 bar, 500 rpm	218
Table 5.6 - Generic equations for the refined mechanism with intermediates: dual site L-H model according to Yang and Hougen tables, n = 2 without H ₂ dissociation, n = 3 with dissociation.	219

Table 5.7 - Calculated parameters for the three models, adsorption constants K_i are in L/mol.....	219
Table 5.8 - Calculated values of the model parameters with 95% confidence interval and regression metrics.	222

List of Papers

Included in this thesis

- A. Rosengart, M. Vizzi, F. Manenti, A. Citterio. Development of an ultrafiltration predictive model to estimate the cost of downstream in biorefineries: Effects of epistemic experimental uncertainties. In *Energy Conversion and Management*, Volume 149, 2017, Pages 875-884.
<https://doi.org/10.1016/j.enconman.2017.03.043>.
- S. Capelli, A. Rosengart, A. Villa, A. Citterio, A. Di Michele, C.L. Bianchi, L. Prati, C. Pirola. Bio-adipic acid production by catalysed hydrogenation of muconic acid in mild operating conditions. In *Applied Catalysis B: Environmental*, Volume 218, 2017, Pages 220-229.
<https://doi.org/10.1016/j.apcatb.2017.06.060>.
- A. Rosengart, S. Capelli, C. Pirola, A. Citterio, C. L. Bianchi, L. Prati, A. Villa. Renewable Adipic Acid From the Hydrogenation of *trans,trans*-muconic acid: Selection of a Three Phases Kinetic Model. In *Chemical Engineering Transactions*, Volume 57, 2017 Pages 931-936.
<https://doi.org/10.3303/CET1757156>
- A. Rosengart, S. Capelli, F. Manenti, C. Pirola. Hydrogenation of *trans,trans*-muconic acid to adipic acid: mechanism identification and kinetic modelling. In *Chemical Engineering Journal*. Submitted October 2017.
- A. Rosengart, M.O. Bertran, J.M. Woodley, R. Gani, A. Citterio, F. Manenti. Process Synthesis for the Production of Sustainable Adipic acid. In *Biotechnology for Biofuels*. Submitted October 2017.

Not Included in this thesis

- A. Rosengart, M.Teresa Cesário, M. Catarina M.D. de Almeida, Rodrigo S. Raposo, Ana Espert, Elena Díaz de Apodaca, M. Manuela R. da Fonseca. Efficient P(3HB) extraction from Burkholderia sacchari cells using non-chlorinated solvents, In Biochemical Engineering Journal, Volume 103, 2015, Pages 39-46.
<https://doi.org/10.1016/j.bej.2015.06.013>.
- V. Barbera, A. Bernardi, A. Palazzolo, A. Rosengart, L. Brambilla, M. Galimberti. Facile and sustainable functionalization of graphene layers with pyrrole compounds. In Pure and Applied Chemistry. In press.
<https://doi.org/10.1515/pac-2017-0708>

Preface

“Chemical engineering is the only engineering discipline founded on all three sciences, and mathematics. As such, it is well positioned for exploring discoveries and advances in chemistry, biology and physics to solve pressing problems in energy, the environment, biosciences, materials and other exciting areas. This makes ChE very relevant and also a lot of fun.” This is what Gregory Stephanopoulos, prominent professor of MIT, says about Chemical Engineering. Being immersed in such an interdisciplinary environment (to chemistry biology, physics and mathematics, let us add economics) it is quite complicated to describe what actually a chemical engineer does. Nevertheless, there are some ideas that are so deeply rooted in chemical engineers’ education that can be used to define their identity. These are the fundamental values of Efficiency and Safety.

What is Efficiency? The need to bind to Nature’s constraints, but also the pursuit of the best for human progress: this induces chemical engineers to search for what is defined “optimal”. Not perfect, as perfection is not achievable, not definitive, as time is limited, not absolute, as knowledge will possibly improve.

What about Safety? Chemical engineers have a major responsibility toward human and environment safety, as their work can have tremendous consequences. Therefore it is not surprising that chemical engineers influenced the first regulation of industrial safety and that the first tools to measure environmental impacts were theorized within chemical engineering applications. Still, the role of the chemical engineer is not to be limited to a merely productive application. The multidisciplinary formation and some “secret” computational tricks of chemical engineers (belonging to the so called “Process Systems Engineering” discipline) can prove themselves useful in laboratory, in a wider context of research and development.

This thesis contains examples for all the mentioned concepts. The most consistent part is related to the feasibility study of a novel and safe manufacturing practice, to promote new environmental friendly technologies. The feasibility study is conditioned by the achievement of an optimal solution for the process flowsheet, and optimality is searched by applying different PSE tools. Also, this Thesis contains some examples of how “theory” can assist practical laboratory research. In fact, even though the objective of a research is defined, the path to reach it is not clear a priori, requiring efforts that can be very resource and time demanding. Is there a way to enhance research efficiency and optimize lab work?

Chapter 1

Introduction

This chapter will provide the reader with the general framework that inspired this work. Paragraph 1.1 gives an overview on the environmental impact mitigation policies that both European Union and United States of America have been promoting in the recent years. Paragraph 1.2 introduces the traditional process for oil-derived adipic acid, characterized by relevant environmental and safety hazards and which make it also economically risky. This framework motivated a strong academic and industrial interest toward alternative productions of adipic acid: paragraph 1.3 presents the main players in this field, focusing on the main challenges that a biorefinery for commodity chemicals should overcome. Finally, the objectives and the structure of this Ph.D. thesis are presented in paragraph 1.4.

1.1 - Green Chemistry and Biorefining

1.1.1 - Environmental impact mitigation: a paradigm for industry

The awareness of the negative impact of human activity on the Earth has pushed policy makers to incentive the search of new solutions to mitigate pollution and reduce resource consumption. The world environmental policy is led by the European Union since Kyoto Protocol (1997): in facts, EU sets the most ambitious objectives for the internal industrial development agenda in the mid and long term.¹ The current reference document for the environmental legislation of the European countries is the 7th Environment Action Programme (7EAP), which entered into force in 2014 and sets the growth targets for 2020.² “Living well, within the limits of our planet” says the official slogan of the programme, as shown Figure 1.1. These few words perfectly represent the logic of changing toward a sustainable production paradigm: the objective is to keep (and improve) the human development, but also to respect the limited resources of our planet.



Figure 1.1 - Official logo and slogan of the EU 7th Environment Action Programme.

The main points of the 7EAP, to be fulfilled before 2020, are the following:

- I. Reduce the 20% of the Greenhouse gas (GHG) emissions (30% if other developed countries pursue the same objective), employ at least 20% of renewable energy, and reduce the 20% of primary energy consumption by improving efficiency.

- II. Halt the loss of biodiversity and the degradation of ecosystems in European territory and restore them as far as possible.
- III. Halt the loss of global cover (by 2030 at the latest) reducing of the 50% the tropical deforestation compared to 2008 level.
- IV. Maintain or improve the status for all EU waters.
- V. Achieve good environmental status in all marine waters.
- VI. Achieve of air quality levels in all the Union territory that do not give any negative impact to human health and environment.
- VII. Produce and use chemicals in a way that minimize the significant adverse effects on human health and environment.
- VIII. Protect human health and environment preventing and reducing the impact of waste generation and management.
- IX. Stimulate the transition to a Green Economy, pursuing the complete decoupling of economic growth and environmental degradation.
- X. Strive to achieve a land degradation neutral world in the context of sustainable development.

These points, adapted from the first lines of the legal publication of 7EAP, represent the most modern and advanced positions toward environmental protection, highlighting the importance of some concepts as “Human health and environment protection”, “Green Economy”, “Sustainable Development”. Being translated into a transnational legal document, these concepts ceased to be mere buzzwords against climate change, and became the main direction for the Economy and Development Ministries of the most advanced countries of the World.

Also, United States of America put much effort in directions similar to the 7EAP, with the “Air, Climate and Energy Strategic Research Action Plan” (ACEStRAP), valid from 2016 to the 2019, even though it is less ambitious on certain targets.³ Still, US nation keeps its role of a privileged speaker on some of the technologies that should promote human sustainable growth.

7EAP and ACEStRAP are the proof that the governments (of the most advanced countries) are taking seriously the priority of protecting environment to guarantee the long-term wellness of citizens. However, if the role of governments and policy makers is to set the general direction to be followed, the road must be traced by the actual responsible of the

environmental impacts, i.e. is industry, as pointed by the diagram in Figure 1.2. The 20% of the GHG emission worldwide, particularly cumbersome among the many anthropogenic impacts as responsible of global warming, is ascribable to the industrial sector. A more detailed insight comes from Figure 1.3 showing the specific contributions of the manufacturing categories.

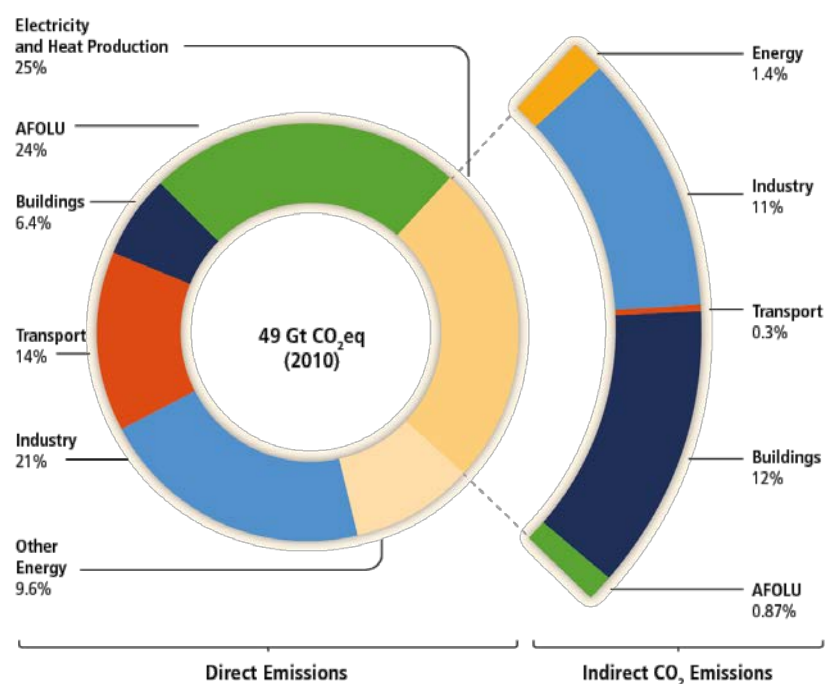


Figure 1.2 - GHG emissions by economic sector adapted from ref.4. The acronym AFOLU stands for “agriculture, forestry and other land use”.

Interestingly, the areas related to chemical industry (waste treatment and chemicals production) account by 30%: any improvement in this fields would hence result in the biggest benefits.⁴ Fortunately, this industrial sector has been developing for years the tools to implement the changes now formally required by the new green production paradigm. It was indeed within these manufacturing sectors that Chemical Engineers, following the mission of plants efficiency while ensuring man and environmental safety, came into the first formulation of the “Human health and environment protection”, “Green Economy”, “Sustainable Development” concepts.⁵

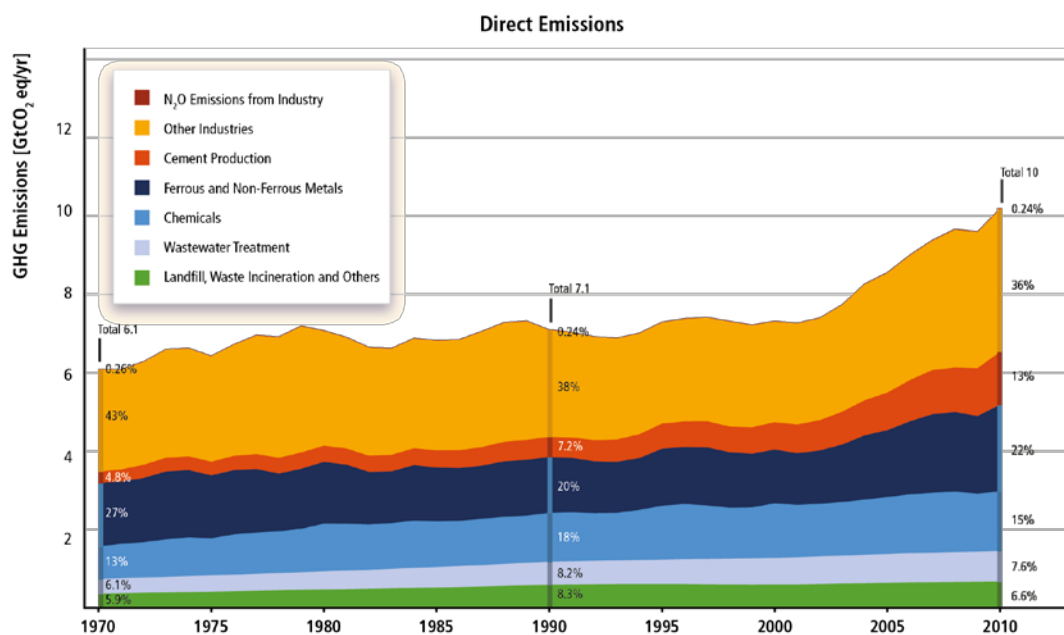


Figure 1.3. - GHG emissions by manufacturing category adapted from ref. 4.

From a more careful analysis however, the renovation of the manufacturing practice toward efficiency and sustainability has always been the only surviving option for western chemical industry. A KPMG report titled “The future of European chemical industry” clearly presented this scenario back in 2008, before the definition of 7EAP.⁶ Accordingly, the main challenges to European industry is the struggle of Middle East and China to become self-sufficient, and even exporters of base chemicals. Those countries can exploit the access to cheap oil feedstocks (67% of oil reserves and 45% of natural gas are located in Middle East) and/or the government support, which encourages with public money the opening of new chemical plants (especially in China). Even though these countries still depend on Western technologies, their aggressive industrial policies have already proven to be successful between 1997 and 2007, as shown in Figure 1.4. China led export growth, and eventually arrived to pass US industry output in 2010.⁷ Europe and US have been continuously losing territory when talking about commodity chemicals, unable to contrast such a fierce competition. For example, about 40 out of the 200 crackers worldwide have been closed before 2015: 14 of these were in Europe.⁶ Similar fate had ethylene glycol plants. European companies are facing major restructuring: Clariant for example cut 3220 positions in 2009, Akzo Nobel reduced the workforce of 20%.⁶

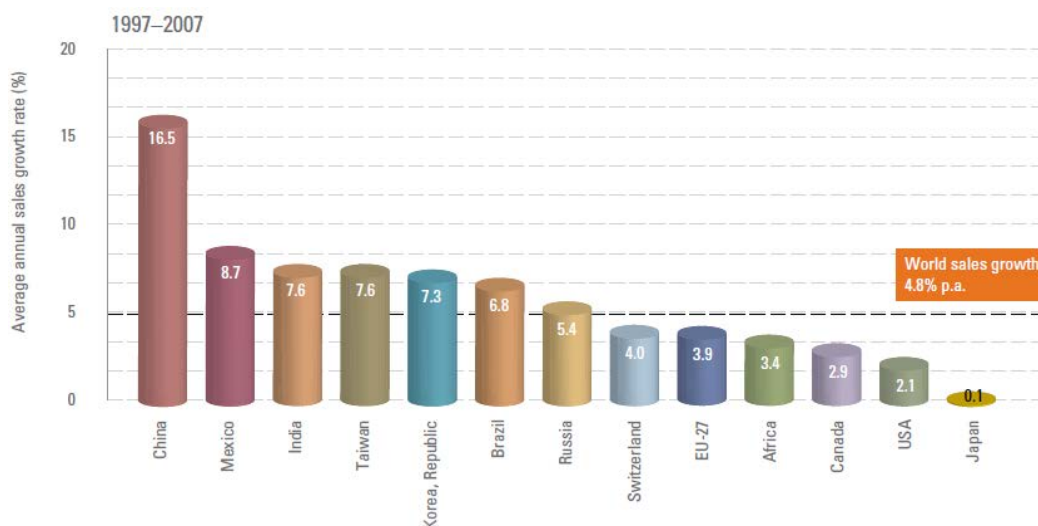


Figure 1.4. Chemical sales growth rates of selected countries between 1997 and 2007

Still, the forecasted scenarios point out a general growth of 5% yearly of the worldwide chemical demand before 2020.⁶ Western countries can benefit from a larger market: the future will simply not be commodity production, intended in the traditional way. The KPMG report indicated the following survive strategies for European companies:⁶

- Move from bulk chemicals to specialty chemicals at the end of the value chain, setting a technological advantage
- Maintain the advantage on Intellectual Property, investing in R&D and novel technology development.
- Strengthen supply chain relationship both with feedstock providers and customers, by means of joint venture programs and Open Innovation approaches.
- Enhance the integration among energy and resource consumption within a manufacturing area (a waste can be a resource for another production). This concept is the BASF “Verbund approach”.⁸

While the third and fourth points involve company-level management decisions, the first two strategies have a much wider influence. These are indeed the purposes of the 7EAP and ACESRAP policies. Even KPMG observed in 2010 how “Using their technological advantage to stay ahead of the market, these (European) companies are uniquely positioned

as leaders in the development of new energy-efficient products, efficient manufacturing processes and alternative feedstocks based on natural materials such as sugar, vegetable oils and plant extracts”.

Environment is therefore not only an industrial constraint, but is actually a leverage to relaunch the industrial competitiveness. In fact, developing countries, that currently underestimate the importance of pollution prevention against economic growth, will eventually understand the importance of preserving human health and environment and will need sustainable solutions. It is therefore in the interest of western countries to be the market leaders and providers of these Green Technologies.

In conclusion, the shift to Green Industry is a necessary action to be taken. This could appear challenging and certainly requires the formulation of new concepts (e.g. Life cycle thinking, Circular Economy, etc.) Also, new forms of production must be understood and used (e.g. the “Verbund” integrated plants or biorefineries).

First of all, it should be clarified what is the actual meaning of the term “Green”.

1.1.2 - The concepts of Green process and the Biorefinery

A univocal definition of “Green” is still missing, and the term is generally used for any application or product that somehow has good ecological performances. A recycled plastic bottle is “green” even though can be responsible of long lasting sea pollution, and a biodegradable bioplastic bag is called “green” even though its production exploits more natural resources than a traditional polypropylene bag.^{9,10}

For industrial production it is possible to apply the definition contained in the 12 principles of Green Chemistry.¹¹ In general, a chemical reaction (and by extension a production process) can be considered “Green” if fulfills the three following points:

- ◆ New processes should enhance material and energy efficiency, minimizing wastes.
- ◆ Renewable feedstocks and energy sources should be preferred.
- ◆ Safe and environmentally benign substances should be used whenever possible.

Even though the complexity of real applications often forces to pursue a trade-off among the three above tendencies, it is clear that efficient bio-processes are generally preferable,

given the lower energy intensity and low hazard level.¹² In this spirit, the concept of Biorefinery took place, as a renewable counterpart of the ill-famed oil industry.^{13,14}

Biorefineries are supposed to produce entire classes of organic chemicals and fuels just as a traditional refinery, with the great difference that the carbon source is no more fossil, but follows the natural cycle of CO₂, which is captured from atmosphere and fixed into living organisms (plants, algae, bacteria).¹⁴ Biorefineries and biorefining-related processes (i.e. production of a specific product from natural sources, as bio-gas) are classified into first, second and third generation.

The first-generation biorefineries exploit feedstocks that have been cultivated and cropped on purpose: these have the issue of causing soil consumption and overlap with food production (e.g. sugar cane for bio-ethanol), which can raise ethical concerns.^{15,16}

A second-generation biorefinery, instead, employs waste material of natural origin, e.g. the residual lignocellulosic material from forestry and agriculture.

The third-generation ones exploit the solar radiation using microalgae as photo bioreactors to produce target products as fuels, polymers and nutraceutical products.

This latter type of biorefinery is still under investigation, while there are many full scale operating plants of first generation technologies (e.g. for ethanol or succinic acid). Second generation plants have reached the demonstrative scale, as Proesa® cellulosic ethanol facility in Crescentino (Italy) with a productivity of 40,000 ton/year, and the first full scale Renmatix® biomass-to-glucose biorefinery (US) will be realized in 2018.¹⁷

Industry is gaining evidence of the sustainability and profitability of these alternative processes, and many other biorefineries are currently being studied for industrialization.¹³

The US Department for Agriculture (USDA) has projected that biobased chemical market share will rise from 2% to more than the 22% by 2025: the world is experiencing the raise of renewable chemical industry.¹²

However, the development of biorefining should face the important constraint of feedstock availability. First and second generation feedstocks (in particular renewable biomass) have lower energy and carbon density than oil, are more expensive to be shipped, and are geographically dispersed. Considering the case of US, the amount of biomass producible in the whole territory would not cover the total demand of crude oil.¹⁸ Therefore, traditional processes and biorefineries are destined to coexist: it is hence of paramount importance to

define carefully the renewable products to be developed, to maximize the benefits for environment and ensure the short-term process feasibility.¹⁹

Energy security considerations have fostered the research toward fuels, but the actual advantage of biorefineries is to be found in chemicals production (specialty but also commodity chemicals).²⁰ As shown in Figure 1.5, renewable feedstocks have hydrogen-to-carbon (H/C) ratios more similar to the feedstock carbohydrates, therefore the production of industrially relevant chemicals requires in theory less transformations.¹⁹ This aspect, together with the higher market prices of value-added products, would ensure higher margins than producing renewable fuels.

When thinking to new biorefining production routes, two main strategies can be followed: a “drop-in strategy” which aims at substituting an oil-derived product with a greener (and cheaper) alternative, or an “emerging product strategy” where a novel compound creates a new market.¹⁹ The advantage of the former is that the market is already mature and large part of the necessary infrastructure and technology already exist, to fast capitalize the new renewable solution. On the other hand, the new technology should compete with fossil equivalents, which are often particularly cost effective. Emerging products, instead, are more challenging as require extensive investments on a long term, but have the advantage of creating a new market, detached from oil counterparts. The choice about the right approach to follow and the type of products to be industrialized is one of the topics that is mostly puzzling academic and industrial research. An important report of 2004 from NREL (National Renewable Energy Laboratory, a US public research institute) reviewed and listed the most relevant “renewable platform chemicals”.^{21,22} Platform chemicals are those compounds, derivable from biomass, which are capable of finding the higher number of applications within the current chemical product market. The list, counting more than 30 chemicals, gives much importance to many carboxylic acids, such as formic acid, acetic acid, malonic acid, fumaric acid, levulinic acid, 2,5-furandicarboxylic acid, adipic acid, citric acid. All these compounds can find application as final products, but they are also interesting as intermediates. Particularly versatile in the perspective of a drop-in biorefinery application, is adipic acid, which has been at the center of industrial attention for the last five years.

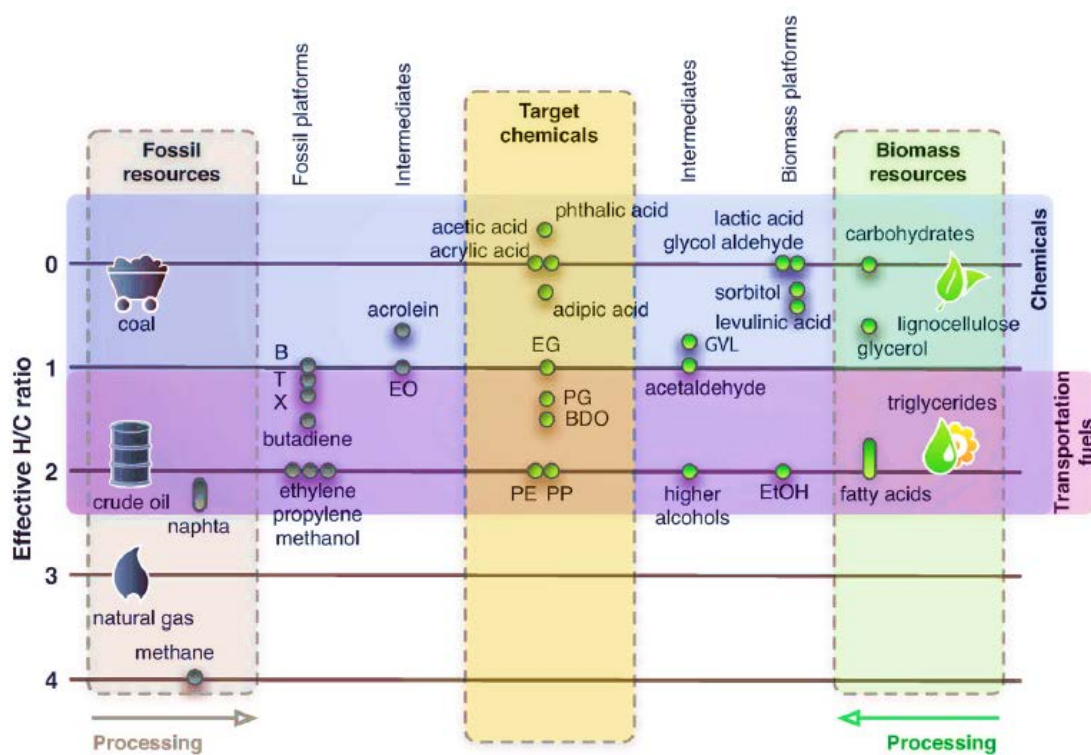


Figure 1.5 - Representation of the effective H/C ratio of bulk and commodity chemicals, with renewable feedstocks and the qualitative degree of processing, adapted from ref. 19.

B benzene, *BDO* 1,4-butanediol, *EG* ethylene glycol, *EO* ethylene oxide, *GVL* γ -valero lactone, *PE* polyethylene, *PG* propylene glycol, *PP* polypropylene, *T* toluene, *X* xylenes.

1.2 - Adipic acid: overview of a strategic platform chemical

1.2.1 - The traditional oil-based processes

Adipic acid (AA) is a high volume bulk chemical, whose market has the size of 3.7 million tons and generates revenues for more than 7 billion USD (Coherent market insights, 20 July 2017).²³ The market is expected to grow at a rate of 4.1% per year in terms of volume in the period 2017-2025, almost entirely due to the expansion of Asian countries.

The 75% of the total output is employed for polyamide fibers production (PA6 and PA6,6), but AA finds application also for polyesters, lubricants, plasticizers and, if further purified, as acidulant in food industry (E355).²⁴

The totality of the current production is petrol based, and is divided between three main types of processes according to the feedstock employed, as represented in Figure 1.6. These are the phenol route, the cyclohexane process, the cyclohexene route: in all these cases, the starting material is benzene. A fourth route has butadiene as a starting material, which is carbonylated to dimethyl adipate and then converted to adipic acid by hydrolysis (BASF). This technology, however, plays a minor role. Most of the worldwide adipic acid in fact derives from Du Pont two-step oxidation of cyclohexane (known as KA-oil process). The main conversion steps are the following: benzene is first hydrogenated to cyclohexane using Ni/Al₂O₃ catalysts under pressure; then cyclohexane is oxidized at 150-170°C with Co based homogeneous catalysts producing cyclohexanone and cyclohexanol (ketone and alcohol, the “KA-oil”); finally the mixture is further oxidized to adipic acid using nitric acid and air in presence of Cu-V catalysts.²⁴ This process is the most cost efficient and is widely employed, even though it still raises serious safety and environmental concerns, in spite of 70 years of technological maturity and continuous optimization.²⁴

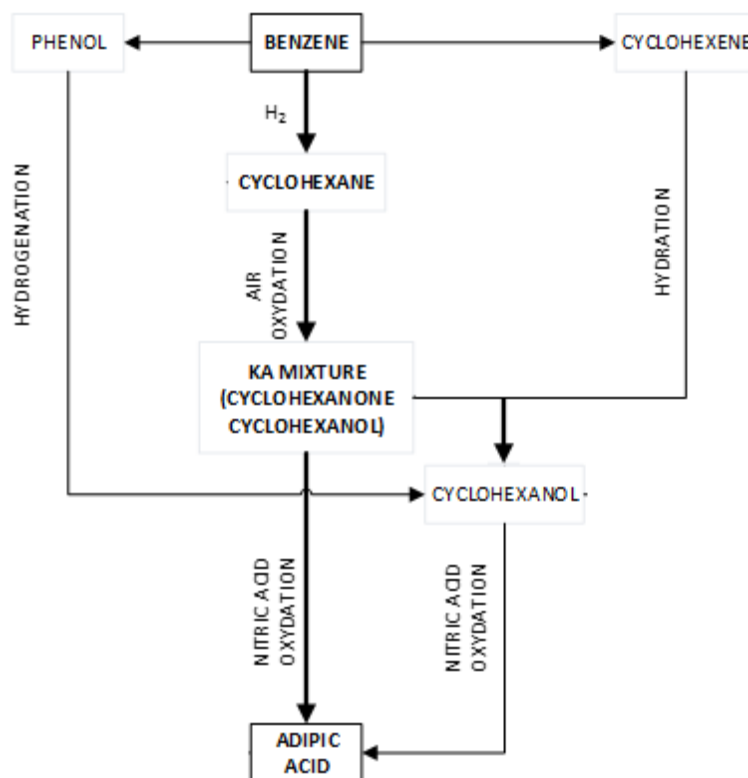


Figure 1.6 - Commercial processes for adipic acid, adapted from ref.24.

Explosion hazard is a real issue for this process, due to the formation of hydroperoxydes in the first oxidation and due to the inner instability of cyclohexane; the second oxidation is dangerous due to the large use of nitric acid under constant threat of runaway exothermic reactions.²⁵ This enforces to keep low conversions in the first step (4%), with high recycle costs. The costs are increased also by the need of corrosion resistant equipment, for the strongly aggressive environment. Indeed, one of the worst disasters in the history of chemical engineering happened on a cyclohexane oxidation plant. In Flixborough (UK), a leak of cyclohexane caused a major explosion in 1974 (see Figure 1.7), that blew the entire site, killing 28 people and injuring 36 of a total of 72 operators. This tragic event deeply shocked the international community of chemical engineers, who began to investigate and define those practices that today constitute the basic regulation of industrial safety and accident prevention.



Figure 1.7 - Original picture of the flames generated by the explosion of reactor 5 in Flixborough cyclohexane oxidation plant, 1974. Ref. 26.

Adipic acid process is also particularly burdensome for the environment.²⁷ The main threats derive: from the need to stock large amounts of dangerous chemicals (benzene for cyclohexane and ammonia for nitric acid production), from the use of homogeneous metal catalysts with the risk of soil contamination, from the production of CO, NMVOCs (non methane volatile organic compounds), nitrous oxide and NO_x gases.²⁸ Remarkably, before the development of highly efficient NO_x abatement technologies in the 90s, adipic acid manufacturing was responsible alone of the 10% of the total anthropogenic nitrous oxides production.²⁸

New and stricter regulations oblige companies to continuously invest on hazard prevention and environment protection, which further erodes the already slight margins of a process dominated by feedstock price and energy requirements.²⁴

1.2.2 - General economic considerations

The main source of apprehensions for adipic acid producers in the last years has been the strong market fluctuations, which can dangerously reduce the span between feedstock and product price and therefore the profits. Considering the trends of the last 10 years, the price of adipic acid has spanned between 900 \$/ton and 2700 \$/ton, according to the

unpredictable fluctuations of benzene and following the expansion/recession periods of manufacturing industry.²⁴ Figure 1.8 reports the trends of the price of benzene in the decade 2006 and 2015 (ICIS news data)²⁹: the lowest value was 130 \$/ton (0.5 \$/gal) and the highest 1455 \$/ton (5.5 \$/gal). The price, normally unstable, actually saw two sudden falls, due to the economic crisis of 2008 (which caused a general market stagnation) and due to the oil price fall after 2014.

Since the market price of adipic acid does not follow automatically the oil price fluctuations (as it is influenced also by demand and existing stocks), the raw material costs peaks can actually strike down the profits of such a delicate plant, that must be run continuously and does not allow to reduce the productivity to follow the market.

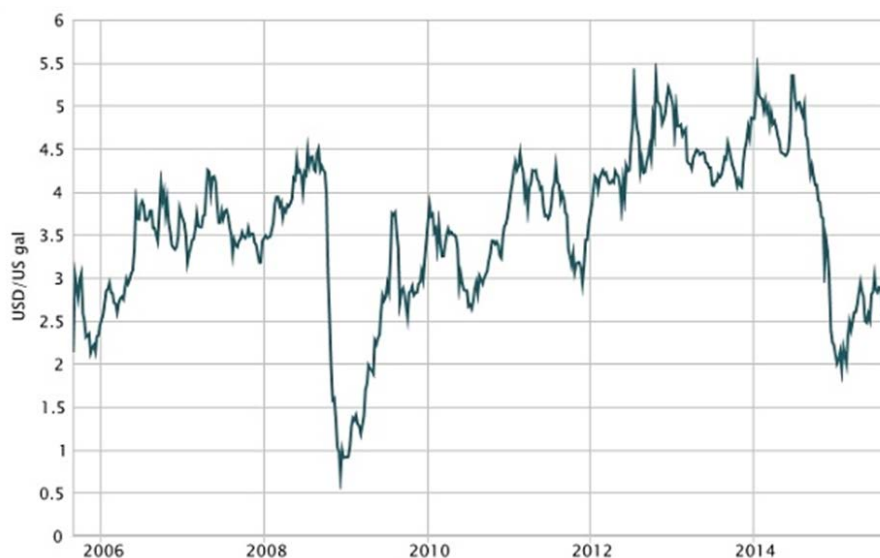


Figure 1.8 - Price trends of benzene FOB in US, for the decade 2006-2015.

(Source ICIS news).²⁹

As a general consequence, only few companies are able to compete in the adipic acid niche, as listed in Figure 1.9. Invista, Rhodia, Ascend and BASF cover the 61% of global production and in a common trend with other chemical industries, they are moving the production to East following the demand (and less restrictive environmental policies).²⁴ From their original role of global exporters, western countries risk becoming importers of

adipic acid, unless a new technology brings a better adipic acid alternative, characterized by an eco-compatible process and, possibly, CO₂ neutral raw materials.

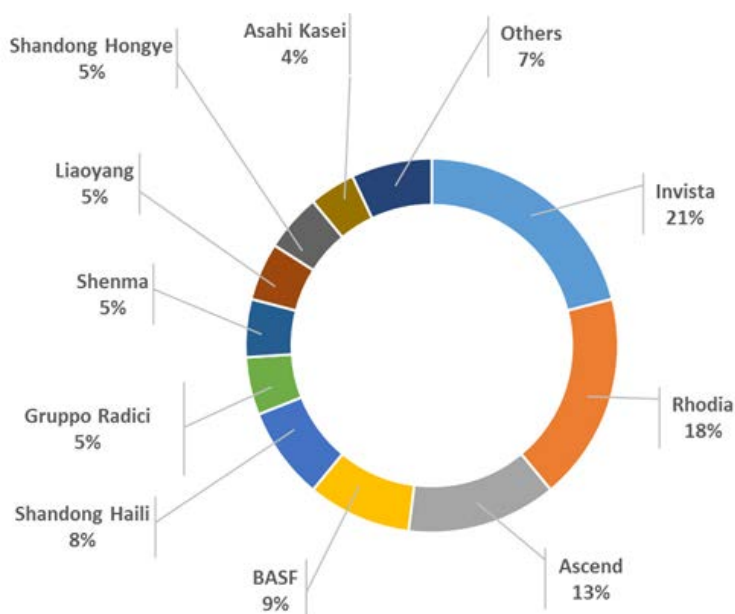







Figure 1.9 Adipic acid market share, adapted from ref. 24.

This economic framework explains the reason why adipic acid has been included in the strategic platform chemical list. A green process would allow exploiting safe and cheaper raw materials (detached from oil fluctuations), would comply with the environmental protection laws without expensive equipment, would stop the trend of manufacture off-shoring, while exploiting the huge and growing adipic acid demand.³⁰

1.3 - The challenges of developing an adipic acid biorefinery.

Provided the strategic role of adipic acid, several companies pioneered some alternative green solutions. The detailed analysis of the patent literature is performed in Chapter 2, while Table 1.1 summarizes the main players.

Table 1.1 - Overview of the companies investing on the development of alternative routes for adipic acid.

	Amyris	Bioconversion of glucose to muconic acid and hydrogenation to adipic.
	Bioamber	Direct bioconversion of glucose to adipic acid.
	Genomatica	Direct bioconversion of glucose to adipic acid.
	Verdezyne	Bioconversion of long chain fatty acids into shorter dicarboxylic acids, as adipic
	Rennovia	Catalytic hydrodeoxygenation of aldaric acids to adipic acid

- a. Acquired the patents of Draths corp.
- b. In joint venture with Celexion.

In the relatively short period of 2000-2010 these knowledge-based companies filed more than 50 patents, covering several possible bio-chemical routes to achieve adipic acid from different feedstocks. Two of these companies, Verdezyne and Rennovia, received consistent investment from big players as DSM and Johnson Matthey, and reached the level of pilot plant experimentation, fostering the rumors of a “soon green adipic acid revolution”.³¹⁻³³ However, the revolution did not really happen and today adipic acid is still derived from fossil sources. None of the renewable projects has been translated into a demonstrative plant and, even if the research on sustainable adipic acid has not stopped (especially in academia), the industrialization seems to be postponed to better times.

This highlights the two biggest weak points of adipic acid drop-in biorefinery.

First, the barrel price fall of 2014 made fossil adipic acid too cheap for taking the risk of innovating. The most advanced technology of the 2014 period (Rennovia) was estimated competitive until a minimum oil price of 60 \$/barrel.³³ Today the price is still very low, around 51 \$/barrel.³⁴

Second, an “emerging bioderived product”, was successfully introduced in the market: succinic acid. This 4-carbon dicarboxylic acid is similar to adipic acid, but still does not overlap entirely with this the other one’s market. Particularly important, bio-derived succinic acid does not have an oil-derived counterpart. Therefore, succinic acid diverted much of the bigger companies’ investment, which were before of adipic acid: in practice the investors applied the wise saying “a bird in the hand is worth two in the bush”.^{35,36}

But could Rennovia, Verdezyne and the others have done more to convince the stakeholders to believe more in their technologies?

The answer is yes, as some recent studies on biorefinery development have pointed out.^{36,37}

A common characteristic of the companies of Table 1.1 is that they are all knowledge-based, being university startups and/or focusing mostly in the area of lab-scale applied research and patenting. All of them (except for Rennovia) are active in biological engineering field, and their core expertise is much more oriented toward genetic engineering, rather than process development. This is clearly reflected by their patents and commercial brochures, where the industrialization challenges are absolutely underrated and the estimated economic performances are supported by very questionable numbers (see Chapter 2 and 3). In fact, good bacterial yield and selectivity are important conditions for a process feasibility, but a viable downstream can be determining for the rapid success of a new technology, as for the case of succinic acid. In fact, an acid fermentation of yeast for succinic acid, though not as brilliant as other *Escherichia coli* neutral fermentation, proved to be more stable against contamination (which means easy scalability of the fermenters) and allowed saving the cost of neutralization chemical and the disposal of the produced counter salts.³⁶ This paved the way to the success of this DSM technology against the competitors, who were still struggling in enhancing the glucose selectivity.

As a consequence, it is evident that the traditional paradigm of “first defining the conversion steps, then optimizing the process” does not hold with the biorefineries as it

used to with traditional chemical industry. New challenges characterize bio-derived commodity processes:^{19,37,38}

- The development of new bacteria (or biocatalysts in general, as for enzymatic transformation) does not follow the same pattern of traditional catalysts.
- There are strict cost constraints for bio-derived commodity chemicals, while bio-processes have often addressed specialty or fine chemicals: the field of bio-optimization is still young.
- The scale and technologies are very different with respect to oil industry, employing solutions more common in pharmaceutical industry.

In practice, large scale bioprocesses can be seen as hybrids between pharmaceutical and petro-chemical processes, needing tailor-made and flexible technologies to overcome the specific needs of the biotransformations, but requiring costs reduction by optimization and standardization.

Provided the fairly recent development of biorefining applications, there is not an established practice for bio-process development, and the rule of thumbs borrowed from the pharma or oil industry, can actually fail in evaluating the competitiveness of biorefineries.³⁸

The approach to process development should be re-defined for biorefining applications, as highlighted by Noorman et al.³⁷, and new tools should be developed, that take advantage of the best practices of both pharmaceutical and oil tradition.

The three critical points of Noorman et al.³⁷ general analysis are:

- I. The product specification and the downstream purification schemes should be set before defining the upstream section.
- II. The feedstock and the product-market combinations should be assumed already in place when developing the new process
- III. The process, and in particular the upstream section should be developed assuming the final full-scale size of the plant

The last point is due to the evidence that the usual scale up rules of chemical industry do not hold against fermentation. A big scale fermenter (order of magnitude 100 m³ and more) presents some transport phenomena completely different from the bench scale reactors. To avoid the risk of major bottlenecks during industrialization, a solution can be the

application of “down-scaling” rules that is reproducing the full-scale conditions in lab-reactors. The traditional approach of commodity chemical industry is consecutive-incremental in scale, i.e. the optimization is carried out at lab scale, then on a miniplant, then on a pilot plant, then at demonstrative scale (Figure 1.10). In a bioprocess, this approach can be risky: for example, an unpredicted inhibition of bacterial growth occurring at an advanced stage could frustrate the results of years of R&D.

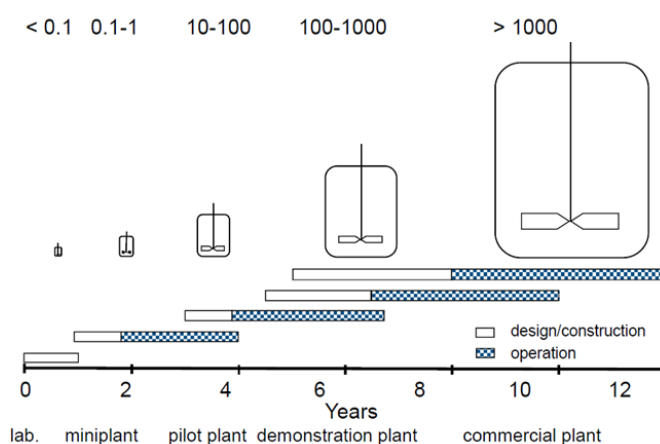


Figure 1.10 Time horizon for the development of a new process following the traditional consecutive step scale up.

The second of the three points is motivated by the large amounts of non-exploited biomass (See Paragraph 2.1.3). The feedstock availability should not be considered as a limit for the process development as long as the processes themselves are designed to be flexible and viable for different feedstocks. Actually, oil industry itself grew up assuming that the petrol availability was not an issue.

The third point stresses the role of downstream and the importance of a holistic approach toward process development. This means that the process shape should influence R&D decisions from the very beginning. Therefore, conceptual design becomes the critical stage of the whole activity of process development.³⁷

In the traditional commodity industry, detailed conceptual design is usually performed after the pilot/demonstrative plant level, while the pharmaceutical industry performs some process engineering estimates far before, as shown in the diagram of Figure 1.11. In fact, the preliminary estimates from the ongoing research can be very useful for identifying the

Best Manufacturing Practices, to ensure the quality of the products, (QbD approach of pharmaceutical industry, See Chapter 3).

Translating this idea to biorefineries and large scale bioprocesses, preliminary data could guide the technology selection to ensure low price of the future commodity chemicals. This would not only allow controlling a priori the costs of the future process, but also can guide research to focus on the best-scalable alternatives.

The challenge for biorefineries is to adapt the reliable conceptual design tools of chemical industry to the uncertainty of early stage design of bioprocesses.³⁸

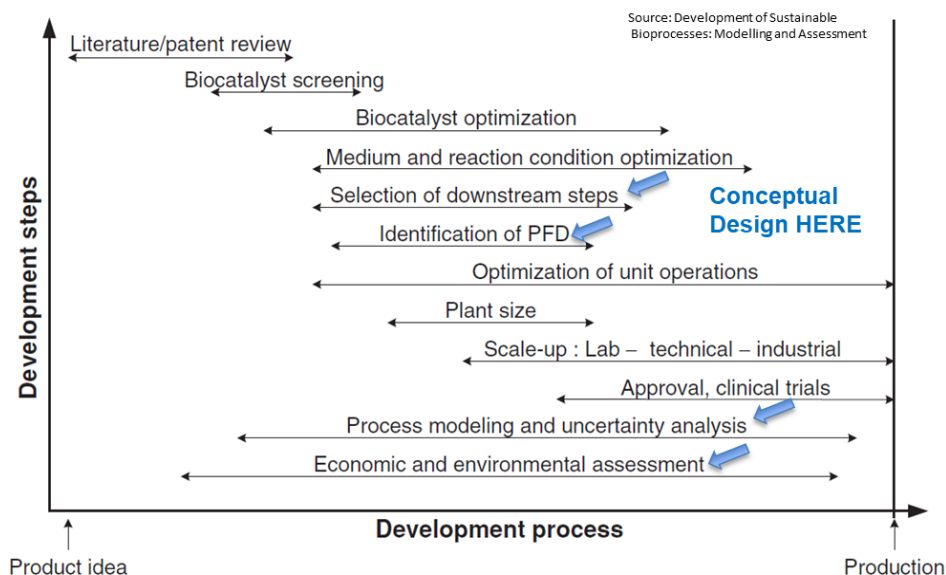


Figure 1.11 - Steps in the development of a pharmaceutical bioprocess from the product idea to the operating plant, adapted from ref. 39. The arrows point the tasks where conceptual design activity is determinant.

In conclusion, the investors seem to have cooled down their initial enthusiasm for adipic acid. From now, any further step will need to be motivated by sound and careful numbers. The case of a “green” adipic acid becomes therefore the best opportunity to test novel approaches for early-stage evaluations of novel bio-based processes.

1.4 - Objectives of the thesis and structure

The main objective of this study is to provide an updated and complete techno-economic analysis of a novel process concept for green adipic acid, analyzing the current technological alternatives.

Such an analysis would be beneficial for industrial stakeholders:

- The maturity level of green adipic acid technology is measured, providing systematic information on the risks/opportunities of investing in this research topic.
- The analysis can be included in a company's market projection to decide future strategies.³⁶

The main benefits would come however for the researchers still involved in the development of a green adipic acid process:

- The scattered and fragmented material from different fields is organized systematically, reviewing the entire process state of the art, from the upstream- to the downstream
- The economic/environmental potential of different concurrent is calculated, helping the researcher to prioritize the best manufacturing solutions, reducing the dispersion of the efforts
- The identification of process bottlenecks or hotspots (particularly expensive, critical) can help to define a series of SMART objectives (Specific, Measurable, Achievable, Relevant, Time-bound) to define an effective strategy of research.⁴⁰

For strategy definition however, it is of paramount importance that the results are the most reliable possible: still, by definition of "early stage" process development, no definitive or reliable data were available for this study.

This requires the application of the methodological approach theorized by Noorman et al.³⁷, using some recently developed concepts from the field of Process Systems Engineering (PSE). PSE offers in fact a pool of mathematical tools able to deal with the uncertainty of preliminary data and the necessity to provide accurate estimates at the same time.

Focusing on the structure of this thesis, the chapters are organized as follows.

Chapter 2 provides the state of the art of the technologies for the production of alternative (non oil-based) adipic acid. Some general green chemistry criteria are applied to identify the processing routes more likely to be environmentally sustainable, and therefore worth for being further investigated.

In Chapter 3, a realistic and sound conceptual flowsheet for a bio-derived adipic acid process is obtained, using preliminary data and with scarce benchmark examples. This is achieved by applying the systematic PSE methodology for processing route synthesis and analysis available in the software pack ICAS, used thanks to the collaboration with Professor Gani of DTU (Denmark Technical University, Copenhagen).

Chapter 4 presents a methodology for first principle modelling of complex and non-standardized bioprocess unit operations, applying fuzzy logic algorithms to study the uncertainty on the model parameters. A case study on broth clarification cross-flow membranes was analyzed, in collaboration with prof. Manenti's sustainable process engineering research group (Politecnico di Milano).

Chapter 5 presents a kinetic study to obtain the model of a key catalytic reaction to achieve adipic acid from the selected route. The study is based on unedited data, experimentally measured for this purpose. This last activity was carried out in collaboration with the laboratories of Industrial Chemistry of Università degli Studi di Milano, with the support of dott. Sofia Capelli.

The chapters are provided of independent introduction and references, as they can be seen as distinct researches on different aspects of the same feasibility study. The general conclusions (chapter 6) will finally recall the main achievements of three years of investigation, presenting the future developments expected from a study that, for its inner constitution, is aimed at paving the way for future research.

1.5 - References chapter 1

1. Schreurs, M. A.; Tiberghien, Y. *Glob. Environ. Polit.* **2007**, 7 (4), 19.
2. European Parliament. Decision No 1386/2013/EU- 7th Environment Action Programme <http://data.europa.eu/eli/dec/2013/1386/oj> (accessed Oct 23, 2017).
3. *Air, Climate, and Energy: Strategic Research Action Plan 2016-2019*; **2015**.
4. IPCC, *Climate change 2014: mitigation of climate change*; Cambridge University Press, 2015; Vol. 3.
5. Gamper-Rabindran, S.; Finger, S. R. *J. Regul. Econ.* **2013**, 43 (1), 1.
6. Harnick, P. *The Future of the European chemical industry*; KPMG press, **2010**.
7. Fung, P. *China's Chemical Industry: The new forces driving change*; KPMG press, **2011**.
8. Kumberger, O. In *The Chemical and Pharmaceutical Industry in China*; Springer, 2005; pp 171–179.
9. Philp, J. C.; Ritchie, R. J.; Guy, K. *Trends Biotechnol.* **2013**, 31 (2), 65.
10. Khoo, H. H.; Tan, R. B. H.; Chng, K. W. L. *Int. J. Life Cycle Assess.* **2010**, 15 (3), 284.
11. Anastas, P. T.; Warner, J. C. *Green Chemistry: Theory and Practice*; Oxford University Press, **2000**.
12. Philp, J. C.; Ritchie, R. J.; Allan, J. E. M. *Trends Biotechnol.* **2013**, 31 (4), 219.
13. Cherubini, F. *Energy Convers. Manag.* **2010**, 51 (7), 1412.
14. Kamm, B.; Gruber, P. R.; Kamm, M. *Biorefineries - industrial processes and products: status quo and future directions*; Wiley-VCH, **2006**.
15. Carus, M.; Dammer, L. *Ind. Biotechnol.* **2013**, 9 (4), 1.
16. Tomei, J.; Helliwell, R. *Land use policy* **2016**, 56, 320.
17. Reisch, M. *Chem. Eng. News* **2016**, 94 (37).
18. Perlack, R. D.; Wright, L. L.; Turhollow, A. F.; Graham, R. L.; Stokes, B. J.; Erbach, D. C. *Biomass as feedstock for a bioenergy and bioproducts industry: the technical feasibility of a billion-ton annual supply*; Oak Ridge National Lab TN, **2005**.
19. Vennestrøm, P. N. R.; Osmundsen, C. M.; Christensen, C. H.; Taarning, E. *Angew. Chemie - Int. Ed.* **2011**, 50 (45), 10502.

20. Naik, S. N.; Goud, V. V.; Rout, P. K.; Dalai, A. K. *Renew. Sustain. Energy Rev.* **2010**, *14* (2), 578.
21. Holladay, J. E.; White, J. F.; Bozell, J. J.; Johnson, D. *Top Value Added Chemicals from Biomass-Volume II, Results of Screening for Potential Candidates from Biorefinery Lignin*; Pacific Northwest National Lab.(PNNL)-National Renewable Energy Laboratory (NREL) **2007**.
22. Werpy, T.; Petersen, G.; Aden, A.; Bozell, J.; Holladay, J.; White, J.; Manheim, A.; Eliot, D.; Lasure, L.; Jones, S. *Top value added chemicals from biomass. Volume 1- Results of screening for potential candidates from sugars and synthesis gas*; DTIC Document, 2004.
23. <https://www.coherentmarketinsights.com/press-release/global-adipic-acid-market-to-surpass-us-1212-billion-by-2025-buoyed-by-increasing-demand-for-nylon-66-216> (accessed Oct 19, 2017).
24. Bart, J. C. J.; Cavallaro, S. *Ind. Eng. Chem. Res.* **2015**, *54* (1), 1.
25. Lees, F. *Lees' Loss Prevention in the Process Industries: Hazard Identification, Assessment and Control*; Elsevier Science, **2012**.
26. Flixborough disaster <http://www.fire-engine-photos.com/picture/number27628>.
27. Clark, J. H.; Macquarrie, D. J. *Handbook of Green Chemistry and Technology*; Wiley, **2008**.
28. Thiemens, M. H.; Trogler, W. C. *Science* **1991**, *251* (4996), 932.
29. <https://www.icis.com/resources/news/2015/08/24/9916603/us-spot-benzene-under-2-gal-a-6-year-low/> (accessed Oct 19, 2017).
30. Bart, J. C. J.; Cavallaro, S. *Ind. Eng. Chem. Res.* **2015**, *54* (2), 567.
31. <http://www.icis.com/Articles/2011/10/10/9498186/Green-Chemicals-DSM-adds-adipic-acid-to-bio-based-chemicals.html> (accessed Jun 7, 2016).
32. De Guzman <http://www.icis.com/blogs/green-chemicals/2011/11/verdezyne-starts-pilot-plant/> (accessed Jun 7, 2016).
33. De Guzman <http://www.icis.com/blogs/green-chemicals/2010/09/introducing-rennovia/> (accessed Jun 7, 2016).
34. Current oil barrel price <http://www.oil-price.net/> (accessed Oct 21, 2017).
35. De Guzman <http://www.icis.com/blogs/green-chemicals/2011/05/myriant-files-for-ipo/> (accessed Jun 10, 2016).

36. Grotkjær, T. In *Fundamental Bioengineering*; Wiley-VCH Verlag GmbH & Co. KGaA, 2015; pp 499–546.
37. Noorman, H. J.; Heijnen, J. J. *Chem. Eng. Sci.* **2017**, *170*, 677.
38. Woodley, J. M.; Breuer, M.; Mink, D. *Chem. Eng. Res. Des.* **2013**, *91* (10), 2029.
39. Heinzle, E.; Biwer, A. P.; Cooney, C. L. *Development of sustainable bioprocesses: modeling and assessment*; John Wiley & Sons, 2007.
40. Doran, G. T. *Manage. Rev.* **1981**, *70* (11), 35

Chapter 2

Green adipic acid: state of the art

In this chapter, the first stage of process innovation is tackled, i.e. the identification of the most promising processing routes with respect to the alternatives available in literature. The purpose is to skim those alternatives worth of further study, employing some simple thus objective criteria. Paragraph 2.1 addresses in general the green routes for adipic acid investigated so far, identifying the best feedstocks on the basis of environmental sustainability and likelihood of a profit. Paragraph 2.2 focuses in detail on the (bio)chemical conversion routes of the best feedstock to adipic acid, analyzing the technology maturity. Once identified the route(s) with the highest industrialization potential, in Paragraph 2.3 the challenges of performing a detailed techno-economic assessment are analyzed. Paragraph 2.4 contains some conclusive comments and introduces the topics of the subsequent chapters.

2.1 - Renewable feedstocks, a green chemistry definition

In more than 30 years of research, several alternative processes for adipic acid production have been suggested, communed by the purpose of achieving a greener process. Figure 2.1 summarizes the main routes, derived from the indications contained in literature.¹⁻⁴

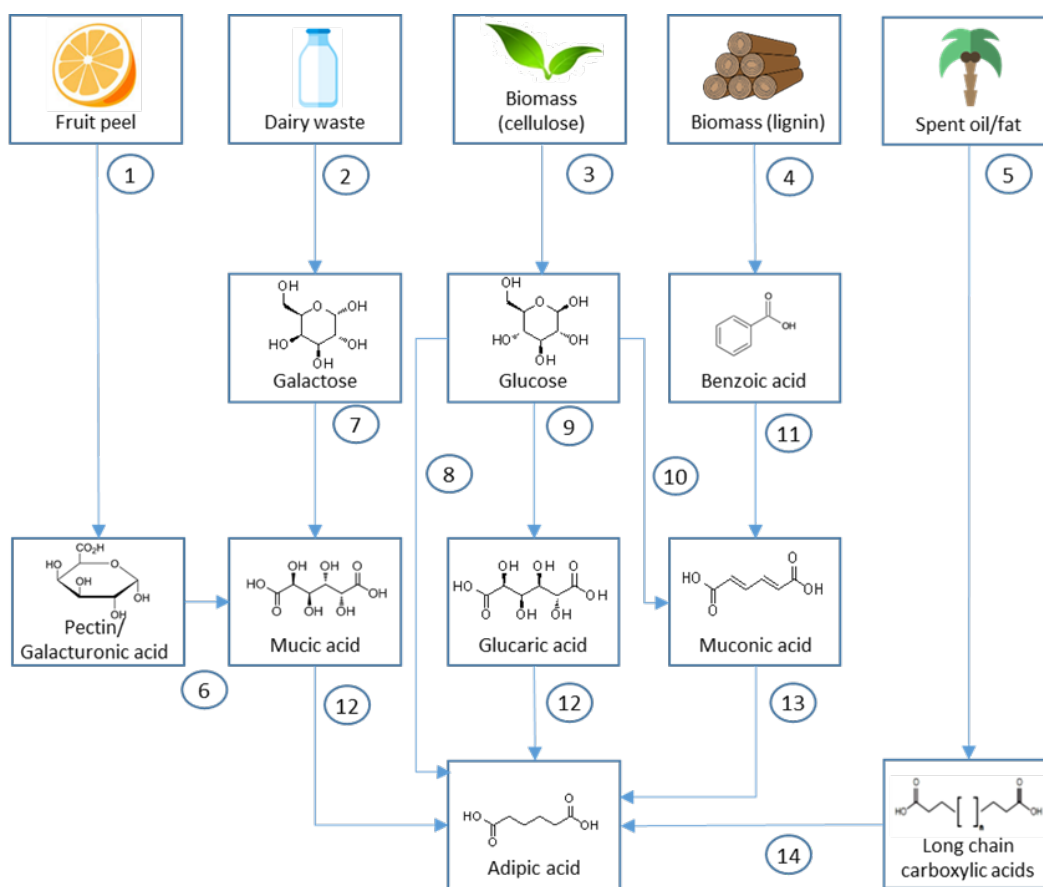


Figure 2.1 - Overview of alternative routes proposed for the production of adipic acid from renewables

In Table 2.1, a list of the main references is provided for each of the transformation steps presented in Figure 2.1.

Table 2.1 - List of fundamental references for each of the routes for renewable adipic acid. Symbols: BIO (biocatalytic approach), CHEM (chemical approach), HYB (hybrid chemical-biochemical approach).

Nr	Description	References
1	Process to extract pectin and hydrolyze it to galacturonic acid from citrus peel.	HYB ⁵
2	Recovery of galactose from serum.	BIO ⁶
3	Production of glucose from cellulose.	HYB ⁷
4	Production of benzoic acid from lignin.	HYB ⁸
5	Conversion of long chain acids into shorter dicarboxylic acids.	BIO Verdezyn ⁹
6	Pectin hydrolysis to galacturonic acid and oxidation to mucic acid.	HYB ¹⁰ ; BIO ¹¹ ; CHEM ¹²
7	Chemical conversion from galactose to mucic acid.	CHEM ¹²⁻¹⁴
8	Biocatalytic conversion of glucose to adipic acid.	BIO Genomatica ^{15,16} ; Bioamber ¹⁷
9	Chemical conversion from glucose to glucaric acid.	BIO ^{18,19} CHEM ¹²
10	Biocatalytic conversion of glucose to muconic acid.	BIO ^{3,20-22}
11	Biocatalytic conversion of benzoate to muconic acid.	BIO ²³
12	Hydrodeoxygenation of aldaric acid to adipic acid.	CHEM ²⁴ ; Rennovia ^{25,26}
13	Hydrogenation of muconic acid isomers to adipic acid.	CHEM ²⁷⁻²⁹
14	Conversion of dicarboxylic acids into adipic acid.	HYB Verdezyn ³⁰

For the establishment of a new process, it is of primary importance to guarantee a stable supply of raw materials, with a price that should be compatible with a source of profit. In addition to these aspects, the the new adipic acid process requires that the feedstock can be classified as “renewable”, or even better as “sustainable”. Renewability of organic compounds is related to the generation of CO₂. If the source does not contain fossil carbon,

then it does not introduce new CO₂ in the environment, which means that the source of materials is able to renovate itself (as crop-derived biomass). Sustainability extends the concept of renewable to the idea that the feedstock production should not affect the society or the environment, i.e. should be mainly of waste origin. This locates the renewable adipic acid development in the field of 2nd generation bio-refining applications, as the overlap with food production should be avoided. Also, for a sustainable process the involved transformations should comply with the “green chemistry” requirements, introduced in Chapter 1. As a support for assessing the “green potential” of a possible production route at the early stage of process development, some easy-to-calculate green metrics were applied, to assess from the very beginning the green potential of the alternative routes Figure 2.1.

The following indexes were considered:

A) *Environmental impact factor*

$$E_{MW} = \frac{\sum MW_{byproducts}}{\sum MW_{products}} \quad \text{Eq. 2.1}$$

where MW stands for molecular weight.

B) *Atom Economy*

$$AE_{MW} = \frac{1}{1 + E_{MW}} \quad \text{Eq. 2.2}$$

which gives a first insight on the use of the reactants. If the reaction itself has an AE value lower than 62%, it cannot be considered particularly brilliant.

C) *Effective Mass Yield*

Similar to the Environmental impact factor, the Effective Mass Yield is defined in terms of mass as

$$E_m = \frac{\sum Mass_{waste}}{Mass_{products}} \quad \text{Eq. 2.3}$$

D) *Reaction Mass Efficiency*

$$RME = \frac{1}{1 + E_m} \quad \text{Eq. 2.4}$$

These metrics apply to single reactions, while to assess chain of transformations, the Total Reaction Yield and the Total Recovery Yield can provide a quick insight on the overall process efficiency. The following points summarize the main transformations necessary to convert different sustainable feedstocks into the actual raw materials to achieve adipic acid.

2.1.1 - Citrus Peel Waste

The renewable feedstock “fruit peel” is distinguished from the more generic term “biomass” (see Paragraph 2.2.3) as it has a different average composition and it can be found in concentrated sources (i.e. not distributed in large territories). In fact, it is a side product of the food industry, a great advantage for the establishment of the supply chain. The so-called “Citrus Processing Waste (CPW)”, the residual of processed lemon and orange fruits, is the main source of pectin (arrow 1 in Figure 2.1), which can be hydrolyzed into its main building block, galacturonic acid, which in turn is oxidized to provide mucic acid (arrow 6 in Figure 2.1), a precursor of adipic acid. The volume of CPW generated only by orange juice industry is around 10 Mton/year, corresponding to a potential of 500 ktons/year of pectin, which is about 12 times its current annual demand for food applications.³¹ Since it is a natural compound, pectin availability can vary in different natural products (e.g. orange peel, lemon peel, apple, pumpkin, etc.) considering also regional and yearly quality.³² An amount of 247 mg/g dry matter of pectic material was recently reported by Müller-Maatsch et al.³² for orange peel, which actually depends on the extraction methods (values from 154 to 204 mg/g were measured before). Pectin is a complex polysaccharide with a linear chain of galacturonic acid units joined by 1 α →4 linkage with molecular weight about 110,000-150,000.³³ In native pectin one free galacturonic acid unit is followed by 5 methyl esters of galacturonic acid, with a degree of esterification (DE) of 83.3%. Branching is present in some regions of the polymer (“hairy regions”) by linear or branched chains of C5 and C6 sugars units, i.e. xylose, rhamnose, galactose, arabinose. Figure 2.2 provides a schematic depiction of the structure and composition of orange peel pectin.

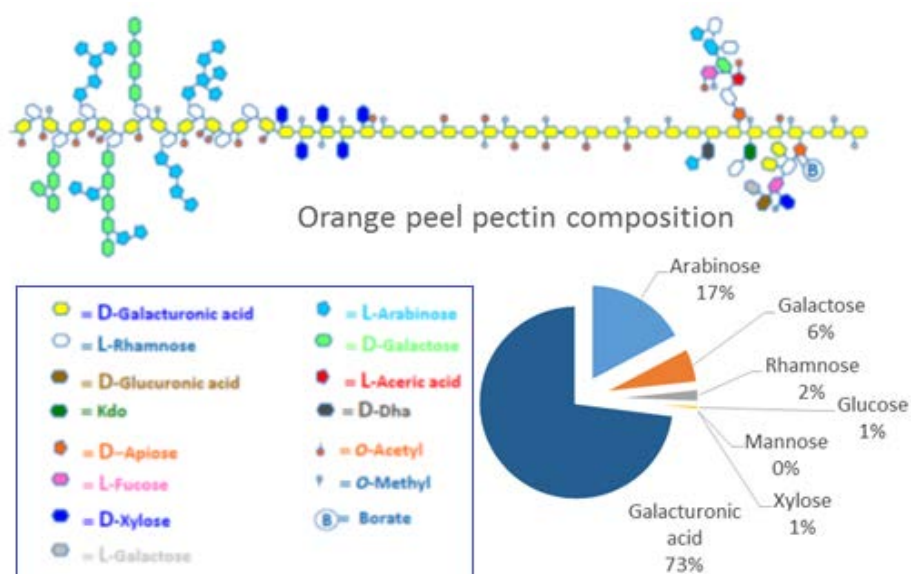


Figure 2.2 – Pectin schematic structure and composition, CP-Kelco® informative material.

DE can be controlled during extraction processing, to obtain low ester (low methoxyl- LM) pectin ($DE < 50\%$) or high ester (high methoxyl - HM) pectin ($DE > 50\%$).³⁴

Limiting the study to citrus peel, which is also the primary source of high quality pectin material with low esterification, it is interesting to consider the transformation chain necessary to achieve mucic acid via separation of galacturonic acid, to achieve the actual raw material for adipic acid. Wet citrus peel, as provided by fruit juice industries, is an inexpensive side product. If not burnt or digested to produce biogas (processes characterized by high inefficiency), the CPW is dried and shipped to different processing sites.^{35,36} Mostly, CPW undergoes to a dehydration process to produce animal feed. The structure of pectin causes it to absorb and hold great amounts of water, which reduce the time-stability of the CPW, enhancing fungal degradation. Hence, a washing with calcium hydroxide promotes the de-methylation of pectin by methylesterase enzymes (naturally present on peels), promoting the coagulation of the chains through interaction with the free calcium ions.³⁷ This structural change causes the release of the internal juices and allows a more efficient mechanical dehydration and pelletization. This quite simple treatment determines a cost of animal-feed citrus peel between 100-220 \$/ton.³⁸ Unfortunately the pectin chains are significantly decomposed, and the final product has no other application

but animal feed. A smaller amount of citrus peel is treated to be sent to pectin recovery facilities, often far from citrus process industries. The process of dehydration becomes more cumbersome as $\text{Ca}(\text{OH})_2$ cannot be used, to avoid lower quality pectins. After milling, the raw citrus peel slurry is washed with counter current water to remove soluble sugars (3 kg water for kg peel), and then the paste is pressed: since the peel ability to hold water is preserved, the efficiency of the screws is reduced of the 50%, with higher costs.³⁹ Then, the slurry is carefully dried at low temperature: the final powder is stable and can be shipped to the pectin extraction facilities, often far from the orange manufacturing plants. The whole process of citrus peel conversion results in a cost of 300-2400 \$/ton.³⁹ To obtain a pure pectin, after the rehydration of the peels, it is necessary to hydrolyze the bonds between galacturonic acid and cellulose. The traditional process requires the heating of the peel aqueous suspension for 30 minutes to several hours with the addition of hydrochloric acid (or other mineral acids) at pH lower than 3. After cooking, the insoluble pulps are removed by vacuum filtration.^{34,40} In the successive transformation, the liquid acidic solution is concentrated, and part of the mineral acid is recovered. The solubilized pectin is then precipitated in alcohol (preferably isopropyl alcohol or ethanol); the precipitate is counter-current washed with different grade alcohol-water solutions, filtered, milled and air-dried.

This traditional process presents several drawbacks: the process requires high dilution to avoid pectin gelification (less than 1%w), it needs expensive acid-proof equipment, requires higher safety and environmental standards for the presence of strong acids. Also it has high cost of distillation for the alcohol recovery, and finally pectin itself could be partially degraded. The general yields are about 20% dry weight of extracted pectin on raw citrus peel (81% of pectin recovery).

Today, thanks to the availability of highly specialized enzymatic formulations, mineral acid can be finally abandoned for low-temperature green enzyme processes, as reported in a recent patent of Cargill, leader producer of pectin.⁴¹ Except for the acidic extraction, the rest of the process remains almost unaltered, introducing simply a pretreatment to inhibit other competing enzymes, naturally occurring in citrus peel. This treatment though is done also for the lower temperature acid extractions: pectin price hence did not change appreciably. For these reasons, the bulk price for commercial pectin ranges from 10,000 to

27,500 \$/ton, according to the final quality.^{39,42} Given these high prices, commercial pectin clearly cannot be taken into consideration for the sake of adipic acid production.

Nonetheless, since only galacturonic acid is needed to obtain mucic acid, there is no use in preserving pectin chain length; moreover, lower purity galacturonic acid can be accepted since the application is not a food-grade product.

Low price galacturonic acid can be achieved applying for example the pectinolytic enzymes required to refine food-grade pectin to the CPW or the feed-grade substrate. Such a process does not exist commercially because the market of galacturonic acid is still at the beginning, but several studies in this direction have already been performed.

An indication on the yield of galacturonic acid in a process to produce mucic acid comes from a recent publication, where detailed kinetics of pectin hydrolysis by commercial enzymes are provided.¹⁰ A yield of 63% of hydrolysed galacturonic acid is reported⁴³, in line with the saccharification yields mentioned in literature: 70% from CPW-orange⁴⁴, 63.8% from CPW grapefruit⁴⁵, 78.7% from CPW with *Apostichopus japonicus* crude enzyme.⁴⁶ Considering a content of 15.12% dw of galacturonic acid in the pectin, the 63.8% yield and the previous indication of the mass yield of pectin, it is possible to calculate the mass E-factor as 41.77 kg waste/kg galacturonic acid.¹⁰ For the green metrics estimates, the reference values are taken of 80% for pectin recovery and 20% for mass yield on raw cattle-feed dried citrus peel.

2.1.2 - Dairy waste

Milk whey is a common residue from dairy industry, which often presents sensible costs of disposal. Its average composition is reported in Table 2.2, distinguishing the whey derived from the cheese production and casein production (obtained by acid precipitation of milk).⁴⁷ Galactose is recovered from lactose, a disaccharide constituted by galactose and glucose units (Figure 2.3). Following the stages of Figure 2.1 number 2, 7, and 9 it is possible to achieve adipic acid from galactose.

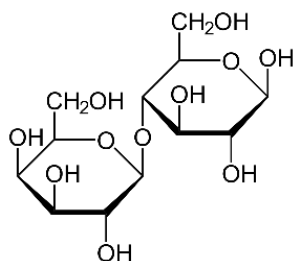


Figure 2.3 – Chemical structure of lactose with on the left galactose and on the right glucose molecules.

The established processes to recover galactose from whey involve a first removal of the protein fraction (by ultrafiltration or acid precipitation), followed by bacterial/enzymatic hydrolysis of lactose, with the subsequent product recovery (multiple crystallization and/or ethanol extraction). The price of lactose powder is about 850 \$/ton (2017), while the original price of liquid whey is lower than 25 \$/ton that indirectly points out the complexity of the required industrial processes.⁴⁸ Since galactose constitutes the 50% by weight of lactose, the price should be at least double (1.7 \$/kg, assuming negligible costs for the hydrolysis and purification). This price for a feedstock is already too high to have a feasible adipic acid process. However, an estimate on the green metrics was performed on the data of a recent patent, which claims a simpler and cheaper process to obtain galactose from whey and serum.⁶

This new process requires a neutral fermentation of milk or milk whey at 37-45 °C (pasteurized but not containing bactericides or bacteriostats) by means of non-modified microorganisms (family of *Lactobacillaceae*, such as *L. bulgaricus*, *L. casei*, and *Streptococcus thermophilus*). Keeping the pH lower than 7.5 the bacteria hydrolyze lactose, consuming preferentially glucose for their metabolism in 16-24 h and therefore leaving the galactose in suspension. A downstream process allows recovering a high purity galactose through the following steps: cell removal, ultra/nanofiltration, electro dialysis and cationic/anionic resin ion-exchange, concentration (and possibly crystallization). The final conversion is 96%, for a 3.5%w lactose starting solution, with a total yield on galactose of 79.5%.

Table 2.2 - Composition of the main sources of lactose in the dairy industry.

	Cheese Whey	Acid Casein Whey
Constituent	%	%
Total solids	6.0	6.4
Water	94	93.6
Fat	0.05	0.05
True protein	0.60	0.60
NPN (non-protein nitrogen)	0.20	0.20
Lactose	4.5	4.6
Ash (minerals)	0.5	0.8
Calcium	0.035	0.12
Phosphorus	0.040	0.065
Sodium	0.045	0.050
Potassium	0.14	0.16
Chloride	0.09	0.11
Lactic acid	0.05	0.05

The molecular weight of lactose is 342, the one of galactose is 180 as for glucose. E_{mw} factor is therefore 1, and the atom economy 0.5. The effective mass yield, considering 1.34 g of galactose per 100 g of solution (water and biomass wasted) can be estimated to have a value of 75 with a reaction mass efficiency of 0.013. These latter values could be improved assuming a closed cycle for the reaction media and a recycle of biomass.

2.1.3 - Biomass, cellulosic fraction.

The term “biomass” comprises, as defined in Directive 2009/28/EC, “the biodegradable fraction of products, waste and residues from biological origin from agriculture (including vegetal and animal substances), forestry and related industries including fisheries and aquaculture, as well as the biodegradable fraction of industrial and municipal waste”.

It is important to stress that a true reduction of environmental impacts would be attained only considering waste biomass, as further deforestation or agricultural intensification will be possibly more harmful. Hence the definition of “environmentally-compatible potential of biomass”, as “the quantity of primary biomass that is technically available for energy generation, based on the assumption that no additional pressures on biodiversity, soil and water resources are exerted compared to a development without increased bioenergy production”.⁴⁹

General examples of biomass are: trees, arable crops, algae, weeds, agricultural and forest residues, livestock effluents, sewage sludge, manure, food production by-products and the organic fraction of municipal solid waste. However, the cited categories do not help much to classify the great number of different feedstocks involved. Variability is an inner characteristic of biomass, and can be described by three main aspects:⁵⁰

1. Waste diversity: biomass comprises different materials that must be treated with specific processes.
2. Local context: geographic and climatic aspects affect the type and the amount of biomass available in each area of interest.
3. Seasonality: especially when dealing with agricultural sub-products, technology should be flexible enough to overcome sensible variation of the biomass quality and availability.

It is possible to simplify the problem of variability, classifying waste-biomass feedstocks into three main families.⁵¹ a) Lignocellulosic feedstocks (agricultural residues, wooden residues, packaging, paper processing residues); b) Plant oils and animal fats (typically by-products of food industry); c) Miscellaneous feedstocks (comprising manure, sewage sludge, etc.). The costs per dry ton vary sensibly according to the location and the nature of the biomass: for example, a rough estimate for forestry residues is between 20 to 70 \$/ton.⁵²

Waste lignocellulosic materials are playing the major role in the strategies of biorefinery development: it is the most abundant feedstock (in the order of 10^{11} ton/year worldwide), and it is highly suitable for chemicals and fuel production.^{49,53,54}

In spite of the variety of natural ligno-cellulosic biomass sources (straw, wooden residues, grass...), three main constituents are always present in higher amount: cellulose, hemicellulose and lignin.⁵⁵ The relative abundance of these components in lignocellulosic substrates are summarized in Figure 2.4,⁵⁰ and, according to their amount in vegetable species, it is possible to classify hardwoods (richer in cellulose), softwoods (richer in lignin) and grasses (richer in hemicellulose).⁵⁵

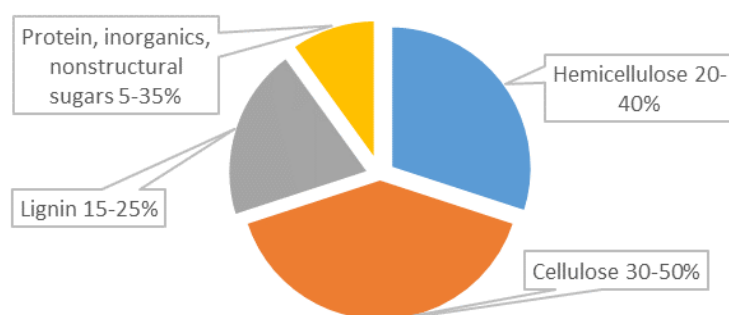


Figure 2.4 – General composition of lignocellulosic biomass, adapted from ref. 50.

Cellulose is a linear highly crystalline polysaccharide made of glucose units linked in $1\beta\rightarrow4$ mode. This polymer is the most abundant source of carbon available in the biosphere.⁵⁶ Hemicelluloses are the co-polymerization products of C5 and C6 sugars, linked in long and branched chains.⁵⁷ They are all amorphous polymers.

Finally, lignin is a complex network of C3-phenols, an insoluble amorphous polymer that covers and protects cellulose and hemicellulose, resulting in the tertiary structure showed schematically in Figure 2.5.⁵⁸

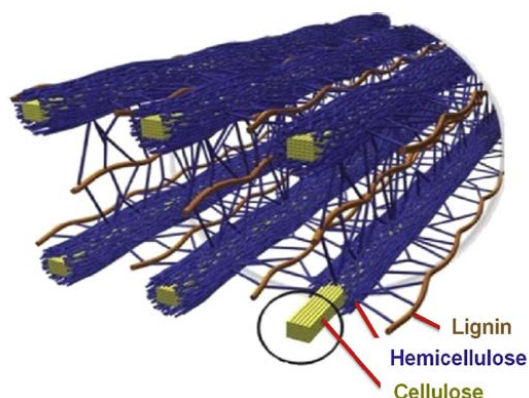


Figure 2.5 – Cellulose crystalline strands surrounded by amorphous hemicellulose and lignin, adapted from ref.58.

Lignocellulosic biomass can be defined as a “natural composite-material”: the disruption of this structure is the first stage of any biorefinery transformation.⁵⁶ This can be attained with different techniques:⁵⁹

- Biological conversion (bacteria and fungi)
- Chemical conversion (acid or basic hydrolysis, ionic liquids, solvents)
- Physical conversion: (microwaves, sonication, other mechanical transformations)
- Thermochemical conversion (pyrolysis, gasification, liquefaction, combustion).

The last class of processes, due to the extreme conditions of temperature, generally decompose the chemical structure of the three main constituents, allowing to obtain homogeneous classes of products (oil, syn-gas, H₂...) even from very different feedstocks. In this paragraph, the derivation of fermentable glucose is assessed, as a starting point for adipic acid production.

Among the many solutions explored to recover the building blocks from lignocellulosic biomass, one process distinguishes for its flexibility, for the good performance and most important for the low price of the final products, comparable with the cheaper first generation sugars: the Plantrose process of the American company Renmatix. In facts, while there are still no industrial scale plants for 2nd generation sugars production, as all the above mentioned disruption techniques present technical issues that make lignocellulosic material exploitation economically unsustainable, Renmatix is already operating a

demonstrative scale process and plans to start building a full-scale (100-300 kton/year) facility in 2018.⁶⁰ The core technology is a supercritical water hydrolysis of biomass in 2 steps, summarized by the company's flow diagram of Figure 2.6.⁶¹

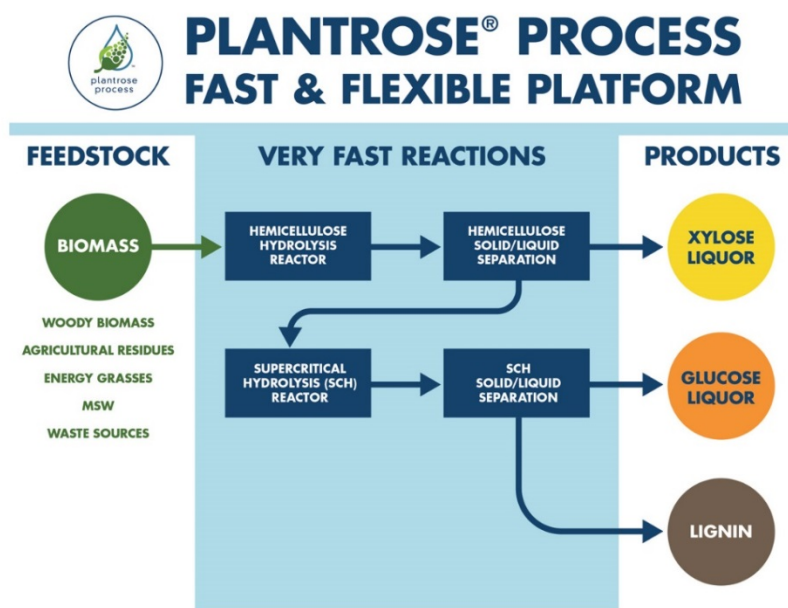


Figure 2.6 – Renmatix process to recover simple fermentable sugars from lignocellulosic biomass, based on supercritical water hydrolysis.

The data disclosed in the reference patent were used to calculate the green chemistry indicators, focusing on the glucose production.⁶¹ On this point the most relevant reaction is the hydrolysis of the glucan chains of cellulose into single glucose molecules, which require one molecule of H₂O for 2 units of glucose. The reaction has no by product, hence the E factor is 0 and AE is 1. The overall yield on glucose is said to be about 40% for softwood (gymnosperm trees as conifers) and hardwood (angiosperm trees as oaks), due to an incomplete conversion of glucan (74% -85%). These performances are expected to be further improved. Under the assumption of water recycle and without considering as a waste the liquid stream of C5 (which is a co-product), the effective mass yield can be estimated in the range of 0.58-0.71 kg waste/ kg product (wastes are the solid residues and galactose traces). The reaction mass efficiency is comprised between 0.58 and 0.63.

2.1.4 - Biomass, lignin fraction

Lignin is the most abundant source of aromatics in nature, counting up to 25% of lignocellulosic biomass weight, but is still an under-exploited source. In fact, some first examples of 2nd generation biorefineries are using biomass to ferment ethanol exploiting only the cellulosic fraction, but lignin is left as a residue and is typically burnt for power generation.⁵⁴ This is due to the inner complexity of lignin and its heterogeneous composition and structure, constituted by three basic building blocks. These can be represented by the three phenol derivatives p-coumaryl, coniferyl, and sinapyl alcohols, whose structure is reported in Figure 2.7.⁶²

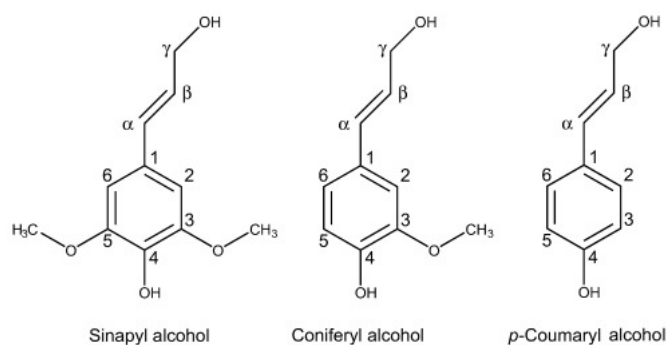


Figure 2.7 – Structure of the three primary monomeric building blocks of the 3D amorphous polymer lignin. Adapted from ref.62.

The current technologies for lignin de-polymerization are:

- Hydrocracking (56-80% yield on alkylated phenols)
- Pyrolysis at 300-600°C
- Fungi decomposition (very slow kinetics, it takes several weeks)
- Acid or Base-catalyzed depolymerization
- Metal catalyzed depolymerization
- Ionic liquid assisted depolymerization
- Supercritical fluids extraction.

Low lignin conversions, low yields for each of the many compounds produced, and high technological costs (temperature and pressure for catalytic processes, reactants for ionic liquids or equipment for supercritical extractions) hinder the establishment of the lignin extraction technology.⁶³

Lignin, once depolymerized can be fractionated to recover value-added compounds (as it is currently done for vanillin or catechol) or can be further treated to obtain de-alkylated mono-aromatics.^{63,64}

The second approach causes strong modifications to the lignin building block structure, as the de-polymerization is accompanied by the hydrogenation/removal of the pending functional groups of the aromatic rings. For example, LtL (lignin to liquid) process gives in one pot alkylated phenols and aliphatic hydrocarbons after heating a mixture of lignin sources and formic acid, with yields from 60 to 95% (based on the phenolic compounds). This process was originally thought to produce fuel additives from renewables.

Hydrocracking processes can yield up to 94% on alkylated phenols, in the form of a so-called lignin bio-oil.⁶⁵ Bio-oil undergoes to a thermal hydro-dealkylation, which yields phenol, benzene, fuel oil and fuel gas. Benzene and phenol are the 34% in weight, and can be further converted to toluene and finally to benzoic acid using the traditional petrochemical technology.⁶⁴

For this series of reactions the E_{MW} factor would be lower than 116 (assuming sinapyl alcohol as starting molecule and assuming the MW of the branching molecules as byproduct). As the entire process does not produce actual wastes (the residues have fuel properties), E_m factor and RME are good. In absence of cost indications for a renewable benzoic acid derived by this route, the reference cost should be the one of commercial benzoic acid, which currently is oil derived, even for food applications.

2.1.5 - Spent oil, fat

The term “fatty acids” considered for the production of adipic acid by Verdezyne, the leader company of this route, comprises a variety of organic acids with long alkyl chain of different origin such as: canola soapstock, FAME (Fatty Acid Methyl Esters), PFAD (Palm Fatty Acid Distillate). These sources are all “renewable” and little expensive, even though

the price is bound to oil fluctuation, as the current application of these feedstocks is mainly in the bio-diesel production. The current price for PFAD is around 600 \$/ton.⁶⁶

The maximum chain length mentioned in the patent literature is C18 (e.g. stearic acid). Genetically engineered microorganisms perform the conversion to adipic acid in more than one step. First, there is the bio-conversion of the mixture of feedstock oils (saturated and unsaturated monoacids, diacids and methyl esters) into linear acids. Then, if unsaturated compounds are present, a metal-catalyzed hydrogenation reaction is applied. Finally the heterogeneous mixture of fatty acids are converted into adipic acid by means of other bio-conversions. The first biochemical step involves the conversion of mixed feed into dicarboxylic acids (exploiting the natural beta-oxidation pathway of microorganism metabolism) has almost quantitative yield, reaching the 99% for sebacic acid from decane and capric acid.⁹ Next step, hydrogenation, again does not present any issue of yield and selectivity. Figure 2.8 summarizes a) the metabolic reactions responsible for the chain reduction to the target adipic acid³⁰ and b) the ω -oxidation metabolic reactions⁹.

Such complex pathways are the actual bottleneck of the technology, which has a maximum theoretical yield of 0.52 g of adipic acid per gram of stearic acid. This performance, not particularly good, is said to be under improvement.³⁰ Considering stearic acid as starting point (MW 284), the E_{mw} factor is 0.94, leading to an atom economy of 0.51. With the little amount of data disclosed by the patent is impossible to estimate the actual amount of waste generated by the process. Also, this technology is yet to be fully developed and industrialized.

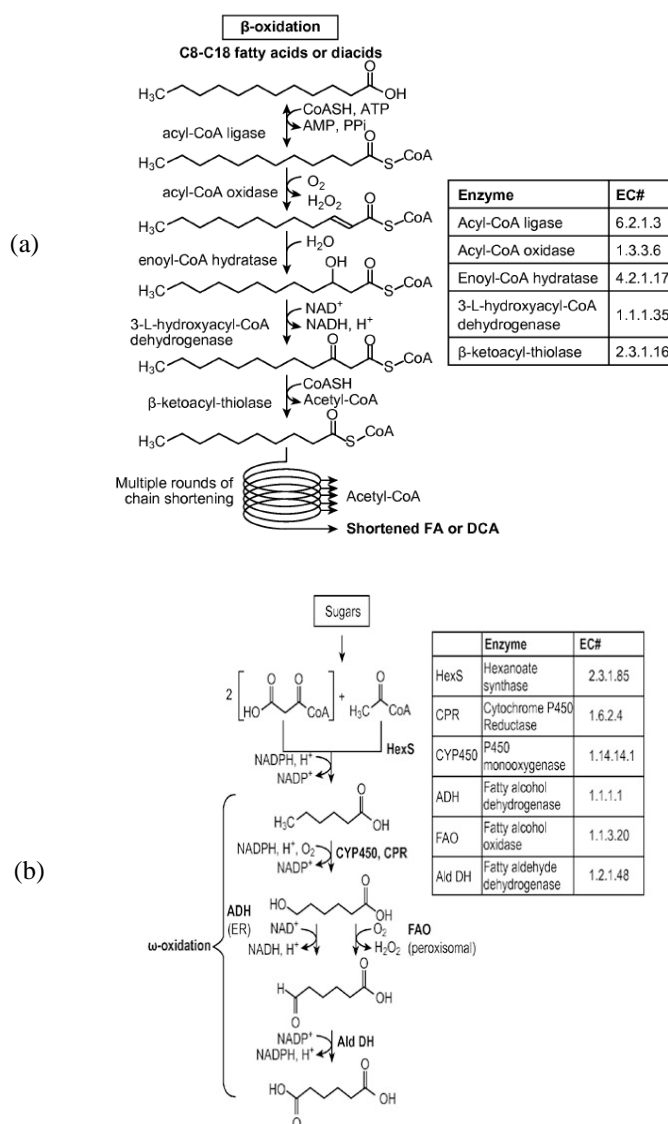


Figure 2.8 – Metabolic pathways of a) the chain reduction of fatty acids and b) ω -oxidation by a *Verdezyne* genetically modified microorganism.³⁰

2.1.6 - Best feedstocks selection

Provided this overview of the potential sources of the building blocks to achieve adipic acid, it is possible to select the ones most likely to become candidates to sustain the new production of adipic acid.

Table 2.3 summarizes the green metrics calculated on the base of these very first preliminary considerations and the associated cost estimates.

When performing preliminary feasibility studies on topics under research and development, the availability of a full-scale operating technology is a positive feature, but it's not determinant, as long as there are scientific evidences of the viability of the process. The aim of these evaluations is in fact the support of decisions on the strategy of ongoing R&D, which will eventually perform the detailed scale-up activity.

Hence, it is possible to see that the "greenest" feedstock is certainly the 2nd generation glucose, which has a price low enough to hypothesize a further process to obtain adipic acid, whose price should be of the order of 1.5-2.5 \$/kg. Also CPW, in spite of higher waste production, seems to have good potential to establish a new route for adipic acid: mucic acid is only one step before adipic acid. Therefore, even if the technology is not mature to have already an operating plant, the condition is not far to be reached (similar technologies exist). On the contrary, the process to extract galactose from whey powder is well established, but this latter feedstock is not suitable to produce adipic acid, as the final galactose has a price higher than the bulk chemical. This route is therefore discarded. It was shown that the technology to achieve benzoic acid from lignin seems far to be economically sustainable: since benzoic acid is currently achieved from nonrenewable sources, the cost to recover it from bio-oil is certainly higher than its commercial price of 1.4 \$/kg.⁴² Still, this route will be taken into consideration for the further analysis, in virtue of the high level of sustainability of waste lignin (virtually no by-products, as for an ideal refinery).

Also, the bacteria responsible for the conversion of benzoic acid to adipic can actually convert heterogeneous mixtures of both benzoic acid derivatives and phenol as shown in Figure 2.9: this could eventually enhance the economy of the route.²³ For this reason many research group in the world are keeping developing the benzoic acid route, even without a secure feedstock source.

Table 2.3 - Summary of the green metrics and cost estimates for the considered feedstocks

Route	Y	E _{mw}	AE	EM	RME	Techno-logy	Raw Mat. Price	Price int.
	g _{prod} /g _{feed}	-	-	g waste/g _{prod}	-	-	\$/kg	\$/kg
Dry CPW to mucic acid	0.12	na	na	10-40	0.02-0.09	Yes*	>0.2	1.6
Whey to galactose	0.3	1	0.5	74	0.013	Yes	0.025	1.8-5
Cellulose to glucose	0.4	0	1	0.58-0.71	0.58-0.63	Yes*	0.03-0.07	0.4
Lignin to benzoic acid	<0.32	1.23	0.45	0	1	No	0.03-0.07	na
Fatty acids to adipic acid	0.51	0.94	0.51	na	na	No	0.6	>1.2

* The technology exists but is not applied for this specific route. A new process should be developed on purpose. na =not available

The use of fatty acids as an adipic acid feedstock, in spite of acceptable green indicators and reasonably good cost forecasts, will not be considered further, due to supply-chain criticalities. The availability of “waste FAME/fatty acids” is in fact too low for supporting the rise of a new bulk production as the one of adipic acid. For example, the yellow grease production (spent oils suitable for the bio-based treatment) is only 900 kton/year in the whole US territory.⁶⁷ The use for adipic acid would enter in fierce competition for the biodiesel production. To support a hypothetical green adipic acid plant, it would be necessary to integrate the feedstock with the use of oleaginous crops harvested specifically to produce adipic acid. This strongly reduces the sustainability of the process and also subtracts resources to the food market. Such a route would be “renewable”, but certainly may be less acceptable as “green and sustainable”.

The following evaluations will therefore assume the availability of glucose/benzoic acid from biomass and mucic acid from PWC, to assess the subsequent steps to achieve adipic acid.

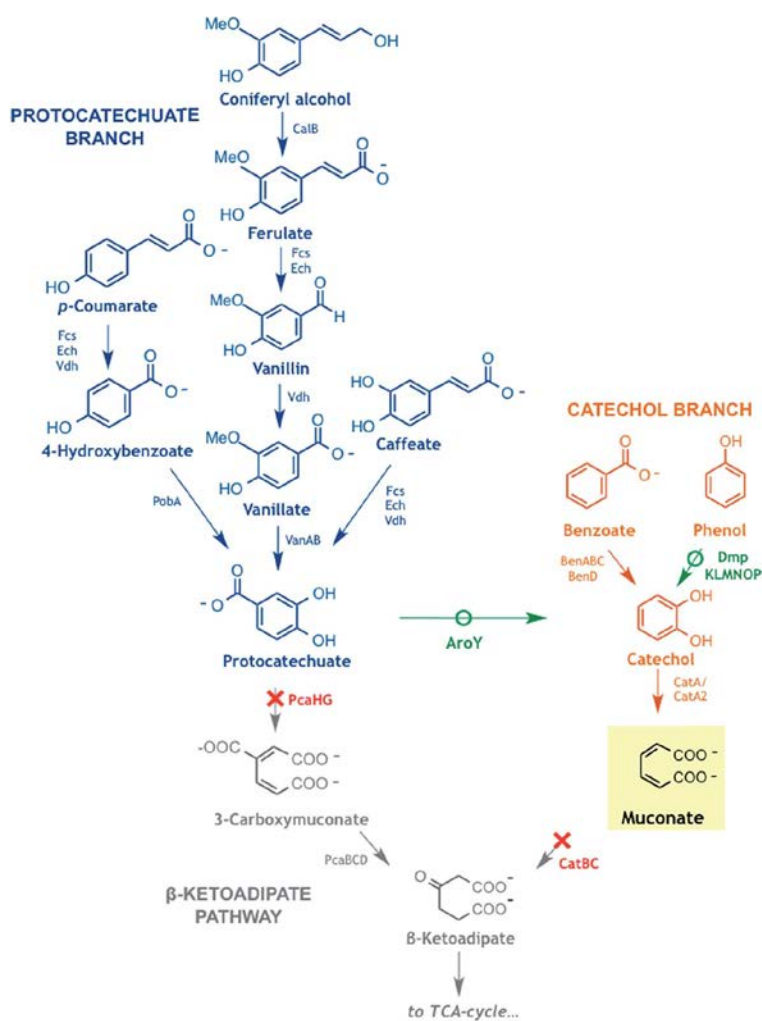


Figure 2.9 – Metabolic pathways to muconic acid (adipic acid precursor, adapted from ref.23). Both phenol and benzoic acid can be processed.

2.2 - Analysis of the routes to adipic acid

Assuming the availability of renewable glucose, benzoic acid, galactose and galacturonic acid, the subsequent conversion steps differ, according to the nature of the employed catalysts. Referring to Figure 2.1, the arrows number 6, 7, 9, and 12 correspond to chemocatalytic conversions, which will be addressed in paragraphs 2.2.1 and 2.2.2. Numbers 8, 10, 11, and 13 involve instead some bio-catalytic reactions, characterized by different mechanisms: they will be described in paragraph 2.2.3.

2.2.1 - Rivertop nitric acid oxidation of C6 sugars

The process involves as a first stage an oxidation reaction to convert the sugars (glucose, galactose, etc.) into the corresponding dicarboxylic aldaric acid, either galactaric acid (from galactose or galacturonic acid) or glucaric acid (from glucose), followed by their hydrodeoxygenation to adipic acid.²⁴⁻²⁶

The oxidation has been thoroughly studied for glucose by the research group of prof. Kiely of the University of Montana (US), who eventually patented and realized a full scale facility, within his own company Rivertop Inc. So far, this is the most advanced example of this kind of oxidation, which is suitable without substantial changes also for galactose and its derivatives, according to the patent literature. The green metrics and preliminary economic estimates are therefore calculated for the Rivertop process. Then, the last reaction of hydrodeoxygenation is assessed according to the patents of another company, Rennovia, and is described in the next paragraph.

The reason why the process for the oxidation of glucose to glucaric acid has been already developed is the existence of market for this specialty chemical. The applications of glucaric acid has space in very different fields. Glucaric acid can be used either for the synthesis or the formulation of pharmaceutical products (e.g. anticancer ingredients), as it is a normal human metabolite. Also, thanks to its chelating properties, can be used for the formulation of cosmetics, in particular for anti-age skin lotions.^{68,69} In industry, it becomes important both as an additive or building-block. Several applications for bio-polymers or hydroxyl-polyamides production are reported in literature, together with interesting uses as

builder for bio-degradable surfactant production.⁷⁰ Glucaric acid is used also as an additive for road de-icing salt as corrosion scavenger, or for dish-washer soap to reduce water hardness.^{71,72}

Glucaric acid, known also as saccharic acid, is an aldose α,ω -dicarboxylic acid having the molecular structure reported in Figure 2.10 (left). Since glucaric acid tends to form δ -lactones, as shown in Figure 2.11, it is difficult to obtain the acid in pure form. For this reason, glucaric acid is commercialized as its salt (mainly potassium glucarate).⁷³

Probably, Rivertop process is the most efficient and optimized nitric acid oxidation of glucose, characterized by a multi-step oxidation that allows fine control temperature and a reduction of the side reactions. A full scale process based on this technology was finally commissioned in the end of 2015.

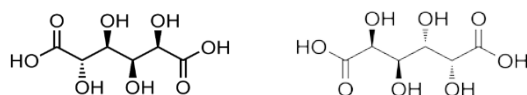


Figure 2.10 – Chemical structure of glucaric acid (left), and its structural isomer galactaric acid (right, also known as mucic acid). The first is optically active, the second not, being a meso form).

Still, it has to be assessed if the process is cheap and sustainable enough to justify the use of the products of the oxidation for the production of a price-constrained product as adipic acid. Focusing on the process disclosed by Rivertop main patents, nitric acid oxidation is only one of the several complex unit operations that glucose undergoes, which together contribute in reducing the environmental performances of the final product.^{12,74}

Neutralization, for example, is a necessary step to exclude the spontaneous lactonization of the acid (Figure 2.11) but requires the consumption of extra chemicals. Figure 2.12 provides an insight of the process shape: no official layouts have been disclosed, and then the one reported derives from the patent interpretation. The main advantage of this process is the higher levels of control of the otherwise little selective oxidation reaction, achieved by the particular reactor shape which:

- Guarantees a better temperature control, thanks to a bi-phase reactor, where the highly exothermic nitrous gas oxidation to nitric acid is performed on the dome of the reactor, provided with an extra cooler.
- Avoids the risk of uncontrolled oxidation, dividing the conversion across more reactors in series.
- Allows the recovery of the nitrous gases.

The main drawback of nitric oxidations of sugar derivatives is the very low selectivity, as consecutive reactions of the products and parallel reaction of the substrate are likely to happen. The conversion on glucose is 100%, while the glucaric acid yield is 45%, which points up the presence of byproducts, not characterized quantitatively in the patent literature. These byproducts are 5-ketogluconic acid, tartaric acid, tartronic acid, oxalic acid; also the quite relevant amount of D-gluconic acid present after the reaction, which is actually an intermediate, can be considered as a by-product since it cannot be recycled. The results of the oxidation of galactose are better, owing the insolubility of mucic acid in the medium, with yields up to 75%.

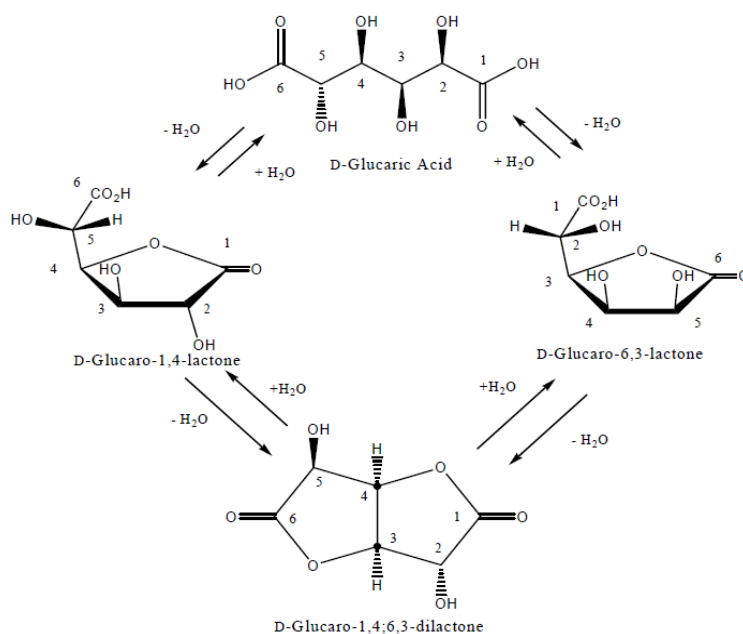


Figure 2.11 – Equilibria between glucaric acid and its lactone derivatives, adapted from ref.73.

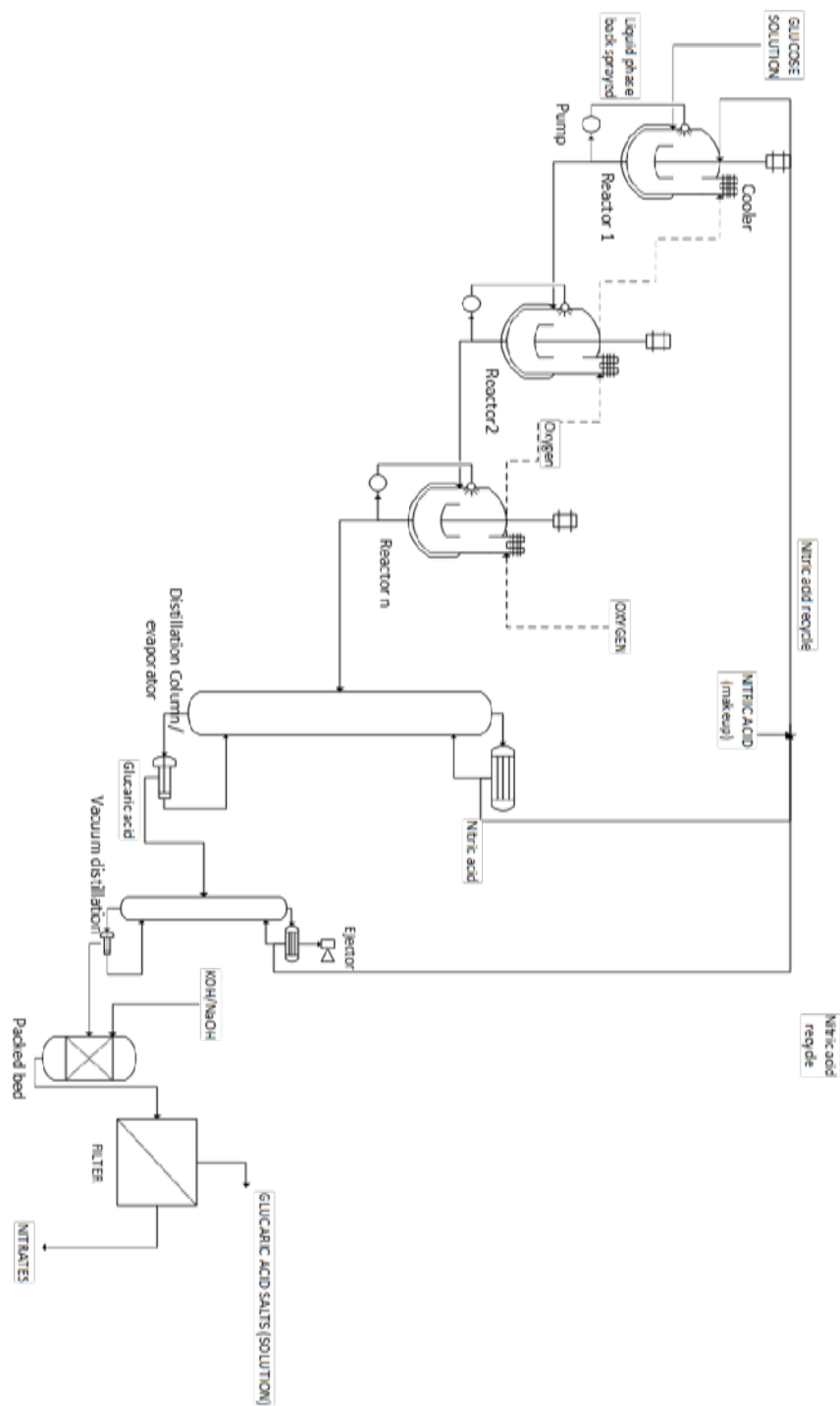


Figure 2.12 – Flowsheet concept base on the Rivertop- DCI facilities.

When assessing the green metrics of the oxidation, it should be noted that the side reactions involved, even if do not alter the balance on glucose (limiting reactant), can increase the stoichiometry of oxygen consumption (in an unknown amount). This aspect results in possibly overestimated green parameters: the actual values should actually be worse than the one reported in Table 2.4.

The workup of the oxidized solution to recover the glucaric acid salts requires a first neutralization of the system residual inorganic and organic acids with KOH, followed by a back acidification (again with nitric acid) until mono potassium glucarate precipitates. Figure 2.13 summarizes the reaction steps involved.

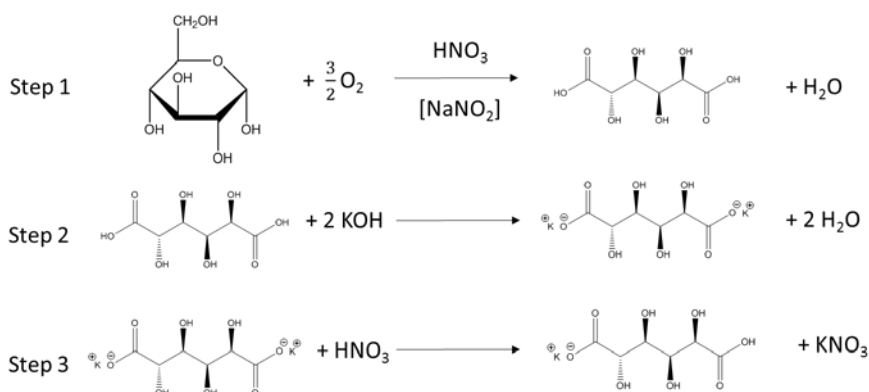


Figure 2.13 – Nitric acid oxidation (step 1) followed by neutralization (step 2) and back acidification (step 3)

Table 2.4 summarizes the green metrics calculated for the three steps, under assumption of complete recovery of catalyst, solvent and byproducts for the first two, as the system is not purified in the intermediate steps. The burden of the reaction wastes are considered in the last step, the acidification, because after product crystallization and separation, the residues have to be disposed and cannot be recycled for another batch, unless they are further treated. It is possible to notice that none of the three reactions is particularly good according to the parameter Atom Efficiency. At the third step, the acidification to recover glucaric acid by differential crystallization, 10 kg of waste are generated per kg of product, giving a reaction mass efficiency far lower than the 0.618 threshold, pointing out the little

sustainability of the overall process. It has to be said that this practice for glucaric acid production is the Best Available Technique: a yield of 45% to glucaric acid more than double with respect to the 20% yield of the traditional oxidation.

These points are already enough to exclude this route, as further transformation would eventually reduce again the environmental performances. The final word comes from the cost-estimates on the so-produced glucaric acid: Rivertop managers stated that their products are sold in the range of 20-30 \$/kg. Such a high price, even though ascribable to the small scale of production and the safe niche of market for glucaric acid applications, points out the difficulties in the purification steps and the little feasibility of the route of glucose oxidation.

Table 2.4 - Main green indicators for the traditional oxidation-recovery steps, on a scale of ca. 150 grams of product as reported in the Rivertop patent examples.

Step	YIELD	E _{mw}	AE	E _M	RME
	mol prod /mol feed	-	-	g waste/ g prod	-
1_OXYD	0.45	0.09	0.920	1.414	0.414
2_BASIF	1	0.126	0.888	0.126	0.888
3_ACID	1	0.406	0.711	9.56	0.095

These considerations hold also for galactose and/or galacturonic acid oxidation. On this latter aspect, the oxidation of galacturonic acid (from de-polimerized pectin) to galactaric acid can be achieved by means of biological transformations or chemo-catalytic. Mojzita et al.⁷⁵ produced for the first time fungal strains able to oxidize galacturonic acid to galactaric. The choice of fungal strains is due to the fact that eukaryotic microorganisms living in decaying plant have several pathways to catabolize pectine and its derivatives, and have the ability to take out D-galacturonate. In the specific case, *Aspergillus Niger* and *Hypocrea jecorina* were first engineered to delete their genes encoding D-galacturonate reductase and to express D-galacturonate dehydrogenase, so that the fungi could not use it as a source of carbon. The study showed how both the strains were very efficient in the

conversion to galactarate, and in particular *H. jecorina* reached the theoretical yield (1.08 grams of galactarate per gram of galacturonate, pH 5.5 in pure D-galacturonate solution). Almost no difficulties were encountered to recover the pure product, due to its low solubility in water, with recovery yields of the 94%.

Another approach identified first a eukaryotic transport protein for D-galacturonic acid in *Nerospora crassa* and then managed to express it in the well-known fermentation host *Saccharomyces cerevisiae*.⁷⁶ After providing to the yeast the genes encoding the pathways to transform D-galacturonate into meso-galactarate, they proved the feasibility of using *S. cerevisiae* to obtain mucic acid, taking advantage of the peculiar resistance to inhibitors and easy industrialization of this microorganism.

A different approach again was patented, in which galactose in aqueous basic solution was oxidized using chlorine gas in presence of a nitroxide catalyst (4-acetamido-2,2,6,6-tetramethylpiperidine-1-oxyl) at 0-5 °C.⁷⁷ This process results in final yield of 75%. Also, ozone can be used as oxidant, to obtain a highly pure crystalline mucic acid without any cost of purification.⁷⁸ Ozone is provided at 20-30°C without any catalyst at a pressure of about 2 bar, and it is produced in situ from liquid oxygen. The starting solution is constituted by galacturonic acid in water (12%) which can be obtained separately through partial oxidation of galactose or better from pectic acids.

All these options still do not compete with nitric acid oxidation costs. Since galactaric acid applications are mostly in the pharmaceutical field, a well-known process as nitric acid oxidation is preferable as long as the products are pure enough, with little care of the final price (30\$/kg is a low price compared to the usual costs of pharmaceutical industry).

2.2.2 - Rennovia hydrodeoxygenation of aldaric acids

A further alternative is the process patented by Rennovia, which addresses the final step of hydrodeoxygenation of glucaric/galactaric acid to adipic by catalytic conversion, and proposes another oxidation reaction to oxidize glucose, without the use of nitric acid. This company, strong of a joint venture with Johnson Matthey for the production of the required catalysts, was among the favorite players in the race toward green adipic acid until 2015. The proprietary process does not present any biocatalytic step, as shown in the block diagram of

Figure 2.14, derived from the analysis of the main related patents.^{25,26}

The reactions present some very good aspects:

- No use of basification-acidification steps, reducing chemicals consumption
- No use of nitric acid for the oxidation, as enriched air is enough
- The hydrodeoxygenation reaches in some cases complete selectivity toward adipic acid (even though 70% was reported in the reference patent example).

However, several drawbacks are visible as well, which probably are the responsible of the delay for the establishment of this technology, together with the unfavorable market conditions. In fact, the two reactions require high pressure (34 bar of oxygen and 56 bar of hydrogen, respectively), the first generates many sub-products and the second is very sensitive to the presence of trace oxygen. The main technological bottleneck is on the separation, because the first step generates many by-products. Simulated moving bed chromatography, suggested for this task, has good performances at laboratory scale, but its scalability must be yet demonstrated. A preliminary calculation of the green metrics of the two reactions shows quite good results: still the waste generation is calculated assuming complete recovery of glucaric/adipic acid in absence of reliable indications on the separation techniques. In reality, EM index could be much higher. With respect to low intensive bio-processes, Rennovia process loses the comparison on sustainability. In fact this process requires massive amounts of halogenidric acid (HBr), organic solvents (acetic acid, green solvent, but less than water) and quite strong process conditions. These aspects and the impossibility to provide further considerations, given the proprietary nature of the key information on the catalysts, forces to suspend the analysis at this point. From an economic point of view, the fact that the process development is still at piloting phase after three years induces to think that the profitability has not been reached yet. The green metrics are reported in Table 2.5.

Table 2.5 - Green metrics on Rennovia process

Step	YIELD	E_{mw}	AE	E_M	RME
	mol prod /mol feed	-	-	g waste/ g prod	-
Glucose- adipic	0.33	0.61	0.62	0.98	0.50

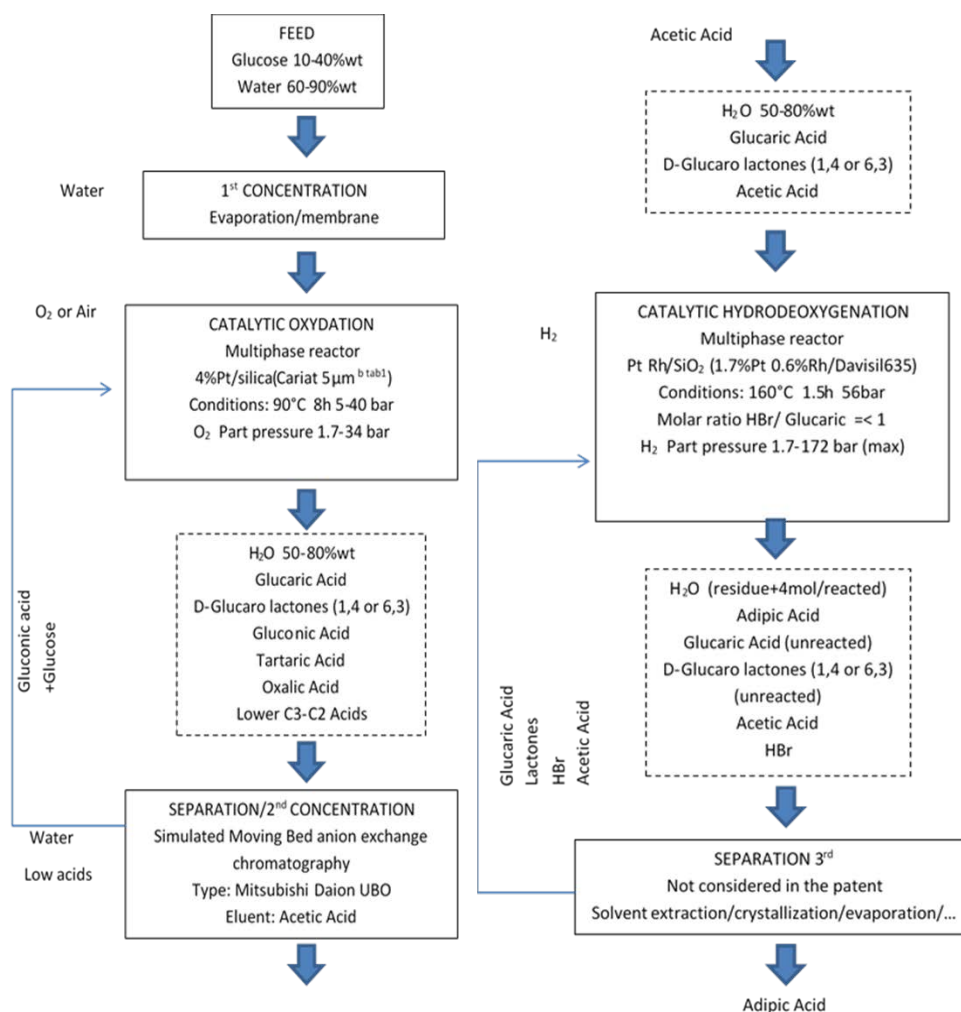


Figure 2.14 – Block flow diagram of the Rennovia process for the production of green adipic acid from glucose.

2.2.3 - The bio-catalytic routes

Since the main bottleneck of chemically oxidative pathways is the selectivity of the reaction and the complexity of the resolution of the product mixtures, most of the last 30 years research focused on bio-catalytic and/or fermentation routes, which have also the advantage of being inherently green and little energy intensive. Table 2.6 is an attempt to summarize the main results achieved so far, starting from literature reviews.¹⁻⁴.

In the specific, the contributions number 1, 2, 3, 4, and 5 can be related directly or indirectly to the activity of Amyris, the American knowledge-based company that acquired the patents of Draths' company and has the most advanced technology for adipic acid production from glucose. This technology is indeed a hybrid biochemical-chemical solution, as the first fermentative step yields muconic acid (Figure 2.15), an intermediate which is purified and then catalytically hydrogenated to adipic acid.

Also the routes 17 and 18 use glucose as starting feedstock, belonging to Genomatica and Bioamber, respectively. However these last solutions seem to present some major challenges when improving the product concentration and the strain stability: this prevented the companies from commercializing the technology. Some of these studies have also performed some preliminary scale-up testing: number 7 produced at 500 L scale, number 5 at 20 L. Nevertheless, the main aspects to consider when comparing the scalability of a bio-based transformation are the reaction yield, the product concentration, and the productivity.⁹² According to these indexes, two strains achieve good performances in all of them: *E. coli* of Amyris²¹ and the *P. putida* of Vardon et al.²³.

Both processes involve schemes that combine biological and chemical conversions. Specifically, a biological process yields a double-unsaturated dicarboxylic acid intermediate, *cis,cis*-muconic acid ((2Z,4Z)-hexa-2,4-dienedioic acid), from glucose in the case of *E.coli* and from benzoic acid in the case of *P. putida*. Muconic acid is then catalytically hydrogenated to adipic acid.² This double step approach has received much attention since it allows more flexibility in the feedstock selection, as both glucose and benzoic acid can be converted, opening to a full exploitation of biomass. In addition, the intermediate can be converted also to other strategic monomers. In fact, *cis,cis*-muconic acid, can be converted to, for example, terephthalic acid for PET production^{21,93} and 3-hexenedioic acid, used in the production of unsaturated polyesters⁹⁴.

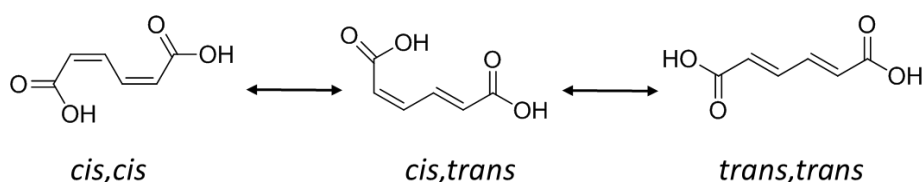


Figure 2.15 – Chemical structure of muconic acid isomers.

Table 2.6 - Overview of the most recent bio-based approaches toward adipic acid

#	Refs	Microorganism	C-source	Yield	C MA [g/L]	Time [h]	Media
1	78	<i>S.cerevisiae</i> BY4741	Glucose	3,86mg/g	0.00014	108	YSC
2	79	<i>E. coli</i> AB2834	Glucose	30%m	3.12	48	M9 pH6.3
3	20	<i>E.coli</i> WN1pWN2.248	Glucose	22%m	36.8	48	M9
4	80	<i>E.coli</i> MYR428	Glucose	-	16	48	M9
5	21	<i>E.coli</i> WN1pWN2.248	Glucose	30,4%m	59.22	88	M9 pH6,8
6	81	<i>E. coli</i> BL21 (DE3)/pEcatA	Cathecol	100%m	59	12	--
7	82	<i>Arthrobacter</i> sp. T8626	Na benzoate	96%m	44.1	256	J pH 7,0
8	83	<i>Arthrobacter</i> sp. T8626	Na benzoate	91%m	4.5	72	pH 7
9	84	<i>Spyngobacterium</i> spM4115	Na benzoate	28%m	0.56	28	SBY3(1-3)
10	85	<i>P. putida</i> KT2440	Na benzoate	89%m	0.16	18	E2 MM pH7
11	23,29	<i>P. putida</i> KT2440	Na benzoate	93%m	34.5	124	pH 7,0
12	86	<i>P. putida</i> sp 1167	Na benzoate	61%m	7.2	12	Given pH 7.2
13	87	<i>C.pseudodiptheriticus</i> M2128	Na benzoate	47%m	3.05	96	? 45deg pH7
14	88	<i>Pseudomonas</i> sp B13	Na benzoate	90%m	7.4	14	Mineral, pH7.2
15	89	<i>P. putida</i> BM014	Na benzoate glucose	100%m	32.4	40	Mineral given NO3
16	90	<i>Pseudomonas</i> sp DCB-71	Toluene, Na ₂ acetate	>90%m	45	96	NO Low phosphate
17	91	<i>E. coli</i> ?	Glucose	64%	0.75	100?	M9
18	17	?	Glucose	<41%	5	59	

Glucose pathway (pentose cycle)

The synthetic pathway expressed in the genetically engineered strain *E. coli* WN1pWN2.248 has been thoroughly investigated and disclosed, as shown in Figure 2.16.²⁰

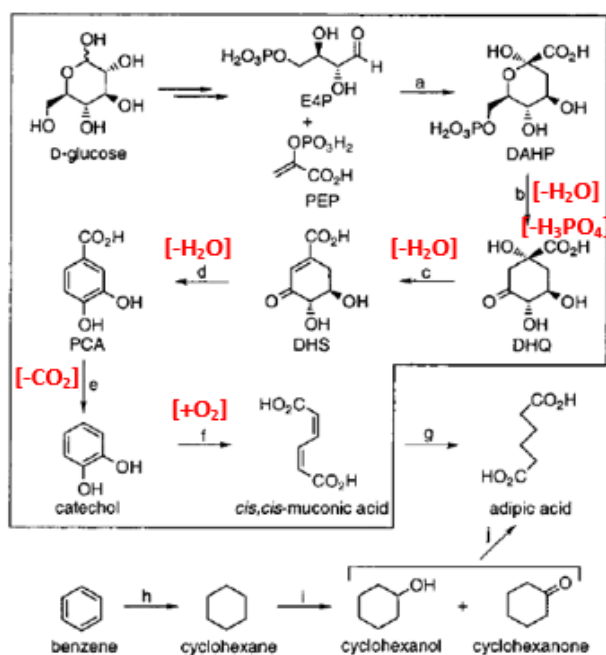


Figure 2.16 – Muconic acid synthetic pathway for *E. coli*, adapted from ref.20.

[E4P, D-erythrose 4-phosphate; PEP, phosphoenolpyruvic acid, DAHP, 3-deoxy-D-arabinoheptulosonic acid 7-phosphate; DHQ, 3-dehydroquinic acid; DHS, 3-dehydroshikimic acid, PCA, protocatechuic acid.]

Glucose is fully metabolized to sustain biomass growth and to synthesize the two intermediates E4P (D-erythrose 4-phosphate) and PEP (phosphoenolpyruvic acid), necessary to achieve DAHP (3-deoxy-D-arabinoheptulosonic acid-7-phosphate) and DHQ (3-dehydroquinic acid). The latter is the actual starting point for simpler reactions of dehydration to yield *cis,cis*-muconic acid. In step c) and in step d) of Figure 2.16, one molecule of H₂O is removed. Step e) produced one molecule of CO₂, while step f) needs one oxygen atom to yield muconic acid.

These pathways require the utilization of many co-factors that play an important role in the cellular metabolism and the DAHP for muconic acid production is diverted from other

cycles for cell self-sustainment. This can be appreciated in the diagram of Patniak et al.⁹⁵, in which 7 moles of glucose produce 3 moles of DAHP (Figure 2.17, A).

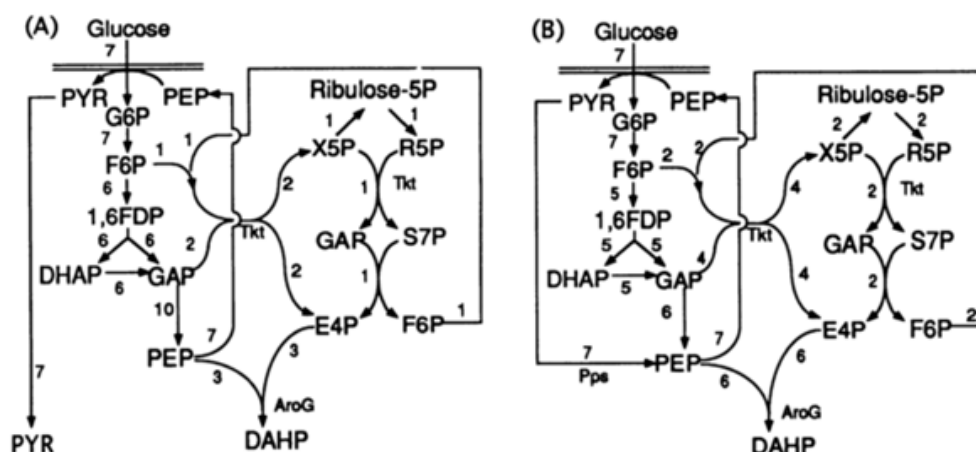


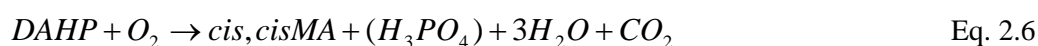
Figure 2.17 – Reaction pathways for the maximal conversion of glucose to DAHP, adapted from ref. 95. [G6P, glucose; F6P, fructose; 1,6FDP 1,6-fructose diphosphate; DHAP, dihydroxyacetone phosphate; GAP, glyceraldehyde 3-phosphate; R5P, ribose 5-phosphate, X5P, xylulose 5-phosphate; S7P, sedoheptulose 7-phosphate; PYR, pyruvate]

E. coli normally follows path A. The overall pseudo stoichiometric equation is the following:



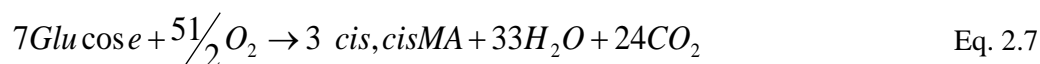
According to this scheme, the maximum theoretical (or stoichiometric) yield is $3/7 = 0.43$. The 10 H₂ molecules in squared brackets on the right side of the equation are necessary to close the balance: in reality the cell does not produce molecular hydrogen, but those atoms are used by the cell for its metabolic activity (e.g. NADH generation, etc.). Therefore, those hydrogens take part to the cellular metabolism and, since they are no more involved in the production of muconic acid, it will be assumed that they eventually produce H₂O. This assumption is motivated by the fact that the fermentation is aerobic and that it is impossible to know a priori the possible byproducts. If we assume that cells are “catalyst”, which oxydate any substrate to CO₂ and water, producing a target product (which is the ideal conditions of work, during steady state fermentation), we can represent in a single pseudo-

stoichiometry the overall reaction performed. In fact the other metabolite (pyruvic acid) produced in Eq. 2.5 is reacted to CO₂ and H₂O in the aerobic citric acid cycle (Krebs cycle). Going back to Figure 2.16, DAHP metabolism to muconic acid gives:



Since phosphoric acid (or better phosphate) is continuously reused by the cell for the first step of glycolysis (i.e. sugar phosphorylation), it can be excluded from our balance.

Merging equation Eq. 2.5 with equation Eq. 2.6 and assuming full oxidation of the metabolites as previously motivated we obtain:

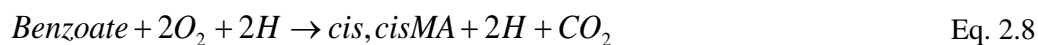


Which gives an idea of the maximum yield attainable by the available engineered *E. coli*. Figure 2.17 however shows how the extra pyruvic acid could be actually employed to produce more DAHP. This solution, which has not been expressed yet successfully in vitro (but in silico is feasible), would lead to double the yield, with 6 moles of muconic acid per 7 moles of glucose, as shown in the pathway B of Figure 2.17.

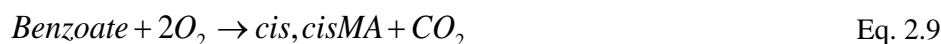
Aromatic pathway: ortho-cleavage of catechol

The metabolic pathway presented in Figure 2.18 is naturally expressed by many species of fungi, able to decompose lignin, where benzoate is available in high amounts. If muconate cycloisomerase is inhibited, the metabolism is stopped and muconic acid accumulates in the system, in a far easier way than with glucose.⁸⁶

The overall reaction is:



It is possible to see how the stoichiometric yield is 100%: one molecule of muconic acid from one of benzoate. The “hydrogen” is added by benzoate dioxygenase consuming an NADH and a proton (H⁺), and the molecule is restored in the further step, hence the balance is 0. Eq. 2.9 is therefore obtained:



Since the interrupted metabolic pathway has been successfully expressed in *P. putida*, another carbon source is required to sustain the normal cellular metabolism.²³

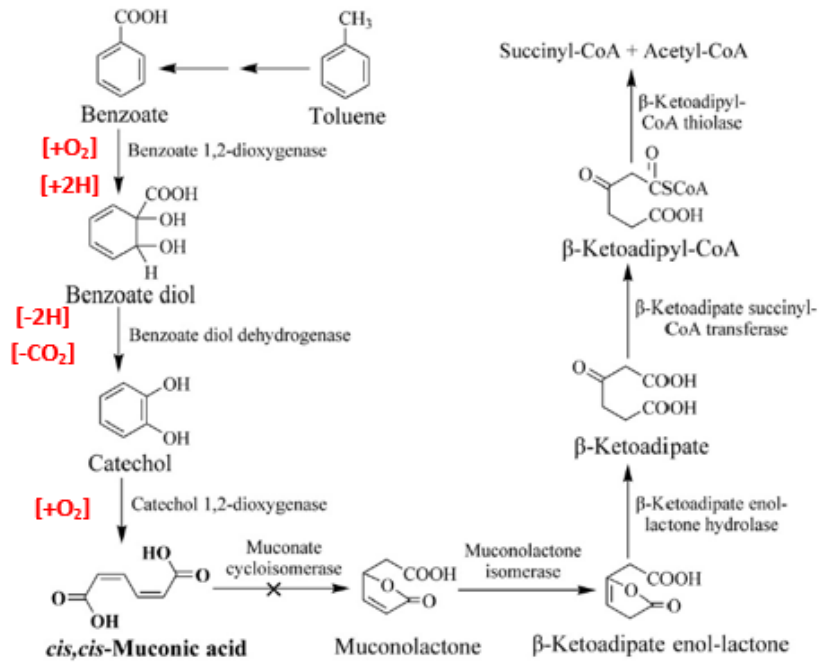


Figure 2.18 – Metabolism from aromatic compounds by ortho-cleavage pathway of catechol. The inhibition of muconate cycloisomerase allows to accumulate muconic acid.

2.3 - Route selection and project management

The good reaction yields, the quantitative fermentation productivity and the high potential for a real technology sustainability make the muconic acid route the most appealing for green adipic acid production. Still, the economic feasibility has to be demonstrated, to motivate further studies toward the scale up and eventually the process realization. Very few literature contributions have addressed this aspect in the past.

The first cost estimates for adipic acid via muconic can be found in Niu et al.²⁰. The analysis was performed applying the analogy approach, therefore estimating the costs without a real process design for bio-adipic acid, but using the economies of a “similar” L-lysine bioprocess. A more detailed study can be found in the LCA analysis performed for muconic acid production from benzoic acid.⁹⁶ In this case, a process flowsheet was provided and simulated to achieve quantitative data on material and energy balances. Still, the economic assessment was secondary with respect to the life cycle assessment, and the hypothesized process was clearly oversimplified. A valuable techno-economic analysis was published in 2015, in which the economic potentials of several innovative bioprocesses were compared.⁹⁷ Unfortunately, this last contribution did not disclose the process flowsheet neither the data at the base of the evaluation, since they were taken from a confidential study performed by Novozymes and the consulting company Nexant. Also, the main reference used for adipic acid assessment was rather outdated, despite the fact that results have been significantly improved in more recent publications.²⁰

For example, muconic acid production from sugar achieved 71% of the theoretical yield: a +40% improvement with respect to the original strain performance.²¹ Also the benzoate route was improved, reaching quantitative amounts of product and opening the process to a feedstock that was previously not considered, the lignin fraction of vegetal biomass.²³ From a downstream point of view, new insights on the physical properties of muconic acid have been disclosed^{98,99}, while new catalytic solutions have been investigated for the hydrogenation to adipic acid: noble metals in organic solvent²⁹, Nickel in aqueous solution¹⁰⁰, electro-catalysis¹⁰¹.

The latest techno-economic analysis published is actually contained in the work of Matthiesen et al.¹⁰², associated to the disclosure of a new electro-catalytic cell. However,

this last study is subordinated to the characterization of the catalytic membrane, therefore several aspects of the technoeconomic analysis lack of sufficient explanation. As a consequence, none of the abovementioned studies is sufficient to motivate any strategic decision to support or abandon the research on the muconic acid fermentation route.

The aim of this Ph.D. project is actually cover this gap of information using some advanced PSE tools to support a systematic strategy definition. To help visualizing the potential of the project and its challenges, a SWOT table is reported (Table 2.7), which highlights the internal and external factors influencing the outcome of the project. The acronym SWOT stands for Strengths (internal factors leading to the success), Weaknesses (internal factors of hindrance), Opportunities (external factors leading to success) and Threats (external factors of hindrance).

The main challenges for a process evaluation, as already mentioned, arise from the lack of complete and high quality data to motivate the results and the assumptions. In facts, any process feasibility study requires as a first key step the definition of the shape of the process itself. If the process definition is biased, so will be the results and the research strategy derived, with a potential loss of time and money. Figure 2.19 summarizes the main open questions associated to the shape of muconic acid production and hydrogenation process.

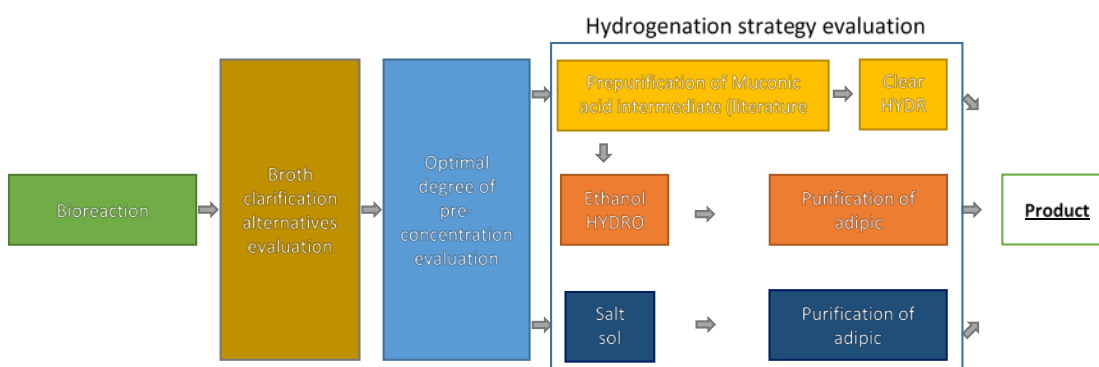


Figure 2.19 – Conceptual map of the decisions to be taken when developing the process shape of green adipic acid process.

Table 2.7 - SWOT matrix for the realization of an early stage techno-economic feasibility study.

Techno-economic analysis of a novel process for green adipic acid production via muconic acid	
Strengths	Weaknesses
<ul style="list-style-type: none"> • Availability of a large corpus of literature • Availability of laboratory facilities to provide experimental measures if needed • Availability of a wide range of PSE tools 	<ul style="list-style-type: none"> • Very limited time horizon • Interdisciplinary topic, involving chemistry, biology and engineering • Lack of studies on several key aspects
Opportunities	Threats
<ul style="list-style-type: none"> • Interest and support by adipic acid producing companies • Formation of an inter-university research group of biologists and chemists 	<ul style="list-style-type: none"> • Unpredictable outcomes/duration of laboratory investigation • Variability of the economic scenarios/ external assumptions at the base of the analysis

1. The first big open issue is the characterization of the bioreaction: nature of the feedstock, availability, fermentation performances and scale up and design are topics that the literature have only cursorily addressed, as the studies never aimed at evaluating experimentally the technology scalability.
2. The second aspect that needs to be specifically addressed is the design of the clarification section of the plant. The technologies of clarification are many and mostly tailor-designed after intensive experimental campaigns, characterizing the flow and filterability processes of the microorganism aqueous suspensions. Unfortunately, these studies are performed at a very advanced stage of the bio-process development, i.e. when the model bacteria can be fermented in quantitative amounts and pilot-plants can be tuned to provide the best economic scalable

solution. As the bacteria under analysis (*E.coli* and *P.putida*) cannot be fermented and assessed experimentally, the process design should be based on a predictive analysis.

3. The third issue is the concentration/recovery of muconic acid. Muconic acid presents three isomers, which have particularly different thermodynamic properties. Very few studies have been performed on this point and, given the very recent interest for this molecule, no experimental-based thermodynamic model is currently available.
4. The fourth main open question is on the hydrogenation strategy and the optimization of the hydrogenation conditions. The main purpose of the previous studies was the demonstration of the feasibility of a muconic acid hydrogenation to adipic, with bench-scale analyses that sometimes were very far away from the acceptable operating conditions of a full scale plant (e.g. very high dilution, high pressure, high temperature, etc.). Moreover, no kinetic studies for a detailed reaction simulation have been disclosed yet.

2.4 - Conclusions

In this chapter the state-of-the-art of technologies to achieve green adipic acid have been reviewed and preliminarily assessed in terms of sustainability potential and likelihood of a profit. Among the many alternatives of feedstock and of production route, the two step process involving a first fermentation of lignocellulosic raw materials (glucose or benzoic acid) to *cis,cis*-muconic acid and its subsequent catalytic hydrogenation to adipic acid proved to have the highest prospective for an industrialization. The main challenges for the achievement of a sound process design and evaluation have therefore been analyzed, given the early stage, incomplete and highly interdisciplinary data available on the topic. Still, PSE can provide a real support to achieve the goal of attaining a process flowsheet and techno-economic estimation. The next chapters will show how different PSE tools are applied to solve the main open challenges of bioprocess development.

2.5 - References chapter 2

1. Bart, J. C. J.; Cavallaro, S. *Ind. Eng. Chem. Res.* **2015**, *54* (2), 567.
2. Xie, N.-Z.; Liang, H.; Huang, R.-B.; Xu, P. *Biotechnol. Adv.* **2014**, *32* (3), 615.
3. Polen, T.; Spelberg, M.; Bott, M. *J. Biotechnol.* **2013**, *167* (2), 75.
4. Kruyer, N. S.; Peralta-Yahya, P. *Curr. Opin. Biotechnol.* **2017**, *45*, 136.
5. May, C. D. *Carbohydr. Polym.* **1990**, *12* (1), 79.
6. Cipolletti, G.; Manoni, M.; Vagnoli, L.; Giacomelli, S.; Biagiolini, S.; Pratesi, C.; Camici, L. WO2005039299A3.
7. Tuck, C. O.; Perez, E.; Horvath, I. T.; Sheldon, R. A.; Poliakoff, M. *Science* (80-.). **2012**, *337* (6095), 695.
8. Lange, H.; Decina, S.; Crestini, C. *Eur. Polym. J.* **2013**, *49* (6), 1151.
9. Beardslee, T.; Picataggio, S.; Eirich, E. D.; Laplaza, J. M. WO2014100504A2.
10. Ghorbanpour Khamseh, A. A.; Miccio, M. *Process Biochem.* **2012**, *47* (11), 1588.
11. Mojzita, D.; Wiebe, M.; Hilditch, S.; Boer, H.; Penttilä, M.; Richard, P. *Appl. Environ. Microbiol.* **2010**, *76* (1), 169.
12. Kiely, D. E.; Hash, K. R. US9162959B2.
13. Merbouh, N.; Bobbitt, J. M.; Brückner, C. US6498269B1.
14. Bonhoure, J. P.; Abboud, H.; Aussenac, T. R.; Coste, C. U.; Hoang, L.; Ralainirina, R.; Rannou, A. C. EP2831028 B1.
15. Burgard, A. P.; Pharkya, P.; Osterhout, R. E. Google Patents December 10, **2009**.
16. Wu, L.; Trefzer, A. C.; DE, W. S. M. A.; Van, D. B. M. A. US9096873B2.
17. Baynes, B. M.; Geremia, J. M. US 8133704 B2.
18. Moon, T. S.; Yoon, S. H.; Lanza, A. M.; Roy-Mayhew, J. D.; Jones Prather, K. L. *Appl. Environ. Microbiol.* **2009**, *75* (3), 589.
19. Solomon, K.; Moon, T. S.; Prather, K. L. J. US 8133704 B2.
20. Niu, W.; Draths, K. M.; Frost, J. W. *Biotechnol. Prog.* **2002**, *18* (2), 201.
21. Bui, V.; Lau, M. K.; MacRae, D.; Schweitzer, D. WO2011085311A1.
22. Thomas, J. M.; Raja, R.; Johnson, B. F. G.; O'Connell, T. J.; Sankar, G.; Khimyak, T. *Chem. Commun.* **2003**, *10*, 1126.

23. Vardon, D. R.; Franden, M. A.; Johnson, C. W.; Karp, E. M.; Guarnieri, M. T.; Linger, J. G.; Salm, M. J.; Strathmann, T. J.; Beckham, G. T. *Energy Environ. Sci.* **2015**, 8 (2), 617.
24. Li, X.; Wu, D.; Lu, T.; Yi, G.; Su, H.; Zhang, Y. *Angew. Chemie - Int. Ed.* **2014**, 53 (16), 4200.
25. Boussie, T. R.; Dias, E. L.; Fresco, Z. M.; Murphy, V. J.; Shoemaker, J.; Archer, R.; Jiang, H. US8669397B2.
26. Diamond, G.; Murphy, V.; Boussie, T. R. *Modern Application of High Throughput R&D in Heterogeneous Catalysis*. Bentham Science Publishers: Sharjah (UAE) 2014, pp 288–309.
27. Capelli, S.; Rosengart, A.; Villa, A.; Citterio, A.; Di Michele, A.; Bianchi, C. L.; Prati, L.; Pirola, C. *Appl. Catal. B Environ.* **2017**, 218, 220.
28. Draths, K. M.; Frost, J. W. *J. Am. Chem. Soc.* **1994**, 116 (1), 399.
29. Vardon, D. R.; Rorrer, N. A.; Salvachúa, D.; Settle, A. E.; Johnson, C. W.; Menart, M. J.; Cleveland, N. S.; Ciesielski, P. N.; Steirer, K. X.; Dorgan, J. R.; Beckham, G. T. *Green Chem.* **2016**, 18 (11), 3397.
30. Picataggio, S.; Beardslee, T. US8241879B2.
31. Kuivanen, J.; Dantas, H.; Mojzita, D.; Mallmann, E.; Biz, A.; Krieger, N.; Mitchell, D.; Richard, P. *AMB Express* **2014**, 4 (1), 33.
32. Müller-Maatsch, J.; Bencivenni, M.; Caligiani, A.; Tedeschi, T.; Bruggeman, G.; Bosch, M.; Petrusan, J.; Van Droogenbroeck, B.; Elst, K.; Sforza, S. *Food Chem.* **2016**, 201, 37.
33. Gómez, B.; Gullón, B.; Yáñez, R.; Parajó, J. C.; Alonso, J. L. *J. Agric. Food Chem.* **2013**, 61 (42), 10043.
34. May, C. D. *Carbohydr. Polym.* **1990**, 12 (1), 79.
35. Mamma, D.; Christakopoulos, P. *Waste and Biomass Valorization* **2014**, 5 (4), 529.
36. Olsen, H. S. US20130330797A1.
37. Hotchkiss, A. T.; Savary, B. J.; Cameron, R. G.; Chau, H. K.; Brouillette, J.; Luzio, G. A.; Fishman, M. L. *J. Agric. Food Chem.* **2002**, 50 (10), 2931.
38. Cameron, R. G.; Chau, H. K.; Manthey, J. A. *J. Chem. Technol. Biotechnol.* **2016**, 91 (10), 2597.

39. Vincent Corporation. <http://www.vincentcorp.com/content/citrus-pectin-peel-preparation> (accessed Oct 23, 2017).
40. Hull, W. Q.; Lindsay, C. W.; Baier, W. E. *Ind. Eng. Chem.* **1953**, *45* (5), 876.
41. Gusek, T. W.; Zullo, L.; Eyal, A. M. WO2006096884A3.
42. <https://www.icis.com/chemicals/channel-info-chemicals-a-z/>.
43. Ghorbanpour Khamseh, A. A.; Miccio, M. *Process Biochem.* **2012**, *47* (11), 1588.
44. Grohmann, K.; Baldwin, E. A. *Biotechnol. Lett.* **1992**, *14* (12), 1169.
45. Wilkins, M. R.; Widmer, W. W.; Grohmann, K.; Cameron, R. G. *Bioresour. Technol.* **2007**, *98* (8), 1596.
46. Li, P.; Xia, J.; Nie, Z.; Shan, Y. *Bioprocess Biosyst. Eng.* **2016**, *39* (3), 485.
47. Bylund, G. *Dairy processing handbook*; Tetra Pak Processing Systems AB, 2003.
48. Dairy products prices <http://www.clal.it/en> (accessed Aug 23, 2017).
49. Wiesenthal, T.; Mourelatou, A. How much bioenergy can Europe produce without harming the environment?; EU government report **2006**.
50. Kenney, K. L.; Smith, W. A.; Gresham, G. L.; Westover, T. L. *Biofuels* **2013**, *4* (1), 111.
51. Drapcho, C. M.; Nhuan, N. P.; Walker, T. H. *Biofuels engineering process technology*; McGraw-Hill New York, NY, USA, 2008.
52. McKendry, P. *Bioresour. Technol.* **2002**, *83* (1), 37.
53. Steubing, B.; Zah, R.; Ludwig, C. *Environ. Sci. Technol.* **2012**, *46* (1), 164.
54. Perlack, R. D.; Wright, L. L.; Turhollow, A. F.; Graham, R. L.; Stokes, B. J.; Erbach, D. C. *Biomass as feedstock for a bioenergy and bioproducts industry: the technical feasibility of a billion-ton annual supply*; Oak Ridge National Lab TN, 2005.
55. Betts, W. B.; Dart, R. K.; Ball, A. S.; Pedlar, S. L. Betts, W. B., Ed.; *Biodegradation*, Springer London: London, 1991; pp 139–155.
56. Malherbe, S.; Cloete, T. E. *Rev. Environ. Sci. Biotechnol.* **2002**, *1* (2) 105.
57. Saha, B. C. J. *Ind. Microbiol. Biotechnol.* **2003**, *30* (5), 279.
58. Ghaffar, S. H.; Fan, M. *Biomass and Bioenergy* **2013**, *57*, 264.
59. Naik, S. N.; Goud, V. V.; Rout, P. K.; Dalai, A. K. *Renew. Sustain. Energy Rev.* **2010**, *14* (2), 578.
60. Renmatix builds full scale plant <http://renmatix.com> (accessed Aug 24, 2017).
61. Kazachkin, D. V.; Colakyan, M.; Moesler, F. J. WO2014012030A1.

62. Abdelaziz, O. Y.; Brink, D. P.; Prothmann, J.; Ravi, K.; Sun, M.; García-Hidalgo, J.; Sandahl, M.; Hulteberg, C. P.; Turner, C.; Lidén, G.; Gorwa-Grauslund, M. F. *Biotechnol. Adv.* **2016**, *34* (8), 1318.
63. Wang, H.; Tucker, M.; Ji, Y. *J. Appl. Chem.* **2013**, 2013.
64. Huibers, D. T. A.; Parkhurst, H. J. US4420644A.
65. Yang, J.; Zhao, L.; Liu, S.; Wang, Y.; Dai, L. *Bioresour. Technol.* **2016**, *212*, 302.
66. PFAD prices <http://www.indexmundi.com> (accessed Aug 25, 2017).
67. Nelson, B.; Searle, S. Projected availability of fats, oils, and greases in the US; ICCT Working Paper, 2016.
68. Saladini, M.; Candini, M.; Iacopino, D.; Menabue, L. *Inorganica Chim. Acta* **1999**, *292* (2), 189.
69. Gupta, S. K. US20090209642A1.
70. Henkensmeier, D.; Abele, B. C.; Candussio, A.; Thiem, J. *Polymer.* **2004**, *45* (21), 7053.
71. Smith, T. N.; Kiely, D. E.; Kramer-Presta, K. US9404188B2.
72. Smith, T. N.; Shirley, R. US9347024B2.
73. Brown, J. M.; Manley-Harris, M.; Field, R. J.; Kiely, D. E. *J. Carbohydr. Chem.* **2007**, *26* (8–9), 455.
74. Kiely, D. E.; Hash, K. R. US9162959B2.
75. Mojzita, D.; Wiebe, M.; Hilditch, S.; Boer, H.; Penttilä, M.; Richard, P. *Appl. Environ. Microbiol.* **2010**, *76* (1), 169.
76. Benz, J. P.; Protzko, R. J.; Andrich, J. M.; Bauer, S.; Dueber, J. E.; Somerville, C. R. *Biotechnol. Biofuels* **2014**, *7* (1), 20.
77. Bonhoure, J. P.; Abboud, H.; Aussenac, T. R.; Coste, C. U.; Hoang, L.; Ralainirina, R.; Rannou, A. C. EP2831028 B1 2015,.
78. Curran, K. A.; Leavitt, J. M.; Karim, A. S.; Alper, H. S. *Metab. Eng.* **2013**, *15* (1), 55.
79. Frost, J. W.; Draths, K. M. US5487987A1.
80. Yocum, R. R.; Gong, W.; Dole, S.; Sillers, R.; Gandhi, M.; Pero, J. G. US20150044755A1.
81. Kaneko, A.; Ishii, Y.; Kirimura, K. *Chem. Lett.* **2011**, *40* (4), 381.

82. Mizuno, S.; Yoshikawa, N.; Seki, M.; Mikawa, T.; Imada, Y. *Appl. Microbiol. Biotechnol.* **1988**, 28 (1), 20.
83. Imada, Y.; Yoshikawa, N.; Mizuno, S.; Mikawa, T. US4871667A.
84. Wu, C. M.; Wu, C. C.; Su, C. C.; Lee, S. N.; Lee, Y. A.; Wu, J. Y. *Biochem. Eng. J.* **2006**, 29 (1–2), 35.
85. Van Duuren, J. B. J. H.; Wijte, D.; Leprince, A.; Karge, B.; Puchałka, J.; Wery, J.; Dos Santos, V. A. P. M.; Eggink, G.; Mars, A. E. *J Biotechnol.* **2011**, 156 (3), 163.
86. Xie, N. Z.; Wang, Q. Y.; Zhu, Q. X.; Qin, Y.; Tao, F.; Huang, R. B.; Xu, P. *Prep. Biochem. Biotechnol.* **2014**, 44 (4), 342..
87. Liu, W.-H.; Li, R.-M.; Kung, K.-H.; Cheng, T.-L. *Food Sci. Agric. Chem.* **2003**, 5 (1), 7.
88. Schmidt, E.; Knackmuss, H.-J. *Appl. Microbiol. Biotechnol.* **1984**, 20 (5), 351.
89. Bang, S. G.; Choi, W. J.; Choi, C. Y.; Cho, M. H. *Biotechnol. Bioprocess Eng.* **1996**, 1 (1), 36
90. Chua, J. W.; Hsieh, J. H. *World J. Microbiol. Biotechnol.* **1990**, 6 (2), 127.
91. Burgard, A. P.; Pharkya, P.; Osterhout, R. E. US8062871 B2.
92. Villadsen, J.; Lee, S. Y.; Nielsen, J.; Stephanopoulos, G. *Fundamental Bioengineering; Advanced Biotechnology*; Wiley, 2016.
93. Lu, R.; Lu, F.; Chen, J.; Yu, W.; Huang, Q.; Zhang, J.; Xu, J. *Angew. Chemie - Int. Ed.* **2016**, 55 (1), 249.
94. Rorrer, N. A.; Vardon, D. R.; Dorgan, J. R.; Gjersing, E. J.; Beckham, G. T. *Green Chem.* **2017**, 19, 2812.
95. Patnaik, R.; Liao, J. C. *Appl. Environmental Microbiol.* **1994**, 60 (11), 3903.
96. Van Duuren, J. B. J. H.; Brehmer, B.; Mars, A. E.; Eggink, G.; dos Santos, V. A. P. M.; Sanders, J. P. M. *Biotechnol. Bioeng.* **2011**, 108 (6), 1298.
97. Grotkjær, T. In *Fundamental Bioengineering*; Wiley-VCH Verlag GmbH & Co. KGaA, 2015; pp 499–546.
98. Carraher, J. M.; Matthiesen, J. E.; Tessonier, J. P. *J. Mol. Liq.* **2016**, 224, 420.
99. Scelfo, S.; Pirone, R.; Russo, N. *J. Mol. Liq.* **2016**, 222 (Supplement C), 823.
100. Scelfo, S.; Pirone, R.; Russo, N. *Catal. Commun.* **2016**, 84, 98.
101. Matthiesen, J. E.; Carraher, J. M.; Vasiliu, M.; Dixon, D. A.; Tessonier, J. P. *ACS Sustain. Chem. Eng.* **2016**, 4 (6), 3575.

102. Matthiesen, J. E.; Suástegui, M.; Wu, Y.; Viswanathan, M.; Qu, Y.; Cao, M.; Rodriguez-Quiroz, N.; Okerlund, A.; Kraus, G.; Raman, D. R.; Shao, Z.; Tessonnier, J.-P. *ACS Sustain. Chem. Eng.* **2016**, *4* (12), 7098.

Chapter 3

Early stage process synthesis and design

In this chapter, the feasibility of a new biotechnological process for adipic acid is evaluated, applying a computer-aided methodology for process synthesis-design to generate the first flowsheet concept. Paragraph 3.1 describes in detail the methodology, providing a clear overview of the workflow and the dataflow required to formulate the problem and introducing the concepts of optimization and Mixed Integer Linear Programming employed. Paragraph 3.2 is centered on the superstructure generation, describing in detail the data and the assumptions provided for each technology included in the process. Paragraph 3.3 comments the results of the optimization, with the economic and environmental sustainability analysis and a multi-scenario assessment. Paragraph 3.4 shows how the results can be used to develop and plan the next R&D activities.

3.1 - A computer aided framework for process synthesis and design

3.1.1 - Historical perspective on Process Design and Optimization

Decisions on strategic topics must be taken with the support of sound calculations. However, when dealing with complex projects based on preliminary data and with many arbitrary degrees of freedom, the risk of being misled is high. This is particularly critical when the investments in terms of money and R&D resources become consistent. Manufacturing companies have developed different approaches for new product/process development, and, focusing on process industry, we can distinguish the bulk chemical (oil and gas) approach and the pharmaceutical approach. The main reference for the former area is the methodology of Douglas¹, which became subject of teaching in all the chemical engineering courses and whose concepts are present with little updates in the main manuals of process design.^{2,3} Douglas approach is based on a hierarchical classification of the process unit operations, and the main steps of the methodology are:

1. Definition of the chain of transformations from a feedstock to the product
2. Detailed modeling of the key unit operations (as reactions and cost intensive separations) on a simulator flowsheet to obtain a base-case.
3. Identification of possible process alternatives, generating as many flowsheet as the alternatives, proceeding from the upstream to the downstream.
4. Iterative update of the process design. When changing a process parameter, the downstream can be affected, but also the upstream in case of recycle.

Such an approach allows rationalizing the process of decision making, proceeding first with the most cost-intensive decisions (this is why is defined hierarchical method) and then defining the rest. Though, the methodology becomes labor intensive for complex processes or when an oversimplification of the flowsheet wants to be avoided, to reduce the risk of wrong decisions. Another drawback of this approach is that makes large use of the process simulators, which, as already stated, are not suitable in presence of uncertain or preliminary data. Why this method is still so popular in oil and gas industry? It is because new process development became rare events in the field of commodity chemicals after the 80s, and, until recently, the need of more refined methods was minimal, and context dependent. However, the new strict regulation on emission and pollution, and the advent of novel bio-

processes, raised again the problem of finding the optimal design of a completely new process, as explained after.

Much different is the case of Pharmaceutical companies, where new API (active pharmaceutical ingredients) are identified every year and the process development must follow the fast evolution of the market. The strict regulation on pharmaceutical product quality led the FDA (Food and Drug Administration office, the reference organism that controls the commercialization of pharmaceutical in the USA) to introduce a series of compulsory guidelines known as GMP (Good Manufacturing Practice).^{4,5}

The guidelines provide the minimum requirements that pharmaceutical manufacturers must meet: since the product reproducibility is of paramount importance, the process design steps are assisted by the guidelines, limiting the degrees of freedom to the selection of the BAT (Best available techniques). This emphasis on the product rather than the process, led to the establishment of a process development practice based on “experience” and “procedure compliance”, which reflects in high costs of production and little sustainability, tolerated in virtue of the high revenues and the strategic importance of the market (at expenses of the environment). Also in this case, there has been a recent change of paradigm, in which a systematic but optimized process design became more relevant. In fact, the new FDA guidelines for pharmaceutical industries introduced the concept of QbD (Quality by Design).⁶⁻¹⁰ Accordingly, the API lifecycle (from R&D to commercialization) must be systematically optimized from the beginning with an appropriate definition of critical quality attributes and process parameters, maximizing the quality, but also minimizing resource exploitation (and costs). Fundamental for this goal is the adoption of Process Analytical Technology (PAT) for in line and at line controls.

The same concepts of “Optimization” apply therefore to pharmaceutical and commodity chemicals process. The scientific branch of mathematics and engineering that addresses the search of “optimal solutions” is defined “Operational Research”: the solution algorithms are useful for problems of physics, economics, supply chain management, network design, resource distribution and virtually any problem that could be written as a minimization of an “objective function”. The term “operational research” was used for the first time during the 2nd World War, by Albert Rowe, a British physicist in charge of developing the first radar system. Also during the War the first powerful algorithm for linear optimization

problems was conceived by the US mathematician George Dantzig, the SIMPLEX method.¹¹ The development of computers, able to deal with the many variables of optimization problems, finally paved the way for a wider application of optimization. Chemical engineering, which represents one of the most challenging fields of application of operative research concepts, saw a systematic use of optimization thanks to the pioneering work of professor Roger Sargent of Imperial College, the father of Process Systems Engineering.¹²

He was among the first to understand the need of optimization and unit operation integration in process design, developing some first nonlinear programming techniques to solve alternatives design selection for distillation columns (the first “superstructure”).^{13–15} Then he addressed also mixed-integer programming (optimization with discrete variables) with his Ph.D. student Ignacio Grossman.¹⁶ This resulted in the establishment of a new research branch, which soon became a chemical engineering school, led by Grossman (who became Professor at Carnegie Mellon University). The school had among its lines great personalities as prof. Floudas, prof. Sahinidis, prof. Pistikopoulos, and prof. Biegler, to cite few of them. In more than 30 years of research, the concepts of “superstructure” and MI(N)LP have been applied to many different problems, from process supply chain definition, to optimal design of unit operations and flowsheets, including data uncertainty in the problem formulation. On this latter field, another prof. Sargent’s former Ph.D. student gave great contributions: professor Rafiqul Gani, head of the KT-consortium (Kemitec Teknik) of Denmark Technical University (DTU, Lyngby-Copenhagen). In particular, he focused on the development of computer aided tools to pursue an integrated approach to manage the complexity of process design problems. The aim is to “*identify the optimal raw material, the product portfolio and select the process technology for a given market scenario together with the optimal material flows through the network (of alternatives) and calculate the corresponding performance and sustainability metrics*”.¹⁷ The models and the framework developed by prof. Gani, dr. Quaglia and other DTU researchers, led to the formulation of a new methodology, which is particularly suitable for novel bio-processes development, and became a user-interface software named Super-O, belonging to DTU/KT-consortium pack of software for Integrated Computer Aided System (ICAS).^{18,19}

This methodology corresponds to the first stage of the more general “3-stage approach for process innovation” theorized by Babi et al.²⁰, which is a strategy for solving the overall design problem in a decomposed manner, following three sequential stages. In stage 1 (synthesis), the process flowsheet is obtained, from a number of alternatives processing routes; in stage 2 (design), detailed design and analysis of the selected process are performed; in stage 3 (innovation), the outputs from stage 2 are used as improvements target and a more sustainable design is obtained. By following this 3-stage approach, the size of the search space is subsequently reduced as the model and data complexity increases.

Thanks to an exchange program promoted to the Ph.D. school of Politecnico di Milano, the author of this work spent 6 months at the Chemical Engineering department of DTU under the supervision of prof. Rafiqul Gani, learning Super-O and applying the process synthesis tools to the case study of renewable adipic acid production.

3.1.2 - The generic framework: main concepts and workflow

The methodology for processing route synthesis-design and analysis developed by Bertran et al.¹⁸ has been adopted in this work and has been applied to find the optimal processing route (flowsheet) for sustainable adipic acid production via *cis,cis*-muconic acid. The methodology has many useful features, being:

- Systematic: a step-wise approach allows to build the documentation of the design decisions and helps to represent the vast amount of fragmented and highly interdisciplinary data, through a specially developed knowledge representation framework.
- Generic: the model structure is common for all the processing intervals, allowing a simple but rigorous definition of the unit operation performance and costs, even when little equipment standardization is feasible.
- Flexible: the synthesis problem formulation and solution methods are adaptable to different problem types and scenarios and can easily accommodate new technologies into an existing superstructure.

- Open: the framework supports benchmarking and reusability of the data, so that published information embedded within the in-house database is available to other users needing the same information.

Figure 3.1 provides an overview of the workflow and data-flow required to achieve a final process concept.

It is possible to notice that the activity consists of three subsequent moments:

1. Problem formulation

The first step consists of defining the synthesis problem in terms of its objective and characteristics. The following must be specified: available raw material(s)/feedstock(s), desired product(s), and geographical location(s).¹⁸ In addition, uncertainties in specified constraints (e.g. feedstock/product prices) are considered through different scenarios that are investigated in terms of their effect on the final process design. The problem objective is defined and later translated into an objective function for the optimization problem. This objective can be: profit maximization, environmental impact minimization or productivity maximization, among others.

2. Superstructure generation and data collection

This step encompasses the gathering of processing alternatives and the associated data. The representation of alternatives is achieved using a “superstructure”, that is a process diagram which includes all the possible processing units and all the relevant interconnections. The generic shape of a superstructure is illustrated in *Figure 3.2*. For each alternative, data are collected systematically and can later be stored in a specially designed database. The main sources for data are literature, industrial or academic partners and online databases.

3. Solution of the optimization problem and analysis

The process alternatives, with the multiple interconnections of the unit operations and their performances, are translated into a mathematical problem using a generic optimization model presented by Quaglia et al.¹⁷ and adapted by Bertran et al.¹⁸. The model uses a Mixed-Integer Nonlinear Programming (MINLP) generic formulation applicable to any problem that fits the PSIN representation. The model reduces to an MILP when multi-stream problems are not considered, that is, when stream split optimization is not desired, and when capital cost functions are piece-wise linearized.

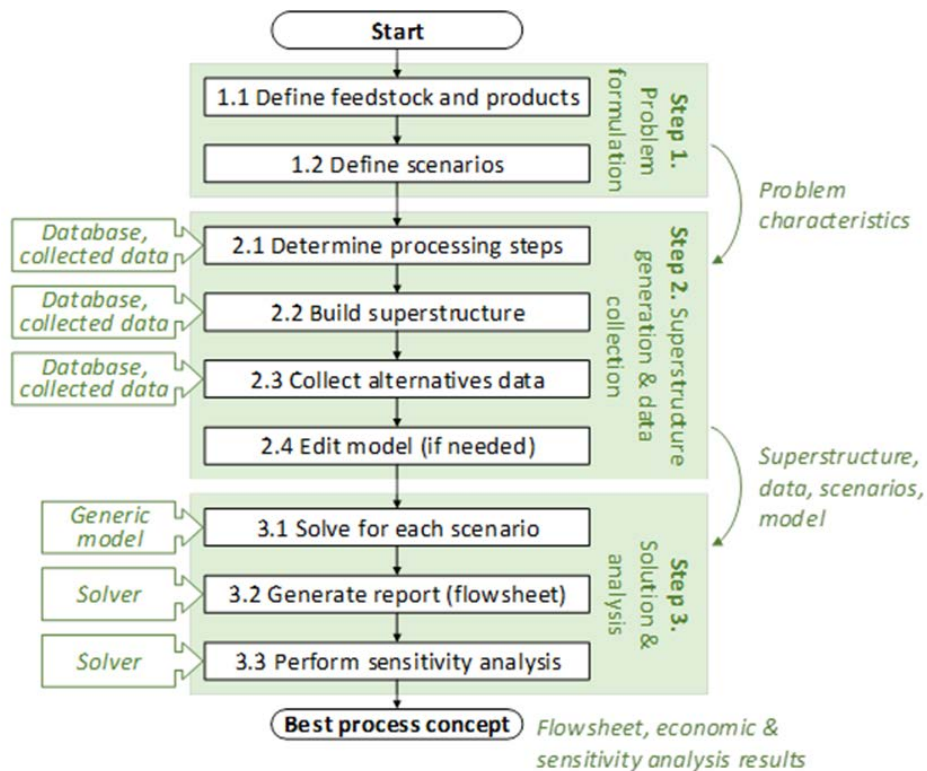


Figure 3.1 - Scheme of the workflow and dataflow for the process synthesis methodology.

The Processing Step-Interval Network representation of Quaglia et al.¹⁷ is used to model the superstructure and formulate the optimization problem (Figure 3.2). The key concept at the base of this representation is the so-called “Interval”, which is a standard and modular unit-operation model (constituted by a set of linear equations and user specified parameters) capable to give a simplified representation of any transformation technology of a processing step.

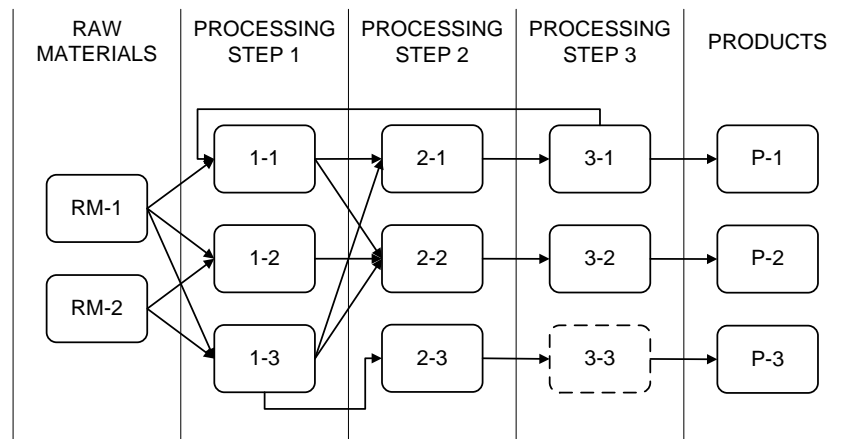


Figure 3.2 - Processing Step-Interval Network (PSIN) representation. Columns represent processing steps (for example, pretreatment, concentration, purification), boxes represent alternative processing intervals (transformation technologies), and arrows represent feasible connections between intervals

The basic idea of this approach is that, at an early stage of process development, when data are few and uncertain, the process units can be described using simpler models that focus on their performances and cost, to speed up the data collection part and include most of the alternatives with little modelling effort. The generic interval model encompasses five basic processing tasks, namely mixing, reaction, waste removal, product separation and utilities consumption. A combination of these interval tasks can successfully represent any real unit operation. Figure 3.3 provides a graphical representation of the interval model, as a block “containing” the basic tasks. In the superstructure, each block introduces a modification (flow rate and/or composition) on the inlet stream(s) and generates one or more outlet streams, connected to other intervals. Material and energy balance consistency is ensured, and the interval model is formulated in a linear form, to give a mixed-integer linear programming problem formulation. The details about the MILP formulation can be found in literature.^{17,21,22}

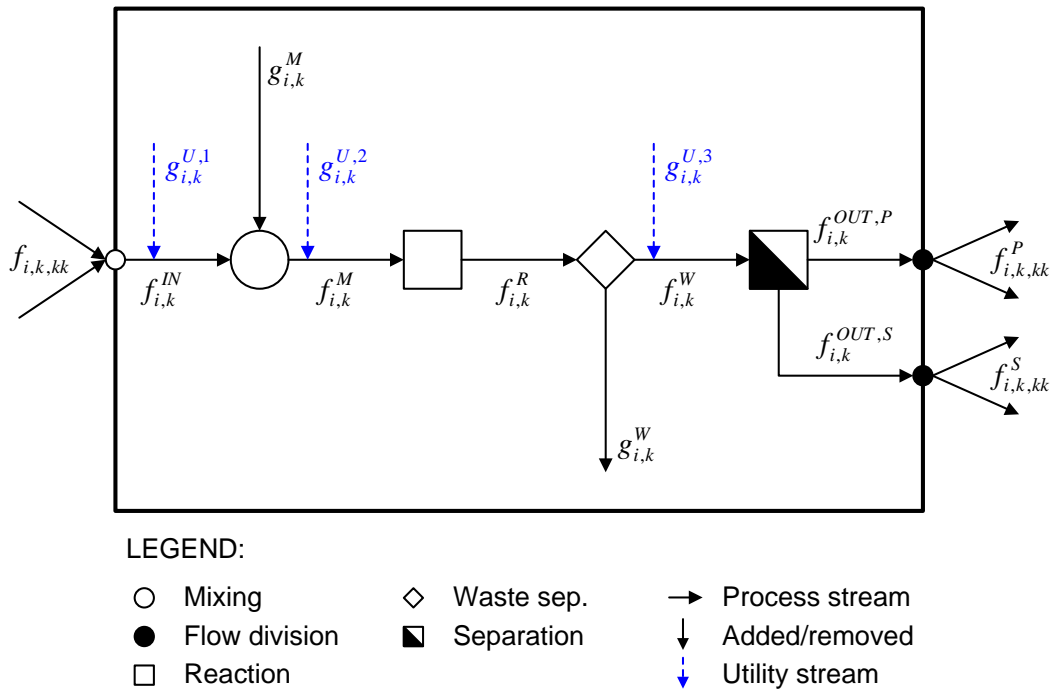


Figure 3.3 - Processing interval scheme with variables used for modelling: index k refers to the interval “ k ”, i refers to component “ i ” in a multi-component flow rate.

The following list describes in detail the five tasks and the symbols of Figure 3.3:

- **Mixing:** used to merge flow rates from upstream units or to introduce new components in the main flow rate, which can be “reactants” or “inerts” (as a solvent, impurities, and so on). For the addition of new components, the flow rate of the new component is scaled according to the mass flow rate of a reference component in the inlet stream (e.g. reactant addition per kg of feedstock) with the user-defined parameter called mixing ratio (symbol μ).
- **Reaction:** this task performs any chemical transformation described by a stoichiometric reaction. The model requires the stoichiometric coefficients of reactants and products, along with the conversion of the limiting reactant.
- **Waste separation:** this task represents the removal of components from the system (not recyclable, represented with the symbol g^W). For example, the gaseous stream

in an aerated fermenter or the waste water from a dehydration step. The required model parameters are the percentage of loss of each component in the inlet flow rate and the associated cost of waste treatment.

- Separation: this task identifies separation operations and has two outlet streams, namely the primary outlet (containing the component of interest) and the secondary outlet (containing the remaining components). It is modelled with the percentage of recovery for each component. Both outputs can be connected to one or more downstream units. For example, this task can represent the top and bottom streams of a distillation column.
- Flow division: an output stream can be split into more than one downstream units by specifying a split parameter on the total flow rate: this task is not used in the present work.

Considering the flow rates included in the model definition, the following symbols are used:

- Variable f : is a flow rate (mass/time). The superscripts inside the interval boundary have the following meaning:
 1. IN: inlet flow rate
 2. M: flow rate after the Mixing task
 3. R: flow rate after the Reaction task
 4. W: flow rate after the Waste task
 5. OUT,P: flow rate after the Separation task, primary stream
 6. OUT,S: flow rate after the Separation task, secondary stream
- Variable g^U : is the flow rate of utilities associated to the interval tasks of unit k , correlated to the flow rate of a component i (e.g. kg of steam required to heat one kg of water) via the utility consumption ratio (symbol β). The utilities considered in this work are Electric Power (EL_PO), Steam High Pressure (ST_HP), Steam Low Pressure (ST_LP), Cooling Water (CO_WA) and Compressed Air (AI_CO). The utility consumption can be referred to a particular task considering three of the interval internal flow rates:
 1. Utilities required by the mixing task
 2. Utilities required by reaction/waste tasks
 3. Utilities required by the separation task

The specification of any of the mentioned parameters activates the task in the interval model; otherwise, the flow rate is not modified.

For instance, a gas-liquid reactor model will require the mixing task specifications (addition of the co-reactant and solvent), the reaction task (the actual stoichiometry and conversion/selectivity), the waste (the gas is assumed wasted). If no separations occur and the output stream is one, the separation task is not specified. As for the utilities, some cooling can be included for the reaction step specifying the parameter $g^{U,2}$. Finally, each block is provided with a set of parameters for the costs of the utilities/added components and with a capital cost function proportional to the flow rate according to a power law. The power-law allows to account for economies of scale, but introduces a non-linearity in the model equations: for this reason Super-O is provided with a piece-wise linearization feature that divides the range of validity of the cost function into equal intervals and linearizes the function in between.

In general, the flow rates, the compositions and the dependence of process economics are calculated only with the user-specified process conditions without the need of providing a detailed model of the units.

Focusing on the mathematical formulation of the model, it is possible to identify 5 typologies of equations: I) objective-function equations, II) logical constraints, III) process interval equations, IV) consumption of utilities, V) connection equations.

I. Objective function equations

For this specific application, the objective is the identification of the most economic processing route for adipic acid. When translated into an objective function, this must consider the annual incomes from the product sales and the annual expenditures, related to both capital investment and operating costs (utilities and consumables), to estimate the profitability of the processing alternatives. The sum of these contributions corresponds to the process economic potential as defined by Douglas¹ and gives a first indication of the process economic feasibility.

Objective function equations:

$$z = S - C_{RM} - C_C - C_U - C_W - C_T - CAPEX \quad \text{Eq. 3.1} \quad \text{Economic Potential}$$

$$S = \sum_i \sum_k P_k^P f_{i,k}^W \quad \text{Eq. 3.2} \quad \text{Product sales}$$

$$C_{RAW} = \sum_i \sum_k P_k^{RAW} f_{i,k}^W \quad \text{Eq. 3.3} \quad \text{Raw materials cost}$$

$$C_C = \sum_k \sum_i P_i^C g_{i,k}^M \quad \text{Eq. 3.4} \quad \text{Chemicals cost}$$

$$C_U = \sum_k \sum_{ut} P_{ut}^U g_{ut,k}^U \quad \text{Eq. 3.5} \quad \text{Utilities cost}$$

$$C_W = P_W \sum_i \sum_k g_{i,k}^W \quad \text{Eq. 3.6} \quad \text{Waste handling cost}$$

$$C_T = \sum_k \sum_{kk} ctr^{k,kk} \quad \text{Eq. 3.7} \quad \text{Transportation cost}$$

$$CAPEX = \sum_k LIN \left[\left(\alpha \sum_i f^{i,k} \right)^\beta \right] \quad \text{Eq. 3.8} \quad \begin{array}{l} \text{Capital cost,} \\ \text{linearized} \end{array}$$

The parameters identified by the symbol P (Price), are user defined. The indexes k and kk identify two distinct connected intervals, as shown in equation 3.7. However, for the case of adipic acid the transportation cost are not considered.

II. Logical constraints

The following equations belong to the big-M solution strategy for MILP, as explained in section 3.1.3. They are meant to guide the mathematical solver toward a feasible solution providing the constraints to avoid meaningless solutions (as more equivalent unit operations for the same step).

Logical Constraints:

$$\sum_{kk} y_{kk} u_{kk,step} \leq 1 + \sum_k \sum_{kk} u_{k,step} \zeta_{k,kk} \omega_{kk} \quad \text{Eq. 3.9} \quad \text{Select one interval per processing step}$$

$$f_{i,k}^W \leq y_k M \quad \text{Eq. 3.10} \quad \text{Activation constraint for raw materials}$$

$$g_{i,k}^M \leq y_k M \quad \text{Eq. 3.11} \quad \text{Activation constraint for chemicals}$$

$$y_k \leq \sum_i f_{i,k}^W M / 1000 \quad \text{Eq. 3.12} \quad \text{Activation constraint for variable } y \text{ downstream}$$

$$\sum_i f_{i,k}^{IN} \leq y_k M \quad \text{Eq. 3.13} \quad \text{Activation constraint for feedstock}$$

The variable y is an integer variable that can assume the values 1 or 0: it is the variable that determines the selection (activation) of a specific interval and/or a specific stream. The symbol $u_{kk,step}$ is the data defining the allocation of intervals to steps (i.e. equals 1 if interval kk is allocated to step st), the symbol ζ_{kk} is a parameter defining the connections existing in the superstructure (i.e. equals 1 if a connection exist between the outlet of interval k and the inlet of interval kk). The parameter ω_{kk} distinguishes if the interval is a product/feedstock (equals 0) or an actual processing step interval (equals 1).

III. Process interval equations.

The following equations correspond to the material balances of each interval, determining the flow rate and composition of the interval streams.

Process interval equations:

$$f_{i,k,kk} = f_{i,k,kk}^P + f_{i,k,kk}^S \quad \text{Eq. 3.14} \quad \text{Overall composition}$$

$$f_{i,k}^{IN} = \sum_k f_{i,k,kk} \quad \text{Eq. 3.15} \quad \text{Inlet mixer}$$

$$g_{i,k}^M = \sum_k \mu_{i,\ddot{i},k} f_{\ddot{i},k}^{IN} \quad \text{Eq. 3.16} \quad \text{Mixing task 1}$$

$$f_{i,k}^M = f_{i,k}^{IN} + g_{i,k}^M \quad \text{Eq. 3.17} \quad \text{Mixing task 2}$$

$$f_{i,k}^R = f_{i,k}^M + \sum_{rr,react} f_{react,k}^M \theta_{react,kk,rr} \frac{\gamma_{i,k,rr}}{\gamma_{i,k,react}} \frac{MW_i}{MW_{react}} \quad \text{Eq. 3.18} \quad \text{Reaction task}$$

$$f_{i,k}^W = f_{i,k}^R (1 - \delta_{i,k}) \quad \text{Eq. 3.19} \quad \text{Waste separation task 1}$$

$$g_{i,k}^W = f_{i,k}^R - f_{i,k}^W \quad \text{Eq. 3.20} \quad \text{Waste separation task 2}$$

$$f_{i,k}^{OUT,1} = f_{i,k}^W \sigma_{i,kk} \quad \text{Eq. 3.21} \quad \text{Product separation primary outlet}$$

$$f_{i,k}^{OUT,2} = f_{i,k}^W - f_{i,k}^{OUT,1} \quad \text{Eq. 3.22} \quad \text{Product separation secondary outlet}$$

$$f_{i,k}^{OUT,1} = \sum_k f_{i,k,kk}^1 \quad \text{Eq. 3.23} \quad \text{Flow division principal outlet}$$

$$f_{i,k}^{OUT,2} = \sum_k f_{i,k,kk}^2 \quad \text{Eq. 3.24} \quad \text{Flow division secondary outlet}$$

The parameters μ , θ , γ , δ and σ are the mixing ratio, the reaction conversion, the stoichiometric coefficient, the waste rate and the separation rate, respectively.

IV. Utilities consumption equations

The utilities are calculated according to the flow rate of the streams at the inlet (before the mixer), before the reaction task and before the separation according to β , a user defined parameter.

Consumption of utilities:

$$g_{ut,k}^{U,1} = \beta_{ut,k}^1 \sum_i f_{i,k}^{IN} \quad \text{Eq. 3.25} \quad \text{Utilities before mixing}$$

$$g_{ut,k}^{U,2} = \beta_{ut,k}^2 \sum_i f_{i,k}^M \quad \text{Eq. 3.26} \quad \text{Utilities before reaction}$$

$$g_{ut,k}^{ut,k} = \beta_{ut,k}^3 \sum_i f_{i,k}^W \quad \text{Eq. 3.27} \quad \text{Utilities before separation}$$

$$g_{ut,k}^U = g_{ut,k}^{U,1} + g_{ut,k}^{U,2} + g_{ut,k}^{U,3} \quad \text{Eq. 3.28} \quad \text{Overall interval utilities consumption}$$

V. Connection equations

The following equations are the mathematical formulation of the PSIN representation of the superstructure and define the feasible connections between intervals.

Connection equations:

$$f_{i,k,kk}^1 \leq f_{i,k}^{OUT,1} S_{k,kk}^P \quad \text{Eq. 3.29} \quad \begin{array}{l} \text{Flow rate of downstream} \\ \text{interval for primary} \\ \text{connections} \end{array}$$

$$f_{i,k,kk}^2 \leq f_{i,k}^{OUT,2} (\zeta_{k,kk} - S_{k,kk}^P) \quad \text{Eq. 3.30} \quad \begin{array}{l} \text{Flow rate of downstream} \\ \text{interval for secondary} \\ \text{connections} \end{array}$$

$$y_{kk} \omega_{kk} \leq y_k \quad \text{Eq. 3.31} \quad \begin{array}{l} \text{Blender must have 1 inlet at} \\ \text{least} \end{array}$$

$$f_{i,k,l}^W = \phi_{i,k,l} f_{k,l}^{RAW} \quad \text{Eq. 3.32} \quad \begin{array}{l} \text{Raw material composition} \\ \text{from different location} \end{array}$$

The parameter $S_{k,kk}$ is the split factor (value between 0 and 1), related to the flow separation task (not used). The parameter $\phi_{i,k,l}$ is the blending factor, defining the quantities of raw materials from different locations: since the supply chain optimization feature is not needed in this location, the equation is not considered.

The parameter definition process is assisted by the graphical interface of Super-O, which generates a Microsoft Excel spreadsheet storing the entire set of input data for the superstructure generation and optimization problem.

3.1.3 - MILP problem structure

The general formulation of a mixed-integer nonlinear problem of optimization is the following:²³

$$\begin{aligned} \min_{y,x} \quad & z = f(x, y) \\ \text{s.t.} \quad & \begin{cases} h(x, y) = 0 \\ g(x, y) \leq 0 \\ x \in \mathfrak{R}^n, y \in \{0,1\}^m \end{cases} \end{aligned} \quad \text{Eq. 3.33}$$

Where, z is the objective function value ($z \in \mathfrak{R}$), $h(x,y)$ is a set of linear or nonlinear equality constraints, and $g(x,y)$ is a set of linear or nonlinear inequality constraints, which determines the feasible region of the problem. The variables are continuous or integer, in the specific case integer-disjunctive as y can assume only the values 1 or 0.

Provided that the problem equations are linear, as shown in the previous section, the problem becomes a mixed-integer linear problem with disjunctive variables, which can be written as:

$$\begin{aligned} \min_{y,x} \quad & z = c^T y + p(x) \\ \text{s.t.} \quad & \begin{cases} h(x) = 0 \\ g(x, y) = Ax + By + c \leq 0 \\ x \in \mathfrak{R}^n, x \geq 0, y \in \{0,1\}^m \end{cases} \end{aligned} \quad \text{Eq. 3.34}$$

The advantage of solving a MILP is that:

1. Inequalities can be transformed into equations introducing new “slater” variables:

$$x_1 + x_2 \leq 2 \rightarrow \begin{cases} x_1 + x_2 + s = 2 \\ s \geq 0 \end{cases} \quad \text{Eq. 3.35}$$

2. The feasible region is convex, therefore the solution exists and is unique.
3. Linear problems are solvable in polynomial time.

In facts, a set of linear constraints determines a polyhedron-shaped feasible region F and the solution lays on an extreme of F . Commercial codes as XPRESS, GUROBI, and CPLEX, the one used for the solution of the superstructure problem, implement the SIMPLEX algorithm or the “barrier interior point method” for the solution of such

problems. The computation time can be reduced using some relaxation formulation of the problem: since the MILP of the generic interval model is further simplified by the use of only disjunctive integer variables, the big-M formulation has been used. A disjunctive condition means that a set of constraints can be either active or inactive, therefore the inactive ones can be relaxed, i.e. written in a way that the equation is always true. Given a set of disjunctive constraints D :

$$\underline{\vee} [A_j x \leq b_j] \quad j \in D \quad \text{Eq. 3.36}$$

Where $\underline{\vee}$ is the logical operator EXOR (mutually exclusive OR), the problem can be relaxed by writing it in the following way:

$$\begin{cases} A_j x \leq b_j + M_j (1 - y_j) \\ \sum y = 1, y_j = \{0,1\} \end{cases} \quad \text{Eq. 3.37}$$

That is

$$\begin{aligned} A_j x \leq b_j &\rightarrow \text{active} \\ A_j x \leq b_j + M &\rightarrow \text{inactive} \end{aligned} \quad \text{Eq. 3.38}$$

The equation for the inactive constraint is always respected for sufficiently big values of M : the relations are kept in the problem but relaxed to be always respected. A simple graphical representation is reported in Figure 3.4.

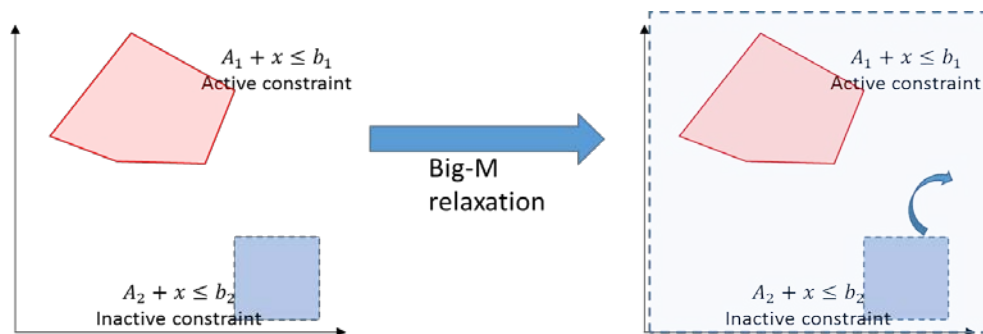


Figure 3.4 - The feasible region is multiplied by a big factor M so to contain also the polyhedron determined by the active constraint

3.2 - Process Superstructure development and assumptions

This section addresses in detail the problem definition and solution for the renewable adipic acid case-study, corresponding to the first two of the three steps of the methodology, namely “problem formulation” and “superstructure generation and data collection”.

The main purpose of the optimization problem solution is the definition of the optimal process configuration, from an economic perspective. The objective functions considers the annual incomes from the product sales and the annual expenditures, related to both capital investment and operating costs (utilities and consumables), formulated as the Economic Potential of Douglas.¹

Since the most updated open-source market analyses are referred to 2014, this year has been chosen as a reference. The economic potential is used to calculate the production cost of adipic acid, which allows calculating and analyzing the profitability of the process.

The generated processing routes are evaluated against the traditional process in terms of the following three environmental indexes: energy required in MJ/kg adipic acid; direct CO₂ emissions (also associated to the energy consumption) in terms of kg CO₂/kg adipic acid; and water consumption in kg H₂O/kg adipic acid.²⁴ Also, the processing routes are assessed in terms of Aquatic Toxicity Potential (ATP), Terrestrial Toxicity Potential (TTP) and Human Toxicity Potential by Exposure (HTPE), which will be calculated through the WAR algorithm.²⁵

In terms of feedstocks and products, two different feedstocks are considered (benzoic acid and glucose) and one product (polymer grade adipic acid). The route is the two step conversion, with a first bio-catalytic transformation of the feedstock to achieve the intermediate *cis,cis*-muconic acid, followed by the catalytic hydrogenation of the intermediate to adipic acid. To reduce the boundaries of this investigation, the availability of renewable feedstocks of lignocellulosic origin is assumed.

In order to use the generic model of Quaglia et al.¹⁷, model parameters are provided for each interval, which are either fixed from the analysis of known process data or estimated

from generated process data. These data can be derived from manuals, technology solutions from similar processes, analogy principles and general material balances.² However, some data may be inaccessible because they are proprietary knowledge or may be too uncertain. In these cases, assumptions are made to obtain a fixed variable value, provided that the estimates can be sufficiently motivated; otherwise, the technology is not included in the network. The cost functions associated to each interval are determined from cost information retrieved from industrial sources, process equipment correlations for level 4 estimates and general utilities cost correlations.^{26,27} For the capital cost annuity estimation, an investment duration of 10 years and a MARR (minimum attractive rate of return) of 7% is considered.² When performing conceptual estimation, the accuracy of the calculated economic potential is around $\pm 30\%$. This accuracy is sufficient to quantify the potential of the sustainable adipic acid biorefinery and to rank the alternative routes.

The generated processing routes are compared under varying design constraints, such as, product price, feedstock price, plant size, strain yield, etc. The different values that these aspects can assume determine different scenarios: the problem solution is repeated for each of the listed scenarios.

Base case scenario

The base case solution considers a plant for 10,000 metric ton/year of adipic acid, located in North America, with an annual productivity of 8150 h. This scenario is identified in the results as SC_1.

Scenario with varying product (adipic acid) price

The following values from 2014 are considered, based on different locations: 1.60 \$/kg for North America (lower bound), 2.61 \$/kg for South America (upper bound), 1.94 \$/kg and 2.28 \$/kg (intermediate values). Note that the high price for South America is due to the anti-dumping resolution approved by the government of Brazil in December 2013.²⁸ These four price values are identified with the letters a, b, c, d respectively and are combined with the other scenarios (e.g. SC_1_a, SC_1_b ...).

Scenario with varying feedstock (glucose) price

The price of glucose from 2014, varies with location too, which is taken into account through different values: 0.428 \$/kg for North America²⁹, 0.210 \$/kg in South America

(Brazil), close to sugarcane mills.³⁰ The former price is considered in the base case scenario, while the latter is used for all the other scenarios.

Scenario for varying plant size

In order to get closer to the recommended size for a commodity chemical biorefinery, a capacity of 200,000 ton/year, corresponding to 20-fold the base case size, is considered as well.³¹ This scenario is identified as “SC_3”: this size is comparable to a medium sized plant for petrochemical-derived adipic acid. The base-case scenario is sufficiently small to not consider raw-material supply chain. Existing bio-gas plants distributed in rural areas have similar order of magnitude of feedstock requirement, either from first or second generation biomass.³² The 200,000 ton/year plant would require instead around 950 kton/year of glucose, which is equivalent to a large scale sugarcane mill in Brazil or a sawmill in US, assuming second generation biomass use.³³ The optimal size of the plant according to the local feedstock availability is not covered in this work.

Scenario for varying strain yield and product concentration

More favorable values have been assumed for fermentation yield and product concentration. This is done to determine which of these has the biggest impact on the solution and should, therefore, be targeted by future research. In the results, SC_4 assumes a higher product concentration (+30%), SC_5 a higher bioconversion selectivity, SC_6 the combination of both higher selectivity and concentration.

For the adipic acid case study, the obtained superstructure is represented in a graphically simplified version in Figure 3.5. It contains 19 processing steps with a total of 40 processing intervals (unit operations), while steps I and XIX correspond to feedstock and product. The actual superstructure treated by the optimizer is reported in APPENDIX 4. In fact, as the flow rates and the model parameters for the two different biological routes are different, two intervals for each operations must be modeled, one for *E. coli* process conditions and one for *P. putida*. The following paragraphs report in detail the process parameters included in the interval models for both the routes.

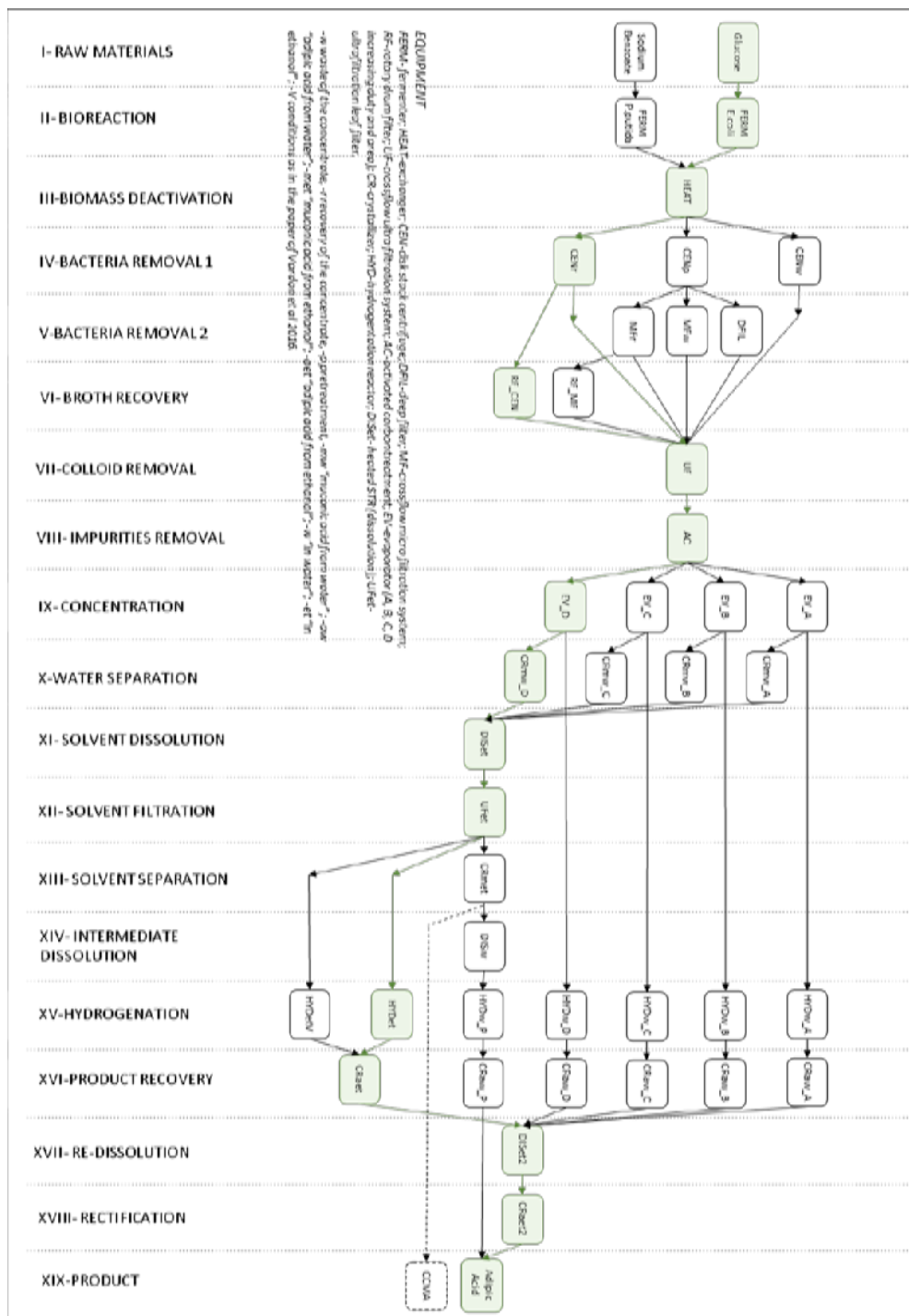


Figure 3.5 - Simplified superstructure for process synthesis and design of a renewable two steps adipic acid process.

3.2.1 - Raw Materials and Component list (processing step I)

The component list included in super-O with the associated information on MW and price is reported in Table 3.1. Four types of components can be identified:

- The “raw-materials” (benzoic acid and glucose), whose flow rate is specified as input parameter (f^{RAW}). The streams of the following units are calculated from this values.
- The “chemicals”, that take part to the reactions modelled in the intervals (MW is provided). They may be raw materials or chemicals added by the task mixer.
- The “pseudo-components”, that do not take part to the reactions and are treated as inert compounds throughout the chain of transformations (can be separated/removed).
- The “products”, whose flow rate is used to calculate the revenues.

The engineered *E. coli* and *P. putida* strains, which express the two fermentation routes considered in this work, need the addition of a growth support to sustain the increasing number of cells during lag and exponential phase. For *P. putida* the support is glucose, in the amount of ca 20 g/L of broth, according to the fermentation conditions of Vardon et al.³⁴ For *E. coli* the growth support is a complex mixture of glucose, vitamins and aminoacids, reported in Table 3.2, which the engineered bacteria are no more able to synthesize.⁴⁴

Table 3.1 - List of the components (RM = raw materials, C component, P product, PC pseudo component)

#	Component	MW	Cost [\$/kg]	Notes
1	Glucose	180 RM	0.210- 0.428	²⁹
2	NaBenzoate	144 RM	1.400	³⁵
3	Muconic Acid	142 C	-	
4	NaMuconate	164 C	-	
5	Na ₂ Muconate	186 C	-	
6	Adipic Acid	146 P	1.600	³⁶
7	Na ₂ Adipate	190 C	-	
8	H ₂ O	18 C	-	
9	O ₂	32 C	-	
10	CO ₂	44 C	-	
11	NaOH	40 C	0.200	³⁵
12	H ₂	2 C	3.615	³⁷ Electrolysis, 53kWh/kg
13	HCl	36 C	0.240	³⁵
14	NaCl	58 C	-	
15	EtOH	46 PC	1.105	³⁵
16	Biomass	- PC	-	
17	Colloids	- PC	-	
18	Impurities	- PC	-	
19	GSupPP	- PC	0.925	See paragraph 3.2.1
20	GSupEC	- PC	1.340	See paragraph 3.2.1
21	Air	- PC		
22	Kieselguhr	- PC	1.069	³⁸
23	Washing water	- PC	7.64e-4	³⁸
24	Activated Carb	- PC	0.60	³⁹ See paragraph 3.2.8

Table 3.2 - Growth support composition for *E. coli* fermentation

Component	Amount [kg/L of broth]	Cost of [\$ /kg]	Notes
Glucose	1.00E-2	0.428	29
L-phenylalanine	4.00E-05	298	40
L-tyrosine	4.00E-05	298	40
L-tryptophan	4.00E-05	990	40
p-hydroxybenzoic acid	1.00E-05	30	40
K p-aminobenzoate	1.00E-05	13.6	25 kg of batch 41 *
2,3-dihydroxybenzoic acid	1.00E-05	931	42

The cost indications reported are mere estimates, in absence of more detailed bulk information. The numbers in fact refer to larger scale laboratory supply. In industrial biotech applications the purchase of certain growth support is typically undergone to make or buy evaluations, and the actual production prices remain confidential. The averaged price of the growth support in Table 3.1. (0.925 \$/kg for *P. putida* and 1.380 \$/kg for *E. coli*) considers also the price of M9 minimal medium, which is the mixture of salts of the buffer solutions, source of the macronutrient phosphorus and nitrogen. M9 contains Na₂HPO₄, KH₂PO₄, NH₄Cl, and NaCl in the amounts of 1.36 g/L, 0.6 g/L, 0.2 g/L, and 0.10 g/L respectively: the prices are taken from ICIS tables.³⁵

3.2.2 - Bioreaction (step II)

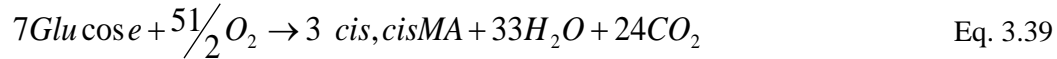
This step involves the conversion of either glucose or benzoic acid to *cis,cis*-muconic acid. The interval “FERM-*E. coli*” employs glucose as the feedstock and represents the biosynthetic pathway expressed in the genetically engineered strain of *E. coli* WN1/pWN2.248, which can accumulate up to 59.22 g/L of *cis,cis*-muconic acid.⁴³ According to the metabolic scheme identified by Niu et al.⁴⁴, this strain of *E. coli* can produce three *cis,cis*-muconic acid molecules per seven glucose molecules, that is 0.43

moles of acid per mole of glucose. The conversion modelled in this interval achieves 0.304 mol/mol, which corresponds to a 71% selectivity with respect to the maximum of the metabolic pathway.⁴³ These performances are the best published so far, and exceed the results of Niu et al. applied in a previous feasibility study.⁴⁵

The second interval, “FERM-*P. putida*” employs benzoic acid as the feedstock to also produce *cis,cis*-muconic acid with an engineered strain *P. putida* KT2440, which accumulates 26.3 g/L of *cis,cis*-muconic acid.³⁴ A yield up to 1 mol of *cis,cis*-muconic acid from 1 mol of benzoic acid can be achieved from this metabolic pathway, with lab-scale applications that reached the 94% of this limit, as modelled in the interval.⁴⁶ Both fermentations are performed at neutral pH, and the product is found in its salt form: the neutralization reaction with NaOH is therefore included in both intervals. The cell propagation and accumulation costs (in terms of carbon source, macro-nutrients and amino acids) are accounted separately, as “growth support expenditures” (see supplementary material), and are considered an unavoidable operating expenditure.

In the intervals model the tasks of mixer, reactor and waste are activated.

The mixing step considers the addition of the species involved in the bio reaction, which converts the feedstock (glucose or benzoic acid) into *cis,cis*-muconate salts according to the pseudo-stoichiometric coefficients of the equations derived in Paragraph 2.2.3.



for *E. coli* and



for the *P. putida* strain.

Also, the mixer considers all the other pseudo-components involved in the actual fermentation (growth supports, biomass, colloids and impurities) to maintain the representativeness of the material balances, even though they do not take part to the pseudo-reaction implemented in the interval. The mixing ratio for the reacting species can be calculated as

$$\mu = \frac{v_x}{v_{\text{reac}}} \frac{PM_x}{PM_{\text{reac}}} \quad \text{Eq. 3.41}$$

where v_x and PM_x are the stoichiometric coefficient and the molecular weight of the co-reactants while v_{reac} and PM_{reac} are the ones of the reference compound. The mixing ratios

for the other species are calculated according to the final concentrations reported in the reference literature.

Table 3.3 - Fermenter mixing ratios

Interval: FERM.			
Description: Fermenter			
Mixing ratio μ [kg/kg reference compound]			
	P. putida	E. coli	Note
O₂	5	5	Ref. to NaBenz and gluc respectively (excess)
H₂O	37.4	17	Ref to NaMuc
NaOH	0.25	0.58	Ref to NaMuc and MucAcid respectively
Biomass	0.0378	0.022	Ref to H2O
Colloids	0.005	0.005	Ref to H2O
Impurities	ppm	ppm	Ref to H2O
Support	0.732	0.01143	Ref to NaBenz and H2O respectively

Biomass, Colloids, and Impurities act as inert in the framework of the interval modelling, therefore their amount do not affect substantially the results. Colloids comprise a class of sub-micron particles of different origin (as cell debris, macro-proteins, etc.) and require specific treatments for the removal (addressed in step VII): the concentration assumed in this work is derived from the indications of Van der Sman et al.⁴⁷ Similar considerations hold for the “impurities” class, which are trace components that can give residual colour to the final product even if in part per million (addressed in step VIII).

As for the waste task, the reactor considers the removal of the 100% of the excess reactants, of the water produced in the reaction and of the CO₂. This simplification adapts the fed-batch operation of the real fermenters to the standard steady-state model of the interval, which does not support other operation modes.

The capital cost function for this interval is derived assuming an air-lift fermenter, provided the suitability of this technology to large scaled up application and the availability of detailed cost information. Due to the rather low productivities of the bacteria considered in

this study, 0.27 kg/m³/h for *P. putida* and 0.67 kg/m³/h for *E. coli*, the target production of 10,000 metric ton/year of adipic acid requires fermentation volumes of the order of 5000 m³ and 2000 m³ respectively. As a first estimate, a system of parallel reactors is assumed, each of 1000 m³ (e.g. diameter 4 m, height 60 m, aspect ratio 15). For common biotechnology applications this volume is remarkable (100 m³ is already considered “big”), however low added value fermentations are normally carried out in very large scale systems, as biogas or ethanol anaerobic fermentations. Big aerated fermenters with the same scale assumed in this work have been successfully employed for succinic acid fermentations.⁴⁸ A techno economic analysis performed on the same fermentation of this study assumed even bigger fermenters, of the size of 3800 m³.⁴⁹

Following the indication of the paper of Moresi⁵⁰, the investment cost for a 1000 m³ fermenter is 870,000 \$ (value updated to 2014, with CEPCI indexes as explained in paragraph 3.2.20), and the power required for the compression and the circulation of the air is 3.5 kw/m³.

The implemented cost function, which needs to be proportional to the interval flow rate [kg/h], is reported in Table 3.4. The equation is the same for both the fermentation routes, as parallel identical fermenters cover the required volumes (linear correlation cost-size).

Table 3.4 - Fermenter cost function [\$(2014)/kg: reference stream *fM*]

Interval: FERM.		
Description: Fermenter		
Cost Function		
	<i>P. putida</i>	<i>E. coli</i>
Cost function (\$2014)	$y = 49.93 x$	$y = 49.93 x$

Fermenters are characterized by a relevant consumption of steam, necessary for the equipment sterilization after the broth discharge. The utility consumption table (Table 3.5), is compiled applying the 6/10 rule.⁵¹

Table 3.5 - Fermenter utility consumption ratios.

Interval: FERM.							
Description: Fermenter							
Utility consumption ratio β [unit/kg reference compound]							
UTILITIES	<i>P. putida</i>			<i>E. coli</i>			Note
	β_1	β_2	β_3	β_1	β_2	β_3	
EL_PO	4.59e-1			2.0e-1			Ref to H ₂ O
ST_LP	5.67e-2			5.67e-2			Ref to H ₂ O

3.2.3 - Biomass deactivation (step III)

This step contains a single interval, representing a heat exchanger, which brings the raw fermentation broth at 80 °C. The thermal treatment on the fermentation broth has three different effects. The first is the deactivation of the bacteria. Increasing the temperature to 80 °C induces the pasteurization of the fermentation broth, preventing any pathogenic risk. The second is the coagulation of the proteic material present in the fermentation broth, which can be later removed via filtration.⁵²

The third effect is to promote the spontaneous isomerization of *cis,cis*-muconate salts to *cis,trans*-muconate, as reported in the equation:²⁰



The reaction is complete at 60 °C for 1.25 h at pH 4. The amount of HCl to be added to reduce the pH in the fermentation buffer (Table 3.6) is estimated applying the virtual titration tool CurTiPot.⁵³ The selected equipment is a simple heat exchanger: the only indication is that the thermal treatment should be no longer than 20 min.⁵⁴

In fact, it has been evidenced that muconic acid undergoes to lactonization reactions when kept at 80 °C for periods of the order of hours: this occurrence should be avoided, in order to prevent a decrease in the process selectivity.⁵⁵ A complete isomerization is important to have homogeneous crystallization conditions in the downstream recovery steps.

Table 3.6 - Heat exchanger mixing ratios.

Interval: HEAT			
Description: Heat exchanger			
Mixing ratio μ [kg/kg reference compound]			
	<i>P. putida</i>	<i>E. coli</i>	Note
HCl	0.0072	0.0072	Ref to H ₂ O

Table 3.7 - Heat exchanger cost function [\$(2014)/kg: reference stream fM]

Interval: HEAT		
Description: Heat exchanger		
Cost Function		
	<i>P. putida</i>	<i>E. coli</i>
Cost function (\$2014)	$y=9.54 x^{0.85}$	$y=18.865 x^{0.79}$

The utility consumption is calculated with a simple energy balance:

$$\dot{m}_{ST_LP} \lambda_{ST_LP} = \dot{m}_{Broth} c_p \Delta T \quad \text{Eq. 3.43}$$

The consumption of low pressure steam for heating is reported in table Table 3.8.

Table 3.8 - Heat exchanger utility consumption ratios.

Interval: HEAT							
Description: Heat exchanger							
Utility consumption ratio β [unit/kg reference compound]							
UTILITIES	<i>P. putida</i>			<i>E. coli</i>			Note
	β_1	β_2	β_3	β_1	β_2	β_3	
ST_LP	9.51e-2			9.51 e-2			Ref to H ₂ O

A final benefit from the higher broth temperature is a lower viscosity, which reduces the pumping costs of the immediate downstream reactions.

3.2.4 - Bacterial Removal 1 (step IV)

This processing steps has three intervals which represent different operating conditions for centrifugation. The raw fermentation broth contains 37.8 g/L and 22 g/L (dry weight) of biomass in the *P. putida* and in the *E. coli* fermentation, respectively. These amounts are too high for being processed economically by membrane filters or kieselguhr, while are suitable for centrifugation.⁵¹ Disk stack centrifuges are the usual choice for high density strain-sensitive fermentation broths. The optimal design of an industrial clarification centrifuge depends on many parameters, which have to be empirically characterized case by case. In absence of these data, a case-study available for *E. coli* selects the Alfa Laval BTPX series centrifuges.⁵⁶ Similar filtration behavior between *E. coli* and *P. putida* are assumed. According to the case study, the complete removal of solids is achieved with a broth recovery of the 90%. This means that the 10% of the broth is diverted to the solid accumulation stream: this slurry can be further processed to recover part of the lost product, otherwise can be treated as a waste. CENw interval implements this latter option, where the 100% of the bacteria and the 10% of the other components are removed as “waste”. CENr models the same performance of separation of CENw, but uses the separation task of the interval. The 100% of the bacteria and the 10% of the other stream components are sent to the secondary stream leaving the interval, which is connected to the downstream operation RF_CEN (process step VI), allowing a partial recovery of the broth. To scale up the case study (performed on BTPX 210, 1.2 m³/h max feed), the same proportion between nominal flow rate and maximum feed flow rate is assumed for the biggest scale BTPX model (BTPX720 10 m³/h max feed throughput).⁵⁷ The number of required units is then calculated as a function of the target productivity. The utility consumption is derived from the technical datasheet. For the equipment purchase cost, the reference is the Perry handbook (180 k\$ in 2004), as for this type of technologies producers are reluctant to provide detailed information. Since the centrifuge system is in parallel the aggregated cost function becomes linear (*Table 3.9*).

Table 3.9 - Centrifuges cost function [\$(2014)/kg: reference stream fM]

Interval: CENw and CENr		
Description: Disk stack centrifuge. Solid waste and Solid recovery		
Cost Function		
	<i>P. putida</i>	<i>E. coli</i>
Cost function (\$2014)	$y=181.37 x$	$y=181.37 x$

Table 3.10 - Utility consumption ratios

Interval: CENw and CENr							
Description: Disk stack centrifuge. Solid waste and Solid recovery							
Utility consumption ratio β [unit/kg reference compound]							
UTILITIES	<i>P. putida</i>			<i>E. coli</i>			Note
	β_1	β_2	β_3	β_1	β_2	β_3	
EL_PO	1.2e-2			1.2e-2			Ref to H ₂ O
CO_WA	3.6e-1			3.6e-1			Ref to H ₂ O
AI_CO	1.2e-3			1.2e-3			Ref to H ₂ O

A third centrifugation alternative is represented by CENp interval. When operating a centrifuge, the nominal throughput can be increased at expenses of the separation performance: the optimal condition is function of several factors as broth filtration properties, energy consumption, productivity, downstream requirements. CENp represent a pre-treatment centrifugation, which allows the removal of only the 90% of the solids but achieves a well de-watered bacterial slurry.

Still the 63.6% of the weight for *P. putida*⁵⁸ and the 68.2% for *E. coli*⁵⁹ are due to water. The product recovery yield is assumed to be of the 94% and 95.7% for *P. putida* and *E. coli* respectively: the broth waste factors are 6% and 4.3% for the broth and 90% of the bacteria. The maximum solid throughput of the BTPX720 is used to calculate the number of centrifuges required.⁵⁷

Table 3.11 - Centrifuges cost function [\$(2014)/kg: reference stream fM]

Interval: CENp		
Description: Disk stack centrifuge. Pretreatment		
Cost Function		
	<i>P. putida</i>	<i>E. coli</i>
Cost function (\$2014)	y=66.14 x	y=66.14 x

Table 3.12 - Centrifuges utility consumption ratios

Interval: CENp							
Description: Disk stack centrifuge. Pretreatment							
Utility consumption ratio β [unit/kg reference compound]							
UTILITIES	<i>P. putida</i>			<i>E. coli</i>			Note
	β_1	β_2	β_3	β_1	β_2	β_3	
EL_PO	4.3e-3			4.3e-3			Ref to H2O
CO_WA	1.29e-1			1.29e-1			Ref to H2O
AI_CO	4.3e-4			4.3e-4			Ref to H2O

An important assumption for this and for the following processing steps is that the waste stream is not accounted as a cost for the process. The big amounts of biomass produced are unlikely to be treated as simple waste sludge: in the worst case, the deactivated slurry can be fermented for bio-gas production, which can compensate the expenditures for the treatment. However, spent fermentation biomass can also become a source of the amino acids for the fermentation: the hydrolysis /recovery costs would be compensated by the savings from the growth support purchase.⁶⁰ Another option, which requires further studies, is to use the biomass as animal feed.⁶¹

3.2.5 - Bacterial Removal 2 (step V)

The clarification of low-density fermentation broths (1% volume fraction or ca 5 g/L dry weight) is performed conveniently with deep filtration and cross-flow microfiltration, which have been modelled in this processing step.^{51,62} The former is a consolidated and cheap technology for beer filtration: an industrial case of beer filtration with Filtrox® candle filters with kieselguhr (200,000 m³/year throughput) is adapted to the case of adipic acid production, using the 6/10 rule.³⁸

From the detailed information in the case study it is possible to know the utility consumption, summarized in *Table 3.15*. The utilities (electric power and steam for sanification) and chemicals (diatomaceous earth and washing media) consumption per kg of filtrate are taken from Filtrox case study. There is an indication also on the disposal cost of the filtration media, which is 1/10 of the purchase cost. In the interval model, both the kieselguhr and the washing media are added (mixing task) and removed (waste task). The interval model assumes 100% of residual bacteria removal and 4% of broth loss.

Table 3.13 - Deep filter mixing ratios

Interval: DFIL			
Description: kieselguhr (diatomaceous earth) candle filter			
Mixing ratio μ [kg/kg reference compound]			
	<i>P. putida</i>	<i>E. coli</i>	Note
Kieselguhr	1.1e-3	1.1e-3	Ref to H ₂ O
WashM	1.44e-4	1.44e-4	Ref to H ₂ O

Table 3.14 - Deep filter cost function [\$(2014)/kg: reference stream fM]

Interval: DFIL		
Description: kieselguhr (diatomaceous earth) candle filter		
Cost Function		
	<i>P. putida</i>	<i>E. coli</i>
Cost function (\$2014)	$\gamma=4107.6x^{0.66}$	$\gamma=4107.6x^{0.66}$

Cross flow filtration via micro-porous membranes is ubiquitous in bioprocesses, but the tools for conceptual design and predictive modelling are yet hard to find, if not completely missing.

Crossflow filtration applications cannot be easily adapted as done for deep filtration, due to the complex relations between operating variables and filtrate properties, which involve non trivial trade-offs between costs and performances. For the estimate of the MFr and MFw parameters, analogous in terms of performances and costs, the model developed in Chapter 4 is used.⁶³

Table 3.15 - Deep filter utility consumption ratios

Interval: DFIL							
Description: kieselguhr (diatomaceous earth) candle filter							
Utility consumption ratio β [unit/kg reference compound]							
UTILITIES	<i>P. putida</i>			<i>E. coli</i>			Note
	β_1	β_2	β_3	β_1	β_2	β_3	
EL_PO	1e-3			1e-3			Ref to H ₂ O
ST_LP	1.68e-3			1.68e-3			Ref to H ₂ O

Four main variables determine the overall permeate flux, hence the size of the filtration unit:

- Membrane geometry and pore size: microfiltration for cell harvesting goes from 0.1 μm to 0.45 μm . This results in quite different initial values of permeate, that are reflected by different steady state fluxes (and plant size & costs). Ceramic membranes are preferable for their durability, the cheapest and scalable geometry is the extruded monolith. Commercial ceramic membranes of the market leader Kerasep are used as reference.
- ΔPTM or Transmembrane Pressure: it is the pressure difference between retentate side and permeate side of the membrane and the driving force of separation. 2-3 bar are often indicated for the bigger pores membrane, while Kerasep modules indicate 6-10 bar as the best ΔPTM for their 0,1 μm membranes.

- Cfv or Crossflow velocity: is the most important variable for preserving the performances of filtration. Velocity should maintain a turbulent flow so that the shear rate prevents the deposition of a cake of bacteria on the membrane and reduces the height of polarization layer. Caking and polarization are in fact the main reasons for permeate flux reduction. Higher velocities enhance filtration duration, but increase dramatically the cost of recirculation pumping, due to bigger fluxes and higher pressure drops. The minimum crossflow velocity is 2 m/s in small hydraulic diameters (2 mm) as for these industrial membranes, even if higher fluxes are advisable. This because most of bacterial suspension have a pseudo-plastic rheology, that means the higher the shear the lower the viscosity. For the bio-adipic acid case study 3-4 m/s are the reference values. This value allows considering 20 hours of filtration exercise followed by 4 hours of cleaning-regeneration.
- CF concentration factor: a dilute cell content corresponds to less fouling and higher permeates, but also reduces recovery ratios. If the cell concentration is not allowed to increase too much in the retentate, high amounts of water and valuable solutes are lost. In continuously operated plants (feed and bleed systems) the cell concentration output can be very high, but depends on the properties of the microorganism (rigid cells vs gelatinous-compressible) and on the scale of the operation. For medium-small batches of high value products, as in pharma industry, high concentrations are attained at higher expenses due to low fluxes and frequent cleaning, even with the use of diafiltration technique. The interval modelling will consider a CF of 20, which corresponds to a broth recovery of 95%, with 100% removal of the residual biomass.

The conditions summarized in table Table 3.16 are simulated for the 2 distinct broths, after the first centrifugation.

Table 3.16 - Process conditions for cross flow filtration units implemented in the model.

Variable	Units	<i>P. putida</i>	<i>E. coli</i>
Cross flow velocity	[m/s]	4	4
Transmembrane pressure	[Pa]	8	8
Concentration factor (95% rec)	[-]	20	20
Duration of a filtration cycle [h]	[h]	20	20
Cleaning time [h]	[h]	5	5
Inlet cell concentration [g/L]	[g/L]	3.78	2.2
Feed throughput [m ³ /h]	[m ³ /h]	44.1	25.8

A single filtration unit consists of 2 modules Kerasep® K99 in series, which contain each 99 monoliths BK-Kompact® (49.5 m² of filtration area.). Each monolith contains 44 squared channels with 2.2 mm of hydraulic diameter and 1178 mm of length.

Each unit is provided with a circulation pump (DP 3 bar, flow rate ca. 230 m³/h), while 6 units are provided a fresh feed pump (DP 8 bar, flow rate ca. 70 m³/h)

The model simulates the fouling mechanism of the membrane, due to polarization resistance and caking (*E. coli* is considered as a reference for the filtration, *P. putida* has similar behaviour) and calculates the average permeate flux for each filtration. The average flux allows to calculate the total area required and the number of units. A cost function is implemented in the algorithm: a linear correlation between installation cost and throughput is achieved, given the equipment modularity.

Table 3.17 - Cross-flow filters cost function [\$(2014)/kg: reference stream fM]

Interval: MFw and MFr		
Description: Cross-flow microfiltration. Solid waste and Solid recovery		
Cost Function		
	<i>P. putida</i>	<i>E. coli</i>
Cost function (\$2014)	y=94.89x	y=68.63x

Table 3.18 Cross-flow filters utility consumption ratios

Interval: MFw and MFr							
Description: Cross-flow microfiltration. Solid waste and Solid recovery							
Utility consumption ratio β [unit/kg reference compound]							
UTILITIES	<i>P. putida</i>			<i>E. coli</i>			Note
	β_1	β_2	β_3	β_1	β_2	β_3	
EL_PO	2.69e-2			2.59e-2			Ref to H ₂ O

The only difference between MFr and MFw is in the disposal of the retentate fraction: in the first the retentate is recovered as a secondary stream, which goes to RF_MF, in the second the retentate is wasted. The considerations provided for CENr and CENw hold also for this case.

3.2.6 - Broth Recovery (step VI)

This step contains two units capable to recover part of the broth (and dissolved product) otherwise wasted in the treatments of the previous clarification units. Both intervals model a rotary drum filter, suitable for concentrated slurries: RF_CEN is connected to CENr (step IV), RF_MF to MFr (step V). The previous published process concepts for *cis,cis*-muconic acid production assumed a simpler one-step centrifuge without any recovery.^{49,64} Every time the cells are separated from the fermentation broth as a “solid” cake in the centrifuge CENw, a consistent part (100-36.4% *P. putida*) and (100-31.8 % *E. coli*) of their weight is still given by the fermentation broth. This reduces to 95% the maximum recovery of the first centrifugation step.

Similarly, assuming a CF=20 (concentration factor) in the microfiltration unit, we achieve a 95% of recovery. 5% of the liquid flow rate during filtration is “lost” in the retentate, which has an output concentration of twice the initial cell concentration (75.6 and 44.0 g/L for *P. putida* and *E. coli* respectively). For example, the volume of the filtered broth is of the order of 2.25 m³/h, with a loss of 632 ton/year of the target product.

The equation to calculate the area of a rotary drum filter is taken from Harrison et al.²⁹:

$$A = \frac{1}{\Psi_f} \left[\frac{\mu_0 \cdot \alpha \cdot \rho_c \cdot V^2}{2 \cdot \Delta P \cdot t} \right]^{0.5} \quad \text{Eq. 3.44}$$

Where μ_0 is the viscosity of the filtrate = $1e-3$ kg/m/s

$\alpha = \alpha_0 \cdot \Delta P^{0.51}$ is the specific cake resistance = $2.73e10 * 6.67e4^{0.51} = 7.88e12$ m/kg, using the parameters valid for *E. coli* available in literature.⁶⁵

$\rho_c = \rho_{wet_cell} \cdot (1 - \varepsilon_c)$ is the cake density = $1220(1-0.364) = 775.92$ kg/m³ for *P. putida* and = $1160(1-0.318) = 791.12$ kg/m³ for *E. coli*

$V = \dot{V} \cdot t$ is the volume of filtrate produced the filtration time = $2.25/3600 * 18 = 0.01125$ m³

ΔP is the suction prevalence, assumed to be 500 torr (66.66 kPa)

t is the filtration time assumed to be the 30% of the duration of a cycle that is 18 s.⁵⁴

Ψ_f is the fraction of the cycle time devoted to filtration.

Together these values result in an active total area of 57 m² for *P. putida*, 34 m² for *E. coli*.

The investment is calculated using the correlations in Couper et al:⁵⁴

$$PurCost_{RDF} = CI \cdot 10.76 \cdot 1.218 \cdot \exp\left\{1.27 + 1.38 \cdot \log(A) + 0.0709[\log(A)]^2\right\} \quad \text{Eq. 3.45}$$

Where A is in m², CI is 1.103 and the installation factor is 1.4. Since the area is function of the volume of filtrate, there is a direct relation between investment and the inlet water flow rate, determined by the separation in the crossflow filter.

The operation costs derive mainly from the electric consumption of the rotation drive, the stirrer in the feed tank, and the suction pump. The first two contributions is estimated in 6 kW cumulated, according to the technical datasheet of the manufacturer Andritz AG.⁶⁶

The vacuum pump requirement is calculated with the following relation.⁶⁷

$$P = \frac{1}{\eta_{iso}} \frac{1}{27 \cdot 10^3} P_{vac} \cdot \tilde{V}_{air} \cdot A \cdot \ln \frac{P_{out}}{P_{vac}} \quad \text{Eq. 3.46}$$

where η_{iso} is the optimal isothermal efficiency, comprised between 0.25 and 0.40 (assumed 0.32)

P_{vac} is the suction prevalence in mmHg (508 = 66.66 kPa)

P_{out} is the pressure of discharge (760 mmHg).

\tilde{V}_{air} is the air suction for squared meter in m³/h and is estimated in 4.25 m³/h, corresponding to the 2.5 cfm suggested by the manufacturer NFM-filter (Salt Lake City, US).⁶⁸ The power requirements are then 57 kW for *P. putida* broth and 34 kW for *E. coli*.

In both RF_MF and RF_CEN the separation is modelled setting a waste ratio, as no further treatments are assumed for the solid fraction. For the slurry coming from MFr a loss of 10% is assumed (waste task), while the loss is 50% for the other.

Table 3.19 - Rotary drum filter (microfiltration recovery) cost function [\$(2014)/kg: reference stream fM]

Interval: RF_MF		
Description: Rotary drum filter- microfiltration broth recovery		
Cost Function		
	<i>P. putida</i>	<i>E. coli</i>
Cost function (\$2014)	$y=23784.6 x^{0.611}$	$y=4246 x^{0.546}$

Table 3.20 - Rotary drum filter (microfiltration recovery) utility consumption ratios

Interval: RF_MF							
Description: Rotary drum filter- microfiltration broth recovery							
Utility consumption ratio β [unit/kg reference compound]							
UTILITIES	<i>P. putida</i>			<i>E. coli</i>			Note
	β_1	β_2	β_3	β_1	β_2	β_3	
EL_PO			2.9e-2			2.9e-2	Ref to H ₂ O

Table 3.21 - Rotary drum filter (centrifuge recovery) cost function [\$(2014)/kg: reference stream fM]

Interval: RF_CEN		
Description: Rotary drum filter- centrifuge broth recovery		
Cost Function		
	<i>P. putida</i>	<i>E. coli</i>
Cost function (\$2014)	$y=1048 x^{0.6258}$	$y=2121 x^{0.5644}$

Table 3.22 - Rotary drum filter (centrifuge recovery) utility consumption ratios

Interval: RF_CEN							
Description: Rotary drum filter- centrifuge broth recovery							
Utility consumption ratio β [unit/kg reference compound]							
UTILITIES	<i>P. putida</i>			<i>E. coli</i>			Note
	β_1	β_2	β_3	β_1	β_2	β_3	
EL_PO			2.9e-2			2.9e-2	Ref to H ₂ O

3.2.7 - Colloids removal (step VII)

The removal of the colloidal matter from the clarified filtration broth is achieved by means of ultra-filtration (UF membranes). Colloids are a class of sub-micron particles of various origin, typically composed by cell debris, proteins and DNA fractions.⁶⁹ As the UF of the pre-clarified broth of this study is not different from any preliminary UF treatment of water depuration plants, the same technology can be assumed. An extensive work of cost classification for water treatment applications is available in literature, with general correlations both for operating costs and capital costs.⁷⁰ A broth recovery factor can be considered as high as 98%.

For the operating cost the following correlation is implemented

$$C_{UF}^{OPM} (\$/1000 gal) = 0.43 \cdot Q^{-0.15} \quad \text{Eq. 3.47}$$

where Q is in mgpd and the estimate of cost is in 1996 \$.

Membrane system installed cost consider membranes, pumps, compressors, piping and valves, I&C, cleaning system. The correlation for capital costs is:

$$C_{UF}^{CAP} (\$/1000gal) = 1.29 \cdot Q^{-0.40} \quad \text{Eq. 3.48}$$

where Q is in mgpd and the estimate of cost is in 1996 \$. The cost is scaled on the plant capacity. Plant capital cost consider membrane system cost plus buildings, electrical supply and distribution, disinfection facilities, pumping, storage, without land acquisition, administration, engineering and site work.

As the operating cost correlation includes implicitly the utility consumption and the membrane regeneration, these contributions are added to the capital costs. This resulted in a general cost function, suitable for the interval model as both CAPEX and OPEX correlations are originally scaled on the plant throughput.

Table 3.23 - Ultrafiltration filters cost function [\$(2014)/kg: reference stream fM]

Interval: UF		
Description: Cross flow ultra filtration membranes		
Cost Function		
	<i>P. putida</i>	<i>E. coli</i>
Cost function (\$2014)	$y=759.45 x^{0.7186}$	$y=816.49 x^{0.712}$

3.2.8 - Impurities removal (step VIII)

The purification of a clarified broth using granular activated carbon (GAC) in packed beds or slurry reactors is often addressed as “decolorization treatment”. These removed impurities are a class of diverse compounds covering aminoacids, polyphenols, and cell debris. In spite of their variety, the impurities are removed thanks to the non-selective adsorption on the activated carbon internal surface. Decolorization steps for high scale applications are quite similar for all the bio-processes: the process specification applied for succinic acid or lactic acid can be transferred to the case of muconic acid.

Activated carbon is used by Vardon et al.³⁴ on *P. putida* fermentation broth: the concentration of GAC for the small scale application is said to be 5 g/L. This concentration

is quite low, denoting the presence of unwanted compounds outside cell membranes: concentrations as high as 20 g/L of GAC are advised in a decolorization process for succinic acid.⁷¹ The AC concentration in a slurry reactor is actually a function of the kinetics of adsorption, determined by the isotherms of the different compounds to be removed. Typically, the plants are sized according to a single target compound. In case of packed columns, the empty bed residence time is decided accordingly. To get a simple and quick cost estimation, the GAC change out rate is enough. Vardon et al.³⁴ reports a consumption of 0.145 kg GAC/kg Na muconate with an 8 L scale application, assuming that the carbon is disposed after each filtration. This would be an anti-economic choice and would impact with 0.10 \$/kg on the final product (cost of GAC 1243 \$/ton). A more consistent estimation can be derived from a patent for lactic acid industrial downstream: 77 L of concentrated broth (116 g/L of lactic acid) are filtered with a GAC packed column.⁷² The change out rate is then 0.08 kg GAC/kg acid, which allows calculating the highest contribution to the operating expenditures: the carbon substitution. It should be noted that GAC can be regenerated, with savings of the 40% on the new carbon purchase (estimate from the commercial producer CarbonCalgon). Unfortunately no information on the duration of the treatment is given: this value is necessary to know the retention time and estimate the CAPEX. An indication on this comes from wastewater treatment plants, which indicate 10-60 minutes as the span of packed bed residence time, with preferred values of 30 minutes.⁷³ In particular, moving bed absorbers are the preferred equipment to maintain a pseudo steady state operation: given the little complication of the unit, the purchase cost is assumed to be the one of a generic process vessel.³

For the bare module cost correction coefficients are used.³ The empty bed volume is calculated according to the residence time, and the value is divided by 0.66, a value of average porosity of GAC with density 550 kg/m³: the correlation provides a continuous cost estimate, even if in reality column sizes are discrete.⁷⁴

In a moving bed column, the amount of lost muconic acid is negligible: the small amount of spent carbon is rinsed with fresh water (returned to the main flux) and the adsorbed muconic acid is not relevant as shown by Vardon et al.³⁴ The consumption of utilities for this unit is negligible (all the operating costs are implicitly carried by the regenerated carbon purchase).

Table 3.24 - Activated carbon treatment mixing ratios.

Interval: AC			
Description: activated carbon treatment			
Mixing ratio μ [kg/kg reference compound]			
	<i>P. putida</i>	<i>E. coli</i>	Note
ActiCarb	8e-2	0.0072	Ref to Na ₂ Muc

Table 3.25 - Activated carbon cost function [\$(2014)/kg: reference stream fM]

Interval: AC		
Description: activated carbon treatment		
Cost Function		
	<i>P. putida</i>	<i>E. coli</i>
Cost function (\$2014)	$y=25.51 x^{0.824}$	$y=41.35 x^{0.78}$

3.2.9 - Concentration (step IX)

In step IX (Concentration), four alternative multi-effect vertical evaporators are considered, with the purpose of evaluating the tradeoff between the benefits of a more concentrated product (higher recovery and smaller downstream equipment) and costs of evaporation (utilities consumption and exchange area). EV_A implements the lowest level of concentration, EV_D the highest. It should be noted that muconic acid has three isomers (*cis,cis*; *cis,trans*; *trans,trans*) characterized by different solubilities.⁷⁵ The isomerization reaction from *cis,cis* to *cis,trans* occurs spontaneously in an acidic environment at temperatures higher than 80 °C, conditions that are found in the evaporators and during the following acidification to induce crystal formation (step X).⁵⁵ In absence of more detailed information about the actual isomers composition, and since the *cis,cis* isomer should be present in larger quantity for short treatments⁵⁵, the *cis,cis*-muconic acid solubility curves of Scelfo et al.⁷⁶ are taken as a first reference.

The design of the evaporators is tightly related to the recovery yields pursued in the downstream crystallizers.

The following relation gives the maximum product recovery in the crystallizer

$$RR\% = \frac{C^{conc} - C^{equil}}{C^{conc}} \quad \text{Eq. 3.49}$$

where C^{conc} is the concentrated broth product titer and C^{equil} is the solubility of the product in the conditions of crystallization: the higher the concentration the higher is the recovery.

Considering the evaporation step, we define CF , concentration factor as

$$CF = \frac{C^{conc}}{C^{broth}} \quad \text{Eq. 3.50}$$

where C^{broth} is the inlet broth titer.

Since the mass of all the solutes does not change during evaporation (non-volatile compounds), the following balance on the water holds:

$$\dot{m}_{H_2O}^{in} = \dot{m}_{H_2O}^{out} - \dot{m}_{H_2O}^{evap} \quad \text{Eq. 3.51}$$

Therefore the duty evaporation is calculated as

$$\dot{m}_{H_2O}^{evap} = \dot{m}_{H_2O}^{in} \left(1 - \frac{1}{CF} \right) \quad \text{Eq. 3.52}$$

The explicit relation between crystallizers and evaporators is given by

$$CF = \frac{C^{equil}}{C^{broth} (1 - RR\%)} \quad \text{Eq. 3.53}$$

As the generic interval structure does not allow introducing any of these correlation in the model (it introduces nonlinearities) four alternative evaporation conditions are hypothesized. Assuming for the cases A, B, C, D a value of water evaporation for *P. putida* broth of 55%, 65%, 75%, and 85% respectively, the subsequent maximum muconic acid recovery in the crystallizer is 91%, 93%, 95%, and 97%. For the more concentrated broth of *E. coli* the evaporation fraction is assumed in 33%, 43%, 53%, and 63%, allowing recoveries of 94%, 95%, 96%, and 97%. The evaporation rates are chosen to get a qualitative indication on the trade-off between higher costs of evaporation or higher product recovery, considering only recoveries higher than 90%, the minimum acceptable. The exact

trade-off and the optimal operation point can be identified only with further studies and detailed process design and optimization.

The design specification of the evaporators are taken from Couper et al.⁵⁴, using the indication of a thermal economy of 2.4 kg of water evaporated per kg of steam in a triple effect configuration, and a value of 3.123 kW/m²/K for the overall heat transfer coefficient. The thermal stability of the products and the use of high pressure steam ensure a temperature difference of 20 °C in each exchanger (in spite of the possible ebullioscopic rise), avoiding more expensive vacuum systems. The purchase cost correlations are taken from Aspen Capital Cost Estimator tool, assuming the installation of vertical tube falling film steel/copper evaporators. A value of 1.9 for installation factor is assumed.⁵⁴

Table 3.26 - Evaporators cost functions [\$(2014)/kg: reference stream fM]

Interval: EV_ A,B,C,D		
Description: Falling film vertical evaporators		
Cost Function		
	<i>P. putida</i>	<i>E. coli</i>
Cost function (\$2014) EV_A	$y=1230.1 x^{0.642}$	$y=563.56 x^{0.642}$
Cost function (\$2014) EV_B	$y=1369.3 x^{0.642}$	$y=1023.4 x^{0.642}$
Cost function (\$2014) EV_C	$y=1510.0 x^{0.642}$	$y=1170.4 x^{0.642}$
Cost function (\$2014) EV_D	$y=1626.5 x^{0.642}$	$y=1307.7 x^{0.642}$

Table 3.27 - Evaporators utility consumption ratio

Interval: EV_A,B,C,D							
Description: Falling film vertical evaporators							
Utility consumption ratio β [unit/kg reference compound]							
UTILITIES	<i>P. putida</i>			<i>E. coli</i>			Note
	β_1	β_2	β_3	β_1	β_2	β_3	
EV_A ST_HP	2.3e-3			1.4e-1			Ref to H ₂ O
EV_A CO_WA	6.55			3.93			Ref to H ₂ O
EV_B ST_HP	2.7e-1			1.8e-1			Ref to H ₂ O
EV_B CO_WA	7.74			5.12			Ref to H ₂ O
EV_C ST_HP	3.1e-1			2.2e-1			Ref to H ₂ O
EV_C CO_WA	8.93			6.31			Ref to H ₂ O
EV_D ST_HP	3.5e-1			2.6e-1			Ref to H ₂ O
EV_D CO_WA	10.13			7.51			Ref to H ₂ O

3.2.10 - Water separation (step X)

The intervals modelled in step X represent OSLO type crystallizers, with different operating conditions and recovery yields according to the level of pre-concentration of the input stream (CRmw_A is connected to EV_A, and so on).

The reactive muconic acid extraction proposed by Gorden et al.⁷⁷ has not been included in the superstructure, as the technology performances have not been yet confirmed for the complex matrixes of a real fermentation broths, while the fractional crystallization is applied successfully at lab scale.³⁴

In this processing step, a mixture of isomers of muconic acid is recovered by means of continuous crystallization.

Given the remarkable complexity of this unit operation, the design and costing of industrial crystallizers is typically achieved after extensive experimental investigation and piloting.⁷⁸

Therefore, any attempt of modelling is impossible at this stage, in absence of both detailed thermodynamic properties of the involved species and crystallization kinetics data. The main limitation of the state of the art knowledge are summarized:

- Almost no solubility data are available for muconic acid: only one paper addressed the problem, providing the first correlations, which are valid only for the *cis,cis* form.⁷⁶ The isomers *cis,trans* and *trans,trans* have not been investigated yet, to the best of the authors' knowledge. However there is experimental evidence that *cis,trans* and *trans,trans* are less-soluble: the available correlation will be used to produce conservative estimations.⁷⁵
- The few data available could actually fail to represent the reality of a full scale plant. In fact, the solubility curves are calculated for model solutions of the sole *cis,cis* form in water, while the real broths contain several other ionic species.
- The solubility correlations proposed by for *cis,cis*-muconic acid have been questioned, since the isomerization equilibria are probably not taken into consideration.⁷⁵
- Neither data on the kinetics of crystallization, nor the crystal characteristics are available in literature.

Some assumptions are made to achieve a first estimate for the four crystallizers performances, according to the four levels of concentration achieved in the previous step. First, the technology for the water crystallization of muconic acid is chosen in analogy with adipic acid, as they are both six carbon dicarboxylic acids.

Second, the curve for *cis,cis* muconic acid is taken as a conservative estimate. The diagram in *Figure 3.6* summarizes four solubility curves for adipic acid: the curve *cis,cis*-muconic acid, generated with the model of Scelfo et al.⁷⁶, are included. It is possible to notice how the solubility of *cis,cis*-muconic acid is lower than adipic acid, and increases slightly in a span of 15 °C (0,5 g/100 g H₂O between 25 °C and 40 °C).

The few reliable data on muconic acid solubility are summarized in Table 3.28. The useful indication derived is that *cis, trans* form is five times more soluble than *cis, cis* form while *trans, trans* form is an order of magnitude less soluble.

The higher solubility of *cis,cis* muconic acid is indirectly confirmed by the material balances on the crystallization performed by Vardon et al.³⁴

Also in this case, the acid is assumed to be in *cis,cis* form, but the final titer of the acid in the filtrate at 5°C and pH 2 is 4.00 g/L. This value agrees with Matthiesen et al.⁷⁹ results, even if the temperature is far lower. Possibly, Vardon et al.³⁴ did not wait until complete equilibration, as the crystals are said to be “readily” formed.

Another consideration can be made on the temperature of crystallization: Vardon et al.³⁴ obtained the crystals both acidifying and chilling the solution at 5 °C. In the absence of an optimized procedure for muconic acid, they followed conditions similar to the adipic acid processing. However, the biggest contribution to crystal formation is due to the pH shift, since temperature is little effective from 35°C downward, as clearly shown by the solubility curves. Cooling is therefore not advised, as would cause higher crystallization costs. The solubility curve for *cis,cis*-muconic acid confirms the low effectiveness of the solution cooling.

Table 3.28 - Solubility points for the isomers of muconic acid available in literature.

	Temperature [°C]	pH	Solubility [kgMA/kgH ₂ O]	Source
cc-MA	25 (room)	2	1.00e-3	⁷⁹
ct-MA	25 (room)	2	5.22e-3	⁷⁹
tt-MA	25 (room)	2	9.00e-5	⁷⁹
tt-MA	15	2	2.00e-5	⁸⁰

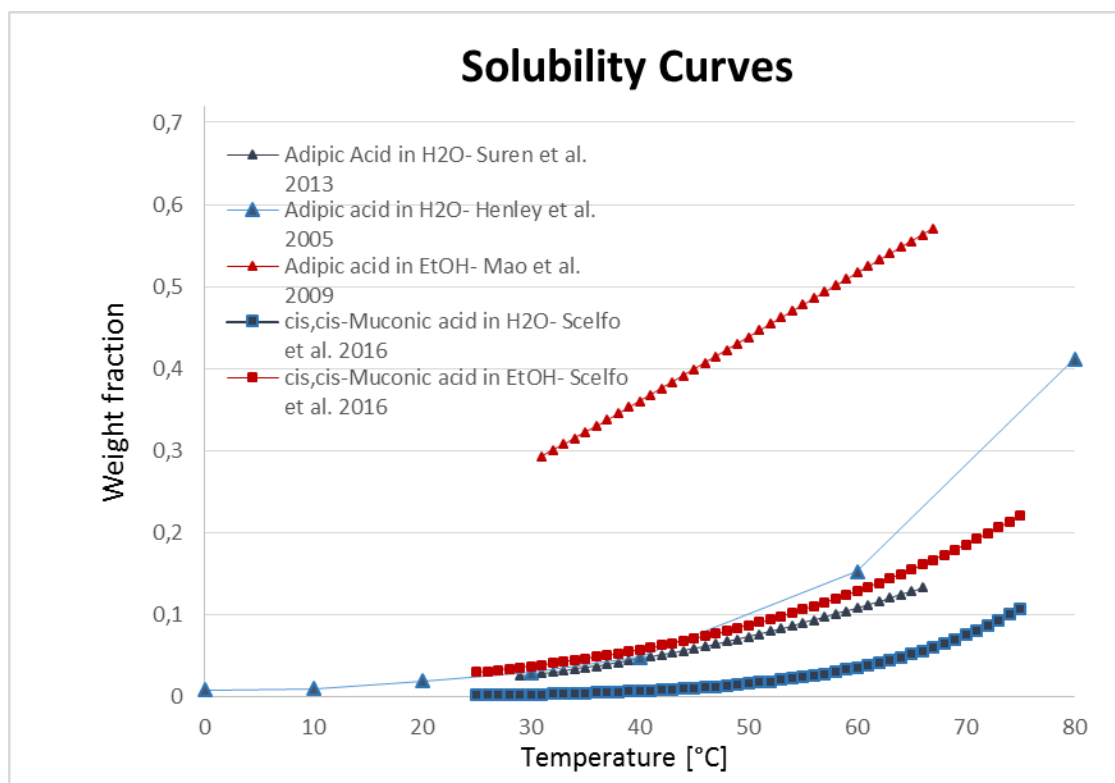


Figure 3.6 - Solubility curves for the isomers of muconic acid and similarity with adipic acid. Refs. 75,81–83.

To derive a first estimate of the design and costs of a crystallizer for *cis-trans*-muconic acid, the following assumptions are made:

- Cost estimates are provided by Aspen Capital Cost Estimator (AspenOne v8.8, Aspentech) for an OSLO type crystallizer with corrosion proof materials installation coefficient 1.9 and for the circulation pumps and the screen bowl centrifuge to separate crystals in the magma (installation factor is 1.2).⁸⁴
- The final concentration in the mother liquor is 5.2 g/L at pH 2.⁷⁹
- Product purity is 100%: there are no indication on the composition of the possible impurities. Other downstream crystallization steps will be included anyway to make sure that this assumption is respected on the final product.
- The kinetics of the crystal nucleation and growth (therefore the design and operation of the equipment) for muconic acid are expected to be similar to the ones of adipic acid.

- The crystallizers are provided with a pre-mixer, in which HCl is added in stoichiometric amount to ensure muconic acid formation from the salt.
- The maximum product recovery set in the process network is 97% (for the highest grade of concentration): higher yields are unlikely, given the necessity to purge the impurities that are present despite the previous workout.

Table 3.29 - Crystallizers mixing ratios

Interval: CRmw_A,B,C,D			
Description: Crystallizer for muconic acid from water			
Mixing ratio μ [kg/kg reference compound]			
	<i>P. putida</i>	<i>E. coli</i>	Note
HCl	3.87e-1	3.87e-1	Ref to Na ₂ Muconate

Table 3.30 - Crystallizers cost function [\$(2014)/kg: reference stream fM]

Interval: CRmw_A,B,C,D		
Description: Crystallizer for muconic acid from water		
Cost Function		
	<i>P. putida</i>	<i>E. coli</i>
Cost function (\$2014) CRmw_A	$y=5519 x^{0.57}$	$y=6273 x^{0.57}$
Cost function (\$2014) CRmw_B	$y=6310 x^{0.57}$	$y=6831 x^{0.57}$
Cost function (\$2014) CRmw_C	$y=7521 x^{0.57}$	$y=7550 x^{0.57}$
Cost function (\$2014) CRmw_D	$y=9710 x^{0.57}$	$y=8521 x^{0.57}$

Table 3.31 - Crystallizers utility consumption ratios

Interval: CRmw_A,B,C,D							
Description: Crystallizer for muconic acid from water							
Utility consumption ratio β [unit/kg reference compound]							
UTILITIES	<i>P. putida</i>			<i>E. coli</i>			Note
	β_1	β_2	β_3	β_1	β_2	β_3	
CRmw_A EL_PO	1.75e-2			9.13e-3			Ref to Mucic acid
CRmw_A ST_HP	5.45			3.72			Ref to Mucic acid
CRmw_A CO_WA	3.55e2			2.42e2			Ref to Mucic acid
CRmw_B EL_PO	1.75e-2			9.13e-3			Ref to Mucic acid
CRmw_B ST_HP	4.3			3.21			Ref to Mucic acid
CRmw_B CO_WA	2.80e2			2.1e2			Ref to Mucic acid
CRmw_C EL_PO	1.75e-2			9.13e-3			Ref to Mucic acid
CRmw_C ST_HP	3.16			2.7			Ref to Mucic acid
CRmw_C CO_WA	2.06e2			1.76e2			Ref to Mucic acid
CRmw_D EL_PO	1.75e-2			9.13e-3			Ref to Mucic acid
CRmw_D ST_HP	2.02			2.19			Ref to Mucic acid
CRmw_D CO_WA	1.31e2			1.42e2			Ref to Mucic acid

3.2.11 - Solvent dissolution (step XI)

The crystals of muconic acid recovered in step X may contain co-crystals of other inorganic salts. Interval DIS_{et} assumes the dissolution of the intermediate crystals in ethanol, as suggested in the lab-procedure of Vardon et al.³⁴ Further studies could identify other alternative solvents for this step.

The interval DIS_{et} represents a coil jacketed stirred tank, to provide a 30 min residence time at 75 °C to ensure the dissolution of the crystallized muconic acid in ethanol.⁵⁴

Table 3.32 - Ethanol dissolution mixing ratios

Interval: DISet			
Description: Dissolution of cis,trans MA in ethanol			
Mixing ratio μ [kg/kg reference compound]			
	<i>P. putida</i>	<i>E. coli</i>	Note
EtOH	3.96	3.96	Ref to muconic acid

Table 3.33 - Ethanol dissolution cost function [\$(2014)/kg: reference stream fM]

Interval: DISet		
Description: Dissolution of cis,trans MA in ethanol		
Cost Function		
	<i>P. putida</i>	<i>E. coli</i>
Cost function (\$2014)	$y=1418 x^{0.53}$	$y=1418 x^{0.53}$

Table 3.34 - Ethanol dissolution utility consumption ratios

Interval: DISet							
Description: Dissolution of cis,trans MA in ethanol							
Utility consumption ratio β [unit/kg reference compound]							
UTILITIES	<i>P. putida</i>			<i>E. coli</i>			Note
	β_1	β_2	β_3	β_1	β_2	β_3	
EL_PO							
ST_HP	5.48e-2			5.48e-2			Ref to EtOH

3.2.12 - Solvent filtration (step XII)

Following Vardon et al.³⁴ lab-scale procedure, a step of ultrafiltration after the ethanol dissolution is necessary to remove the mineral crystals co-precipitated with muconic acid. The only reference for muconic acid solubility in ethanol is the correlation of *cis,cis*-muconic acid of Scelfo et al.⁷⁵ These data are worth as a preliminary estimate. A poly-ether sulphone (PES) UF filter, in a vertical pressure leaf configuration is assumed for this task:

this piece of equipment is indicated for flammable systems.⁸⁵ The cost of the membrane is of the order of 100 \$/m².⁸⁶ An average flow of 960 L/h/m² at 4 bar transmembrane pressure is assumed to size the module. The cost function assumes an installation factor of 1.4.⁵⁴ The interval can be alternatively connected to the interval of step XIII or XV.

Table 3.35 - Solvent ultrafiltration cost function [\$(2014)/kg: reference stream f^M]

Interval: UFet		
Description: Ethanol ultrafiltration		
Cost Function		
	<i>P. putida</i>	<i>E. coli</i>
Cost function (\$2014)	$y=4090 x^{0.34}$	$y=4090 x^{0.34}$

Table 3.36 - Solvent ultrafiltration utility consumption ratios

Interval: UFet							
Description: Ethanol ultrafiltration							
Utility consumption ratio β [unit/kg reference compound]							
UTILITIES	<i>P. putida</i>			<i>E. coli</i>			Note
	β_1	β_2	β_3	β_1	β_2	β_3	
EL_PO	2.69e-4			2.69e-4			Ref to EtOH

3.2.13 - Solvent separation (step XIII)

In this step the muconic acid in ethanol solution is crystallized again, in a mixture of *cis,cis* and *cis,trans* form. In this case the driving force for crystallization is no more the pH shift nor the concentration: supersaturation is achieved by means of cooling, from 75°C to ambient temperature (25°C). This unit allows a 100% recovery of the dissolved muconic acid (purges are negligible given the high purity of muconic acid at this point) and assuming a 100% removal of ethanol, which is recycled to the dissolver: therefore the cost of fresh ethanol is not included in the economic evaluation. The single interval model CRmet encompasses three distinct equipment: a heat exchanger cooled with the utility CO_WA

with installation factor 2.2, a draft tube crystallizer with installation factor 1.9, a decanter centrifuge for the crystal recovery with installation factor 1.2.⁵⁴

Table 3.37 - Crystallizers (ethanol system) cost function [\$(2014)/kg: reference stream fM]

Interval: CRmet		
Description: Crystallizer for muconic acid from ethanol		
Cost Function		
	<i>P. putida</i>	<i>E. coli</i>
Cost function (\$2014)	$y=17338 x^{0.47}$	$y=17338 x^{0.47}$

Table 3.38 - Crystallizers (ethanol system) utility consumption ratios

Interval: CRmet							
Description: Crystallizer for muconic acid from ethanol							
Utility consumption ratio β [unit/kg reference compound]							
UTILITIES	<i>P. putida</i>			<i>E. coli</i>			Note
	β_1	β_2	β_3	β_1	β_2	β_3	
EL_PO	1.26e-2			1.26e-2			Ref to Muconic acid
CO_WA	2.88			2.88			Ref to Ethanol

3.2.14 - Intermediate dissolution in water (step XIV)

The crystals of *cis,cis* and *cis,trans* muconic acid are dissolved in hot water in the interval DISw, ready to be hydrogenated in the following step.

The equipment of this step is analogous to the one of step XI, with the difference that the solvent is water and NaOH is added to increase solubility, obtaining a muconate solution. The highest reported solubility for *cis, trans*-sodium muconate is 100 g/L.⁷⁵

Table 3.39 - Water dissolution mixing ratios.

Interval: DISw			
Description: Dissolution of <i>cis,trans</i> MA in water			
Mixing ratio μ [kg/kg reference compound]			
	<i>P. putida</i>	<i>E. coli</i>	Note
H ₂ O	1.31e1	1.31e1	Ref to muconic acid
NaOH	5.63e-1	5.63e-1	Ref to muconic acid

Table 3.40 - Water dissolution cost function [\$(2014)/kg: reference stream fM]

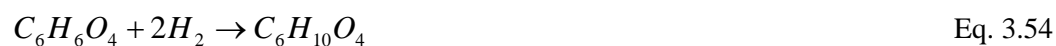
Interval: DISw		
Description: Dissolution of <i>cis,trans</i> MA in water		
Cost Function		
	<i>P. putida</i>	<i>E. coli</i>
Cost function (\$2014)	$y=1302 x^{0.53}$	$y=1302 x^{0.53}$

Table 3.41 - Water dissolution utility consumption ratios

Interval: DISw							
Description: Dissolution of <i>cis,trans</i> MA in water							
Utility consumption ratio β [unit/kg reference compound]							
UTILITIES	<i>P. putida</i>			<i>E. coli</i>			Note
	β_1	β_2	β_3	β_1	β_2	β_3	
ST_HP	7.16e-2			7.16e-2			Ref to H ₂ O

3.2.15 - Hydrogenation (step XV)

In step XV, the chemical hydrogenation of *cis,cis*-muconic acid to adipic takes place, as represented by Eq. 3.54, which simplifies the actual multi-step reaction.⁸⁷



where C₆H₆O₄ and C₆H₁₀O₄ are the minimal formula of *cis,cis*-muconic acid and adipic acid respectively. *cis,cis*-muconic acid hydrogenation has been extensively studied and

several catalysts have been proposed for different reaction conditions. The best performing ones are modelled in the intervals, following the three main strategies of hydrogenation presented in literature, namely hydrogenation of the clarified broth, of a pure water solution, or of an organic solvent solution. The intervals HYDw_A, B, C, and D model the hydrogenation of the pre-concentrated broths according to step IX. The performance of the Ni/Al₂O₃ catalyst recently described by Scelfo et al.⁸⁸ are assumed for these intervals. The catalyst performance of Capelli et al.⁸⁷ is modelled also in interval HYDw_P, where the solvent is pure water. For the hydrogenation in ethanol, the Pd/C catalyst performance of Vardon et al.^{34,89} are modelled: HYDet assumes the reactant concentration coming from the upstream dissolution step, HYDetV includes a further dilution, to align with the literature reference concentrations. The electro-catalytic hydrogenation presented by Matthiesen et al.⁷⁹ is not included in the superstructure definition, as the experimental conditions and results do not apply to the higher muconic acid concentrations reached by *P. putida* and *E. coli* included in this work.

All the intervals assume the application of a system of an agitated jacketed reactors in parallel, with volume 10 m³ and a shape factor H/D of 4, to ensure the longer contact time between the gas and the liquid phase. The cost correlation is taken from the literature and considers Guthrie's pressure factor (e.g. 2.05 for 10 bar reactions).³

The most important assumptions to model this processing step are the following:

- The conversion is complete and selective to adipic acid (no sub-products). The best results published are very close to this ideal condition.
- Hydrogen is produced by means of electrolysis (its cost is calculated according to electric power cost). This assumption wants to enhance the green vocation of the process.
- The reaction is not affected by the full scale plant conditions: the data from lab-scale experiences refer to lower solute and higher catalyst concentrations, which are little compatible with the economic constraints of an industrial hydrogenation. Further studies should address with more detail the scale-up issues.

Table 3.42 - Hydrogenation reactors mixing ratios.

Interval: HYD			
Description: Hydrogenation of cis,trans MA to adipic acid			
Mixing ratio μ [kg/kg reference compound]			
	P. putida	E. coli	Note
H₂	2.82e-2		Ref to muconic acid
H₂	2.15e-2		Ref to sodium muconate

Table 3.43 - Hydrogenation reactors cost function [\$(2014)/kg: reference stream fM]

Interval: HYD		
Description: Hydrogenation of cis,trans MA to adipic acid		
Cost Function		
	P. putida	E. coli
Cost function (\$2014) HYDw_A	$\gamma=325.7 x$	$\gamma=325.7 x$
Cost function (\$2014) HYDw_B	$\gamma=319.2 x$	$\gamma=308.8 x$
Cost function (\$2014) HYDw_C	$\gamma=308.1 x$	$\gamma=301.1 x$
Cost function (\$2014) HYDw_D	$\gamma=285.1 x$	$\gamma=290.1 x$
Cost function (\$2014) HYDw_V	$\gamma=389.9 x$	$\gamma=389.8 x$
Cost function (\$2014) HYDet	$\gamma=225.6 x$	$\gamma=225.6 x$
Cost function (\$2014) HYDetV	$\gamma=224.9 x$	$\gamma=224.9 x$

The interval HYDetV considers also a task of dilution (mixer as in step XI) and of concentration to ensure the same stream composition of the equivalent HYDet: this changes the cost function and requires to include the corresponding utilities.

Table 3.44 - Hydrogenation reactors utility consumption ratios

Interval: HYDetV							
Description: Hydrogenation of cis,trans MA to adipic acid according to [37]							
Utility consumption ratio β [unit/kg reference compound]							
UTILITIES	P. putida			E. coli			Note
	β_1	β_2	β_3	β_1	β_2	β_3	
ST_HP	3.97e-1			3.97e-1			Ref to Ethanol
CO_WA	6.48			6.48			Ref to Ethanol

3.2.16 - Product recovery (step XVI)

In this step, the crystallization of adipic acid after the hydrogenation is modelled. CRaw_A, B, C, D and CRAet are then connected to step XVII for another step of dissolution-crystallization. Crawl_P provides instead sufficiently pure adipic acid, as the hydrogenation is performed on pre-purified substrates. For these intervals, similar considerations to step X hold. The only difference is that the equipment is no more an OSLO type, but an internal daft tube crystallizer, cooled at 5 °C, as the industrial practice for adipic acid suggests. For this reason a 2 step cooling is considered: a first exchanger lowers the temperature to 27 °C from the 60 °C of the hydrogenation using cooling water, the second exchanger uses salt brine modelled as a pseudo component to be added and removed (to compute its cost). The loss of product due to the different level of concentration is 16%, 12%, 9% and 5% respectively for the four alternatives.

Table 3.45 - Adipic acid crystallizers (broth) mixing ratios.

Interval: CRaw_A,B,C,D			
Description: Crystallizer for adipic acid from water (conc. broth)			
Mixing ratio μ [kg/kg reference compound]			
	P. putida	E. coli	Note
HCl	3.87e-1	3.87e-1	Ref to Na ₂ Adipate
Brine	2.63	2.63	Ref to H ₂ O

Table 3.46 - Adipic acid crystallizers (broth) cost function [\$(2014)/kg: ref. stream fM]

Interval: CRaw_A,B,C,D		
Description: Crystallizer for adipic acid from water (conc. broth)		
Cost Function		
	<i>P. putida</i>	<i>E. coli</i>
Cost function (\$2014) CRaw_A	$y=4816 x^{0.55}$	$y=5316 x^{0.55}$
Cost function (\$2014) CRaw_B	$y=5929 x^{0.54}$	$y=6009 x^{0.55}$
Cost function (\$2014) CRaw_C	$y=7508 x^{0.53}$	$y=6859 x^{0.54}$
Cost function (\$2014) CRaw_D	$y=10023 x^{0.52}$	$y=7938 x^{0.54}$

Table 3.47 - Adipic acid crystallizers (broth) utility consumption ratios

Interval: CRaw_A,B,C,D							
Description: Crystallizer for adipic acid from water (conc. broth)							
Utility consumption ratio β [unit/kg reference compound]							
UTILITIES	<i>P. putida</i>			<i>E. coli</i>			Note
	β_1	β_2	β_3	β_1	β_2	β_3	
CRaw_A EL_PO			1.27e-2			1.78e-2	Ref to adipic acid
CRaw_A CO_WA		3.30			3.30		Ref to H ₂ O
CRaw_B EL_PO			1.27e-2			1.78e-2	Ref to adipic acid
CRaw_B CO_WA		3.30			3.30		Ref to H ₂ O
CRaw_C EL_PO			1.27e-2			1.78e-2	Ref to adipic acid
CRaw_C CO_WA		3.30			3.30		Ref to H ₂ O
CRaw_D EL_PO			1.27e-2			1.78e-2	Ref to adipic acid
CRaw_D CO_WA		3.30			3.30		Ref to H ₂ O

The data of the adipic acid crystallizers from pure water are hereafter summarized.

Table 3.48 - Adipic acid crystallizers (pure water) mixing ratios.

Interval: CRaw_V			
Description: Crystallizer for adipic acid from pure water			
Mixing ratio μ [kg/kg reference compound]			
	<i>P. putida</i>	<i>E. coli</i>	Note
HCl	3.87e-1	3.87e-1	Ref to Na ₂ Adipate
Brine	2.63	2.63	Ref to H ₂ O

Table 3.49 - Adipic acid crystallizers (pure water) cost function.

Interval: CRaw_V		
Description: Crystallizer for adipic acid from pure water		
Cost Function		
	<i>P. putida</i>	<i>E. coli</i>
Cost function (\$2014)	$y=8335.4 x^{0.51}$	$y=8335.4 x^{0.51}$

Table 3.50 - Adipic acid crystallizers (pure water) utility consumption ratios

Interval: CRaw_V							
Description: Crystallizer for adipic acid from pure water							
Utility consumption ratio β [unit/kg reference compound]							
UTILITIES	<i>P. putida</i>			<i>E. coli</i>			Note
	β_1	β_2	β_3	β_1	β_2	β_3	
EL_PO			1.22 e-2			1.22 e-2	Ref to adipic acid
CO_WA		3.30			3.30		Ref to H ₂ O

The estimated product loss is 12% for the adipic acid crystallization from water.

Regarding the adipic acid crystallization in ethanol, the reference for the solubility of adipic acid at high temperature in ethanol is Mao et al.⁸² According to the concentration of the inlet stream, the theoretical crystallization recovery would be only the 81% maximum. To

avoid an excessive loss of product, an evaporation treatment is included in the model CRAet (which therefore comprises an evaporator, a condenser, the cascade water-brine exchanger, the draft tube crystallizer and the centrifuge). In this way the product losses are reduced to 4%. The data of the ethanol crystallizers for adipic acid are summarized in the following tables.

Table 3.51 - Adipic acid crystallizers (ethanol) mixing ratios.

Interval: CRAet			
Description: Crystallizer for adipic acid from ethanol			
Mixing ratio μ [kg/kg reference compound]			
	<i>P. putida</i>	<i>E. coli</i>	Note
Brine	7.97e-1	7.97e-1	Ref to Ethanol

Table 3.52 - Adipic acid crystallizers (ethanol) cost function [\$(2014)/kg: ref. stream fM]

I Interval: CRAet		
Description: Crystallizer for adipic acid from ethanol		
Cost Function		
	<i>P. putida</i>	<i>E. coli</i>
Cost function (\$2014)	$y=16961 x^{0.49}$	$y=16961 x^{0.49}$

Table 3.53 - Adipic acid crystallizers (ethanol) utility consumption ratios

Interval: CRAet							
Description: Crystallizer for adipic acid from ethanol							
Utility consumption ratio β [unit/kg reference compound]							
UTILITIES	<i>P. putida</i>			<i>E. coli</i>			Note
	β_1	β_2	β_3	β_1	β_2	β_3	
EL_PO			1.22 e-2			1.22 e-2	Ref to adipic acid
ST_HP		3.86e-1			3.86e-1		Ref to Ethanol
CO_WA		6.30	3.06		6.30	3.06	Ref to Ethanol

3.2.17 - Re-dissolution (step XVII)

The adipic acid crystals obtained on step XVI are dissolved in ethanol in interval DISet2. The polymer grade adipic acid should reach a purity of minimum 99.8%, therefore a final recrystallization is included for all the streams but C_{Raw_V} (which underwent to already three subsequent steps). The first step is the dissolution of the adipic acid into ethanol. The interval model is analogous to DISet of step XI.

Table 3.54 - Ethanol re-dissolution mixing ratios

Interval: DISet2			
Description: Dissolution of adipic acid in ethanol, rectification.			
Mixing ratio μ [kg/kg reference compound]			
	<i>P. putida</i>	<i>E. coli</i>	Note
EtOH	6.48e-1	6.48e-1	Ref to adipic acid

Table 3.55 - Ethanol re-dissolution cost function [\$(2014)/kg: reference stream fM]

Interval: DISet2		
Description: Dissolution of adipic acid in ethanol, rectification.		
Cost Function		
	<i>P. putida</i>	<i>E. coli</i>
Cost function (\$2014)	$y=2654 x^{0.53}$	$y=2654 x^{0.53}$

Table 3.56 - Ethanol re-dissolution utility consumption ratios

Interval: DISet2							
Description: Dissolution of adipic acid in ethanol, rectification.							
Utility consumption ratio β [unit/kg reference compound]							
UTILITIES	<i>P. putida</i>			<i>E. coli</i>			Note
	β_1	β_2	β_3	β_1	β_2	β_3	
EL_PO							
ST_HP	5.48e-2			5.48e-2			Ref to EtOH

3.2.18 - Rectification (step XVIII)

This last step of crystallization (interval CRaet2) allows the recovery of pure adipic acid. It is possible to see that the superstructure is generated to include at least two crystallization steps for each possible configuration (on muconic acid or adipic acid). This is an important difference from the flowsheets proposed previously, assuming the recovery of 99.96% pure adipic acid (polymer grade) in a single step of crystallization.^{49,64} A single crystallization step is unlikely even for the oil-derived process, which operates with more clean substrates.⁹⁰

This final interval comprises a double cooler exchanger (CO_WA utility and brine), a draft tube crystallizer and a solid bowl centrifuge for the crystals harvest. A complete product recovery is assumed (purge is negligible). As for step XIII, the ethanol cost is not accounted as it is recycled.

Table 3.57 - Adipic acid re-crystallization mixing ratios.

Interval: CRaet2			
Description: Crystallizer for adipic acid from ethanol, rectification.			
Mixing ratio μ [kg/kg reference compound]			
	<i>P. putida</i>	<i>E. coli</i>	Note
Brine	1.38	1.38	Ref to Ethanol

Table 3.58 - Adipic acid recrystallization cost function [\$(2014)/kg: reference stream fM]

Interval: CRaet2		
Description: Crystallizer for adipic acid from ethanol, rectification.		
Cost Function		
	<i>P. putida</i>	<i>E. coli</i>
Cost function (\$2014)	$\gamma=29371 x^{0.47}$	$\gamma=29371 x^{0.47}$

Table 3.59 - Adipic acid re-crystallization utility consumption ratios

Interval: CRAet2							
Description: Crystallizer for adipic acid from ethanol, rectification.							
Utility consumption ratio β [unit/kg reference compound]							
UTILITIES	<i>P. putida</i>			<i>E. coli</i>			Note
	β_1	β_2	β_3	β_1	β_2	β_3	
EL_PO			1.22 e-2			1.22 e-2	Ref to adipic acid
CO_WA		2.88			2.88		Ref to Ethanol

3.2.19 - Product (step XIX)

The “adipic acid interval” represents the final product of the process, polymer grade adipic acid from renewable biomass. CCMA interval is a dummy step included for a further development of the superstructure. In fact, the purified *cis,cis/cis,trans*-muconic acid can be diverted to another process for terephthalic acid production, for example. This step allows the extension of the processing network.

3.2.20 - Economic aspects

As already defined, the reference year for the economic data included in this case study is 2014. CEPCI Cost Indexes are used to relate cost estimates of different years to the reference.²⁷ The capital cost estimates are calculated using Guthrie multipliers on the equipment purchase cost.^{3,54} The annuity is calculated assuming a 10 years investment with a 7% interest.² Taxes, depreciation, salvage values are not considered. Regarding the labour cost impact, Matthiesen et al.⁴⁹ used the approach of workers per unit operation per shift as presented in Peters et al.⁹¹, obtaining a value of 5% of the total operating expenditures. However, the reference considers traditional oil industry plants, and provides as a general rule of thumb for labor impact the 5-15% of the total operating costs. The straight application of this traditional approach could lead to questionable results: as the majority of the operating costs for this case-study is due to the feedstock, any improvement on the yield would dramatically reduce the labor cost. However, the layout of the plant would not

change sensibly and so the number of workers. For these reasons and since an error of ca 5% in the final estimate is acceptable, labor cost is not included in this analysis.

Regarding the dependence of the capital cost estimates and the plant size, the correlations presented throughout this section are benchmarked for the full span of productivity of the sensitivity analysis (10,000- 200,000 ton/year of adipic acid). The reported cost equations provide the final installed cost value: since the plant overhead can impact on the 1% of the final production costs, this value is not included as well. For the sake of the solution of a MILP, the nonlinear cost-size correlation are piece-wise linearized according to the method presented by Bertran et al.¹⁸

The price for the utilities are summarized in Table 3.60.²⁶

Table 3.60 - Utility costs summary.

Utility	Abbreviation	Cost	Unit	Notes
Electric power	EL_PO	0.0723	\$/kWh	US energy mix base
High pressure steam	ST_HP	0.0168	\$/kg	8 bar steam, 170 °C
Low Pressure Steam	ST_LP	0.0160	\$/kg	2 bar steam. 120 °C
Cooling Water	CO_WA	2.09E-05	\$/kg	River water 15 °C
Compressed Air	AI_CO	0.07157	\$/kg	Compressed air

3.3 - Superstructure optimization and results analysis

Super-O, after the generation of the Microsoft Excel file containing the input data, launches a GAMS script. The script compiles automatically the code reading the input data and solves the problem, printing the results of the optimization in another Excel flowsheet. The main output of the simulation are: the vector of integer variables y (providing the shape of the selected flowsheet and raw materials/products), the flow rates at each interval with associated utility consumptions, the calculated expenditures and the total profit. The GAMS program has to be run as many time as the number of perturbations of the input parameters. The optimizer yields always one solution, the optimal, hence, to generate a ranking of 2nd, 3rd, ... best solution the code has to be modified inserting some integer-cuts. These are extra constraints that induce the exclusion of the 1st best solution, of the 2nd and so on. The integer cut analysis is useful to have a deeper insight of the best processing strategy, comparing the concurrent technologies. These results are reported in Paragraph 3.3.1. The sustainability of the best process configuration is assessed (Paragraph 3.3.2) both from an economic and from an environmental point of view: the preliminary cost estimates are also useful to highlight the unit operations requiring most resources, which therefore deserve a more careful design and optimization. Finally, the solution has been repeated to explore a range of variation of the performances of the bioreaction step (Paragraph 3.3.3). This sensitivity analysis allows identify the variables that affect most the profitability of the process, setting the milestones for the ongoing research.

3.3.1 - The best process configurations ranking

The best processing route selected by superstructure optimization is evidenced in Figure 3.5. The solver provided the same processing route for all the considered scenarios, indicating that this optimal solution is not affected by the uncertainties in variable specifications and other conditions considered in different scenarios. Table 3.61 lists the top-ranked process configurations according to their economic potential: the detailed process flowsheet corresponding to the optimal processing route is depicted in Figure 3.7.

Table 3.61 - Integer cut analysis, ranking of the best process configurations

#	Selected Network																EP
	FERM	HEAT	CEN	RF CEN	UF	AC	EV D	CRmw D	DISet	UFet	HYDd	CRaet	DISet2	CRaet2	CRaet2	CRaet2	
1	FERM	HEAT	CEN	RF CEN	UF	AC	EV D	CRmw D	DISet	UFet	HYDd	CRaet	DISet2	CRaet2	CRaet2	CRaet2	-0.25%
2	FERM	HEAT	CENp	MFt	RF MF	UF	AC	EV D	CRmw D	DISet	UFet	HYDd	CRaet	DISet2	CRaet2	CRaet2	-0.59%
3	FERM	HEAT	CEN	RF CEN	UF	AC	EV C	CRmw C	DISet	UFet	HYDd	CRaet	DISet2	CRaet2	CRaet2	CRaet2	-1.19%
4	FERM	HEAT	CEN	RF CEN	UF	AC	EV R	CRmw R	DISet	UFet	HYDp	CRaet	DISet2	CRaet2	CRaet2	CRaet2	-1.80%
5	FERM	HEAT	CEN	RF CEN	UF	AC	EV A	CRmw A	DISet	UFet	HYDd	CRaet	DISet2	CRaet2	CRaet2	CRaet2	-2.15%
6	FERM	HEAT	CEN	RF CEN	UF	AC	EV D	HYDw D	CRaw D	DISet2	CRaet2						-3.27%
7	FERM	HEAT	CEN	RF CEN	UF	AC	EV C	HYDw C	CRaw C	DISet2	CRaet2						-3.60%
8	FERM	HEAT	CENp	DFIL	UF	AC	EV D	CRmw D	DISet	UFet	HYDd	CRaet	DISet2	CRaet2	CRaet2	CRaet2	-4.21%
9	FERM	HEAT	CENp	MFw	UF	AC	EV D	CRmw D	DISet	UFet	HYDd	CRaet	DISet2	CRaet2	CRaet2	CRaet2	-4.64%
10	FERM	HEAT	CENw	UF	AC	EV D	CRmw D	DISet	UFet	HYDd	CRaet	DISet2	CRaet2	CRaet2	CRaet2	CRaet2	-5.50%
11	FERM	HEAT	CEN	RF CEN	UF	AC	EV B	HYDw B	CRaw B	DISet2	CRaet2						-6.67%
12	FERM	HEAT	CEN	RF CEN	UF	AC	EV A	HYDw A	CRaw A	DISet2	CRaet2						-19.65%
13	FERM	HEAT	CEN	RF CEN	UF	AC	EV D	CRmw D	DISet	UFet	CRaet1	DISw	HYDw V	CRaw V	CRaw V	CRaw V	-45.04%
14	FERM	HEAT	CEN	RF CEN	UF	AC	EV D	HYDw D	CRaw D	DISet2	CRaet2						-45.04%

*. Best process route for the feedstock benzoic acid; all other routes have glucose as feedstock.

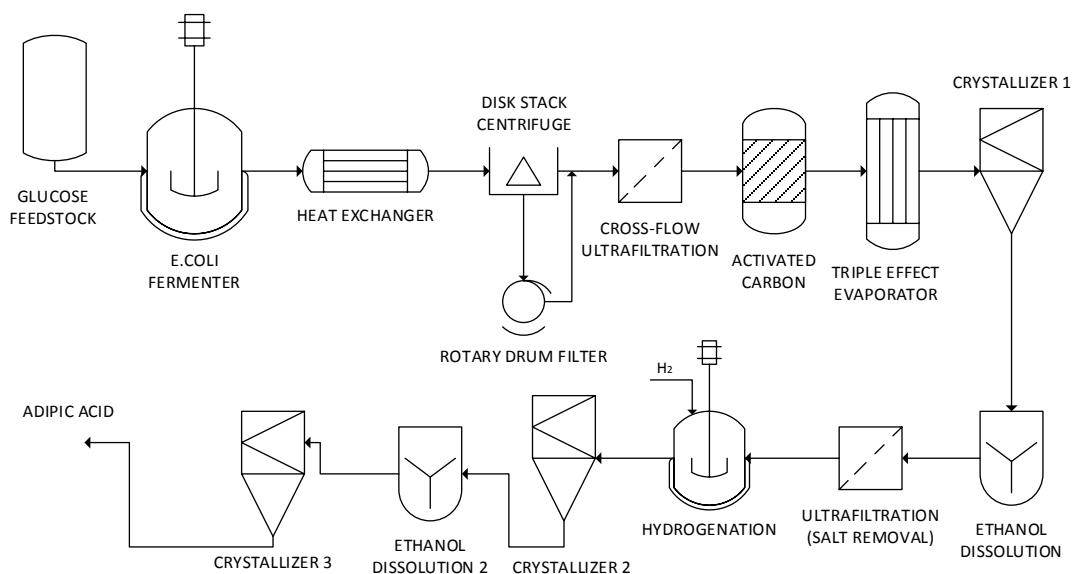


Figure 3.7 – Flowsheet of the best processing route.

An important result of the superstructure optimization is that the glucose route (*E. coli* fermentation) is preferable over the benzoic acid route. A process based on benzoic acid (*P. putida* fermentation) corresponds to a production cost of at least 45% higher than the optimal process with the glucose route. This is due to higher benzoic acid costs, but mostly due to the lower strain productivity and lower product concentration.

In terms of the alternatives for the broth clarification (from step IV to VI), the best solution is a single step operation (CEN_r), followed by broth recovery with rotary drum filtration (RF_CEN). However, a different configuration with centrifugation pre-treatment (CEN_p), cross-flow microfiltration (MFr) and retentate broth recovery (RF_MF) would decrease the economic potential by only 0.25%. In fact, cross flow filters have higher electricity consumption, but require lower investments.⁶³ This processing route (the second best - see Table 2) could actually become more effective at higher cell concentrations.⁵¹

Other alternatives to achieve a clarified broth are listed in Table 3.61, such as the processing route number 8 (pre-treatment and depth filtration), number 9 (pre-treatment and cross-flow filtration without recovery), and number 10 (single step centrifugation without

recovery). These processing alternatives lower the economic potential by 3.60%, 4.21% and 4.64%, respectively. The conclusion of this analysis is that the economic potential is enhanced by selecting those technologies that maximize product recovery, which also reflects in lower raw material consumption. A similar conclusion can be made for the alternatives in step IX (concentration). The optimal route includes the most costly evaporator, to give a higher product concentration: concentrated broths are beneficial for product recovery in crystallizers. Assuming a milder evaporation (EV_C), as per solution number 3 in Table 3.61, the economic potential decreases by 0.59% (*cis,cis*-muconic acid recovery of 96% instead of 97%). This value further decreases by 1.19% (EV_B, solution number 4) and 1.80% (EV_A, solution number 5), corresponding to 95% and 94% of product recovery. This indicates that the savings in process expenses do not compensate the loss in productivity.

As for the hydrogenation strategy, ethanol is the preferred solvent. In fact, hydrogenation in water (directly in the clarified fermentation broth) leads to higher costs, reducing the economic potential from 2.15% (HYDw_D, solution 6) to 6.67% (HYDw_A, solution 12), depending on the level of pre-concentration in the evaporator. A downstream set-up with a pre-purification of *cis,cis*-muconic acid followed by its re-dissolution in water for hydrogenation (HYDw_P), would involve 20% higher costs (solution number 13 in Table 3.61). This last processing route involves extra steps of neutralization (to dissolve *cis,cis*-muconic acid) and acidification (to crystallize adipic acid). Therefore, ethanol hydrogenation is preferable not only because of the higher concentrations achievable (both for *cis,cis*-muconic acid and adipic acid) which reduce equipment size, but also because it leads to significant savings in chemicals expenditure. On this latter aspect, it is preferable to hydrogenate at higher muconic acid concentrations.

3.3.2 - Sustainability analysis

The calculated economic potential can be used to provide a first estimate of the bio-derived adipic acid production costs, assessing the level of maturity of the technology and the feasibility of the plant.

Economic sustainability

Under the conditions of the base-case scenario (SC_1 in Table 3.62), the optimal flowsheet is economically feasible for a price of adipic acid of 3.60 \$/kg. This value is more than double the reference price of adipic acid in North America. Still, different market scenarios confirm the potential of industrialization.

Table 3.62 – Multiscenario analysis and process profitability

		Profit on sales [\$ /kg adipic acid]			
SC_1	Base case	-2.00	-1.66	-1.32	-0.99
SC_2	Sugar price (0.210 \$/kg)*	-1.00	-0.67	-0.33	0.00
SC_3	Scale up (200 kton/year AA)	-0.93	-0.59	-0.25	0.08
SC_4	Concentration (+30%)	-0.75	-0.41	-0.07	0.26
SC_5	Selectivity (93%)	-0.76	-0.42	-0.08	0.25
SC_6	Selectivity (93%)+Conc.	-0.51	-0.17	0.17	0.50
Adipic acid selling price [\$ /kg]		a-1.6	b-1.94	c-2.28	d-2.61

not feasible
 -20% to -5%
 -5% to 0%
 breakeven/profit

*This sugar price applies also to the following scenarios

For a benzoic acid based process, on the other hand, the economic performances would be always worse, requiring a selling price higher than 5.00 \$/kg for the base case, and unacceptable price values even in the most optimistic scenarios. As a general indication, the current benzoic acid route is not as good as the glucose one for the industrial scale-up. Regarding the glucose-based process, the multi-scenario analysis reported in Table 3.62 considers the price of glucose for a plant located in Brazil (SC_2). In this case, when adipic acid is sold at 2.28 \$/kg (SC_2_c), the estimated loss is within the uncertainty of the cost estimates and profitability is reached at 2.61 \$/kg (SC_2_d), which is the actual Brazilian

selling price of 2014 given the protectionist measures. Therefore, the process for sustainable adipic acid production becomes economically feasible under Brazil's market conditions, assuming no improvements in the current technology. The development of new technologies to achieve cheaper glucose from second generation biorefineries could eventually allow extension to other countries.⁹²

Considering the solutions for the plant size (SC_3 series), it is observed that an increase of the plant production up to 20-fold that of the reference does not affect the result significantly: the plant feasibility maintains its dependency on external incentives. Interestingly, with an assumed improved upstream performance (increased fermentation yield and product concentration), profitability could be reached for prices of adipic acid lower than the 2.00 \$/kg threshold (SC_6_b, c, d).

Environmental sustainability

Focusing on the first indications coming from the early stage environmental assessment, the validity of a shift toward a bio-based technology is confirmed. Table 3.63 shows a comparison of the metrics for the traditional process and the best flowsheet under some selected scenarios. The energy demand for the bio-derived adipic acid from glucose is lower, and so are the associated CO₂ emissions. On the contrary, the higher dilution of *P. putida* based process results in values higher than the traditional process. The water consumption index is better for the traditional petrochemical process, where water has a minor role. The mitigation of water resource impact will be the actual environmental challenge for the bio-based adipic acid: higher concentration fermentation could be a possible solution. Still, the environmental cost of waste-water treatment can be considered to span between 1 and 2.4 kg CO₂ equivalent per kg of COD removed⁶⁵: closed-loop water use, efficient water treatment and optimized fermentations (e.g. more concentrated) could be of some use. The WAR algorithm, whose results are presented in Table 3.64, confirms the better environmental performances of the intensified *E. coli* processes, but also presents *P. putida* process as the one with the lowest environmental impacts: this indication is in line with the low impacts of lignin-derived aromatics evidenced by Van Duuren et al.⁶⁴

The base-case cost distribution diagram of Figure 3.8 provides a more detailed insight into the critical aspects of the process that need to be improved. The main cost contribution comes from the feedstock, as high as 55% of the total production costs, a result which is in

line with other bio-refining applications for commodity chemicals.⁴⁵ The second largest contribution is the consumption of chemicals, which accounts for 22% of the production costs. The growth support expenditures, acid (HCl) and base (NaOH) for pH modifications contribute the most. The consumption of NaOH and HCl, in particular, cannot be reduced with the present neutral pH fermentation: an acid fermentation could possibly reduce these costs, as attained for succinic acid, although new strains need to be sought.⁴⁵

Table 3.63 - Environmental impact factors, comparison with the traditional oil-based process.

	Energy Required [MJ/kg AA]	Water consumption [kgH ₂ O/ kg AA]	CO ₂ emissions [kgCO ₂ /kg AA]
Traditional process	104.00 ^a	5-0.6 ^b	6.7 ^c
SC_1: E. coli, base case.	82.50	21.69	4.63 ^d
SC_3: E. coli, 20kton/year.	82.34	21.69	4.62
SC_4: E. coli, concentration +30%.	62.75	17.15	3.52
SC_6: E. coli, selectivity 93%.	62.75	16.62	3.52
SC_1: P. putida, base case.	246.58	42.50	13.83

a- Value from ref.64.

b- Value from ref.90.

c- Value from ref.37.

d- The CO₂ emissions for the bioprocess assume natural gas as energy source⁹³

With an impact of 17%, utilities account for the third largest contribution to production costs. In this case, the highest expenditure is for the electricity (76%), used mainly by the upstream section. The compressors that provide aeration and broth stirring for the aerated fermenters modelled in step II (Bioreaction) require a larger amount of power than other energy intensive operations such as centrifugation or evaporation (which consumes the largest share of high-pressure steam).

Table 3.64 - WAR algorithm evaluation results for selected solution scenarios. ATP is Aquatic Toxicity Potential; TTP is the Terrestrial Toxicity Potential; and HTPE is the Human Toxicity Potetial by Exposition.

	Bioprocess Potential Environmental Impact [PEI/kg AA]		
	ATP	TTP	HTPE
SC_1: E. coli, base case.	8.4	9.1	0.0073
SC_3: E. coli, 20kton/year.	8.4	9.1	0.0072
SC_4: E. coli, concentration +30%.	7.3	8.4	0.0073
SC_6: E. coli, selectivity 93%.	5.7	8.8	0.0049
SC_1: P. putida, base case.	2.49	8.3	0.0022

Cost distribution and process bottlenecks analysis

Finally, the overall capital cost is estimated to be 15.2 M\$ for the base-case plant, the annualized amount of which corresponds only to 6% of the production costs. The largest contributions to the capital expenditures come from centrifuges (31.82%) and crystallizers (31.14%), which are the most complex pieces of equipment in the process layout.

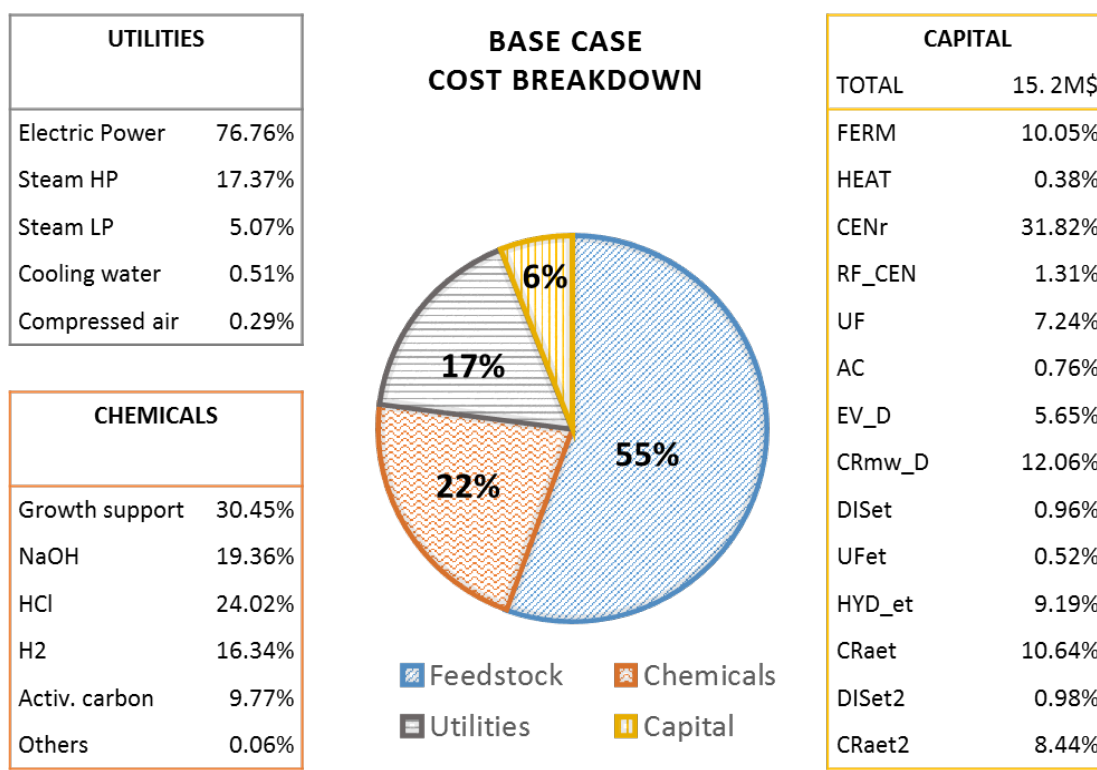


Figure 3.8 - Cost breakdown for the optimal processing configuration.

3.3.3 - Sensitivity analysis for the glucose route

The multi-scenario analysis indicates that better upstream performances can improve the process economics. Therefore, the sensitivity analysis presented in Figure 3.9 addresses those fermentation metrics that research aims at enhancing, focusing on the optimal flowsheet and the actual *E. coli* fermentation. The input parameters for the sensitivity analysis are bacteria productivity, product concentration in the fermenter, and yield on feedstock. These are perturbed to assess the effects of their variation (ranging from -30 to +40% with respect to base case conditions) on the production cost.

The first parameter perturbation results in minimal changes to the production cost. More relevant is the contribution of *cis,cis*-muconic acid concentration in the broth: the sensitivity coefficient is 0.25 for positive variations (i.e. a 1% increase of *cis,cis*-muconic

acid broth concentration results in a 0.25% reduction in the adipic acid production cost), while for negative variations it is 0.375: more diluted fermentation should thus be avoided. In fact, *cis,cis*-muconic acid final concentration in the final broth determines the flow rates (and thus the size) of the downstream equipment and reflects also in the energy consumption for the evaporation. A similar trend characterizes an improvement in the bioconversion yield (sensitivity coefficient 0.25), which can be reached by enhancing bacteria selectivity towards *cis,cis*-muconic acid. For example, the best *E. coli* selectivity reached so far in the stationary phase is 71%.⁴³ There is room for further improvement, for example following the strategies described by Niu et al.⁴⁴ Normally, for a fixed amount of feedstock, yield and product concentration are correlated: an improved strain would increase both, as a bad fermentation would reduce them. The achievement of higher selectivity (up to +40% of the base case performance, with consequent higher broth concentration) would give the best benefits, with a sensitivity coefficient of 0.4 for positive variations (higher yield and concentration). The effect of bad fermentations on the process economics is even stronger, with a coefficient of 0.7. This result points out the importance of developing strains which should be stable to mutations and stress resistant, to avoid any reduction of conversion or selectivity.

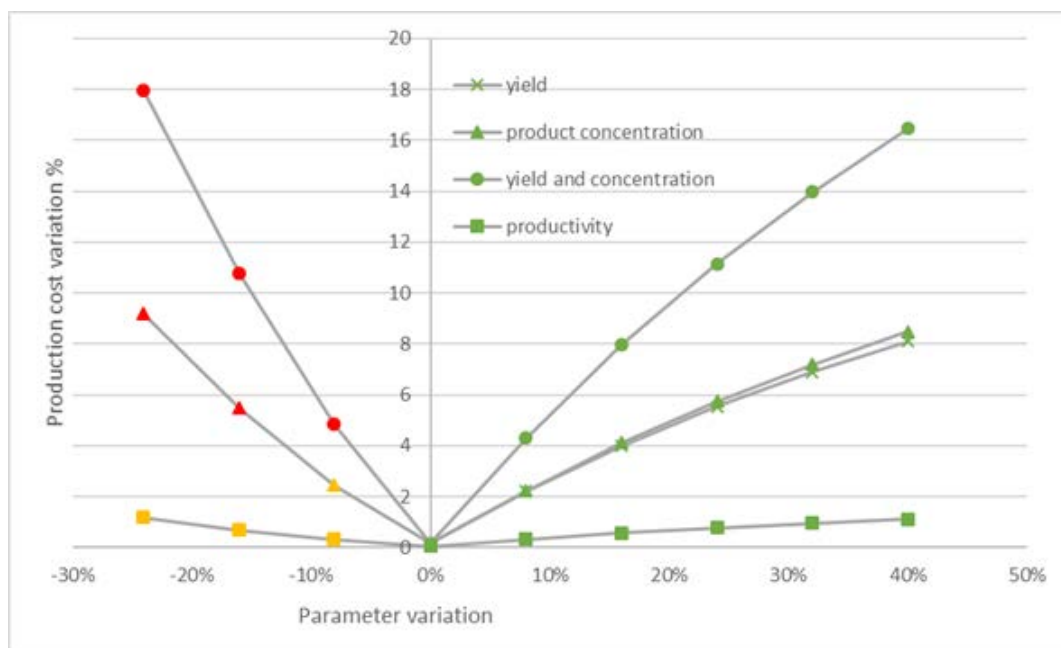


Figure 3.9 - Sensitivity analysis of different variables on the production cost. In green, the points improving the process feasibility, in yellow and red, the ones negatively affecting it.

3.4 - Conclusions

This work applied a systematic methodology for early-stage process synthesis and design to obtain a sustainable process design for the production of bio-derived adipic acid. A large number of reported technologies associated with bio-conversions and downstream separation operations were employed in the model of the process superstructure formulation. This included also the best and most updated information about bio-catalytic and chemical conversions, related to the transformation of renewable feedstocks to adipic acid. The obtained optimal processing route confirms the indications of previous studies, thus providing more information for the process development, derived from the application of a rigorous optimization-based methodology and not using simplified analogy principles. The main insights on the sustainable process design for adipic acid are: the preference to the glucose feedstock (*E. coli* fermentation) instead of the benzoic acid feedstock (*P. putida* fermentation); the need to reduce the product losses during the downstream purification; and the advantages of converting the intermediate product (*cis,cis*-muconic acid) hydrogenation in an organic solvent (ethanol). The economic analysis in different scenarios confirmed that a bio-adipic acid production is affected by the availability of cheap feedstock. In this specific case, the adipic acid process can be profitable if it is located in Brazil, using first generation glucose at a price not higher than 0.21\$/kg. To complete the sustainability analysis, some preliminary environmental indicators were calculated and they confirmed the potential sustainability of glucose-based adipic acid. Finally, since the data used in this work are derived from early-stage and lab-scale investigations, the estimates can be further refined, as soon as new insights are provided by the ongoing R&D. The superstructure based synthesis-design method employed in this work is able to implement and extend new sections in the superstructure, including new technologies or even new conversion mechanisms to other products, in addition to adipic acid. The indications on the current technological bottlenecks, the main assumptions done while defining the superstructure and the sensitivity analysis are useful to indicate the priority aspects to be further investigated. In Appendix 1, a list is presented, containing the SMART objectives for research derivable from this feasibility study.

3.5 - References chapter 3

1. Douglas, J. M. *AIChE J.* **1985**, 31 (3).
2. Biegler, L. T.; Grossmann, I. E.; Westerberg, A. W. *Systematic methods of chemical process design*; Prentice-Hall international series in the physical and chemical engineering sciences; Prentice Hall PTR, **1997**.
3. Turton, R.; Bailie, R. C.; Whiting, W. B.; Shaeiwitz, J. A. *Analysis, synthesis and design of chemical processes*; Pearson Education, **2008**.
4. FDA. Questions and Answers on Current Good Manufacturing Practices for Drugs <https://www.fda.gov/Drugs/DevelopmentApprovalProcess/Manufacturing/ucm124740.htm> (accessed Oct 27, 2017).
5. Medicines and Healthcare products Regulatory Agency. *Rules and Guidance for Pharmaceutical Manufacturers and Distributors*; Pharmaceutical Press: London, 2014.
6. Drennen, J. K. *J. Pharm. Innov.* **2007**, 2 (3), 65.
7. ICH guidelines. Pharmaceutical development Q8(2R) **2009**.
8. ICH guidelines. Quality risk management Q9 **2005**.
9. ICH guidelines. Pharmaceutical quality system Q10 **2008**.
10. ICH guidelines. Development and manufacture of drug substances (chemical entities and biotechnological/biological entities) Q11 **2012**.
11. Dantzig, G.; Orden, A.; Wolfe, P. *Pacific J. Math.* **1955**, 5 (2), 183.
12. Doherty, M. F.; Grossmann, I. E.; Pantelides, C. C. *AIChE J.* **2016**, 62 (9), 2951.
13. Sargent, R. W. H.; Murtagh, B. A. *Trans Inst Chem Eng* **1969**, 47 (4).
14. Sargent, R. W. H.; Murtagh, B. A. *Math. Program.* **1973**, 4 (1), 245.
15. Sargent, R. W. H. *Chem. Eng. Prog.* **1967**, 63 (9), 71.
16. Grossmann, I. E.; Sargent, R. W. H. *Ind. Eng. Chem. Process Des. Dev.* **1979**, 18 (2), 343.
17. Quaglia, A.; Sarup, B.; Sin, G.; Gani, R. *Comput. Chem. Eng.* **2012**, 38, 213.
18. Bertran, M. O.; Frauzem, R.; Sanchez-Arcilla, A. S.; Zhang, L.; Woodley, J. M.; Gani, R. *Computers and Chemical Engineering*. January 2016.

19. Bertran, M. O.; Frauzem, R.; Zhang, L.; Gani, R. *Comput. Aided Chem. Eng.* **2016**, *38*, 685.
20. Babi, D. K.; Holtbruegge, J.; Lutze, P.; Gorak, A.; Woodley, J. M.; Gani, R. *Comput. Chem. Eng.* **2015**, *81*, 218.
21. Quaglia, A.; Sarup, B.; Sin, G.; Gani, R. *Comput. Chem. Eng.* **2013**, *59*, 47.
22. Quaglia, A.; Sarup, B.; Sin, G.; Gani, R. *Comput. Aided Chem. Eng.* **2013**, *32*, 661.
23. Duran, M. A.; Grossmann, I. E. *AIChE J.* **1986**, *32* (4), 592.
24. Lopez-Arenas, T.; Gonzalez-Contreras, M.; Anaya-Reza, O.; Sales-Cruz, M. *Comput. Chem. Eng.* **2017**, *107*, 140.
25. Kalakul, S.; Malakul, P.; Siemanond, K.; Gani, R. *J. Clean. Prod.* **2014**, *71*, 98.
26. Ulrich, G. D.; Vasudevan, P. T. *Chem. Eng.* **2006**, *113* (4), 66.
27. Dysert, L. R. *Cost Eng.* **2003**, *45* (6), 22.
28. Godinho, M. D. *Ministério do Desenvolvimento, Indústria e comércio exterior-Secretaria de Comércio Exterior: Circular n75 de 13 Dezembro 2013*; Brasilia, 2013.
29. Harrison, R. G.; Todd, P.; Todd, P. W.; Rudge, S. R.; Petrides, D. P. *Bioseparations Science and Engineering*; Topics in chemical engineering; Oxford University Press, 2015.
30. Bigaton, A.; Danelon, A. F.; Torres, H. J. da S.; Xavier, C. E. O.; Marques, P. V. *Rev. iPecege* **2016**, *1* (1), 103.
31. Wright, M.; Brown, R. C. *Biofuels, Bioprod. Biorefining* **2007**, *1* (3), 191.
32. Walla, C.; Schneeberger, W. *Biomass and Bioenergy* **2008**, *32* (6), 551.
33. Neves, M. F.; Trombin, V. G.; Consoli, M. *São Paulo UNICA* **2011**.
34. Vardon, D. R.; Rorrer, N. A.; Salvachúa, D.; Settle, A. E.; Johnson, C. W.; Menart, M. J.; Cleveland, N. S.; Ciesielski, P. N.; Steirer, K. X.; Dorgan, J. R.; Beckham, G. T. *Green Chem.* **2016**, *18* (11), 3397.
35. <https://www.icis.com/chemicals/channel-info-chemicals-a-z/> (accessed Sep 4, 2017).
36. Bart, J. C. J.; Cavallaro, S. *Ind. Eng. Chem. Res.* **2015**, *54* (1), 1.
37. Holladay, J. D.; Hu, J.; King, D. L.; Wang, Y. *Catal. Today* **2009**, *139* (4), 244.
38. Filtrox case study [https://www.vlb-berlin.org/sites/default/files/Seite/Bangkok Conference 2011 - Downloads/thu04-filtrox.pdf](https://www.vlb-berlin.org/sites/default/files/Seite/Bangkok%20Conference%202011%20-%20Downloads/thu04-filtrox.pdf) (accessed Sep 4, 2017).
39. <http://www.ibisworld.com/procurement/activated-carbon.html> (accessed Sep 4, 2017)
40. Aminoacids price <http://www.ajiaminoacids.com> (accessed Sep 4, 2017).

41. Aminobenzoate <http://www.bulksupplements.com/> (accessed Sep 4, 2017).
42. DHB acid <https://www.alfa.com/it/catalog/B24016/> (accessed Sep 4, 2017).
43. Bui, V.; Lau, M. K.; MacRae, D.; Schweitzer, D. WO2011085311A1.
44. Niu, W.; Draths, K. M.; Frost, J. W. *Biotechnol. Prog.* **2002**, *18* (2), 201.
45. Grotkjær, T. In *Fundamental Bioengineering*; Wiley-VCH Verlag GmbH & Co. KGaA, 2015; pp 499–546.
46. Xie, N.-Z.; Liang, H.; Huang, R.-B.; Xu, P. *Biotechnol. Adv.* **2014**, *32* (3), 615.
47. van der Sman, R. G. M.; Vollebregt, H. M.; Mepschen, A.; Noordman, T. R. *J. Memb. Sci.* **2012**, *396*, 22.
48. Lubben, M. No Title <https://www.bio.org/sites/default/files/WorldCongress/MarcelLubben.pdf> (accessed Oct 25, 2017).
49. Matthiesen, J. E.; Suástegui, M.; Wu, Y.; Viswanathan, M.; Qu, Y.; Cao, M.; Rodriguez-Quiroz, N.; Okerlund, A.; Kraus, G.; Raman, D. R.; Shao, Z.; Tessonnier, J.-P. *ACS Sustain. Chem. Eng.* **2016**, *4* (12), 7098.
50. Moresi, M. *Biotechnol. Bioeng.* **1981**, *23* (11), 2537.
51. Todaro, C. M.; Vogel, H. C. *Fermentation and Biochemical Engineering Handbook*; Elsevier Science, 2014.
52. Van De Graaf, M. J.; Vallianpoer, F.; Fiey, G.; Delattre, L.; Schulten, E. A. M. US20120238722A1.
53. Gutz, I. G. R. CurTiPot-pH and Acid-Base Titration Curves: Analysis and Simulation freeware. **2015**.
54. Couper, J. R.; Penney, W. R.; Fair, J. R. *Chemical Process Equipment: Selection and Design*; Elsevier Science, 2012.
55. Carraher, J. M.; Pfennig, T.; Rao, R. G.; Shanks, B. H.; Tessonnier, J.-P. *Green Chem.* **2017**, *19*, 3042.
56. Datar, R. V; Rosén, C.-G. In *Biotechnology Set*; Wiley-VCH Verlag GmbH, 2008; pp 469–503.
57. BTPX-<http://www.alfalaval.com/products/separation/centrifugal-separators/separators/btpx/> (accessed Oct 25, 2017).
58. Bratbak, G.; Dundas, I. *Appl. Environ. Microbiol.* **1984**, *48* (4), 755.

59. Godin, M.; Bryan, A. K.; Burg, T. P.; Babcock, K.; Manalis, S. R. *Appl. Phys. Lett.* **2007**, *91* (12).
60. Verstraete, W.; Clauwaert, P.; Vlaeminck, S. E. *Bioresour. Technol.* **2016**, *215*, 199.
61. Vriens, L.; Nihoul, R.; Verachtert, H. *Biol. Wastes* **1989**, *27* (3), 161.
62. Belfort, G.; Davis, R. H.; Zydney, A. L. *J. Memb. Sci.* **1994**, *96* (1–2), 1.
63. Rosengart, A.; Vizzi, M.; Manenti, F.; Citterio, A. *Energy Convers. Manag.* **2017**, *149*, 875.
64. Van Duuren, J. B. J. H.; Brehmer, B.; Mars, A. E.; Eggink, G.; dos Santos, V. A. P. M.; Sanders, J. P. M. *Biotechnol. Bioeng.* **2011**, *108* (6), 1298.
65. Tanaka, T.; Usui, K.; Kouda, K.; Nakanishi, K. *J. Chem. Eng. Japan* **1996**, *29* (6), 973.
66. Drum Filter https://www.andritz.com/se-kmfiltr-05_11_prayes_en.pdf (accessed Sep 4, 2017).
67. Bannwarth, H. *Liquid Ring Vacuum Pumps, Compressors and Systems: Conventional and Hermetic Design*; Wiley, 2006.
68. Aspects of Rotary Vacuum Filter Design and Performance http://www.nfm-filter.com/userfiles/file/Aspects_of_Rotary_Vacuum_Filter_Design_and_Performance.pdf (accessed Sep 4, 2017).
69. Bacchin, P.; Si-Hassen, D.; Starov, V.; Clifton, M. J.; Aimar, P. *Chem. Eng. Sci.* **2002**, *57* (1), 77.
70. Adham, S. S.; Jacangelo, J. G.; Laîné, J.-M. *J. / Am. Water Work. Assoc.* **1996**, *88* (5), 22.
71. Hong, W. H.; Lee, S. Y.; Hong, Y. K.; Won, H. J.; Huh, Y. S.; Song, H.; Lee, E. Z. WO2009082050 A1.
72. Lum, O. L.; Venkidachalam, G.; Neo, Y. C. US20110028759 A1.
73. Burton, F.; Tchobanoglous, G.; Tsuchihashi, R.; Stensel, H. D.; Metcalf & Eddy, I. *Wastewater Engineering: Treatment and Resource Recovery*; McGraw-Hill Education, 2013.
74. Clements, M.; Haarhoff, J. *Water SA* **2004**, *30* (1), 89.
75. Carraher, J. M.; Matthiesen, J. E.; Tessonier, J. P. *J. Mol. Liq.* **2016**, *224*, 420.
76. Scelfo, S.; Pirone, R.; Russo, N. *J. Mol. Liq.* **2016**, *222* (Supplement C), 823.

-
77. Gorden, J.; Zeiner, T.; Sadowski, G.; Brandenbusch, C. *Sep. Purif. Technol.* **2016**, 169, 1.
 78. Mersmann, A. *Crystallization Technology Handbook*; CRC Press, 2001.
 79. Matthiesen, J. E.; Carraher, J. M.; Vasiliu, M.; Dixon, D. A.; Tessonnier, J. P. *ACS Sustain. Chem. Eng.* **2016**, 4 (6), 3575.
 80. S Scherer, G.; Renner, T.; Meger, M. *J. Chromatogr. B Biomed. Appl.* **1998**, 717 (1–2), 179
 81. Henley, E. J.; Seader, J. D.; Roper, D. K. *Separation Process Principles*; Wiley, 2011.
 82. Mao, Z.; Sun, X.; Luan, X.; Wang, Y.; Liu, G. *Chinese J. Chem. Eng.* **2009**, 17 (3), 473.
 83. Suren, S.; Sunsandee, N.; Stolcova, M.; Hronec, M.; Leepipatpiboon, N.; Pancharoen, U.; Kheawhom, S. *Fluid Phase Equilib.* **2013**, 360.
 84. ScreenBowl-<http://www.flsmidth.com/en-US/Industries/Categories/Products/Classification/Centrifuges/ScreenbowlCentrifuge/ScreenbowlCentrifuge> (accessed Apr 12, 2017).
 85. Leaf_filter-<http://www.solidliquid-separation.com/pressurefilters/verticalleaf/verticalleaf.htm> (accessed Sep 6, 2017).
 86. Cheryan, M. *Ultrafiltration and Microfiltration Handbook*; Taylor & Francis, 1998.
 87. Capelli, S.; Rosengart, A.; Villa, A.; Citterio, A.; Di Michele, A.; Bianchi, C. L.; Prati, L.; Pirola, C. *Appl. Catal. B Environ.* **2017**, 218, 220.
 88. Scelfo, S.; Pirone, R.; Russo, N. *Catal. Commun.* **2016**, 84, 98.
 89. Vardon, D. R.; Franden, M. A.; Johnson, C. W.; Karp, E. M.; Guarnieri, M. T.; Linger, J. G.; Salm, M. J.; Strathmann, T. J.; Beckham, G. T. *Energy Environ. Sci.* **2015**, 8 (2), 617.
 90. Castellan, A.; Bart, J. C. J.; Cavallaro, S. *Catal. Today* **1991**, 9 (3), 237.
 91. Peters, M. S.; Timmerhaus, K. D.; West, R. E.; Timmerhaus, K.; West, R. *Plant design and economics for chemical engineers*; McGraw-Hill New York, 1968; Vol. 4.
 92. Kazachkin, D. V.; Colakyan, M.; Moesler, F. J. WO2014012030A1.
 93. GHG_Protocol. *The greenhouse gas protocol: a corporate accounting and reporting standard*; Sustainable, W. B. C. for, Institute, Eds.; World Resources Inst, 2017
 94. Keller, J.; Hartley K. *Water Sci. Technol.* 2003, 47(12), 43.

Chapter 4

Development of a predictive model for microfiltration

This chapter describes the development of a model able to predict the flux reduction of a cross flow membrane for broth clarification. The main modelling challenges of this common (but little understood) unit operation are introduced in Paragraph 4.1. Paragraph 4.2 describes the statistical tools applied to study the uncertainty propagation from the model-semi empirical parameters to the simulation results. The model is defined in Paragraph 4.3, with the theoretical background to understand the multi-scale phenomena that affect filter performances. The results of model validation and the analysis of uncertainty propagation are reported in Paragraph 4.4, followed by the general conclusions of Paragraph 4.5.

4.1 - Broth Clarification, a challenge for modelling

High throughput and contained costs are primary aspects for any downstream operation in the field of biorefinery. Chemicals and fuels derived from biomass must compete with the low price of oil, though introducing a number of new technological challenges related to seasonality, dilution, non-homogeneous substrates. Bio-products recovery and purification can account up to the 80% of the final price and the removal of the microorganisms from the fermentation broth can become one of the most delicate downstream operations.^{1,2}

For large-scale applications, crossflow filtration is widely used, as a support to centrifugation or even in its substitution, thanks to a much sharper particle size cut-off and a lower energy consumption. As for many other operations in bioprocesses, the method to scale up filtration units is strongly empirical, because of the variability of filterable substrates and because of the diverse possible operation conditions.³ However, when assessing the economic feasibility of a new process at its early stage of study, it is not always possible to proceed with the usual empirical approach. Still, Quality by Design (QbD) practice requires quick estimations of process layout and costs even at the first stages of bio-chemical routes investigations, when the available data are minimal. In this way, the economic and environmental performances of the future plant are taken into account from the beginning, both for pharma bioprocesses or biorefining applications (examples are available for bio-ethanol,⁴ bio-butanol,⁵ polyhydroxy-alkanoates⁶).

For the adipic acid case study, the small scale experimental information and the general lack of standardized data for ultrafiltration units complicate any predictive approach.

The problem of representing microorganism suspensions in industrial crossflow filters has been extensively studied, but the results are always strongly dependent on the experimental conditions and little reproducibility has been achieved, even for the same bacterial strains. Tarleton and Wakemann stated in the middle of the 90s that previous studies suffered of “conflicting experimental data”, and tried to de-couple the different mechanisms of biological fouling.⁷ The main obstacles for a good modelling were later identified in the complexity of biological solutions, the weakness of the theoretical models and the non-linear interactions between different causes.⁸ Table 4.1 lists the main phenomena that can affect the filtration behaviour of a membrane.

Table 4.1 - List of the phenomena influencing the cake formation and flux reduction

	Phenomenon	Causes	Scale level
1	Cell shape (spheroidal, rod-like, flat)	Type of culture	Nano and micro-scale
2	Cell compressibility	pH, ionic strength	
3	Cell Size distribution	Type of culture	
4	Cell age	Process conditions	
5	Presence of extracellular colloids	Proteins, DNA, etc	
5	Membrane roughness/hydrophobicity	Surface treatments	Micro and meso scale
6	Membrane pore size and distribution	Production process	
7	Filtration module geometry	Membrane selection	
8	Cross-Flow velocity	Operation mode	Macro scale (operation)
9	Trans membrane pressure	Operation mode	
10	Cell concentration	Operation mode	

The easiest representation of the flux of permeate in a filter is the Darcy law with additive resistance contribution, reported in Eq.4.1:

$$J_p = \frac{\Delta P_{TM}}{\mu_p \sum_{i=1}^n R_i} \quad \text{Eq. 4.1}$$

where ΔP_{TM} is the applied transmembrane pressure, μ_p is the dynamic viscosity of the permeate and R_i is the resistances to the flux due to the specific fouling mechanism. The research activity of the late 80s and first half of the 90s was mainly devoted in recognizing which phenomena contribute to membrane fouling (for example bio-film formation, polarization, clogging, etc.), with some first attempts to model the effects.^{9,10} The main aspects of the fouling mechanism were qualitatively understood, but a general paradigm valid for any type of microorganism was far from being achieved. For this reason, subsequent research efforts changed approach, directing to different purposes.

A first trend in modern filter modelling is the characterization of very specific filtration applications, using adaptive models (Standard Blocking, Complete Blocking and Intermediate Blocking models are some of the most popular) to represent empirical data.¹¹ The representation is good in most of the application, but the results are highly context

dependent, as for yeast filtration in beer industry.¹² Another trend is the development of highly detailed computational fluid dynamics (CFD) simulations of cross-flow filters, to gain a deep and detailed insight of the system.¹³ CFD simulations, however, are both computationally and time demanding, applicable only to simplified systems. Also, due to the evasiveness of the fouling mechanisms, another approach is the one of using artificial neural network models.¹⁴ For conceptual design estimations, neither fully adaptive models, nor CFD simulations are suitable due to their lack of flexibility. Instead, a model with a sound physical interpretation, but with few and constrained parameters as Darcy equation, could provide reasonable values to predict the performances of complex (and little investigated) fermentation broths, as some uncertainty is tolerable for preliminary estimates.

The uncertainty in the calculated quantities derives from the application of semi-empirical models whose experimental parameters have been only roughly estimated or have been extended for analogy from similar systems. This lack of knowledge is defined “epistemic uncertainty” and requires statistical concepts from the field of Possibility Theory. In this framework, an original and flexible model for representing the biological fouling in cross-flow ultrafiltration units is proposed, with the purpose of estimating filtration costs. An uncertainty propagation algorithm, based on the Possibility Theory, is implemented to deal with the lack of experimental knowledge of certain biological systems. To the authors’ knowledge, this is the first study that applies possibility theory as a supporting tool to process conceptual design, in the field of industrial bio-filtration.

4.2 - Manage uncertainty with fuzzy logic: possibility theory

Empirical science has always been dealing with the concepts of error and uncertainty. Refined statistical tools have been developed down the last centuries, all based on the concept of “probability”, whose axiomatic definition was given only in 1933 by Kolmogorov.¹⁵

The “classical” interpretation of probability is applicable to any situation where the “principle of indifference” holds, that is where the known possible outcomes are equally likely. This is the case of random sampling in a well-known system, as for the dice game, where the probability of an event is always 1/6. This interpretation however is no more suitable when measuring unknown quantities, because neither the real value, nor the set of the possible events, are known a priori. In this case, the “frequentist” interpretation is used, which defines probability as the ratio between the number of observed events A and the number of experiments, for an infinite number of experiments (Eq. 4.2).

$$P_f(A) = \lim_{n \rightarrow \infty} \frac{n_A}{n} \quad \text{Eq. 4.2}$$

Since the number of experiments cannot be infinite for real applications, measures provide an estimate of the probability of a certain event, which is closer to the expected value for a high number of experiments, according to the law of large numbers. Obviously, the conditions of independence and repeatability (P_A exists and is the same for all the observations) of the experiments must hold. Hence, statistical analysis is carried out to estimate the frequentist probabilities in all situation that can be modelled using a probability distribution (Gaussian, binomial, and so on), i.e. the ones characterized by an high number of observations.

However, in many cases the “large amount of repetitions” is not viable. Is it possible to estimate the propagation of uncertainty, also in these conditions? De Finetti¹⁶ in 1930 and Ramsey¹⁷ in 1931 introduced the “subjective probability interpretation”, opening to the mathematical study of previously unmanageable problems. Subjective probability can be written as $P(A/K)$, which means that the value of probability given to the event A is conditioned to the current knowledge K of the system. If the knowledge changes, also the

value of probability might change: Bayes theory is the formal tool developed to tackle rigorously these problems. The concept of “Imprecise probability” is used instead to interpret the cases with a very poor knowledge of the system, defining an upper and a lower probability limit. Imprecision becomes then the representation of the lack of knowledge. A similar theoretical background can be found in the so called “Possibility Theory”, developed by Zadeh to treat the uncertainty deriving from a limited number of available measures (epistemic uncertainty) and any partial belief on the likelihood of an event, as the experience of a professional.¹⁸

These general statistical concepts can be consulted in dedicated books and manuals.^{19,20} Numerical methods based on Zadeh’s Possibility theory will be applied to study uncertainty propagation in the context of the present work. Since the experimental knowledge on cross-flow filters is not detailed enough to use a probability distribution for the uncertain parameters, the so called “*Possibility distribution of the event y , belonging to a set S* ”, in symbols $\pi(y)$, becomes a central concept. The statement $\pi(y)=0$ means that the outcome of y is impossible, while $\pi(y)=1$, means that the event y is likely, or in other words “unsurprising”, “possible”. The degree of knowledge expressed by $\pi(y)=1$ is far lower than $P(y)=1$ (i.e. 100% of probability, or “certain event”): it is like to say that one of the y in the set S is the true value. Two measures were defined to interpret a possibility distribution. The Possibility of an event in the subset A of S , is defined as:

$$\Pi(A) = \sup_{y \in A} \pi(y) \quad \text{Eq. 4.3}$$

and the Necessity of an event A , is defined as:

$$N(A) = 1 - \Pi(\bar{A}) = \inf_{y \notin A} (1 - \pi(y)) \quad \text{Eq. 4.4}$$

Let $P(\pi)$ be the family of the possible probability distribution for all events A so that

$$N(A) \leq P(A) \leq \Pi(A) \quad \text{Eq. 4.5}$$

then

$$N(A) = \inf_{P(\pi)} P(A) \quad \text{and} \quad \Pi(A) = \sup_{P(\pi)} P(A). \quad \text{Eq. 4.6}$$

In this way, Necessity and Possibility can be considered as the upper and lower limits of the probability of the same event. Any form of statistical distribution (Gaussian, log-normal, etc.) could describe the probability of the event within these limits, however, due to the already mentioned lack of knowledge, the possibility distribution does not provide

any further information. For example, taking into consideration Figure 4.1, given two physical limits $[a,b]$ to the compressibility index and a most likely value c , the triangular possibility distribution represents the family of all the probability density functions with support $[a,b]$ and mode c . Another shape for possibility distribution is the rectangular, which mean that the real value is comprised between $[a,b]$, but in the interval all values equally possible. Taking an average number, the most common practice in these cases, would result in a false assumption (i.e. the average value is “better”). Possibility distributions are useful to represent epistemic uncertainty, and can be successfully applied to study uncertainty propagation in modelling problems.

Given a generic function $G = f(x_1, \dots, x_N)$, the output value G will be affected by an uncertainty if the N input variables are uncertain. The input uncertainty can be probabilistic, possibilistic or a combination of both. In this application only possibilistic uncertainty propagation will be considered.

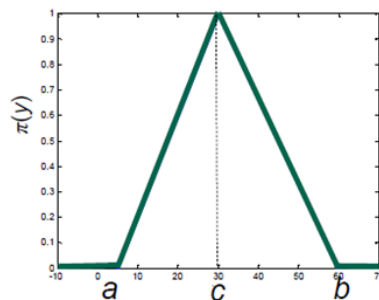


Figure 4.1 - Example of triangular possibility distribution

Uncertainty propagation in possibilistic problems is performed applying the “extension principle of fuzzy set theory”. If x_1, \dots, x_n are real variables described by the possibility distributions $\pi_1(x_1), \dots, \pi_N(x_N)$ and G is a single real quantity, the principle extends the function $G = f(x_1, \dots, x_N)$ to a function that maps from and to the class of all the defined possibility distributions $\pi_i(x_i)$.¹⁹ In other words, the extension provides the possibility distribution for the values of G , as defined in Eq. 4.7:

$$\pi_G(G) = \sup_{\bar{x}, g(\bar{x})=G} \min\{\pi_1(x_1), \dots, \pi_N(x_N)\} \quad \text{Eq. 4.7}$$

In particular

$$\min\{\pi_1(x_1), \dots, \pi_N(x_N)\} = \pi_{x_1, \dots, x_N}(x_1, \dots, x_N) \quad \text{Eq. 4.8}$$

where $\pi_{x_1, \dots, x_N}(x_1, \dots, x_N)$ are the joint possibility distributions of the N input quantities.

An alternative formulation of the extension principle is based on the representation of the output possibility distribution in the form of a nested set of intervals

$$A_\alpha = [\underline{G}_\alpha, \bar{G}_\alpha] = \{G : \pi_G(G) \geq \alpha\} \quad \text{Eq. 4.9}$$

which are usually referred to as “ α -cuts”.

Indicating as $X_{1\alpha}, \dots, X_{N\alpha}$ the α -cuts of the input quantities x_1, \dots, x_N , the extension principle becomes, for a given value of α in $[0, 1]$:

$$\underline{G}_\alpha = \inf(g(x_1, \dots, x_N), x_1 \in X_{1\alpha}, \dots, x_N \in X_{N\alpha}) \quad \text{Eq. 4.10}$$

$$\bar{G}_\alpha = \sup(g(x_1, \dots, x_N), x_1 \in X_{1\alpha}, \dots, x_N \in X_{N\alpha}) \quad \text{Eq. 4.11}$$

This second formulation has been implemented in the ultrafiltration algorithm, whose scheme is summarized in Figure 4.2. Detailed information on the numerical method of the α -cuts to apply the fuzzy-set extension principle is available in literature.²¹

The intervals of variability of the three uncertain variables are calculated for each value of the α -cut, defining the search space for the optimization algorithm. As shown in Figure 4.2, the optimization tool calls the fed-batch filtration model, providing the values of the uncertain parameters. Then, the stiff DAEs system is solved (Matlab ode15s function) for each search point. The average permeate flux value is returned to the optimizer, for its minimum and maximum calculation. These values are the extremes of the nested sets of intervals mentioned in Eq. 4.9. A genetic algorithm (Matlab GA function) was applied to limit the number of the required evaluations of the stiff system of DAEs and accelerate the problem solution. The main output of the simulation is the uncertainty profile of the average permeate flux, i.e. its possibility distribution together with its two corresponding limit-cumulative density functions (CDF). The average flux values are associated to capital and operating expenditures (CAPEX and OPEX) by the implemented cost function. In this way, the possibility distributions and CDF plots are provided also for the cost estimates.

The quantity of information deriving from the application of this method is higher than a simpler sensitivity analysis, and could be considered as a more powerful “worst condition design” approach. In fact, possibility theory allows distinguishing those parameters that are to be treated with a pure conservative estimation (e.g. the pumping cost to guarantee turbulence) and those parameters with experimental uncertainty associated. Uncertain inputs identify a range of variability also on the output, ascribable to the experimental uncertainty. If the purely conservative assumptions can be re-considered and corrected only in the phase of detailed-engineering, the range of variability determined by the limit CDFs can be revised earlier, with laboratory and pilot plant investigation. In addition, the cost ranges determined by the uncertain parameters give an indication of the “economic value” of this investigation.

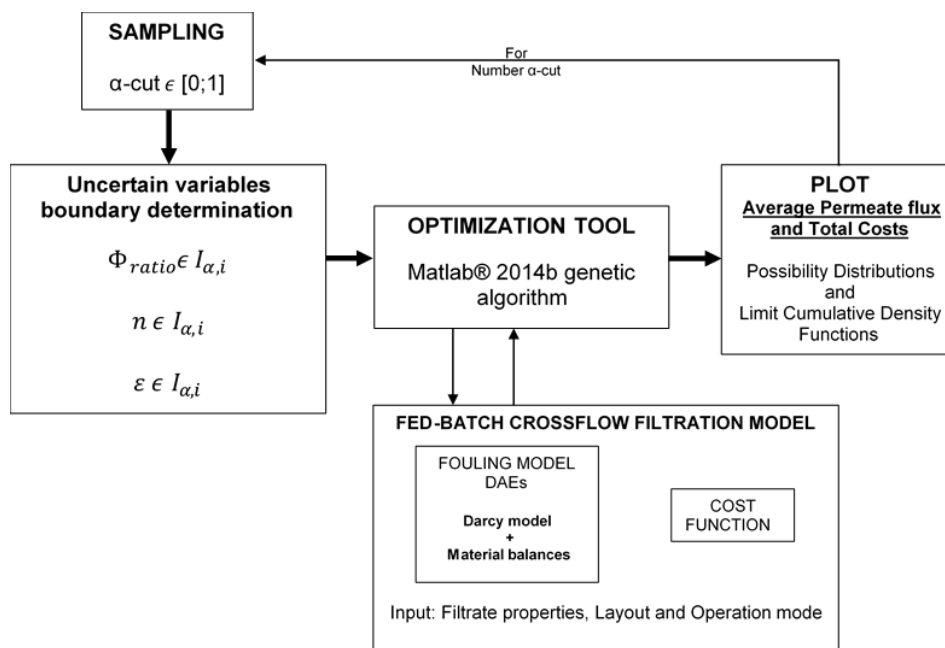


Figure 4.2 - Algorithm scheme: each α -cut determines the variation intervals for the uncertain parameters, defining the search space for the min/max optimization algorithm. The results are used to build the possibility distributions for the permeate flux and costs.

4.3 - Theory of filter fouling and model development

The permeate flux reduction due to membrane fouling is determined mainly by three aspects: the type of filtration equipment, the operation mode, and the fouling properties of the filtrate.

For the first two, the model will consider the unit layout with fed-batch operation presented in Figure 4.3: each feed pump is assumed to serve 24 parallel membrane modules, and each recirculation pump 4 modules (equipment detail will be described in the next sections). This layout is a simplification of the real possible dispositions (multiple array with booster pumps, Christmas-tree network, etc.), which allow an optimization of the pumping expenses.²² Such a level of detail is not advisable during conceptual design. Also, the variability of the filter geometries is remarkable, with alternatives such as hollow fiber, spiral wound, flat sheet, tubular and capillary filters.³ Several technological solutions have applied to enhance filter performances (e.g. vibrating modules, pulsed operation, etc.), resulting in an even wider range of equipment shapes.²³ To avoid excessive complications, the membrane implemented in the model has a simple multi-channel tubular layout, highly suitable for fouling systems as bacterial suspensions. A ceramic module was chosen, more expensive than plastic ones, but resistant to chemical cleaning and durable. The fouling behavior of the microorganism suspension is predicted solving the dynamic material balances on the single unit, calculating the permeate flux according to Eq. 4.1. The contributions of the different fouling mechanisms that progressively reduce the membrane permeability are reported in the next paragraphs.

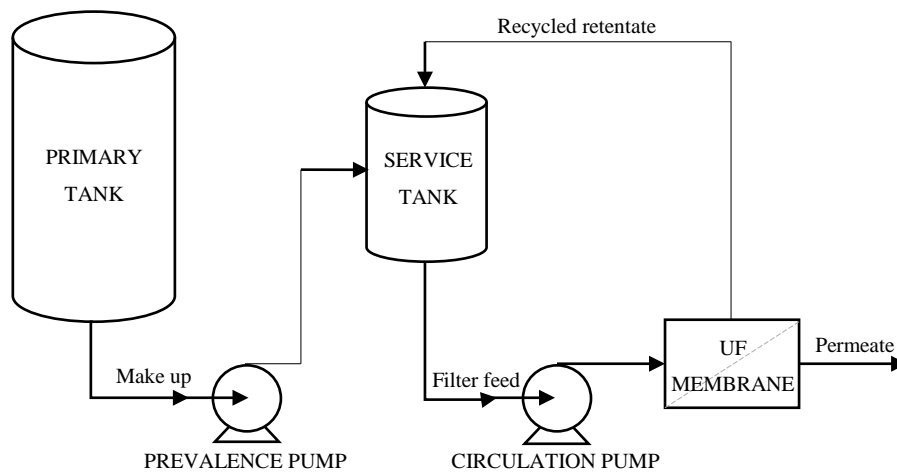


Figure 4.3 - Fed batch filtration unit with buffer tanks, simplified scheme.

4.3.1 - Clean membrane resistance

R_m can be derived from the “free water flow” indication, usually provided in the technical datasheet of commercial membranes. A new membrane has a lower resistance than a used and regenerated one, due to irreversible fouling and aging.²⁴ Considering an industrial plant, it is advisable to consider a free water flow reduced of the 20%, or, in other words, a corresponding R_m increased of the 25%.²⁵ Analytical equations for R_m are available, if the physical properties of the membrane are known.¹⁰

4.3.2 - Adsorption resistance

R_{ads} is caused by the adsorption fouling, when smaller particles enter the membrane pores and adsorb to the channel walls. This reduces the channel diameter, enhancing flow resistance. The rate of fouling is function of the surface material and of the broth composition; experimental evidence states that R_{ads} reaches a maximum when there is no more surfaces available for adsorption. It is important to notice that adsorption fouling does not clog entirely the membrane, while according to standard blocking model a “steady state resistance” does not occur and fouling continues until the flux is stopped.¹² It was shown

for *Escherichia coli* fermentation broths that the “steady state” resistance value exists and is not sensitive to transmembrane pressure, neither to cross flow velocity.²⁶ This was confirmed later also for *Lactobacillus delbrueckii*.²⁷ To measure the value of R_{ads} , the membrane is put in contact with the broth for 24 hours, then the surface is rinsed with fresh water and the permeate flux at a given pressure is measured. Very different experimental values are reported in literature, as adsorption is a complex phenomenon depending on the nature of the solutes, the thermodynamics of the system, the surface shape and the materials of the membrane.^{28,29} Without experimental data, it is impossible to provide the right value for this type of fouling: a first conservative guess could be 9 times the membrane resistance, the highest known contribution.³⁰ Also, the dynamics to reach the steady state are not univocally expressed. Following an approach reported in literature, the adsorption resistance will be:²⁷

$$R_{ads} = R_{ads}^{StSt} (1 - e^{-\beta t}) \quad \text{Eq. 4.12}$$

where β is a time constant of the order of 10^{-4} s^{-1} .²⁷

4.3.3 - Polarization resistance

R_{pol} is caused by the colloidal particles suspended in the fermentation broth. The Gel Layer Theory states that in proximity of the membrane, on the retentate side, the rejected molecules form a layer characterized by higher concentration and viscosity, which contrast the solvent flux.³¹ Two main trends have been observed in micro, ultra and nano-filtration, which describe the layer build-up from the beginning of the filtration to a pseudo-stationary value of polarization resistance.

First, the smallest rejected particles (colloids or macromolecules up to 100 nm of equivalent diameter), carried by the permeating flux, accumulate at the membrane surface, but Brownian back diffusion re-suspend them. The gel layer thickness reaches a stationary value, since the diffusion is equal to the rate of deposition. Brownian diffusivity is a complex phenomenon depending on the thermodynamics of the system and the fluid-dynamics, which can be calculated only for simple mixtures, i.e. with a limited number of solutes and well characterized monodisperse colloids.³² Second, bigger particles (larger than 500 nm) also accumulate in an analogous way. The thickness of the layer reaches a

pseudo-stationary value as well, because particles are swiped away by the tangential flux of retentate, causing the “shear-induced diffusion”.^{33,34} It is possible to predict the diffusion coefficient from the shear rate of the flow, using the correlations between mass and momentum transport, which are available in literature for a number of different shaped conducts.

The difficulty in estimating R_{pol} derives from the fact that in any industrial fermentation there is a population of colloidal particles (cell debris or macro-molecules) with a distribution of sizes and shapes, affected by either Brownian or Shear induced diffusion. Nonetheless, considering the specific type of membrane of this study it is possible to simplify the problem.

As a first assumption, the rejected particles must be larger than 100 nm; the smaller ones can permeate and pass the membrane. Moreover, the particles responsible of the polarization layer should be smaller than the bacteria (4 μm). Due to the high shear-rates resulting from the turbulent flow operation (cross flow velocity higher than 2 m/s), particles larger than 1 μm are lifted away. This second assumption is further supported by the evidence of the shear-induced particle segregation, which causes only smaller particles to deposit on the membrane.³⁵ The deposition of larger particles will be treated with the cake model. The particle sizes spanning from 100 to 500 nm are the most complex to model: these particles are too heavy for Brownian diffusivity and too small to be subject to the shear lift, hence no predictive equations are available. Therefore, these values have been measured directly, as shown in Figure 4.4.³⁶

The minimum value of diffusivity ($4\text{e-}12 \text{ m}^2/\text{s}$) was identified for 500 nm colloids, in correspondence with the transition of the mechanism dominating the particle mobility. These particles will be the major responsible of the gel layer build up.

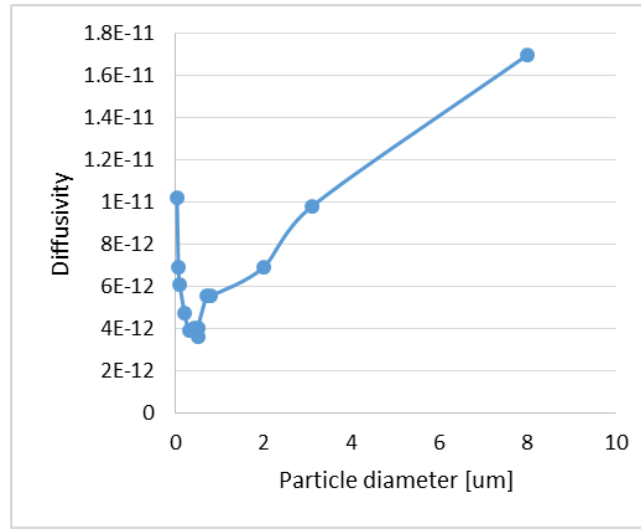


Figure 4.4 - Measured values for diffusivities of colloidal particles according to ref 36.

The material balance on the gel boundary layer yields Eq. 4.13.³⁷

$$\frac{dm_x^{gel}}{A dt} = J_p c_x^{bulk} - k_{mat} (c_x^{gel} - c_x^{bulk}) \quad \text{Eq. 4.13}$$

At steady state, applying the Darcy equation of flux and approximating $c_x^{gel} \gg c_x^{bulk}$ the equation becomes:

$$J_{pol}^{StSt} = k_{mat} \frac{(c_x^{gel} - c_x^{bulk})}{c_x^{bulk}} \approx k_{mat} \frac{c_x^{gel}}{c_x^{bulk}} = k_{mat} \frac{\Phi_x^{gel}}{\Phi_x^{bulk}} = \frac{\Delta P_{TM}}{\mu \cdot R_p} \quad \text{Eq. 4.14}$$

The concentration ratio is expressed with the particle volume fraction (solidosity)

$$\Phi_x^{gel} / \Phi_x^{bulk} \quad .38$$

The polarization layer is increased by the new particles carried by the permeate flux, while the combined effect of shear and Brownian diffusion determines the colloid resuspension, represented by the overall mass transfer constant. The variables in the equations are function of the axial coordinate z . To simplify the model, the following assumptions are made: a) bulk composition does not change along the membrane channel, since the permeate flow rate is far lower (<1%) than the bulk flow rate.³⁹ b) the flux is fully developed. k_{mat} is the overall convective mass transfer coefficient, that can be calculated for membranes using the correlations for fully developed flux, derived from Chilton-

Colbourn analogies in different geometries and for rough ducts (see explicit models in Appendix 2) .⁴⁰ These semi-empirical correlations provide axial averaged mass transfer coefficients, resulting in a simplification of the real dynamics of a permeating membrane. Another aspect to consider is that most of the available literature correlations were originally calculated for non-permeating ducts, and extending them to the case of membranes can lead to relevant approximations. However, the simplifications of this approach are less noticeable with high turbulence, since the flow profile is not disturbed by permeation with $Re > 2e4$.¹⁰

The Sh number correlation employed in this work applies for membranes in the polarization layers under turbulent crossflow⁴⁰:

$$Sh = 0.00929 \cdot \left(\frac{e_R}{d_h} \right)^{0.15} \cdot Re \cdot Sc^{0.5} \cdot \left(1.11 + 0.44 Sc^{-1/3} - 0.7 Sc^{-1/6} \right) \quad \text{Eq. 4.15}$$

where d_h is the channel hydraulic diameter, e is the channel absolute roughness height, Re is the Reynolds number and Sc is the Schmidt number, whose explicit equations are respectively:

$$Re = \frac{\rho \cdot v \cdot d_h}{\mu} \quad \text{Eq. 4.16}$$

and

$$Sc = \frac{\mu}{\rho \cdot Diff} \quad \text{Eq. 4.17}$$

where μ is the medium viscosity, ρ is the density, and $Diff$ is the diffusivity, estimated from the experiments. The equation assumes a pseudo-homogeneous flowing medium as the density difference of bacteria and fermentation broth is negligible.

The overall mass transfer coefficient is calculated as

$$k_{mat} = \frac{Sh \cdot Diff}{d_h} \quad \text{Eq. 4.18}$$

Wall particle solidosity, or gel concentration, is a pressure dependent value, but depends also on the nature of the gel. As it is complex (or impossible) to measure directly the dynamic gel concentration on the membrane, the use of the limit values of gel solidosity could lead to preferable conservative estimations. For example, if the colloidal particles

were monodisperse and spherical, Φ_x^{gel} would have the maximum analytical value of 0.64.⁴¹ However due to experimental evidence, it is preferable to consider an interval comprised between 0.58³⁸ and 0.75.⁴² Given also the range of bulk colloidal fractions Φ_x^{bulk} , comprised between 0.1% and 0.3%, which covers the typical concentrations for fermentation broths it is possible to calculate a range of variation for the ratio $\Phi_x^{gel} / \Phi_x^{bulk}$ that spans from 193 to 750.³² These limit values determine the shape of the possibility distribution for $\Phi_x^{gel} / \Phi_x^{bulk}$ shown in Figure 4.5. The transient formation of the gel layer is taken into consideration applying for J_{pol}^{StSt} the same dynamics of Eq. 4.12.

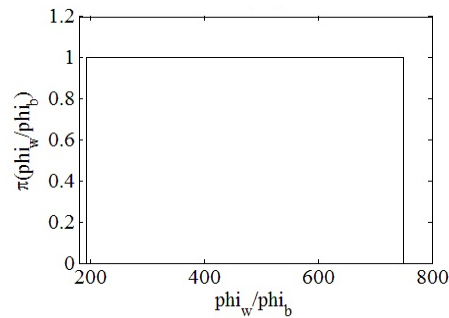


Figure 4.5 - Possibility distribution of the solidosity ratio.

4.3.4 - Cake resistance

R_c is caused by the filtered particles that build up a compressible cake layer on the surface of the membrane. In dead-end filters cake resistance is responsible of the most of the permeate flow reduction, outstanding rapidly the other resistances. Caking becomes relevant also for cross-flow configuration in case of a high suspension concentration or laminar flow conditions, but the usual industrial operations, with high tangential velocities and enhanced shear stress, reduce this occurrence.¹⁰ Similarly to polarization concentration, an equilibrium is reached between the transport of particles from the bulk to the membrane (due to permeation) and from the cake layer to the bulk (due to shear induced diffusion). As the phenomenon of caking concerns the bigger particles at higher concentrations, in this case the microorganisms, Brownian diffusion is negligible and the back diffusion is determined mostly by the shear stress. Carman-Kozeny equation, which defines specific

cake resistance for incompressible spheres of the same size, can describe the flux resistance across packed particles. However, microorganisms are compressible, and except few cases, their shape is far from spherical.

It is preferable to use the empirical specific cake resistance defined in Eq. 4.19.⁴³

$$\alpha = \alpha_0 \cdot \Delta P_{TM}^n \quad \text{Eq. 4.19}$$

The equation relates the experimental specific cake resistance constant α_0 , measured at constant pressure in dead-end or crossflow configuration, and the resistance at other pressures according to n , the compressibility index. As the macroscopic properties of bacterial cakes depend on many interconnected variables, there are multiple values of both α_0 and n , even for the same strain of bacteria. Table 4.2 reports α_0 and n values for several industrially relevant microorganisms. It is possible to notice how the compressibility index is lower for spheroidal microorganisms as yeasts, denoting a better packing, whereas resistance for rod shaped bacteria is sensitive to pressure because, in dead end filters, a higher pressure results in particle rearrangement. This rearrangement is less significant in cross-flow filters (lower n) because of shear induced particle orientation, which causes a more close packing. From the data of Table 4.2, the epistemic distributions of Figure 4.6 for rod-shaped and of Figure 4.7 for spheroidal microorganisms are derived.

Table 4.2 - Filtration cake properties of selected microorganisms

Microorganism	Shape	Size		α_0 [m/kg /Pa ⁿ]	n		Ref.
		Diameter r [μm]	Length [μm]				
<i>K. martianus</i>	Rod/ filamentous	5	-	2.88E+09	0.5	DE	41
<i>L. delbrueckii</i>	Rod	1	8	1.20E+09	0.63	CF	23
<i>L. delbrueckii</i>	Rod	0.5	3 to 6	2.02E+07	1	DE	39
<i>E. coli</i>	Rod	0.5	2 to 3	2.73E+10	0.51	DE	39
<i>S. cerevisiae</i>	Spheroidal	5	-	-	-	DE	44
<i>S. cerevisiae</i>	Spheroidal	5.35	-	1.01E+09	0.7	DE	43
<i>B. subtilis</i>	Rod	-	-	3.53E+08	0.8	DE	45

DE: dead end filter measurement
CF: cross-flow filter measurement

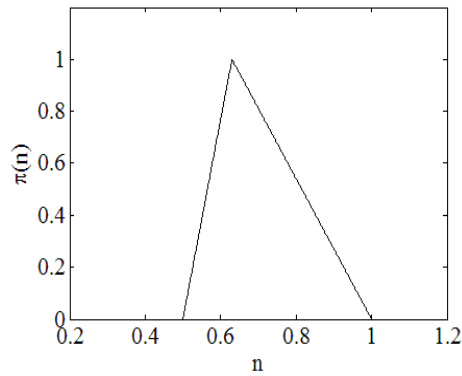


Figure 4.6 - Possibility distribution of the compressibility index for rod shaped microorganisms.

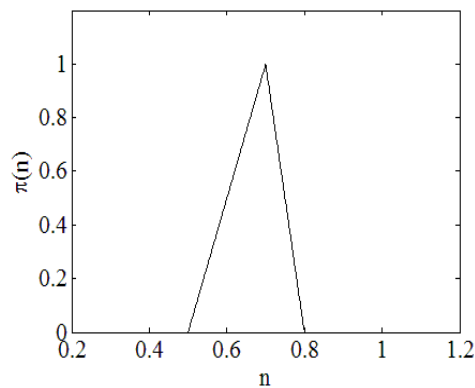


Figure 4.7 - Possibility distribution of the compressibility index for spheroidal microorganisms

The value for cake resistance is determined by Eq. 4.20:

$$R_c = \alpha \cdot w = \alpha \cdot \frac{m_c}{A} \quad \text{Eq. 4.20}$$

where m_c is the mass of particles deposited, A is the filtration area, assumed to be constant.

$$A = 2\pi(d_h - \delta) \cdot L \cong 2\pi \cdot d_h \cdot L \quad \text{Eq. 4.21}$$

In fact δ , cake layer thickness, is negligible in the operating conditions assumed for this work. To quantify the mass of deposited particles, the following material balance holds:

$$\frac{dm_{cells}^{cake}}{A dt} = J_p c_{cells}^{bulk} - K_{mat} (c_{cells}^{cake} - c_{cells}^{bulk}) \quad \text{Eq. 4.22}$$

K_{mat} is the overall convective mass transport constant, calculated with the same adimensional relation for turbulent flux used for R_{pol} . The shear induced diffusion coefficient is calculated applying the empirical equation proposed for particles with equivalent diameter of the order of 1 μm .³⁶

$$D_{shear} = D' \dot{\gamma} d_p^2 = 0.05 \cdot 2 \frac{u}{d_h} d_{cells}^2 \quad \text{Eq. 4.23}$$

The physical meaning of the predicted values is maintained introducing the following constraint:

$$\frac{d(m_{cells}^{cake}/A)}{dt} = J_p \cdot c_{cells}^{bulk} - K_{mat} (c_{cells}^{cake} - c_{cells}^{bulk}) \geq 0. \quad \text{Eq. 4.24}$$

The equation simply guarantees that the caking is an irreversible process, unless the filtration is stopped and the filter is regenerated. In fact, differently from the case of polarization resistance, a “pseudo-steady state” filtration condition would give an unrealistic prediction of the fouling behaviour. The bulk concentration of cells grows steadily, affecting the transport phenomena and consequently the permeate flux: because c_{cells}^{bulk} is far higher than the colloidal concentration, its variation causes appreciable changes. When c_{cells}^{bulk} reaches a specific value that enhances the cake formation (with a quick drop of the permeate flux), membranes must be cleaned. The cell concentration on the cake c_{cells}^{cake} is defined as:

$$c_{cells}^{cake} = \rho_{cells} (1 - \varepsilon) \quad \text{Eq. 4.25}$$

where ρ_{cells} is the micro-organism wet based density and ε is the cake porosity. Modern experimental techniques allow a precise measurement for bacterial density: for example, for yeast cell is around 1100 kg/m^3 , while for *E. coli* is 1160 kg/L m^3 .^{46,47} Cake porosity ε , instead, is a derived variable, which cannot be measured directly but is rather deduced from Carman-Kozeny (CK) relation: the calculated value is hence affected by unavoidable experimental errors, and approximated by the fact that CK model was originally developed only for spheroidal and incompressible particles.⁴⁸ Geometrical considerations on the

packing of particles allow setting a lower value to the epistemic distribution of porosity, while the little amount of data in literature sets the upper: the values are showed in Figure 4.8 for rod-shaped and in Figure 4.9 for spheroidal microorganisms.

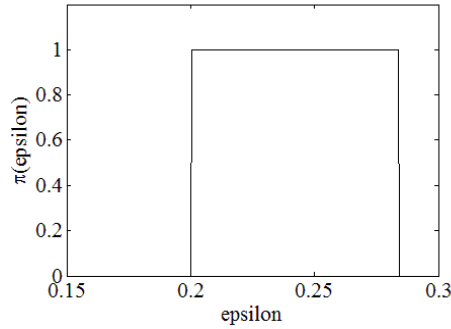


Figure 4.8 - Possibility distributions of the cake porosity for rod shaped microorganisms.

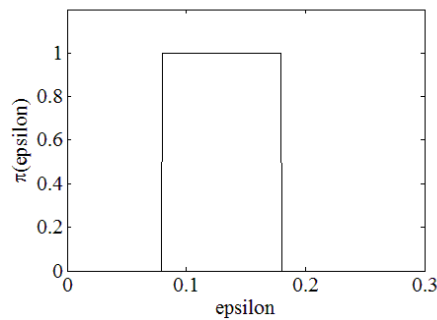


Figure 4.9 - Possibility distributions of the cake porosity for spheroidal microorganisms.

4.3.5 - Model for a filtration unit

To obtain the permeate flux reduction profile, the system of differential-algebraic equations (DAEs) of Eq. 4.26 is solved. The material balances denote a fed-batch operation system with constant holdup volume, as presented in Figure 4.3. The integration time is stopped, and membrane “cleaning and regeneration” is considered, when one of the following conditions is reached:

- The final bulk cell concentration is 8 times the initial one (87.5% permeate recovery).
- The permeate flux is 10% the initial one.

- The time limit of 20 h is reached.

$$\left\{ \begin{array}{l}
 J_p(t) = \frac{\Delta P_{TM}}{\mu_p \left(R_m + (R_{ads}^{StSt} + R_{pol}^{StSt})(1 - e^{-\beta t}) + \alpha_0 \cdot \left(\frac{\Delta P_{TM}}{\Delta P_{TM,0}} \right)^n \cdot \frac{m_c}{A} \right)} \\
 \frac{d(m_c/A)}{dt} = J_p \cdot c_{cells}^{bulk} - K_{mat} (c_{cells}^{cake} - c_{cells}^{bulk}) \\
 V \frac{dc_{cells}}{dt} = c_{cells}^0 \cdot J_p(t) \cdot A \\
 \frac{dV}{dt} = 0
 \end{array} \right. \quad \text{Eq. 4.26}$$

The average flux for the single filtration membrane is calculated, and the result is used to estimate the overall cost of the process. For this purpose, the general equations must be contextualized for a specific case study. An industrial filtration of *L. delbrueckii* for the production of lactic acid is assessed, as the benchmark data are available from a pilot plant.

²⁷ Table 4.3 reports the technical characteristics of the hypothesized industrial filtration.

Table 4.3 - Simulated fermentation broth characteristics and membrane properties.

Fermentation Broth ^a		Membrane ^b	
Microorganism	<i>L. delbrueckii</i>	Shape	Tubular/multichannel
Shape	Rod	Channel diameter	5.75 [mm]
Size d/L	1/8 [μm]	Module length	1.178 [m]
Equivalent diameter	2.28 [μm]	Channels/module	368
Wet cell density	1100 [kg/m ³]	Module Area	7.8 [m ²]
Wet cell concentration	2.6 [kg/m ³]	Material	Ceramic ^c
Viscosity	0.78e-3 [Pa s]	Pore diameter	100[nm]
Temperature	48 [°C]	Roughness height	5e-6 [m]
Permeate volume	11.26e-3 [m ³ /s]	Membrane resistance	3.27e11 [m ⁻¹]
Colloidal content	01-0.3 [kg/m ³]	Unit volume holdup ^c	0.120 [m ³]
		Cleaning Time ^d	0.33 [h]

a- Data from ref.27.²⁷

b- Commercial membrane Kerasep K01BX

c- Comprehensive of the membranes, piping, pumps and buffer tanks.

d- Value reported in ref.25.²⁵

Once the flux reduction profile is known, it is possible to calculate the average permeate flux, considering also the time for membrane cleaning and regeneration, which reduces further the throughput. The number of units to be installed is given by the ratio of the average flux per single unit and the desired permeate productivity. For the calculation of the filtration expenses, a cost function based on literature data and industrial reports was implemented.^{25,49} It should be observed that, for a better representation of real industrial costs, the function should be based on updated quotes from filters manufacturers. Therefore, the calculated values are mere estimates, though in line with industrial filtration costs (Table 4.4). Also, the pumps and modules disposition, the assumed cross-flow velocity and the transmembrane pressure require further optimization. For the sake of this study, the achievement of a “cost value” helps to understand the effects of epistemic uncertainty propagation, from highly specific experimental parameters to the economic performances of a full-scale process. The Matlab codes implementing the model are reported in Appendix 2.

Table 4.4 - Cost function composition

General assumptions		Simulated variability	
Duration	10 years	Ceramic module cost	500 \$/m ²
Interest rate	15%	Number of modules	98-200
Reference year	2014	Permeate cost per liter ^b	0.0022-0.0037\$
Capital Expenditure ^a		Operating Expenditure ^a	
Membrane cost	20%	Electric Power	45%
Pumps	40%	Maintenance & Chemicals	19%
Others	40%	Manpower	36%
a- Cost evaluation for the example case of 36 L/m ² /h of average flux			
b- In the case of wine ultrafiltration, the cost is about 0.0018 \$/L. ⁵⁰			

4.4 - Results and discussion

4.4.1 - Model validation

The proposed Darcy additive resistances model was tested with the detailed experimental data provided in literature for the filtration of *Lactobacillus delbrueckii* used for the production of lactic acid ($C_3H_6O_3$).²⁷ The simulated system was a pilot plant with the same specifications of Table 4.3, but a smaller 7 channels unit and batch operation mode.

At first, the proposed model was tested through a sensitivity analysis in order to verify the qualitatively response by changing the main macroscopic variables.

Cross-flow velocity acts directly on the membrane fouling mechanism, in particular on cake deposition. As velocity increases, the back transport of cells from membrane wall to bulk becomes faster. This determines a lower cake thickness that affects the overall cake resistance. The developed model respects this trend: a sharp flux decline is observed at low velocity, causing lower steady state permeate flux, as shown in Figure 4.10.

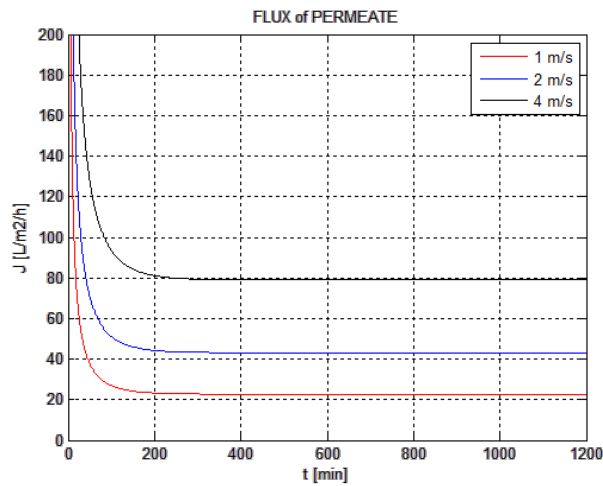


Figure 4.10 - Flux reduction profiles for batch *L. delbrueckii* cross flow ultrafiltration: sensitivity analysis for crossflow velocity variation.

Filtration units are pressure-driven systems, so an increase in pressure determines higher performances in term of permeate flux. However, there is not a linear correlation between ΔP and J (flux) because trans-membrane pressure also affects the cake compressibility and, as consequence, the specific cake resistance. This can be appreciated in Figure 4.11.

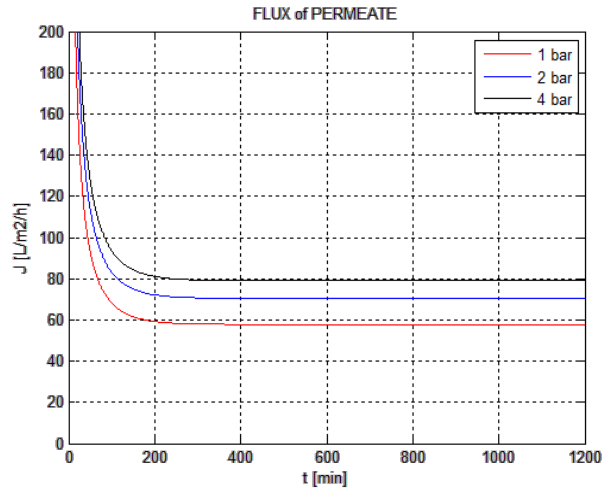


Figure 4.11 - Flux reduction profiles for batch *L. delbrueckii* cross flow ultrafiltration: sensitivity analysis transmembrane pressure

The model response for different particle size is shown in Figure 4.12: it is possible to see that a strong deviation occurs for particles with 500 nm diameter. As Cho et al.³⁶ explained, this type of particles are in the transition region between two mobility mechanisms, Brownian and Shear-induced diffusion models, hence the rate of fouling is sensibly different.

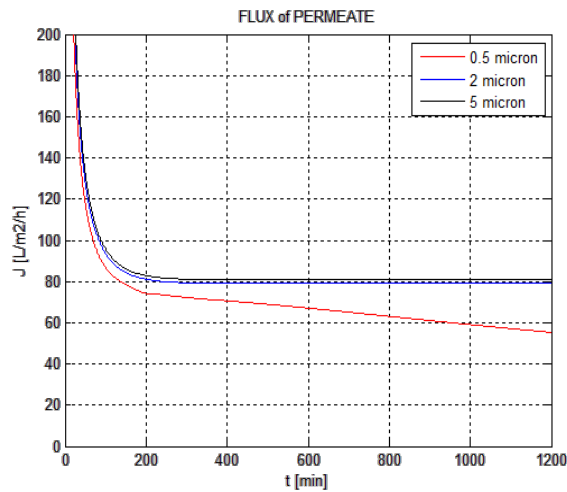


Figure 4.12 - Flux reduction profiles for batch *L. delbrueckii* cross flow ultrafiltration: sensitivity analysis for filtrate particle size.

For longer filtration time the model is able to predict a secondary flux decline determined by an increasing in cake resistance: this time usually represents the “switch off” of the filtration operation and it means that is no more convenient to continue and that a cleaning procedure is needed. The sudden change of slope shown in Figure 4.13 represents the moment when the clogging becomes irreversible and the membrane should regenerated.

In order to validate the model not only on a qualitative base, the exact conditions of the reference *L. delbrueckii* filtration were reproduced. As shown in Figure 4.14, the modelled flux decline is in good agreement with the pilot plant measured values.

Proven the capability of the model in a known boundary, the next step was to evaluate its predictive ability associating the uncertainty propagation.

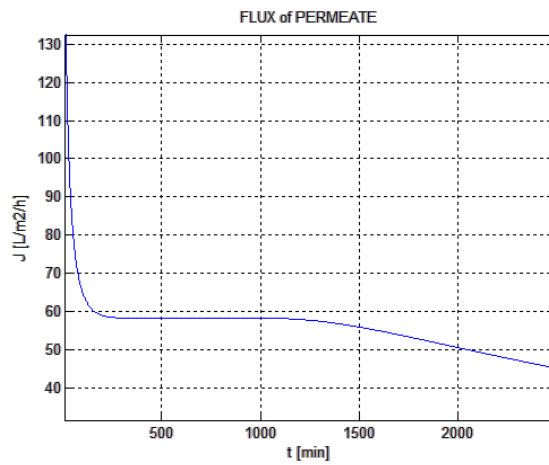


Figure 4.13 - Flux reduction and irreversible clogging.

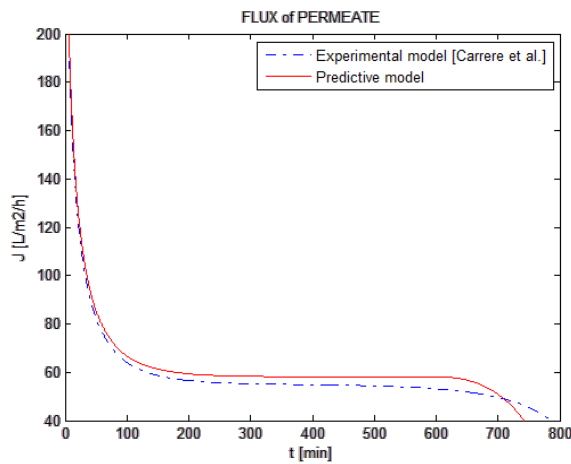


Figure 4.14 - Flux reduction profiles for batch *L. delbrueckii* cross flow ultrafiltration: comparison between the measured and calculated values.

4.4.2 - Uncertainty propagation

The full-scale plant was simulated, with target productivity of 350,000 m³/year of permeate, corresponding to ca 30,000 metric tons of lactic acid production per year. The operating conditions, reported in Table 4.3 are intended to reproduce typical industrial

settings. A transmembrane pressure of 200 kPa and a crossflow velocity of 4 m/s were assumed. A Montecarlo sampling was also implemented in order to study the model sensitivity with respect to both pressure and velocity: in the investigated domain of 100-400 kPa and 3-5 m/s (to ensure turbulence flow), a deviation of $\pm 10\%$ for the average flux was found.

The resistances were calculated with the α -cut method, without using the experimental parameters of literature for a specific case, but using the extended epistemic intervals.

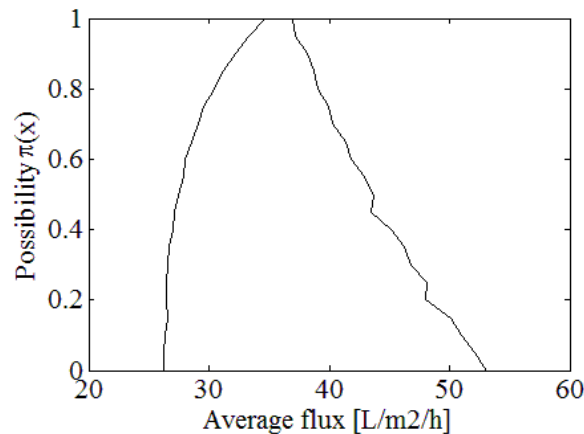
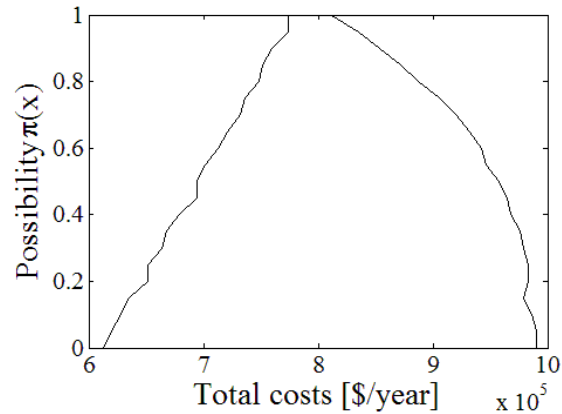


Figure 4.15 - Average permeate flux possibility distribution for a full-scale fed-batch ultrafiltration of *L. delbrueckii* (time step 10s - 20 α -cuts).

The calculated results provide lower values of permeate flux with respect to the ones measured in the pilot plant. In fact, the possibility distribution in Figure 4.15 tells that the likely average fluxes span between 26 and 53 L/h/m², with the most realistic values around 36 L/h/m², lower than the 60 L/h/m² of the pilot studies. This is because the average flux considers also those moments when the system is not productive (cleaning and maintenance), but also because a conservative approach was followed. Similarly, the cost estimates are conservative too, as shown in Figure 4.16 and Figure 4.17. The first plot presents the estimated annualized cost as a possibility distribution, while the second plot shows the corresponding limit cumulative density functions. The advantage of the CDF

representation is the easier interpretation of the data: in terms of cumulative probability, given a 95% of confidence, the higher costs of the proposed filtration plant will be comprised between 774,000 \$/year and 986,000 \$/year. A purely conservative approach would take 986,000 \$/year as the final estimation to be included in the feasibility study considerations. The application of possibility theory, instead, adds the extra information that an amount of 212,000 \$/year is the contribution of the lack of knowledge on the system. In the framework of a process feasibility study carried out when research is still ongoing, this information can help to set the priority of the aspects to be investigated, given the risk of extra expenses high as the variation range.



*Figure 4.16 - Cost possibility distribution for a full-scale biorefinery fed-batch ultrafiltration plant, for the clarification of a *L. delbrueckii* fermentation broth (time step 10 s – 20 α -cuts).*

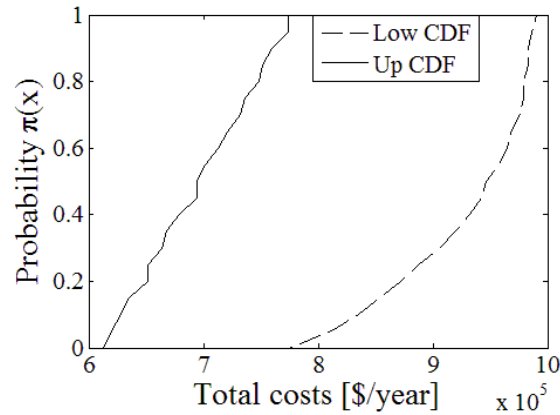


Figure 4.17 - Limit cumulative probability functions, corresponding to the cost possibility distribution of figure 4.16.

To better assess the potential of the model, the same full-scale plant configuration was simulated for *E. coli* and *S. cerevisiae*, some of the most interesting strains for industrial bioprocesses.⁵¹ In these cases an industrial/pilot plant benchmark is not considered, as the purpose is to show the effects on the output uncertainty changing the uncertainty in the input parameters.

Baker's yeast is widely used in industrial applications and its filtration behavior has been well investigated. Typically, the cells are spherically shaped, with an average cell size of 5 μm . The possibility distribution of Figure 4.9 was used for porosity and Figure 4.7 for the compressibility index. The less broad distribution denotes a higher agreement between literature data. This is reflected by the simulation results, in which the span between the limit upper costs is reduced to 47,000 \$/year as shown in Figure 4.18. Differently, *E. coli* is rod shaped, which complicates the packing properties, and shows very different filtration performances from case to case, due to the variability cell physical properties (depending on the type of strain, growth conditions, etc.). Hence, a rectangular possibility distribution for the compressibility index was used, bounded by the lowest and highest values available in literature. As a consequence of the poorness of input data, the simulation results in a wider span of 422,000 \$/year for the limit cumulate cost, as shown in Figure 4.19.

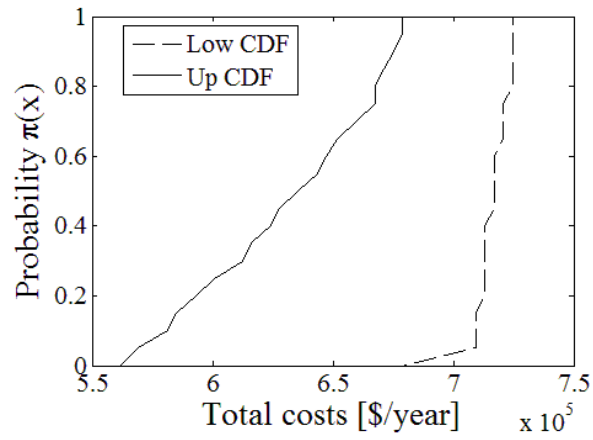


Figure 4.18 - Limit cumulative probability functions for a full-scale fed-batch ultrafiltration of *S. cerevisiae* (time step 10s - 20 α -cuts).

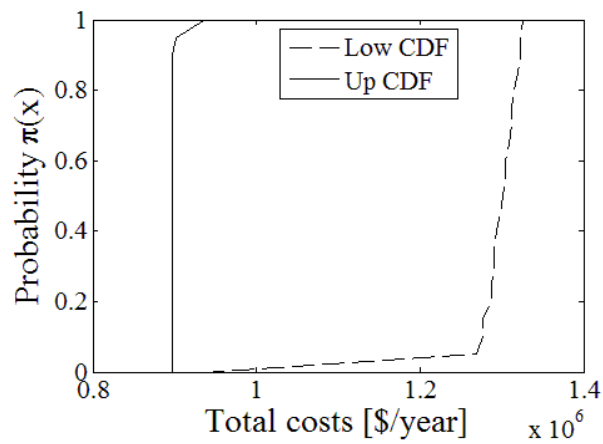


Figure 4.19 - Limit cumulative probability functions for a full-scale fed-batch ultrafiltration of *E. coli* (time step 10s - 20 α -cuts).

4.5 - Conclusions

The proposed conceptual design and cost estimation approach for cross-flow filtration units combines a predictive permeate flux reduction model and an uncertainty propagation algorithms. The flux reduction model is based on a Darcy equation with additive resistances, which is preferred for the simple formulation and the opportunity to extend it to different systems. The lack of experimental knowledge is treated with the Possibility Theory, which applies the Fuzzy set extension principle to estimate the uncertainty propagation from multiple uncertain input parameters to the final overall cost. In this way the model can be applied for predictive filtration simulations, and provides an indication of the contribution of uncertainty to the final result.

The model and the uncertainty propagation approach were tested on the industrial case of a *L. delbrueckii* broth clarification, for lactic acid production. The results show that the simulation yields conservative cost estimations, as desirable in conceptual design evaluations; the results are compatible with the data of a pilot plant experimentation. Some aspects require further investigation, to extend the applicability of the model also to other systems, with different filtration layouts and/or type of membranes. For example, the same model could be applied to simulate polymeric membranes, provided that the appropriate parameters are modified. More extensive benchmarking on industrial filtrations could characterize better the flexibility of the model in representing other microorganisms, and eventually could improve the cost function precision.

To conclude, bio-separations are more complex to standardize than in oil-industry and predictive models become more desirable, even in presence of preliminary experimental data. In this context, the developed method provides a predictive tool to assess the costs of fermentation broths clarification, estimating the uncertainties involved, and giving an indication of the economic impacts of more detailed research.

4.6 - Nomenclature

Given the large number of symbols employed in this Chapter, the following tables are reported, to help the reader in following the equations' meaning.

A	membrane area (m ²)	N	necessity
C	concentration (kg m ⁻³)	n	cake compressibility index
D	diffusion coefficient (m ² s ⁻¹)	P	possible probability distribution
d	diameter (m)	R	resistance (m ⁻¹)
J	flux (m s ⁻¹)	t	time (s, min, h)
K	mass transfer coefficient, cells (m s ⁻¹)	u	cross flow velocity (m s ⁻¹)
k	mass transfer coefficient, colloids (m s ⁻¹)	V	holdup volume (m ³)
L	module length (m)	w	cells mass per square meter (kg m ⁻²)
m	mass (kg)		

Greek symbols

α	specific cake resistance (m kg ⁻¹)	ϵ	cake porosity (-)
α_{cuts}	alfa-cuts	μ	dynamic viscosity (Pa s)
β	time constant (s ⁻¹)	Π	possibility
$\dot{\gamma}$	shear rate (s ⁻¹)	ρ	density (kg m ⁻³)
ΔP	pressure difference (Pa)	Φ	solidosity (particle volume fraction)
δ	cake thickness (m)	K	

Superscripts

<i>bulk</i>	bulk phase	<i>cake</i>	cake
<i>gel</i>	membrane gel layer	<i>StSt</i>	steady state

Subscripts

O	reference	<i>mat</i>	material
<i>ads</i>	adsorption	<i>P</i>	permeate
<i>c</i>	cake	<i>pol</i>	concentration polarization
<i>cells</i>	cells	<i>shear</i>	shear
<i>h</i>	hydraulic	<i>TM</i>	trans membrane
<i>K</i>	experimental coefficient	<i>x</i>	colloid

4.7 - References chapter 4

1. Harrison, R. G.; Todd, P.; Todd, P. W.; Rudge, S. R.; Petrides, D. P. *Bioseparations Science and Engineering*; Oxford University Press, **2015**.
2. Cherubini, F. *Energy Convers. Manag.* **2010**, *51* (7), 1412.
3. Drioli, E.; Giorno, L. *Comprehensive Membrane Science and Engineering*; Comprehensive Membrane Science and Engineering; Elsevier Science, **2010**.
4. Abdullah, S. S. S.; Shirai, Y.; Ali, A. A. M.; Mustapha, M.; Hassan, M. A. *Energy Convers. Manag.* **2016**, *108*, 233.
5. Qureshi, N.; Saha, B. C.; Cotta, M. A.; Singh, V. *Energy Convers. Manag.* **2013**, *65*, 456.
6. Morgan-Sagastume, F.; Heimersson, S.; Laera, G.; Werker, A.; Svanström, M. *J. Clean. Prod.* **2016**, *137*, 1368.
7. Tarleton, E. S.; Wakeman, R. J. *Chem. Eng. Res. Des.* **1993**, *72* (A3), 339.
8. Foley, G.; MacLoughlin, P. F.; Malone, D. M. *Sep. Sci. Technol.* **1995**, *30* (3), 383.
9. Nakanish, K.; Tadokoro, T.; Matsuno, R. *Chem. Eng. Commun.* **1987**, *62* (1–6), 187.
10. Belfort, G.; Davis, R. H.; Zydney, A. L. *Journal of Membrane Science*. 1994, pp 1–58.
11. Iritani, E. *Drying Technology*. 2013, pp 146–162.
12. Van der Sman, R. G. M.; Vollebregt, H. M. *J. Memb. Sci.* **2013**, *435*, 21.
13. Paipuri, M.; Kim, S. H.; Hassan, O.; Hilal, N.; Morgan, K. *Desalination* **2015**, *365*, 151.
14. Ní Mhurchú, J.; Foley, G. *J. Memb. Sci.* **2006**, *281* (1–2), 325.
15. Kolmogorov, A. N. *Foundations of the Theory of Probability*. **1950**.
16. De Finetti, B. *Fondamenti logici del ragionamento probabilistico*; Azzoguidi, 1930.
17. Ramsey, F. P. *Foundations of mathematics and other logical essays*; Routledge, 2013.
18. Zadeh, L. A. *Fuzzy Sets Syst.* **1978**, *1* (SUPPL. 1), 3.
19. Aven, T.; Zio, E.; Baraldi, P.; Flage, R. *Uncertainty in Risk Assessment: The Representation and Treatment of Uncertainties by Probabilistic and Non-Probabilistic Methods*; Wiley, 2013.

20. Ross, T. J. *Fuzzy Logic with Engineering Applications*; Wiley, 2016.
21. Baudrit, C.; Dubois, D.; Guyonnet, D. *IEEE Trans. Fuzzy Syst.* **2006**, *14* (5), 593.
22. Harker, J. H.; Backhurst, J. R.; Richardson, J. F. *Chemical Engineering*; Elsevier Science, 2013.
23. Charcosset, C. *Biotechnol. Adv.* **2006**, *24* (5), 482.
24. El Rayess, Y.; Albasi, C.; Bacchin, P.; Taillandier, P.; Mietton-Peuchot, M.; Devatine, A. *Innov. Food Sci. Emerg. Technol.* **2012**, *16*, 398.
25. Guerra, K.; Pellegrino, J. In *Science and Technology Program Report*; 2012; Vol. 174.
26. Li, S. L.; Chou, K. Sen; Lin, J. Y.; Yen, H. W.; Chu, I. M. *J. Memb. Sci.* **1996**, *110* (2), 203.
27. Carrère, H.; Blaszkow, F.; Balmann, H. R. De. *J. Memb. Sci.* **2001**, *186* (2), 219.
28. Meireles, M.; Aimar, P.; Sanchez, V. *J. Memb. Sci.* **1991**, *56* (1), 13.
29. Möckel, D.; Staude, E.; Guiver, M. D. *J. Memb. Sci.* **1999**, *158* (1–2), 63.
30. Ma, L.; Li, X.; Du, G.; Chen, J.; Shen, Z. *Colloids Surfaces A Physicochem. Eng. Asp.* **2005**, *264* (1–3), 120.
31. Bowen, W. R.; Jenner, F. *Adv. Colloid Interface Sci.* **1995**, *56* (C), 141.
32. Bacchin, P.; Si-Hassen, D.; Starov, V.; Clifton, M. J.; Aimar, P. *Chem. Eng. Sci.* **2002**, *57* (1), 77.
33. Nagata, N.; Herouvis, K. J.; Dziejwski, D. M.; Belfort, G. *Biotechnol. Bioeng.* **1989**, *34* (4), 447.
34. Tiwari, P.; Antal, S. P.; Podowski, M. Z. *Comput. Fluids* **2009**, *38* (4), 727.
35. Chellam, S.; Wiesner, M. R. *J. Memb. Sci.* **1998**, *138* (1), 83.
36. Cho, J.; Park, Y. J.; Sun, H.; Kim, S.; Yoon, Y. *Colloids Surfaces A Physicochem. Eng. Asp.* **2006**, *274* (1–3), 43.
37. Song, L. *J. Memb. Sci.* **1998**, *139* (2), 183.
38. Mondor, M.; Moresoli, C. *Desalination* **2002**, *145* (1–3), 123.
39. Song, L.; Elimelech, M. *J. Chem. Soc. Faraday Trans.* **1995**, *91* (19), 3389.
40. Gekas, V.; Hallström, B. *J. Memb. Sci.* **1987**, *30* (2), 153.
41. Elimelech, M.; Bhattacharjee, S. *J. Memb. Sci.* **1998**, *145* (2), 223.
42. Porter, M. C. *Ind. Eng. Chem. Prod. Res. Dev.* **1972**, *11* (3), 234.
43. Tanaka, T.; Tsuneyoshi, S.-I.; Kitazawa, W.; Nakanishi, K. *Sep. Sci. Technol.* **1997**, *32* (11).

44. Fillaudeau, L.; Carrère, H. *J. Memb. Sci.* **2002**, *196* (1), 39.
45. Tanaka, T.; Usui, K.; Kouda, K.; Nakanishi, K. *J. Chem. Eng. Japan* **1996**, *29* (6), 973.
46. Bryan, A. K.; Goranov, A.; Amon, A.; Manalis, S. R. *Proc. Natl. Acad. Sci.* **2010**, *107* (3), 999.
47. Godin, M.; Bryan, A. K.; Burg, T. P.; Babcock, K.; Manalis, S. R. *Appl. Phys. Lett.* **2007**, *91* (12), 123121.
48. Mota, M.; Teixeira, J. A.; Yelshin, A. *Sep. Purif. Technol.* **2002**, *27* (2), 137.
49. Green, D.; Perry, R. *Perry's Chemical Engineers' Handbook, Eighth Edition*; McGraw Hill professional; McGraw-Hill Education, 2007.
50. Bared.srl. Wine Filtration <http://www.bared.it/en/prodotti/filtrazione-tangenziale-a-membrana/> (accessed Oct 30, 2017).
51. Balat, M. *Energy Convers. Manag.* **2011**, *52* (2), 858.

Chapter 5

Kinetic study of muconic acid hydrogenation

In this chapter, the last step of sustainable adipic acid production is investigated. Paragraph 5.1 presents a survey of the state of the art of the hydrogenation of muconic acid to adipic acid. Paragraph 5.2 describes the experimental apparatus and the analytical techniques set up to obtain new and more accurate information on this reaction. The empirical study allowed identifying a catalyst with optimal performances in very mild conditions, providing the data points for the first kinetic study on the mechanism of muconic acid hydrogenation. The reaction characterization and the model regression results are presented in Paragraph 5.3. Finally, Paragraph 5.4 provides an overview on the further developments which will possibly generate from the obtained results.

5.1 - Muconic acid hydrogenation: state of the art

Most of the past research on the production of muconic acid was driven by the pursuit of renewable adipic acid, hence the final hydrogenation step has already been investigated in different reaction conditions on a number of different catalyst, as briefly reported in Table 5.1. Surprisingly, only qualitative insights of the reactions mechanism have been provided so far and these early studies aimed at demonstrating the reaction feasibility, giving much more attention to the genetic engineering achievements.¹

However, without an optimization of reaction parameters such as temperature, pressure, catalyst/substrate ratio and reaction duration, this latter step risks to become the bottleneck for the whole process. The available literature itself, with the exception of two recent contributions, clearly shows how the studies have been performed without a real technological scalability purpose. For example, Draths et al.² achieved in their pioneering work the complete conversion of *cis,cis*-muconate salts (ccMA) in aqueous solutions in mild conditions of temperature (25 °C) and pressure (3.5 bar). However, they used rather expensive noble catalysts (10% Pt on carbon), for a long reaction (3 h) which showed unacceptable yields for a purified substrate (90%). In a further publication of the same research group, the selectivity was increased to 97%, but they had to increase the pressure to 34 bar without any substantial improvement of the reaction rate (2.5 h).³ To overcome the issues of the low solubility of muconic acid isomers and to avoid the need of forming muconate salts, some organic solvents have been tested as well. Methanol, ethanol, pentanol and butanol have been used, with the problem of forming adipate esters to be eventually hydrolyzed.⁴⁻⁷ Also, the good yields and selectivities of the former works were not achieved. The choice of alcohols was motivated by the need of using eco-friendly solvents (otherwise the claimed sustainability of bio-derived adipic acid would be questionable) but even ethanol, commonly accepted as a “green solvent” undergoes to specific safety regulation.⁸ Another interesting paper investigating green hydrogenation solutions proposed a catalytic reaction where the hydrogen was produced on site by bacteria.⁹ In spite of the very innovative approach, this last method is far from being scalable.

Table 5.1 - Main literature contributions list on muconic acid hydrogenation.

Catalyst	T [°C]	P [bar]	Time [h]	Conversion.	Yield	Note	Ref
Pt/C 10%	25 °C	3.5	3	100%	90%	Aqueous solution.	2
Pt/C 10%	25 °C	34	2.5	100%	97%	Aqueous solution.	3
Ru ₁₀ Pt ₂ /SiO ₂	80 °C	30	5	91%	96%	Solvent ethanol, adipate esters formation.	4
Pt/C 5%	160 °C	na	12	na	99%	Solvent Pentanol, adipate esters formation.	5
Re/TiO ₂	210°C	68	5	100%	90%	Solvent:methanol, adipate esters formation	6
Pd/C 10%	25 °C	7	4	na	62%	Solvent n-butanol adipate esters formation.	7
Royer	37 °C	1	18	na	75%	Small scale, H ₂ provided by bacteria	9
Pd/C 1%	24 °C	24	0.3	>97%	>97%	Solvent ethanol.	10
Ni/Al ₂ O ₃ 14.2%	60 °C	10	5	100%	>99%	Aqueous solution. Inexpensive catalyst.	11

The last two papers in Table 5.1 disclose the best reaction performances achieved so far. Vardon et al.¹⁰ achieved quantitative conversion and 97% selectivity of ccMA to AA with a 1% Pd/C catalyst in only 20 minutes, at room temperature in ethanol, while Scelfo et al.¹¹ achieved even better performances using low-cost Ni/Al₂O₃ 14.2% catalysts in aqueous solution. However, the former still requires rather high pressure (24 bar) and explosion/fire proof technologies, which reflect on equipment that is more expensive. The latter, in spite of lower pressures, presents high dilution and slow kinetics, which require high residence times and bigger reactors. To justify an industrial application of the reaction, an economic (cheap or reusable) catalyst has to be found with high conversion and selectivity for the target product, able to operate at low temperatures and low pressures and shorter times. The pursuit of such catalysts motivated the experimental campaign performed in collaboration with the group of Industrial Chemistry of prof. Carlo Pirola of Università degli Studi di Milano. In particular, the experimental effort of the Ph.D. student Sofia Capelli led to the identification of a good catalyst candidate, and allowed the collection of

the experimental points necessary for the kinetic study here presented. A detailed kinetic study is necessary steps in the perspective of a scale up of the reaction: the regression of kinetic models can provide better insights on the pathways of MA hydrogenation by comparing different reaction mechanisms. This can lead to a more rational optimization of the reaction conditions^{12,13} and allow simulating and comparing industrial reactor configurations, to assess with reliable numbers the economics of this catalytic hydrogenation against concurrent technologies, such as electro-catalysis.¹⁴

5.2 - Materials and Methods

5.2.1 - Experimental setup

5.2.1.1 - Reactants and chemicals.

Previous studies on muconic acid hydrogenation addressed only *cis,cis*-muconic acid (ccMA), without considering that the *cis,cis* isomer is the most unstable of the three possible forms (showed in Figure 5.1) and spontaneously evolves into the configurational isomer *cis,trans* (ctMA) in acidic environment at temperatures above 30 °C.¹⁵ Also, it has been extensively proven that both ccMA and ctMA tend to isomerize to *trans,trans*-muconic acid (ttMA) in presence of metals that strongly bind hydrogen molecules.^{5,16} The choice of ccMA for previous kinetic studies was motivated by the fact that the *cis,cis* isomer is the one produced by the microorganism: this assumption still is not entirely acceptable from a full-process perspective.

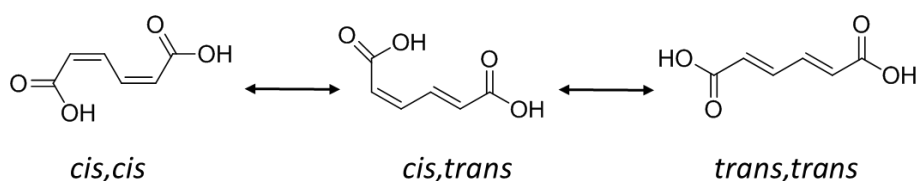


Figure 5.1 – Chemical structure of muconic acid isomers and related equilibria.

Considering in fact the most plausible downstream operations for the ccMA rich fermentation broth described in Chapter 3, the *cis,cis* form is unlikely to be preserved. Indeed, the filtered broth undergoes to a crystallization step achieved by pH shift, and, due to the thermal deactivation of the bacteria and the evaporation steps, an increase of temperature above 80 °C is required. The coupled conditions of acidic environment and higher temperatures are therefore a realistic scenario, and the hydrogenation will be possibly performed on a mixture of the three isomers. The presence of muconic lactones, which actually can be formed in these conditions (and can reduce the hydrogenation selectivity), can be avoided by shorter treatments.¹⁵

Therefore, *trans,trans*-muconic acid (ttMA) was selected as the model chemical for this hydrogenation study. Even though a real application would probably deal with mixtures of MA isomers from the purified broth (as assumed during the development of the superstructure in Chapter 3), the analysis on the sole ttMA has several advantages. First, due to the lower solubility and higher heat of formation, ttMA is the most recalcitrant isomer to react.¹⁴ Therefore, the reaction conditions valid for ttMA apply also for the other isomers, leaving space for further optimizations. Second, the analytics are simplified and accelerated, removing some of the other possible intermediates: 3-hexanedioic acid, for example, is detected when hydrogenating ccMA,¹ but it is not formed in measurable amounts with ttMA.^{6,17} Finally, for the sake of the mechanism modelling, ttMA allows excluding the isomerization equilibria of the reactant between *cis,cis*, *cis,trans* and *trans,trans* forms, reducing the number of equations and parameters to regress. In this way, a deeper understanding of the reaction mechanism is possible, removing parallel or concurrent pathways. All the analyses in water were performed on sodium muconate salts, as ttMA is very insoluble in water in its acid form.

The chemicals employed for the experimental activity were all purchased from Sigma Aldrich and used without further purifications. The list of the chemicals and their purity is: *trans,trans*-muconic acid (98%), *cis,cis*-muconic acid (97%), sodium phosphate dibasic (>99.5%), potassium phosphate monobasic (>98%), sodium chloride (>99%), dimethyl 2,4-hexadiene-1,6-dioate (>99%), dimethyl (3E)-3-hexenedioate (>99%), methanol (99.8%), ethanol (>99%), butanol (>99%), sulfuric acid (98%), sodium hydroxide (98%), adipic acid (>99%), (2E)-2-hexenedioic acid (*trans*-beta-hydrumuconic acid) (98%) and dimethyl adipate ($\geq 99\%$). Milli-q reverse osmosis purified water was employed. Ultra-high-purity hydrogen (99.9%), Nitrogen and Helium were purchased from Sapio. The catalyst, purchased from Sigma Aldrich, is a commercial Pt/C 5%, Taminco G9025 Belgium, in fine powder form.

5.2.1.2 - Reactor design and transport phenomena.

The tests were performed on a 25 mL batch pressurized slurry reactor, with magnetic stirring. The jacketed autoclave is equipped with temperature and pressure control systems, as showed in Figure 5.2. In detail, it is possible to see the cylindrical steel reactor (1) which

contains a glass tube to avoid the catalytic effect of Ni traces in the metal. The reactor is placed in the heating jacket (2) provided by thermocouple for temperature control (4) and placed on the heating plate (3). The valve (5) on the right duct is used to inject the reagent solution, while the left duct contains in order: a pressure gauge for pressure monitoring (6), a valve for gas exclusion (7), a three way valve (8) to select either hydrogen or helium (nitrogen) to quench the reaction. Finally, valves (9) and (10) are put to exclude hydrogen as a further safety measure. All the sealings are Teflon O-rings.

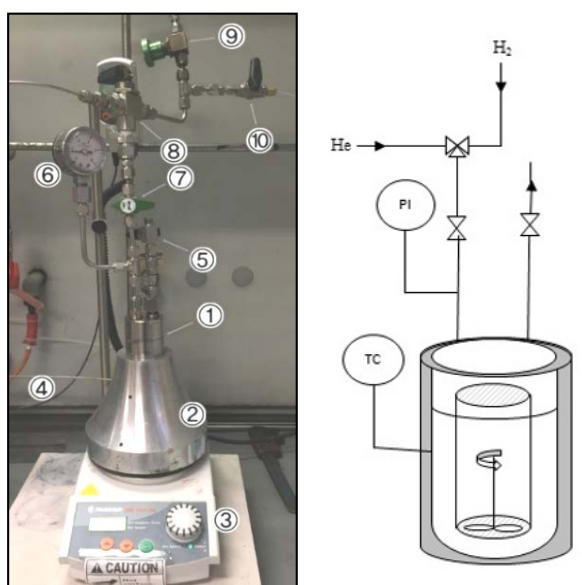


Figure 5.2 - Reactor scheme adapted from MSc thesis of Giulia Locatelli. Ref.18

This configuration ensures the highest safety standards, but hydrogen cannot be bubbled directly into the broth, providing only a static head. Agitation becomes therefore important to ensure good mass transfer and homogeneous conditions in the reactor.

Indeed, an aspect that could significantly affect the performance of a slurry reactor is the insurgence of mass-transfer resistances between the gas (hydrogen), the liquid (water and reactants dissolved) and the solid (catalyst particles) phases. Although slurry reactors usually minimize transport phenomena issues, the confirmation of a pure kinetic regime is necessary if the reactor layout and the results are meant for further mechanism studies.

Some practical criteria to exclude mass transfer resistances were presented by Chaudari and Rajashekharam.¹⁹⁻²¹ They proposed qualitative indexes to assess whether any external or intraparticle mass transfer phenomena are the rate determining step, rather than the reaction itself. The values of the parameters cited in the mathematical formulation of the criteria are reported in Table 5.2.

The calculations are based on the definition of the initial rate of the reaction:

$$R_A = \lim_{t \rightarrow 0} \frac{1}{V_i} \frac{dC_i}{dt} \quad \text{Eq. 5.1}$$

where C_i is the concentration of a reference specie, in this case ttMA. The calculated approximated value is 1.26 kmol/m³/s. The contribution of gas-liquid mass transfer is evaluated by the index defined in equation 5.2, which should be lower than 0.1 to exclude its contribution from the overall kinetics.

$$\alpha_1 = \frac{R_A}{k_{l}a_B C_{H_2}^*} < 0.1 \quad \text{Eq. 5.2}$$

where $k_{l}a_B$ is the overall mass transfer coefficient (gas side-film theory) for stirred reactors, and $C_{H_2}^*$ is the equilibrium concentration of hydrogen. Machado addressed the problem of estimating the gas-liquid mass transfer coefficient for bench-scale stirred reactors.^{22,23} A range of 0.05-0.5 s⁻¹ was considered representative for the smaller hydrogenation reactors. Even with the more conservative values, the system under study resulted in α_1 values lower than 0.05. The calculated value for ttMA was 0.03 that is safely under the threshold to exclude gas-liquid resistance. Liquid-liquid mass transfer limitation was excluded performing a series of hydrogenations under the same conditions but varying the stirring speed from 250 to 700 rpm. The essays revealed that for higher speed than 500 rpm the system is no more sensitive to stirring, hence no more liquid-liquid transport is relevant on the overall kinetics Figure 5.3: the reactor can be considered a CSTR, therefore the hydrogen concentration in liquid bulk is assumed constant.²⁴

Table 5.2 - Parameters required for the evaluation of the mass transfer phenomena

Reaction conditions	
Hydrogen pressure	4 bar
Hydrogen gas-liq. transf. rate (k_{iAB})	0.1 s^{-1}
Liquid density	$1000 \text{ kg}\cdot\text{m}^{-3}$
Liquid viscosity	$6.5 \times 10^{-4} \text{ Pa s}$
Reactor properties	
Volume	0.025 L
Reactor materials	glass
Impeller power number	5
Diameter of the impeller	2.5 mm
Rotation speed	8.33 rps
Catalyst properties	
Support	Activated charcoal
Pt content	5% wt/wt
Catalyst loading	$10 \text{ g}_{\text{cat}}\cdot(\text{L}_{\text{solution}})^{-1}$
Catalyst porosity	0.95
Particle diameter	$40 \times 10^{-6} \text{ m}$
Particle skeletal density	$2 \times 10^3 \text{ kg}\cdot\text{m}^{-3}$

Liquid-solid mass transfer can be assessed by the index in equation 5.3.

$$\alpha_2 = \frac{R_A}{k_s a_p C_{H_2}^*} < 0.1 \quad \text{Eq. 5.3}$$

where k_s is the liquid-solid mass transfer coefficient, a_p is the interface area of liquid-solid boundary. The latter is defined by equation 5.4:

$$a_p = \frac{6w}{\rho_p d_p} \quad \text{Eq. 5.4}$$

where w is the catalyst load, ρ_p and d_p are particle density and diameter respectively.

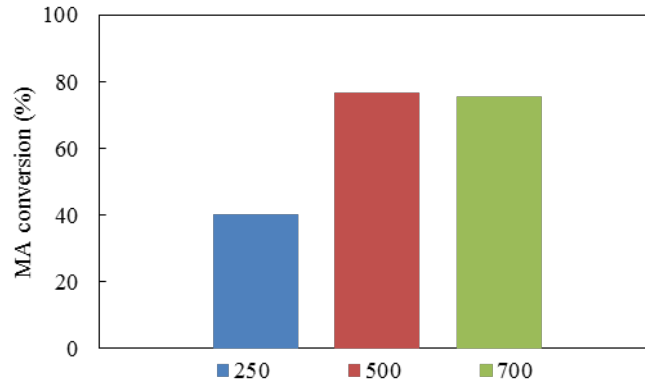


Figure 5.3 - Sodium trans,trans-muconate conversion at 250, 500 and 700 rpm $T=60^{\circ}\text{C}$, $P(\text{H}_2)=4$ bar, reaction time= 60 min, sub/cat= 10 (wt/wt) and $[\text{MA}]=7\cdot 10^{-2}\text{M}$

Particle diameter was set up using sieves and it was at about $40\ \mu\text{m}$ (325 and 400 mesh – TYLER series). The parameter k_s is obtained using a literature correlation.²⁵

$$\frac{k_s d_p}{D_{\text{H}_2} F_c} = 2 + 0.4 \left(\frac{d_p^4 \rho_l^3 e}{\mu_l^3} \right)^{0.25} \left(\frac{\mu_l}{\rho_l D_{\text{H}_2}} \right)^{0.33} \quad \text{Eq. 5.5}$$

where D_{H_2} is the molecular diffusion of hydrogen in water, F_c is a shape factor assumed to be 1 for spherical particles, μ_l and ρ_l stand for liquid viscosity and density respectively, e is the energy supplied to the liquid by the stirrer, given in equation 5.6:

$$e = \frac{N_p n^5 l^5}{V} \quad \text{Eq. 5.6}$$

where N_p is the impeller power number, l is the impeller diameter, n is the rotation speed (in rps). The calculated value for α_2 is 0.019, which allows excluding liquid-solid mass transfer limitations.

Finally, pore diffusion can be considered negligible if the parameter ϕ_{exp} is lower than 0.2:

$$\phi_{\text{exp}} = \frac{d_p}{6} \left(\frac{\rho_p R_A}{w \text{Diff}_e C_{\text{H}_2}^*} \right)^{0.5} < 0.2 \quad \text{Eq. 5.7}$$

where d_p is the particle diameter, w is the catalyst load, D_e is the effective diffusivity calculated as

$$D_e = \frac{D\varepsilon}{\tau} \quad \text{Eq. 5.8}$$

where ε is the catalyst porosity and τ is the tortuosity factor. The latter parameter is usually little characterized: it is a complex function of the type of charcoal, of the adsorbed substrate, and the reaction medium, often regressed from indirect diffusion measurements.²⁶ Nonetheless, in carbon-supported platinum hydrogenation catalysts, the parameter was estimated in the range between 3 and 7.²⁷ The calculated ϕ_{exp} was lower than 0.04 even for the most conservative values of tortuosity in the conditions of this study, allowing the exclusion of external mass transfer and internal pore diffusion limitations.

5.2.2 - Analytical methods

5.2.2.1 - Catalyst characterization

After some preliminary and unsuccessful tests on a series of Ni/Al₂O₃ catalysts prepared at Politecnico di Milano (not included in this dissertation), the commercial catalyst Pt/C 5%, Taminco G9025-Belgium achieved very good performances, so that some further characterization were considered necessary.

- A TPD/R/O 1100 ThermoQuest Instruments was used for TPR (Temperature-Programmed Reduction) analyses: an amount of 40 mg of catalyst was dried in oven and then analyzed. The sample was pre-treated with argon flow from room temperature to 200 °C with a temperature ramp of 30 °C·min⁻¹ and maintained at this temperature for 60 min. The analysis was then conducted from 50 °C to 900 °C at 8 °C·min⁻¹ at 1 bar. The gaseous mixture was 5.04% of hydrogen in argon and it was fluxed within the instrument at 14 mL·min⁻¹.
- The BET surface areas of the as-purchased Pt/C 5% were determined using Sorptometer 1042 Costech.
- SEM images were obtained using a Field Emission Gun Electron Scanning Microscopy LEO 1525 (ZEISS). The samples were investigated by Inlens detector for secondary electrons, AsB detector for backscattered electrons and elemental composition was determined using a Bruker Quantax EDS.
- TEM images were obtained using a Philips 208 Transmission Electron Microscope.

The results of these analyses are not included here as not essential for the development of the kinetic model. High definition images of the catalyst are though provided in the full paper derived from this research and attached to the thesis.

5.2.2.2 - Analytical procedure for conversion and selectivity evaluation

The conversion of the *trans,trans*-sodium muconate salt was evaluated by UV-Vis analysis, quenching the reaction (cooling and substituting H₂ with He or N₂) at fixed time and sampling the entire content of the reactor. After the catalyst filtration, the solution was analysed in a spectrophotometer T60 UV-Visible PRIXMA from 400 to 190 nm. The maximum absorption was at 264 nm while the absorption at 210 nm was attributed to intermediates. The calibration of the analysis was performed with sodium *trans,trans*-muconate prepared by titration of ttMA with sodium hydroxide. No isomerization of ttMA was observed during the neutralization process. The filtrate was also analysed by ICP-OES to check for noble metal leaching.

The selectivity was estimated by gas chromatographic analyses on methyl esters derivatives, prepared following the experimental work validated by Vardon et al.¹ The filtered samples were dried in oven at 70 °C. The white solid residues were reacted with methanol (7 ml) in large excess and sulfuric acid (50 µL) and left at slow stirring at 70 °C for 48 h. Before, the esterification with different alcohols was performed on pure ttMA, AA, and monounsaturated compounds to verify if the acidic environment could influence the isomers distribution: no isomerization was detected and methanol was therefore selected as the best alternative. Since MA esterification did not complete even after 48 h, it was not possible to evaluate the hydrogenation conversion of this compound by GC-TCD analyses: the UV-Vis spectrophotometer was therefore the only technique applicable.

Methyl esters were analysed by GC (Master GC Fast Gas Chromatograph Dani Instrument) equipped with TCD detector operating in split mode (1:3). Butanol was used as internal standard. The GC was outfitted with an Aldrich Supelcowax 10 (60 m x 0.53 mm id, 1 µL), and helium (15 mL·min⁻¹ column flow) was used as carrier at 5 mL·min⁻¹ flow rate. The GC-TCD method consisted of an inlet temperature of 210 °C and TCD transfer line at 240 °C. A starting temperature of 60 °C was set and then ramped at 18 °C·min⁻¹ to a temperature of 120 °C. Then from 120 °C to 160 °C ramped at 20 °C·min⁻¹. From 160 °C to 260 °C the temperature increased at 15 °C·min⁻¹ and held for 1 minute to purge the column.

Dimethyladipate (DMA), dimethyl 2,4-hexadiene-1,6-dioate, and dimethyl-*trans*- β -hydromuconate synthesized from *trans*- β -hydromuconic acid were used for the instrument calibration, using butanol as internal standard. The recognition of the reaction intermediates was performed with GC coupled with mass detector (TraceISQ QD Single Quadrupole GC-MS) on the corresponding products. The inlet temperature was 280 °C and scan ranged from 50 MHz from 400 MHz. The temperature ramp was the same adopted for the GC-TCD analysis and the helium flow was 10 mL·min⁻¹ with a split ratio of 20. For a further control, dimethyl 2,4-hexadiene-1,6-dioate (by Sigma Aldrich) was injected to verify the retention time, while dimethyl (3E)-3-hexenedioate standards was used to evaluate *trans,trans*-MA esterification. Figure 5.4 presents a schematic representation of the main step of conversion and selectivity characterization.

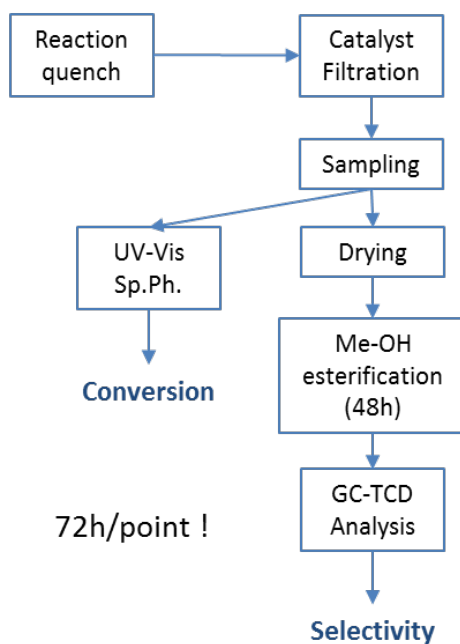


Figure 5.4 - Workflow scheme of the analytical procedure for obtaining the conversion and the selectivity of the hydrogenation.

5.2.3 - LHHW models and nonlinear regression

The Langmuir-Hinshelwood-Hougen-Watson (LHHW) model was used to express the reaction rate equations, assuming as the rate-determining step the reaction on the surface.²⁸ This formulation, which decomposes the mechanism of adsorption-reaction-desorption occurring on the catalyst into elementary steps, allows considering the competitive adsorption equilibria of the species, and the hypotheses of molecular or dissociated hydrogen reaction. The generic reaction rate equation is:²⁸

$$R_{ij} = \frac{C_t \cdot k_{ij} \cdot K_{H_2} \cdot C_{H_2} \cdot K_i \cdot C_i}{\left[1 + K_{H_2} \cdot C_{H_2} + \sum_{k \neq H_2} K_k \cdot C_k \right]^a} \quad \text{Eq. 5.9}$$

where K_i are the adsorption constants, k_{ij} is the kinetic constant of component i in the reaction j , C_i is the concentration of the species, C_t is the active sites concentration, a is a coefficient representing the mechanism with molecular hydrogen reaction ($a=2$) or hydrogen dissociation ($a=3$). The kinetic constant temperature dependence can be expressed by the Arrhenius equation 5.10:

$$k_{ij} = A_{ij} \exp\left(\frac{-E_{att,ij}}{RT}\right) \quad \text{Eq. 5.10}$$

Also K_i can be made temperature dependent with the Van't Hoff formulation, but for liquid phase hydrogenations the temperature dependence of adsorption can be neglected in the hypothesis of high surface coverage and the number of parameters can therefore be reduced.²⁹ However, even though LHHW is among the most popular models in reaction engineering, its mathematical structure is little suitable for nonlinear regression applications, as the parameters are strongly collinear and can lead to ill-conditioned problems.³⁰ This means that while performing the parameters regression, the minimization of the residues becomes difficult even for robust solvers, and the results can be strongly affected by any small perturbation of the input data (in case of experimental error). These shortcomings are particularly relevant for models with many reaction steps and adaptive parameters, which require the solution of large size nonlinear regression problems, coupled with the dynamic solution of the stiff ODEs system derived from the chemical species material balances. To reduce the computational effort, a common approach is the re-

parametrization of the model, and, if possible, the removal of the less significant parameters. Equation 5.9 was therefore re-parametrized as Eq. 5.11:

$$R_{ij} = \frac{\tilde{k}_{ij} \cdot C_i \cdot C_{H_2}}{\left[1 + K_{H_2} \cdot C_{H_2} + \sum_{k \neq H_2} K_k \cdot C_k \right]^3} \quad \text{Eq. 5.11}$$

where the kinetic constant of the numerator is expressed as a modified Arrhenius equation as reported in Eq. 5.12:

$$\tilde{k}_{ij} = \exp \left[\tilde{A}_{ij} - \frac{E_{att,ij}}{R} \left(\frac{1}{T} - \frac{1}{\bar{T}} \right) \right] \quad \text{Eq. 5.12}$$

Where \bar{T} is an average temperature in the investigated range (333K). The constant contributions at the numerator of Eq.5.9 (i.e. K_{H_2} , K_{itMA} , C_i) are all lumped in the factor \tilde{A}_{ij} which is calculated as one of the arguments of the exponential function. The formulation of Eq. 5.12 is fully equivalent to Eq.5.10, but, from a mathematical perspective, helps in reducing the condition number and therefore simplifies the optimization problem.³⁰ The equations could be possibly further re-parametrized, but this would result in non-physically interpretable parameters, which does not allow the definition of physical constraints to the kinetic constants. The advantage of this formulation is in fact that the activation energies of the Arrhenius equations or the adsorption constants can be bounded in the well-known ranges available in literature. In particular, the apparent activation energy for double carbon bond hydrogenations on noble metal catalysts can be confined in the range 10 -120 kJ/mol.^{10,21,31-33} As for the adsorption constants, values taken from similar systems modelled with LHHW span between 10^{-1} and 10^4 L/mol.^{19,32,34} This wide range is enough to reduce sensibly the search space and accelerate the convergence. The objective function to be minimized for the parameter calculation is the sum of squared errors (SSE):

$$SSE = \sum (Y_{i,exp} - Y_{i,calc})^2 \quad \text{Eq. 5.13}$$

where $Y_{i,exp}$ and $Y_{i,calc}$ are respectively the experimental and the calculated composition of specie i .

The model fitting quality was assessed comparing the final value of the SSE and the coefficient of determination, defined as:

$$R^2 \% = 1 - \frac{SSE}{\sum (Y_{i,\text{exp}} - \bar{Y}_{i,\text{exp}})^2} \quad \text{Eq. 5.14}$$

where $\bar{Y}_{i,\text{exp}}$ is the average experimental value.

The optimization method adopted to achieve the best parameters is based on the class of robust minimization of BzzMath library in C++ language.³⁰ The 95% confidence interval on the regressed parameters were calculated using least square method analysis tools both in Matlab environment (lsqnonlin function) and C++, to confirm the results applying different solvers. The codes used for the regression and the model evaluation are reported in Appendix 3.

5.3 - Results and discussion

5.3.1 - Hydrogenation to adipic acid in mild conditions

As already mentioned, the reaction tests were performed in a glass cylindrical tube placed inside the stainless steel reactor to avoid that the Ni traces presents in the steel could invalidate the results due to its catalytic activity. A fixed amount of Pt/C 5% (0.01-0.1 g) was reduced for 3 h at 200 °C under 6 bar of static hydrogen within the cylindrical glass tube, following the indication of the TPR analysis conducted on the fresh catalyst. The temperature was maintained constant by heating the external metal jacket. After cooling to the desired reaction temperature, 10 mL of degassed ttMA salt solution (0.07 M) were added to the reactor. The batch hydrogenations were conducted at 40°C, 50°C, 60°C and 70°C at 4 bar of static hydrogen with a magnetic stirring of 500 rpm up to 4 h.

These conditions apply to the experimental campaign used to generate the data for the kinetic study.

In addition, other tests were conducted at 70 °C, 4 bar of hydrogen and 500 rpm on *cis,cis*-MA using a synthetic salt solution which reproduces a clarified fermentation broth as the one of Niu et al.³ These tests consider the possibility of avoiding a MA crystallization step before hydrogenation reaction, preventing the solution acidification and the risk of MA isomerization. The synthetic fermentation broth contained ccMA (28 g/L), Na₂HPO₄ (50 g/L), KH₂PO₄ (15 g/L), NaCl (2.5 g/L) and NaOH (40 g/L).

Initially, different tests at varied substrate/catalyst ratio were performed keeping constant temperature (40 °C), hydrogen pressure (4 bar) and reaction time (60 min), to select the best amount of catalyst.

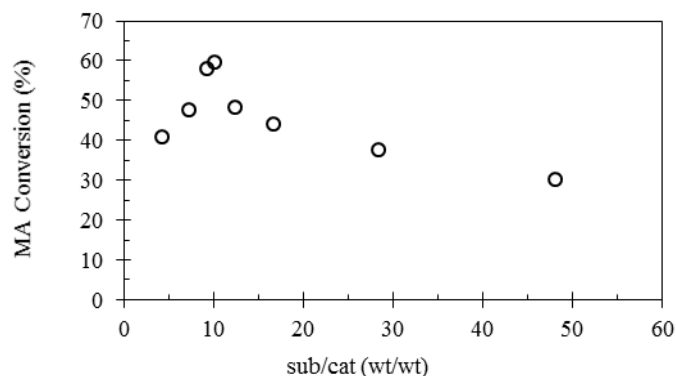


Figure 5.5 - Conversion evaluation at different substrate/catalyst ratio and at 60 °C, stirring=500 rpm, $P(H_2) = 4$ bar, $[MA] = 7 \cdot 10^{-2}$ M, time 4 h.

The results reported in Figure 5.5 show that, for a substrate/catalyst ratio equal to 10 (wt/wt), the reaction has the highest conversion, with good selectivity to AA (>65 %). Once fixed the amount of catalyst, the hydrogenation tests were carried out investigating different temperatures, as shown in Figure 5.6.

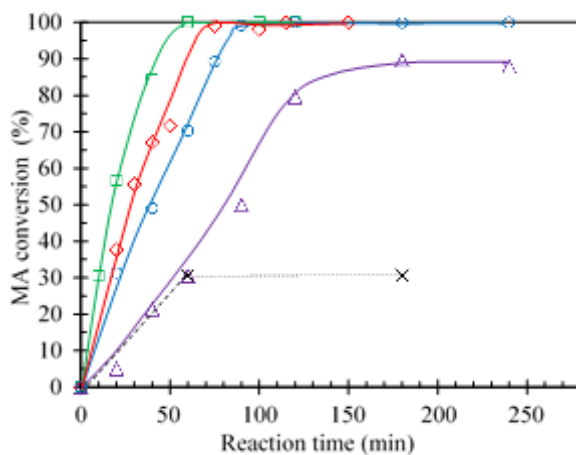


Figure 5.6 - Sodium *trans,trans*-muconate conversion at (Δ) 40°C, (\circ) 50°C, (\diamond) 60°C, (\square) 70°C, and (\times) and 40°C with catalyst removal after 60 min by hot filtration. In all samples $P(H_2) = 4$ bar, stirring = 500 rpm, sub/ca t=10 (wt/wt), $[ttMA]^0 = 7 \cdot 10^{-2}$ M

It is clear that a complete conversion was achieved only at temperatures higher than 40 °C. At 70°C the reaction was complete in only 1 hour, while at 50°C the complete conversion

was achieved in 90 minutes: the selectivity in these cases was 100% for AA. Interestingly, the reaction at 40 °C presented an induction period and did not achieve full conversion even after 4 hours, denoting too slow kinetics for any practical application. This lag time is often detected in heterogeneous catalytic systems that work at low temperatures, and it is due to the strong absorption of the organic species on the active site of the catalyst that gradually moves toward deactivation. Low temperatures are not sufficient to support the desorption step, and for this reason full conversion can not be achieved, as suggested also by Vardon et al.¹ An increase of temperature eliminates the lag time and allows complete conversion in only 1.5 h. Another remarkable aspect is that no metal leaching was observed after hot filtration, thus confirming the heterogeneous behaviour of the reaction. For this experiment, the catalyst was filtered off after 1 h and the solution was allowed to remain under hydrogen atmosphere for other 2.5 h, in the same operating conditions. No further conversion of MA was observed. Moreover, ICP analysis on the reaction media did not reveal the presence of metal, confirming the exclusion of any noble metal leaching.

Recycling tests on the catalyst were performed to obtain information about the stability of the catalyst. The possibility to reuse the catalyst is a key point in an industrial perspective. The test was performed at 70 °C with 10 substrate/catalyst ratio (wt/wt) by using a muconate solution at 8×10^{-2} M. The catalyst was filtered after 2 h and reused without any further activation step with a fresh solution of MA. Even after 10 cycles, a full conversion of MA and a full selectivity toward adipic acid was obtained after 2 hours. The results are reported in Table 5.3 . Once proven the good performances of the catalyst on ttMA, the same hydrogenation conditions were repeated on the *cis,cis* form, with the same good results. However, thinking to the industrial process, a solution with the sole *cis,cis* isomer is unlikely to be found, given the spontaneous rearrangement to the *cis,trans* form in acidic environment.

Table 5.3 - catalyst recycling tests results at $P(H_2) = 4$ bar, stirring = 500 rpm, $sub/cat = 10$ (wt/wt), $[MA] = 7 \cdot 10^{-2}$ M

Test #	MA conversion (%)	AA selectivity (%)
1	100	100
2	100	100
3	100	>99
4	>99	>99
5	>99	>99
6	>99	>99
7	>99	>99
8	>99	>99
9	>99	>99
10	>99	>99

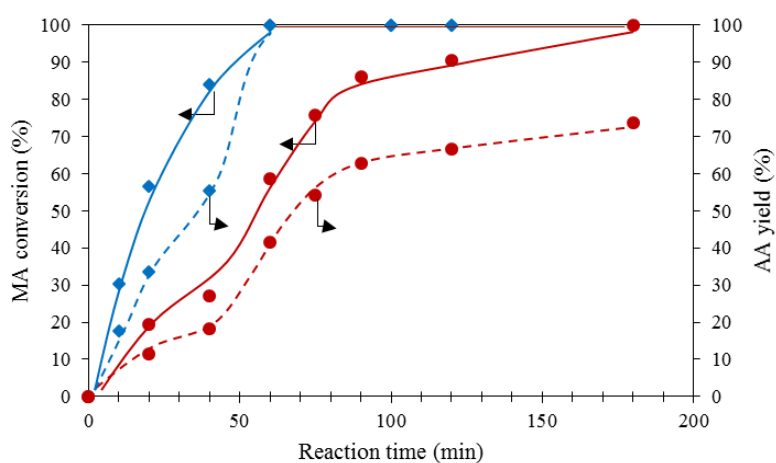


Figure 5.7 - MA conversion (solid line) and AA selectivity (dashed line) - (○) *cis,cis*-MA in the synthetic salt fermentation broth and (◇) in pure water: $P(H_2) = 4$ bar, $T = 70$ °C, stirring = 500 rpm.

Still, the *cis,cis* form could be preserved, as long as any crystallization step on the fermentation broth is excluded. Consequently, a synthetic ccMA solution with inorganic salts was hydrogenated, mimicking the salt buffer of the fermentation. The main assumption were that the broth was previously clarified from the microorganisms, then treated by means of ultrafiltration and activated carbon to remove all the biological matter. The results are reported in Figure 5.7. In presence of salts, the reaction is sensibly slower: The AA yield after 180 min is only 73%. This result can be explained considering the salts concurrent adsorption on the catalyst surface, and confirms the need to perform the hydrogenation on a substrate with the highest possible purity. This would be beneficial also for the duration of the catalyst, as in absence of the growth support salts the noble metal poisoning is prevented.

5.3.2 - Kinetic modelling

Considering the reasonably low reaction temperature, the short reaction time, the very low hydrogen pressure (4 bar), and the catalyst recyclability, the studied hydrogenation outperformed the previously mentioned Ni and Pd based ones.^{1,10,11} At the present state of the art, the published results are the best and the more likely to be scalable, therefore the conditions were satisfactory to perform a detailed kinetic study, the first for ttMA hydrogenation.³⁵

5.3.2.1 - Preliminary study at fixed temperature

In line with the suggestions of Scelfo et al.¹¹, a temperature of 60°C was chosen to collect the first series of experimental point at different times to perform the kinetic study. Many batches were required and the complex and time-demanding workout to characterize the samples (more than 48 hours for each sample) limited the number of available points. To simplify the data collection, the intermediates were considered initially as a single pseudo-component, referred as “IN” in Figure 5.8. The scheme actually shows all the four possible intermediate isomers, as the hydrogenation catalyst promotes double bond isomerization.³⁶

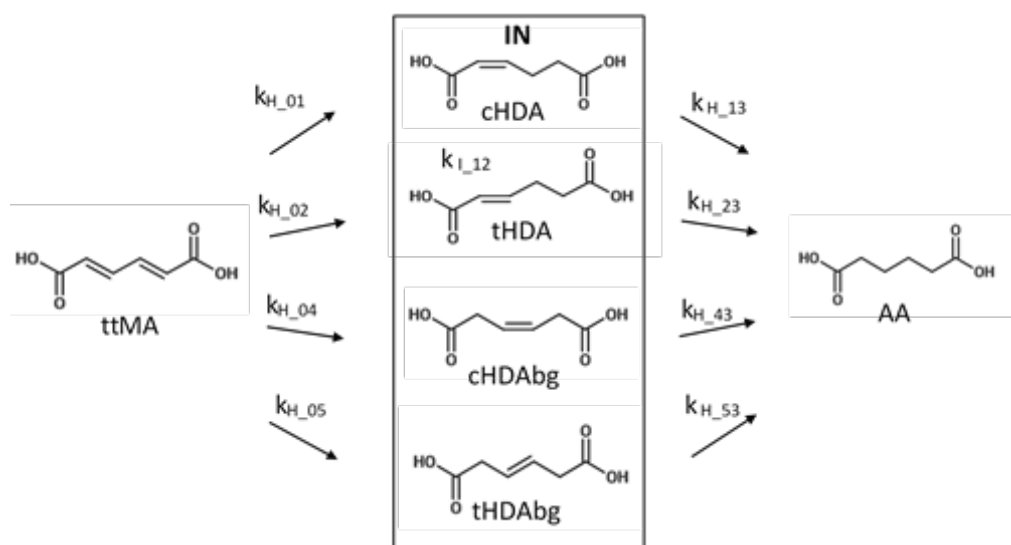


Figure 5.8 - Reaction scheme with all the possible monounsaturated intermediate isomers. The species reported are *trans,trans*-muconic acid (MA), α,β -*cis*-hexenedioic acid (cHDA), α,β -*trans*-hexenedioic acid (tHDA), β,γ -*cis*-hexenedioic acid (cHDAbg), β,γ -*trans*-hexenedioic acid (tHDAbg), adipic acid (AA). In the simplified mechanism, all the intermediates were considered as a single pseudo-component “IN”.

Two models based on LHHW adsorption mechanism were evaluated. Model A, considered the dissociation of molecular hydrogen when adsorbed on the catalyst, while model B, assumed no dissociation. The reaction rate equations are reported in Table 5.4. Each hydrogenation step is considered irreversible and rate-determining, if compared to the kinetics of adsorption and desorption of all the species.

In both cases, the calculations failed to represent properly the experimental data. In particular, the model showed an overestimation of the reactant and the intermediate concentrations, as evidenced in Figure 5.9.

This trend, common in both the models, introduced a doubt on the reliability of the experimental measures, later confirmed by the material balances. A lack of molar quantities up to -20 % was observed during the reaction, which reduced to 0 as long as the reactants were consumed.

Table 5.4 - Generic equations for the simplified mechanism with intermediate pseudo component. Dual site L-H model according to Yang and Hougen tables, $n=2$ without H_2 dissociation, $n=3$ with dissociation.

Kinetic equation	Reaction rate
$R_1 = \frac{\bar{k}_1^* \cdot C_{ttMA} \cdot C_{H_2}}{\left(1 + \sum K_i C_i\right)^n}$	MA hydrogenation to IN
$R_2 = \frac{\bar{k}_2^* \cdot C_{IN} \cdot C_{H_2}}{\left(1 + \sum K_i C_i\right)^n}$	IN hydrogenation to AA

This peculiar trend could only be explained by some errors in the quantification of the intermediate. After repeating the experiments and increasing the resolution of the gas chromatograph, it was possible to identify two distinct intermediates with different retention times. The analytical technique was then improved, so that all the intermediates were considered (table 4) in the successive modelling.

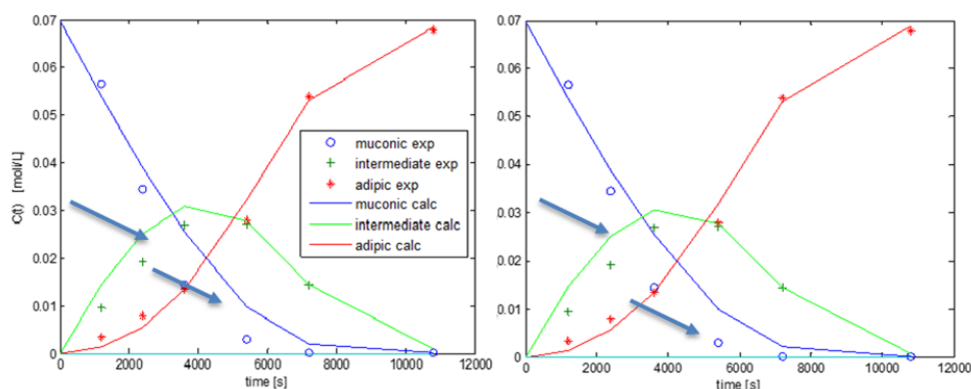


Figure 5.9 - Concentration profiles for the hydrogenation of ttMA on Pt/C 5% catalyst at 4 bar hydrogen at 60°C. Results of the preliminary regression with the pseudo intermediate, (left without hydrogen dissociation, right with). The arrows point the systematic overestimation of the intermediate concentration.

After careful analyses, the β,γ unsaturated intermediates were not detected in significant amounts, in line with the previous indication of She et al.⁶: the reaction scheme was thus simplified. The dataset for the regression at 60°C is reported in Table 5.5.

Table 5.5 - Species concentration in time for the reaction $T=60\text{ }^{\circ}\text{C}$, $Pt/C\ 5\ \%$, $P(H_2)=4\ \text{bar}$, $500\ \text{rpm}$

Time [min]	C_{MA} [mol/L]	C_{cHDA} [mol/L]	C_{tHDA} [mol/L]	C_{AA} [mol/L]
0	7.00E-02	0.00E+00	0.00E+00	0.00E+00
20	5.69E-02	1.36E-03	8.25E-03	3.48E-03
40	4.28E-02	9.79E-03	9.50E-03	7.94E-03
60	2.93E-02	2.85E-03	1.53E-02	2.26E-02
90	1.46E-02	4.69E-03	2.00E-02	3.28E-02
120	1.19E-03	3.52E-03	1.10E-02	5.43E-02
180	1.75E-03	0.00E+00	0.00E+00	6.10E-02
240	1.00E-09	1.00E-09	1.00E-09	7.00E-02

Three reaction pathways were taken into consideration:

- Model C: Mechanism LHHW without hydrogen dissociation ($a = 2$) $T = 60\text{ }^{\circ}\text{C}$ with irreversible isomerization of $cHDA$ to $tHDA$.
- Model D: Mechanism LHHW with hydrogen dissociation ($a = 3$) with irreversible isomerization of $cHDA$ to $tHDA$
- Model E: Mechanism LHHW with hydrogen dissociation ($n=3$) with isomerization equilibrium between $cHDA$ and $tHDA$.

The equations used for modelling the reaction rates are reported in Table 5.6. Given the higher number of species and reactions with respect to the first modelling attempt, the number of kinetic parameters increases, resulting in different models which all performed a fairly good fitting (R^2 higher than 95% in all the cases). The residues for model C were 0.0327, 0.0249 for model D, and 0.0226 for model E. The comparison of the residues of model C and D, equivalent in the number of parameters, shows that hydrogen dissociates on the catalyst surface. Model E therefore assumes the hydrogen dissociation and includes on the isomerization reaction. Another tested model, analogous to Model E but without dissociation, gives a poorer fit, confirming once again the dissociation of hydrogen.

Table 5.6 - Generic equations for the refined mechanism with intermediates: dual site L-H model according to Yang and Hougen tables, $n = 2$ without H_2 dissociation, $n = 3$ with dissociation.

Kinetic equation	Reaction rate
$R_{h01} = \frac{\bar{k}_{h01}^* \cdot C_{tMA} \cdot C_{H2}}{(1 + \sum K_i C_i)^n}$	MA hydrogenation to cHDA
$R_{h02} = \frac{\bar{k}_{h02}^* \cdot C_{tMA} \cdot C_{H2}}{(1 + \sum K_i C_i)^n}$	MA hydrogenation to tHDA
$R_{h02} = \frac{\bar{k}_{h13}^* \cdot C_{cHDA} \cdot C_{H2}}{(1 + \sum K_i C_i)^n}$	cHDA hydrogenation to AA
$R_{h23} = \frac{\bar{k}_{h23}^* \cdot C_{tHDA} \cdot C_{H2}}{(1 + \sum K_i C_i)^n}$	tHDA hydrogenation to AA
$R_{h12} = \frac{\bar{k}_{i12}^* \cdot C_{cHDA} - \bar{k}_{i12}^* \cdot C_{tHDA}}{(1 + \sum K_i C_i)^n}$	Isomerization equilibrium cHDA \leftrightarrow tHDA

Table 5.7 - Calculated parameters for the three models, adsorption constants K_i are in L/mol

	K MA	KcHDA	K tHDA	K AA	K H2	kH_01	kH_02	kH_13	kH_23	ki_12 (I_21)
C	67.36	77.17	2.14e-3	2.83	1.75e-1	6.61e-1	5.96e-1	4.60	5.09e-1	1.01e-3
D	15.90	2.60e-1	1.87e-2	3.25	2.33e-2	1.86e-1	1.70e-1	1.28	1.51e-1	1.0e-1
E	12.46	14.91	1.0e-5	2.92e-2	1.08e-2	0.113e-1	9.93e-2	9.52e-1	1.0e-5	2.27e-4
										(5.14e-4)

Observing the parameter values of Table 5.7, however, it was clear that the model had to be further refined. In fact, the *trans* configuration of the intermediate should be

theoretically favored due to its lower steric hindrance, however, comparing the two kinetic constants reported, the reaction seems to move backward.

These results therefore served as an indication, before more experimental data became available. In addition, the kinetic constants showed an undue variability from model to model, especially for model D. It is however impossible to compare the values to other published literature, since no data for muconic acid and derivatives are available for benchmarking. Nonetheless, some confirmation on the relative values of the adsorption constants can be found in Chaudhari et al.³⁷, who studied the kinetics of hydrogenation of maleic acid to succinic acid in a slurry reactor, a similar system to MA. They observed that the unsaturated acid adsorbs preferably, confirming the relative magnitude of the calculated constants, even though their investigated temperatures were far higher than 230 °C.

5.3.2.2 - Model regression with temperature dependency

The reaction mechanism identified in the preliminary tests is presented in Figure 5.10.³⁸ The first step of hydrogenation on ttMA yields two isomers, namely (2Z)-2-hexenedioic acid (cHDA) and (2E)-2-hexenedioic acid (tHDA), in a single irreversible step. The concentration of the intermediates is regulated by an equilibrium isomerization reaction. The second step of hydrogenation yields adipic acid from both the intermediates.

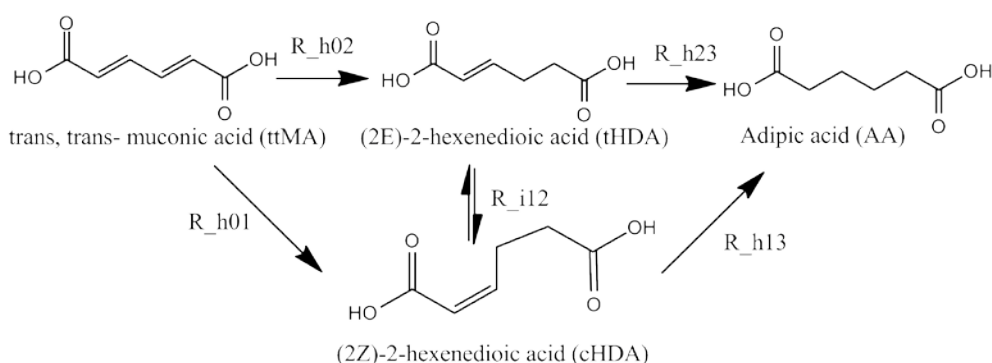


Figure 5.10 - Hypothesized reaction scheme of model LHHW_17P.

The set of ordinary differential equations reported in Eq. 5.15 describes the mechanism (identified from now on as LHHW_17P) and presents 17 adaptive parameters. The results of the regression, listed in Table 5.8, seem particularly encouraging: the regression shows

a R^2 close to 99%. The good fitting can be appreciated also in the concentration time profiles and in the dispersion diagram reported in Figure 5.11.

$$\left\{ \begin{array}{l} \frac{d \text{ttMA}}{dt} = -R_{h01} - R_{h02} = -\frac{\bar{k}_{h01}^* \cdot C_{\text{ttMA}} \cdot C_{H_2}}{(1 + \sum K_i [C_i])^3} - \frac{\bar{k}_{h02}^* \cdot C_{\text{ttMA}} \cdot C_{H_2}}{(1 + \sum K_i [C_i])^3} \\ \frac{d \text{cHDA}}{dt} = +R_{h01} - R_{h13} - R_{i12} = \frac{\bar{k}_{h01}^* \cdot C_{\text{ttMA}} \cdot C_{H_2}}{(1 + \sum K_i [C_i])^3} - \frac{\bar{k}_{h13}^* \cdot C_{\text{cHDA}} \cdot C_{H_2}}{(1 + \sum K_i [C_i])^3} - \frac{\bar{k}_{i12}^* \cdot C_{\text{cHDA}} - \bar{k}_{i12}^* \cdot C_{\text{tHDA}}}{(1 + \sum K_i [C_i])^3} \\ \frac{d \text{tHDA}}{dt} = +R_{h02} - R_{h23} + R_{i12} = \frac{\bar{k}_{h02}^* \cdot C_{\text{ttMA}} \cdot C_{H_2}}{(1 + \sum K_i [C_i])^3} - \frac{\bar{k}_{h23}^* \cdot C_{\text{tHDA}} \cdot C_{H_2}}{(1 + \sum K_i [C_i])^3} + \frac{\bar{k}_{i12}^* \cdot C_{\text{cHDA}} - \bar{k}_{i12}^* \cdot C_{\text{tHDA}}}{(1 + \sum K_i [C_i])^3} \\ \frac{d \text{AA}}{dt} = R_{h13} + R_{h23} = \frac{\bar{k}_{h13}^* \cdot C_{\text{cHDA}} \cdot C_{H_2}}{(1 + \sum K_i [C_i])^3} + \frac{\bar{k}_{h23}^* \cdot C_{\text{tHDA}} \cdot C_{H_2}}{(1 + \sum K_i [C_i])^3} \\ \frac{d H_2}{dt} = 0 \end{array} \right.$$

Eq. 5.15

Still, the statistical analysis of results shows little consistency on the regressed parameters, with a wide confidence interval for all the parameters. This highlights the limits of the dataset, which lacks of an estimate of the experimental error so to exclude possible outliers, and the limits of a too flexible model, able to follow the concentration profile in virtue of the many adaptive parameters. Another critical aspect of LHHW_17P model is the value of the activation energy for the first hydrogenation, which is close to the boundary limit. This model was therefore discarded, pursuing a simpler formulation. A 15 parameters model was hence obtained, excluding from the mechanism the reaction step R_{h01} . This step in fact assumes a combined isomerization and hydrogenation of ttMA: even possible, the isomerization reaction is unlikely in a strong reducing environment.

In spite of the lower number of parameters, model LHHW_15P decreases its coefficient of determination of only 0.6%, while sensibly reducing the uncertainty of many of the parameters. Also, the values of the apparent activation energy assumed a value more in line with the previously estimated 70 kJ mol^{-1} for Pt/C in ethanol.¹⁰

However, the results were still unsatisfactory.

Table 5.8 - Calculated values of the model parameters with 95% confidence interval and regression metrics.

Parameter	LHHW_17P		LHHW_15P		LHHW_13P		LHHW_11P	
K_{ttMA}	1.49E+01	±190%	6.97E+01	±35%	7.85E+02	±13%	8.10E+02	±7%
K_{cHDA}	4.86E+03	±81%	9.16E+02	±56%	9.03E+03	±50%	9.85E+03	±45%
K_{tHDA}	5.81E+00	±500%	1.00E+00	±43%	2.15E+02	±126%	2.19E+02	±102%
K_{aa}	6.53E+01	±133%	3.57E+01	±35%	4.72E+01	±184%		
K_{H2}	4.20E+02	±400%	1.02E+00	±96%	1.00E+00	±186%		
A_{h02}	4.72E+00	±93%	3.86E+00	±27%	1.01E+01	±5%	1.02E+01	±2%
Ea_{h02}	1.20E+05	±146%	7.41E+04	±34%	6.30E+04	±24%	6.20E+04	±13%
k_{h23}	4.35E+00	±43%	2.31E+00	±46%	1.03E+01	±5%	1.04E+01	±2%
Ea_{h23}	2.96E+04	±264%	1.23E+04	±140%	1.03E+05	±16%	1.02E+05	±16%
k_{i12}	2.98E+00	±63%	5.51E+00	±42%	4.62E+00	±13%	4.59E+00	±10%
k_{i21}	5.43E-01	±306%	3.61E+00	±65%	2.98E+00	±24%	2.98E+00	±19%
Ea_{i12}	4.03E+04	±116%	1.63E+05	±119%	1.40E+05	±27%	1.37E+05	±20%
Ea_{i21}	1.17E+05	±43%	2.24E+05	±83%	1.60E+05	±24	1.53E+05	±18%
k_{h13}	8.63E+00	±19%	5.74E+00	±18%				
Ea_{h13}	8.59E+04	±33%	8.37E+04	±27%				
k_{h01}	6.45E+00	±25%						
Ea_{h01}	7.77E+04	±60%						
SSE	2.51E-04		5.38E-04		5.58E-04		5.57E-04	
RR	99.49%		98.90%		98.86%		98.86%	

It is clear that the equilibrium is strongly shifted towards tHDA, therefore, the hydrogenation of the cHDA intermediate is expected to have little effect on the overall mechanism. The reaction R_h13 was therefore neglected, obtaining a more simplified model with 13 parameters, referred as LHHW_13P with comparable residuals. Interestingly, the Arrhenius reaction rates parameters converged to acceptable values with a reduction of the confidence interval, but the adsorption constants saw a broadened confidence. Focusing on the adsorption constants of the dual site Langmuir Hinshelwood model, it should be noted that the values are still comparable with the estimates for 2,4-dinitrotoluene hydrogenation on carbon dispersed catalysts at similar temperatures.³²

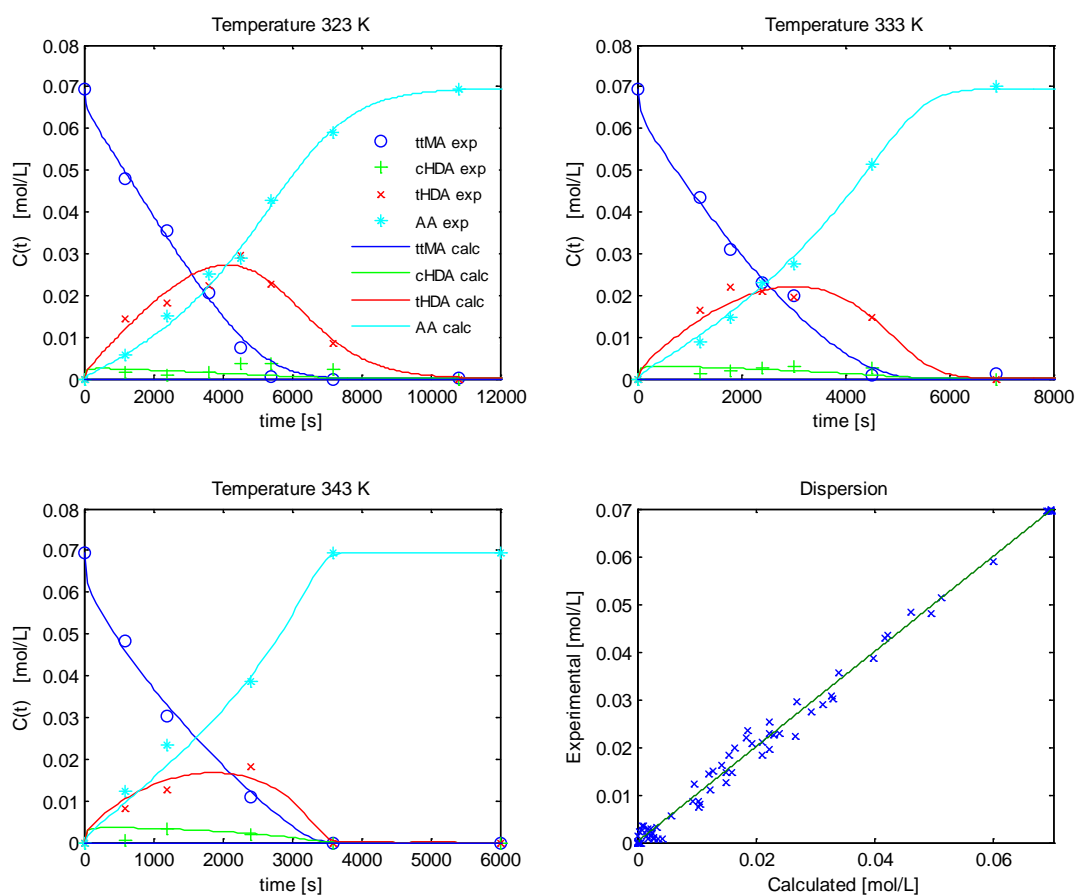


Figure 5.11 - Concentration profiles for the hydrogenation of ttMA on Pt/C 5% catalyst at 4bar hydrogen. Results of the regression with model LHHW_17P.

The large confidence interval for the adsorption constants depends on the fact that the denominator parameters are the most correlated, as shown by a least square analysis performed with BzzMath library tools. The t-test and p-test pointed K_{tHDA} , K_{AA} and K_{H_2} as “redundant parameters”. This model was further analyzed performing a sensitivity analysis on the parameters, whose results are shown in Figure 5.12.

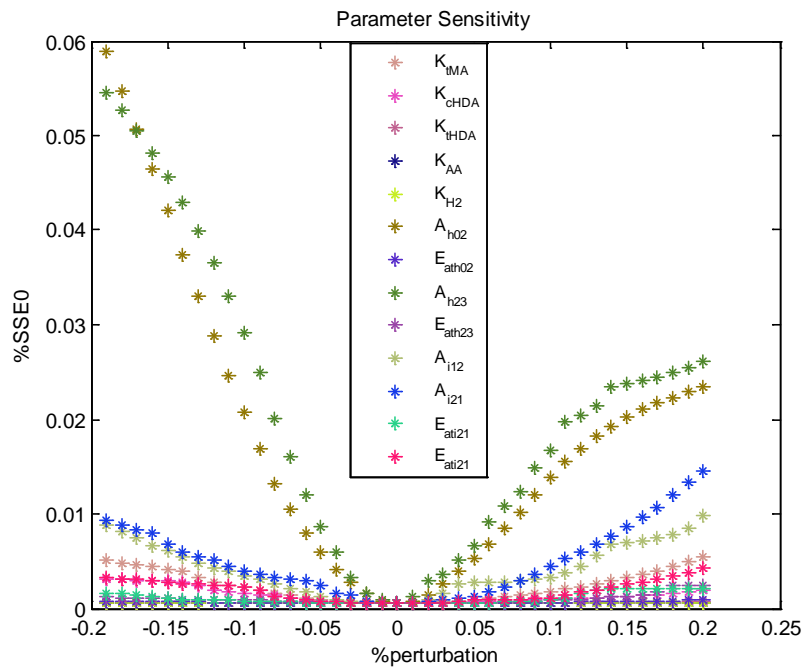


Figure 5.12 - Sensitivity analysis on the parameters of model LHHW_13P.

The parameters that minimally affect the regression results are, in order from the less relevant, K_{H2} , K_{AA} and K_{IHDA} . Provided the constant concentration of H_2 and the lower value of the adsorption constant (close to the lower limit) the contribution of the group $K_{H2}C_{H2}$ could be neglected ($\ll 1$). Also, the group $K_{AA}C_{AA}$ was neglected, as the adsorption constants of saturated compounds is far lower than saturated ones. The obtained model had therefore 11 parameters (identified as LHHW_11P), resulting in a minimal reduction of the coefficient of determination. The statistical analysis showed that K_{IDA} was still affected by collinearity, but all the other values presented acceptable confidence intervals as shown in Table 5.8. The concentration time profiles and in the dispersion diagram for LHHW_11P are presented in Figure 5.13. In conclusion, the LHHW_11P model is to be preferred as simple but sound in representing the experimental data.

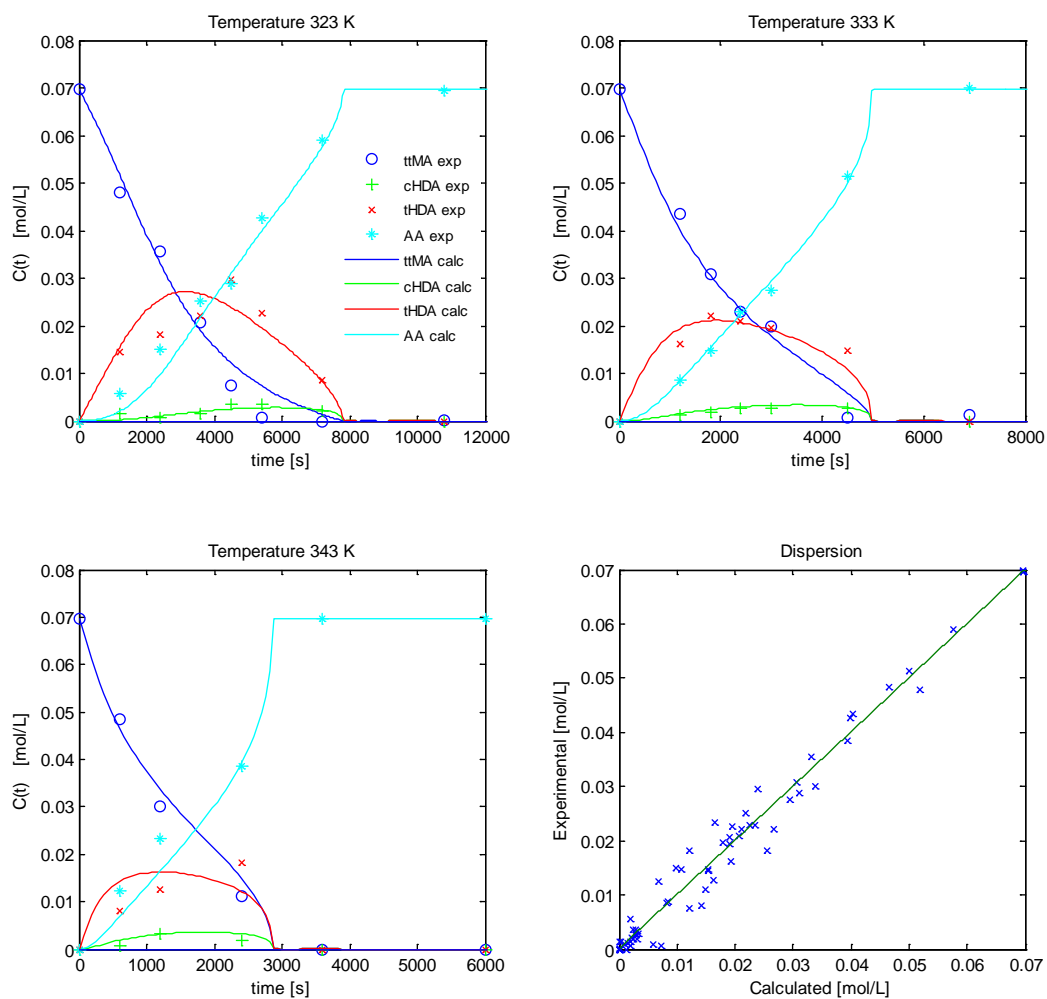


Figure 5.13 - Concentration profiles for the hydrogenation of ttMA on Pt/C 5% catalyst at 4bar hydrogen. Results of the regression with model LHHW_11P.

5.4 - Conclusions

This investigation offers a first insight on the hydrogenation mechanism of *trans,trans*-muconic acid to obtain adipic acid on a Pt/C catalyst. The catalyst employed achieved the highest yields in the mildest conditions compared to the other catalysts at the current state of the art. These hydrogenation performances were used for the design of the hydrogenation interval during the superstructure development described in chapter 3. Kinetic data were collected and used to suggest different plausible reaction pathways and to derive some preliminary kinetic models. Several models were used to interpret the experimental values, developed according to the LHHW theory, which considers the species adsorption-desorption equilibria of the involved species. A dual-step hydrogenation mechanism was demonstrated, characterized by hydrogen dissociation on the metal. The mechanism is the following: ttMA is hydrogenated first to tHDA, that undergoes an isomerization reaction to cHDA, promoted by the catalyst activation of the double bond. The intermediates are further hydrogenated to AA. This led to the formulation of a first model with 17 adaptive parameters, able to fit the data but strongly affected by multicollinearity. The parameters number was therefore reduced to 11, to achieve a final model with a good fit of the experimental data and characterized by kinetic constants in line with previous literature estimates of similar systems.

This very first detailed study of the hydrogenation of muconic acid provided an insight of the kinetic parameters, which currently are the sole reference values for this system. Even though the model was able to fit satisfactorily the experimental data, some topics deserve further investigation.

- I. An aspect that has a key role in the hydrogenation dynamics is the adsorption/desorption of the species on the catalyst. Even though LHHW model takes into account these phenomena, the model has been questioned, as performs many simplifications. For this reason, a specific study on the adsorption equilibria of muconates on the catalyst support needs to be performed. The aim is including in the kinetic equations an explicit and detailed temperature-dependent adsorption model. This will eventually reduce also the computational efforts for the kinetic regression.

- II. The present model can be further refined exploring and modelling the effects of a wider range of reaction conditions, collecting data on the effects of the catalyst amount, the initial species concentration, a wider span of temperatures, and possibly different reactor configurations. In this way the model could be better employed for simulating scaled-up applications, to estimate the performance and the costs of an industrial hydrogenation process of muconic acid.
- III. Following the indication of the superstructure optimization, hydrogenation in ethanol could actually be preferable from an economic perspective. The industrial chemistry group of Università degli Studi di Milano is currently testing new catalysts in ethanol. In particular, some preliminary results anticipate a different reaction mechanism, which involve hydrogenation by hydrogen transfer from a donor solvent.

In general, the hydrogenation model development and the optimization of the reaction conditions gave very encouraging results, but the work is still at its beginning. The path opened for the characterization of a “simple hydrogenation” proved to be extremely challenging and stimulating, so that required the joined efforts of two Ph.D. students. This resulted in several scientific publications, whose number will possibly grow.

From the engineering point of view, it has been particularly interesting to see how model regression tools (from PSE) were useful to guide and direct the practical laboratory research even at the first preliminary assessments, proving the general hypotheses of the methodology of this Ph.D. project. Indeed, it was the preliminary regression to point out the necessity to re-calibrate the GC instrument to explain the error in the material balances. The search of mild pressures rather than room temperature reactions was as well supported by process level indications deriving from the analyses of Chapter 3 (e.g. a simple jacketed reactor is far cheaper than a pressurized one).

As a concluding remark, it is possible to say that this empirical work for the hydrogenation characterization did also empirically prove the importance of a proactive collaboration between laboratory research and Process Systems Engineering.

5.5 - References chapter 5

1. Vardon, D. R.; Rorrer, N. A.; Salvachúa, D.; Settle, A. E.; Johnson, C. W.; Menart, M. J.; Cleveland, N. S.; Ciesielski, P. N.; Steirer, K. X.; Dorgan, J. R.; Beckham, G. T. *Green Chem.* **2016**, *18* (11), 3397.
2. Draths, K. M.; Frost, J. W. *J. Am. Chem. Soc.* **1994**, *116* (1), 399.
3. Niu, W.; Draths, K. M.; Frost, J. W. *Biotechnol. Prog.* **2002**, *18* (2), 201.
4. Thomas, J. M.; Raja, R.; Johnson, B. F. G.; O'Connell, T. J.; Sankar, G.; Khimyak, T. *Chem. Commun.* **2003**, 10, 1126.
5. Li, X.; Wu, D.; Lu, T.; Yi, G.; Su, H.; Zhang, Y. *Angew. Chemie - Int. Ed.* **2014**, *53* (16), 4200.
6. She, X.; Brown, H. M.; Zhang, X.; Ahring, B. K.; Wang, Y. *ChemSusChem* **2011**, *4* (8), 1071.
7. Shiramizu, M.; Toste, F. D. *Angew. Chemie - Int. Ed.* **2013**, *52* (49).
8. Henderson, R. K.; Jiménez-González, C.; Constable, D. J. C.; Alston, S. R.; Inglis, G. G. A.; Fisher, G.; Sherwood, J.; Binks, S. P.; Curzons, A. D. *Green Chem.* **2011**, *13* (4).
9. Sirasani, G.; Tong, L.; Balskus, E. P. *Angew. Chemie - Int. Ed.* **2014**, *53* (30).
10. Vardon, D. R.; Franden, M. A.; Johnson, C. W.; Karp, E. M.; Guarneri, M. T.; Linger, J. G.; Salm, M. J.; Strathmann, T. J.; Beckham, G. T. **2015**, *8* (2), 617.
11. Scelfo, S.; Pirone, R.; Russo, N. *Catal. Commun.* **2016**, *84*, 98.
12. Levenspiel, O. *Chemical reaction engineering*; Wiley, 1999.
13. Froment, G. F.; Bischoff, K. B.; De Wilde, J. *Chemical Reactor Analysis and Design, 3rd Edition*; John Wiley & Sons, Incorporated, 2010.
14. Matthiesen, J. E.; Carraher, J. M.; Vasiliu, M.; Dixon, D. A.; Tessonier, J.-P. *ACS Sustain. Chem. Eng.* **2016**, *4* (6).
15. Carraher, J. M.; Pfennig, T.; Rao, R. G.; Shanks, B. H.; Tessonier, J.-P. *Green Chem.* **2017**.
16. Frost, J. W.; Miermont, A.; Schweitzer, D.; Bui, V.; Wicks, D. A. US8367858 B2 2013
17. Capelli, S.; Rosengart, A.; Villa, A.; Citterio, A.; Di Michele, A.; Bianchi, C. L.; Prati, L.; Pirola, C. *Appl. Catal. B Environ.* **2017**.

18. Locatelli, G. Bio-adipic acid production by heterogeneous catalyzed hydrogenation reaction, Università degli studi di Milano, **2017**.
19. Chaudhari, R. V; Rode, C. V; Deshpande, R. M.; Jaganathan, R.; Leib, T. M.; Mills, P. L. *Chem. Eng. Sci.* **2003**, 58 (3–6), 627.
20. Chaudhari, R. V.; Ramachandran, P. A. *AIChE J.* **1980**, 26 (2), 177.
21. Rajashekharan, M. V; Nikalje, D. D.; Jaganathan, R.; Chaudhari, R. V. *Ind. Eng. Chem. Res.* **1997**, 36 (3), 592.
22. Fillion, B.; Morsi, B. I.; Heier, K. R.; Machado, R. M. *Ind. Eng. Chem. Res.* **2002**, 41 (4), 697.
23. Machado, R. M. *ALR Application Note 01-2007*. 2007, pp 1–14.
24. Hájek, J.; Murzin, D. Y. *Ind. Eng. Chem. Res.* **2004**, 43 (9), 2030.
25. Sano, Y.; Yamaguchi, N.; Adachi, T. *J. Chem. Eng. JAPAN* **1974**, 7 (4).
26. McKetta, J. J. *Encyclopedia of Chemical Processing and Design: Volume 46 - Pumps: Bypass to Reboilers*; Chemical Processing and Design Encyclopedia; Taylor & Francis, 1993.
27. Acres, G. J. K.; Cooper, B. J. *J. Chem. Technol. Biotechnol.* **1972**, 22 (6), 769.
28. Froment, G. F.; Bischoff, K. B.; De Wilde, J. *Chemical reactor analysis and design 3rd Ed.*, 3rd ed.; Wiley New York, 2011; Vol. 2.
29. Lylykangas, M. S.; Rautanen, P. A.; Krause, A. O. I. *Ind. Eng. Chem. Res.* **2004**, 43 (7), 1641.
30. Buzzi-Ferraris, G.; Manenti, F. *Interpolation and Regression Models for the Chemical Engineer: Solving Numerical Problems*; John Wiley & Sons, 2010.
31. Veldsink, J. W.; Bouma, M. J.; Schöön, N.-H.; Beenackers, A. A. C. M. *Catal. Rev. - Sci. Eng.* **1997**, 39 (3).
32. Neri, G.; Musolino, M. G.; Milone, C.; Galvagno, S. *Ind. Eng. Chem. Res.* **1995**, 34 (7), 2226.
33. Jones, W. H. *Catalysis in Organic Syntheses*; Elsevier Science, 2013.
34. Zhang, Z.; Jackson, J. E.; Miller, D. J. *Ind. Eng. Chem. Res.* **2002**, 41 (4), 691.
35. Capelli, S.; Rosengart, A.; Villa, A.; Citterio, A.; Di Michele, A.; Bianchi, C. L.; Prati, L.; Pirola, C. *Appl. Catal. B Environ.* **2017**, 218.
36. Frost, J. W.; Miermont, A.; Schweitzer, D.; Bui, V. US 20100314243 A1.

37. Chaudhari, R. ; Rode, C. .; Deshpande, R. .; Jaganathan, R.; Leib, T. .; Mills, P. .
Chem. Eng. Sci. **2003**, 58 (3), 627.
38. Rosengart, A.; Capelli, S.; Pirola, C.; Citterio, A.; Bianchi, C. L.; Prati, L.; Villa, A.
Chem. Eng. Trans. **2017**, 57, 931.

General conclusions

The Doctoral project presented in this Thesis addressed the feasibility study of a novel bioprocess for the production of a drop-in commodity chemical, adipic acid. The topic belongs to the general framework of renovation of the traditional oil-based industry toward a sustainable manufacturing, as required by the most recent European Union policies.

The peculiar and interdisciplinary context of biorefinery presents new challenges to the usual project engineering practice: in facts, a shared and standardized methodology for process design, as the ones for pharmaceutical or oil industry, is still missing. In addition, the case study of adipic acid is characterized by a very early stage of process development, with incomplete and preliminary data on some key aspects for a reliable process design.

For these reasons, a novel methodology for early stage process design and R&D strategy definition has been investigated and implemented, giving a contribution to fill the gap of large-scale bioprocess development practice. In particular, different Process Systems Engineering tools have been used to tackle data uncertainty and provide sound technoeconomic estimations.

A number of technologies associated with bio-conversion and downstream separation have been analyzed and included in the systematic formulation of a process-alternatives network. By optimizing this superstructure, a feasible processing route has been identified, avoiding the arbitrary decisions usually included by designing a process in “analogy” with similar existing processes. In this way, the obtained flowsheet gives indications on the feedstock to be selected, on the best strategy for broth clarification, on the degree of broth concentration, and, in general, on the best downstream practice. The alternatives are associated to different values of the objective function (related to the process profitability), therefore the design choices can be motivated by unbiased numbers. Most important, the process-related indications can be used to define some priorities for the ongoing research, identifying proactively the occurrence of bottlenecks and measuring the impacts of the uncertainty of the preliminary data available.

Both experimental studies and theoretical modelling have been performed to retrieve the basic information and to provide some sound full-scale estimates, when literature information is not sufficient.

The kinetic study on the hydrogenation of the bioderived intermediate (muconic acid) to achieve adipic acid belongs to the “empirical” activity carried out for this Doctoral project. The published data provide the first reference for this reaction, and give also the first mechanism hypothesis.

The “theoretical predictive modelling” activity addresses instead the design and cost estimation of a key unit operation (broth clarification by membrane filtration). Usually ultrafiltration units design relies on extensive experimental studies that can be performed only at more advanced design stages. In this study the impact on the process economics has a more detailed estimate than generic rule of thumb cost value. A grey-box model is proposed, applying fuzzy-logic algorithms to study the parameter uncertainty effect on the final cost estimates. This method of uncertainty propagation, widely used in risk analysis, is still a novelty in the field of chemical process design.

In general, the modelling activity carried out in this Doctoral Study concerned different types of optimization problems: from mixed integer linear programming, to uncertainty propagation through algebraic-differential equations systems, to computational-expensive regression problems. However, this work did not only apply different computational methods to different types of problems, but has also spaced between topics that can appear quite distant from each other (biology, chemistry, and engineering). This is the consequence of an interdisciplinary field that needs an interdisciplinary approach. A collaborative attitude between complementary expertise was necessary to achieve the most rigorous evaluation in a rather limited time horizon. Provided that the initial objectives of the project have been fulfilled, the obtained results can become the starting point for further investigations, in each of the above mentioned disciplines.

The adipic acid producers can employ the economic assessments of this Thesis to understand in the mid-long term if the renewable alternative is a threat or an opportunity. From this side, an Italian industrial group active in the field of adipic acid has already used some of the data here presented. In addition, the final process flowsheet has been used to

perform a new and updated LCA study by the researchers of Università degli Studi di Milano, which will be soon published.

The assumptions, taken for the full scale estimation, have been translated into some SMART Objectives (Specific, Measurable, Assignable, Realistic, Time bound) than can set the next research and development strategy. These milestones can be related to the future economic performances of the plant, providing a ranking of priorities. For example, the main purpose of biological R&D should be an increased yield on sugar and guarantee the stability of the strains. Similarly the first objective for engineering R&D should be the detailed characterization of the thermodynamics and the crystallization properties of the species, so to validate and refine the process concept approximations.

The hydrogenation model development and the optimization of the reaction conditions can be investigated further, starting from our very encouraging results of this work. New catalysts are currently being tested, and, in the light of the superstructure optimization, hydrogenation by hydrogen transfer from a donor solvent (ethanol) could be preferable. Finally, the methodologies presented in this thesis can possibly be perfected and extended to other problems. An interesting aspect, for example, could be the combination of the membrane models with a centrifuge model, to have a predictive tool to design hybrid systems, which nowadays are becoming widely used in virtue of higher process flexibility. The uncertainty propagation algorithm itself can be applied to any model characterized by some sort of epistemic uncertainty. Regarding the superstructure optimization, since most of the data used in this work are derived from early-stage and lab-scale investigations, the estimates can be updated, as soon as new insights are provided by the ongoing R&D.

Hopefully, continuing this fruitful dialogue between chemistry, biology, and process engineering will accelerate the ability of providing effective technological solutions to renovate manufacturing and establish a Green Industry.

Appendix 1

SMART OBJECTIVES TABLE

The table lists some of the research activities that can generate from the indications contained in this Doctoral Thesis. SMART is the acronym of Specific, Measurable, Assignable, Realistic and Time-constrained, qualities that should pertain to the objectives of a good research project (Doran, G. T. *Manage. Rev.* 1981, 70 (11), 35.). The project management approach theorized by Doran aims at organizing a complex research, by defining some short- or mid-term milestones. In this way it is easier to measure the effectiveness of the investigation effort and understand if the research line is worth of further investments, applying a fail-fast philosophy. These smart milestones are:

- Specific, as they should deal with defined topics with clear targets (e.g. increase yield on glucose can reduce feedstock costs of -20%).
- Measurable, as the results have to be quantified in term of improvement from the previous state of the art (e.g. detailed solubility curves of MA, vs scattered preliminary points)
- Assignable, as they should be easy to be referred to specific areas of expertise. In the following table the area is indicated according to the main three areas of research involved: biology (BIO), chemistry (CHE), process engineering (ENG).
- Realistic: the objective should never be too ambitious, especially for applied research.
- Time-bound: time is a strategic variable for industrial R&D, therefore new research projects should carefully be identified not to be too far away.

The following list was compiled considering the main open questions in the field and the biggest assumptions taken when designing the process. The priority was decided according to the importance of the assumption and the potential benefits that could derive for the industrialization of sustainable adipic acid.

Priority	Area	Title	Description
High	BIO	Optimization of <i>E. coli</i> WN1/pWN 2.248	Currently this strain reached the 71% of the maximum theoretically achievable for this metabolic pathway. The lower selectivity is ascribable to insufficient oxygen availability (depending on the bioreactor and the feed addition) and to interferences between included plasmids (references in Par. 3.2.2). Another aspect worth of investigation is the enhanced pathway presented in par. 2.2.2.
High	BIO	Scalability of <i>E. coli</i> WN1/pWN 2.248 fermentation	The highest scale investigated so far is the 20 L fermentation of patent US20130030216A1 (references in Par. 3.2.2). The investigation should address industrial fermenters (e.g. air lift type) or apply the down-scaling rules mentioned in Par. 1.3.
High	BIO	Genetic stability of <i>E. coli</i> WN1/pWN 2.248	The stability to mutations of the GMO strains of <i>E. coli</i> WN1/pWN2.248 has not been assessed yet. The bacteria stability has been assumed for the process synthesis. Also, resistance to contamination should be demonstrated.
High	CHE	Isomerization kinetics of ccMA	This topic has not been investigated with sufficient detail to define the right conditions and the final concentrations at the end of the thermal treatment. References in Par.3.2.3.
High	CHE/ ENG	Solubility curves of MA isomers and salts	The solubility curves published in literature have been questioned, but so far the data have not been integrated or corrected. This information are of primary importance to perform detailed estimates on the concentration/crystallization operation, and should address MA and salts of all the isomers, in water and other relevant solvents. References in Par. 3.2.9.
High	CHE/ ENG	Crystallization kinetics of MA isomers and salts	The importance of this task is primary due to the necessity of ensuring very high product purity, then due to the relevant contribution of crystallization to the total product costs (30% of capex and 40% of opex). The role of temperature, the kinetics of nucleation, the best crystallization strategy are

			aspects that deserve specific and thorough analyses. References in Par.3.2.10, 3.2.2.
High	CHE/ ENG	Kinetic study on MA hydrogenation in ethanol	This aspect has been already investigated in some preliminary studies. The mechanism, probably involving hydrogen transfer from the solvent, has not been fully characterized. References in Par. 5.4.
Mid	ENG	Validate the cost estimates for broth clarification	This task can be performed provided the production of sufficient amounts of fermentation broth and the availability of the centrifugation/filtration pilots. Still such investigation is important to confirm or correct a capital expenditure of the order of 5 M\$. References in par. 3.2.4, 3.4.5 and 3.3.2.
Mid	CHE	Activated Carbon Adsorption on MA derivatives	This analysis should characterize the adsorption of MA isomers on carbon for two purposes: to optimize the amount of AC for purifying the broth before crystallization (Par. 3.2.8) and to provide a more detailed hydrogenation kinetic model (Par. 5.4)
Mid	ENG	Wastewater treatment	The hypothesized process requires relevant amounts of NaOH and HCl for shifting pH, in particular during the crystallization from water. This results in the production of large amounts of salty water. A closed loop would be beneficial for the environmental performances of the plant: it could be interesting to investigate the possibility to recover part of the original HCl and NaOH by means of electrolysis. References in Par. 3.2.10.
Mid	ENG	LCA analysis	The availability of a nontrivial process flowsheet, with associated material balances, can be used for a more detailed environmental performances estimation, applying for example LCA analysis. References in Par. 3.3.2

Mid	BIO	Muconic acid from <i>S. cerevisiae</i>	Recently, <i>S. cerevisiae</i> has been proved able to express the metabolic pathways to achieve muconic acid, still with low yields. Yeast, however, has the advantage of being easy to industrialize, and could probably allow an acid fermentation, resulting in savings of chemicals. References in Par.2.2.1.
Low	BIO	Extractive fermentation	Among the many techniques to enhance product concentration or fermentation yields, there is the removal of the product (especially when it has inhibiting effects). References in Par. 3.3.3.
Low	CHE	Sulfuric acid for pH control	The acidification steps could benefit from the use of a cheaper acid, as sulfuric acid instead of hydrochloric acid. This alternative has not been considered in literature.
Low	ENG	Estimate of the capital costs of inoculum preparation and propagation	The structure of Super-O did not allow including any batch-fed batch operation, and this aspect has not been included in the process design and in the economic assessment. This information can be useful for a more detailed estimate.
Low	ENG	New solvents for MA and AA extraction/hydrogenation	Ethanol and water are the only solvents without contraindications during hydrogenation. Still, this field has been little investigated: other solvents can maybe allow a solvent extraction purification avoiding one step of crystallization. A first thermodynamic study of the properties of MA derivatives is therefore recommended. Reference in Par.3.2.11,3.2.12
Low	ENG	Secondary metabolites recovery from spent bacteria	The addition of growth supports for <i>E. coli</i> fermentation impacts for the 6% of the final cost of adipic acid. Recovering part of useful amino acids and metabolites from the spent bacteria could help reducing the costs of wastewater treatment. References in Par.3.2.1. and Par.3.2.3

Appendix 2

Code for the cross flow micro-ultra filtration membrane uncertainty propagation. Language Matlab. The algorithm is organized into two functions:

1. Ultrafiltration_epistemic.m
2. Ultrafiltration_universal

Function 1: Ultrafiltration_epistemic.m (MATLAB)

Scope: Applies the algorithm for epistemic uncertainty propagation and generates the diagrams. The flux reduction calculations are performed solving the ADE system contained in the sub function Ultrafiltration_universal.

```

%% Crossflow ultrafiltration model. ALE MODIFICATO
% Generic system
% Crossflow ultrafiltration model: resistances in series
% Implementation of a basic cost function
% Uncertainty epistemic propagation

clear all
close all
clc

global int_epsi int_n int_phiR R_m DP mu Cx_b_in Ra_ss Rp_ss b A Cm alfa
k_m rho

%% Epistemic values
num = 5; % Number of values
% Range of phiR [a b]
int_phiR = [193 750 193.001 749.9999]; % Range of phiR [a b]
int_n = [0.5 1 0.63 0.63]; % Range of n [a b]
int_epsi = [0.08 0.18 0.08000001 0.17999999]; % Range of epsi [a b]

p_phiR = linspace(int_phiR(1),int_phiR(2),num); % Vector phiR
p_n = linspace(int_n(1),int_n(2),num); % Vector n
p_epsi = linspace(int_epsi(1),int_epsi(2),num); % Vector epsi

p_matrix = combvec(p_phiR,p_n,p_epsi)'; % [phiR n epsi] Each row
represents a triplet
size_m = size(p_matrix);

```

```

rows = size_m(1);
columns = size_m(2);

%% Data and operative conditions (fixed values)

% Data
Q_target = 11.26e-3;           % [m3/s] Objective permeate
production

DP = 4*100000;                % [Pa] Transmembrane pressure
DP0 = 1*100000;
mu = 0.78*10^-3;              % [Pa*s] Dynamic viscosity
rho = 1000;                    % [kg/m3] Density
v = 4;                          % [m/s] Crossflow velocity

% Resistances (Carrere, 2001)
R_m = 3.27e11;                 % [1/m] Clean membrane resistance
3.27e11 da specifica

Ra_ss = 2.7e12;                % [1/m] SS adsorption resistance
b = 3.0e-4;                    % [1/s] Parameter

alfaK = 1.2e9;                 % [m/kg/Pa^n] Cake resistance
coefficient

% Particle size
dps = 2e-6;                    % [m] Exp diameter

% Membrane size
di = 5.75e-3;                  % [m] Internal diameter
L = 1.178; % [m] Module length
%ACHTUNG--NR CHANNEL DA VERIFICARE
n_channel = 368; %7;           % [-] Number of channels:
Sez = pi*(di^2)/4;             % [m2] Section
A = pi*di*L*n_channel;         % [m2] Total filtration area single
unit!
e = 5e-6; % [m] Absolute roughness heigth
%ACHTUNG--VOL HOLDUP ARBITRARIO!
V0 = pi*di^2/4*L*n_channel+0.12; % [m3] System holdup volume [120L
tank+volume della membrana- holdup tubi non considerati]

% Diffusivity: Cho (estimated)
dh = di;                       % [m] Hydraulic diameter
Diff = 0.005*2*v*(dps^2)/dh;   % [m2/s] Diffusion coefficient

% Mass transfer coefficient
Re = rho*v*dh/mu;
Sc = mu/rho/Diff;
Sh = 0.00929*(((e/di)^0.15)*Re*(Sc^0.5)*(1.11+0.44*Sc^(-1/3))-0.7*Sc^(-
1/6)));
k_m = Sh*Diff/dh;              % [m/s] Turbulent flow

% Polarization resistance (colloids)
Diff_coll = 3.64e-12;          % [m2/s] Colloids (500nm) diffusion
coefficient
Re_coll = rho*v*dh/mu;
Sc_coll = mu/rho/Diff_coll;

```

```

Sh_coll =
0.00929*((e/di)^0.15)*Re_coll*(Sc_coll^0.5)*(1.11+0.44*Sc_coll^(-1/3)-
0.7*Sc_coll^(-1/6));
k_coll = Sh_coll*Diff_coll/dh;          % [m/s] Turbulent flow

% Inlet cell concentration (wet)
Cx_b_in = 2.6;                          % [kg/m3]

% Flux specification
DPm = 2e5;                              % [Pa] Clean membrane TMP
J0 = DPm/mu/R_m;                        % [m/s] Free water flux

%% Triplets [phiR, n, epsi]
phiR=zeros(rows, 1);
n=zeros(rows, 1);
epsi=zeros(rows, 1);
tri_poss=zeros(rows, 1);
C_total_year=zeros(rows, 1);
J_realwtf=zeros(rows, 1);

tic
for i = 1:rows
    phiR(i) = p_matrix(i,1);            % Solidosity
    n(i) = p_matrix(i,2);              % Cake compressibility index
    epsi(i) = p_matrix(i,3);          % Cake porosity

    % Possibility
    poss = possibility(phiR(i),n(i),epsi(i)); % Possibility values for
    phiR,n,epsi

    tri_poss(i) = min(poss);          % Triplet possibility

    % Dependent values
    alfa0 = alfaK*(DP0^n(i));         % [m/kg] Cake resistance at DP0
    alfa = alfa0*(DP/DP0)^n(i);      % [m/kg] Cake resistance at DP
    J_p_ss = k_coll*phiR(i);         % [m/s] SS polarization flux
    Rp_ss = DP/mu/J_p_ss;            % [1/m] SS polarization
resistance
    Cm = rho*(1-epsi(i));            % [kg/m3] Membrane cell
concentration

    % Filtration cycle
    time = 0;
    Cx_b0 = Cx_b_in;

    t_span = [time:1:20*3600];      % [s] 20 ORE MASSIMO
    y0 = [Cx_b0 J0 1e-3 V0];

    M = zeros(4,4);
    M(1,1) = 1;
    M(3,3) = 1;                      %l'equazione 2 è algebrica
    M(4,4) = 1;
    options = odeset('Mass',M,'MassSingular','yes'); % 'RelTol',1e-2
    [t_sol, y_sol] =
ode15s(@Ultrafiltration_universal,t_span,y0,options);

```

```

Cx_b_vector = y_sol(:,1);           % [kg/m3] C_b
J_vector = y_sol(:,2);             % [m/s] J
m_cake = y_sol(:,3)*A;            % [kg] m_cake
V = y_sol(:,4);                   % [m3] V

%Blocking system

rows_t = 0;                        %NON MI PIACE
for t = 1:length(t_span)
    if (J_vector(t) >= 0.1*J0)
        rows_t = rows_t+1;
    elseif (Cx_b_vector <= 80)
        rows_t = rows_t+1;
    else
        rows_t = rows_t+1;
    end
end
filtration_time = t_sol(1:rows_t); % [s] Effective filtration time
cleaning_time = 20*60;             % [s]
total_time = filtration_time(end)+cleaning_time; % [s]

J_real = mean(J_vector)*filtration_time(end)/total_time; % [m/s] Real
average flux
J_realwtf(i)=J_real*3600*1000;     % [l/m2/h]
N_units = Q_target/J_real/A;       % Number of membrane modules
A_tot = A*N_units;                 % [m2] Total required membrane
area

% Resistances
R_a = Ra_ss*(1-exp(-b*filtration_time)); % [1/m] Adsorption
resistance
R_p = Rp_ss*(1-exp(-b*filtration_time)); % [1/m] Concentration
polarization resistance
R_c = y_sol(1:rows_t,3)*alfa;      % [1/m] Cake resistance

% Costs evaluation
m_cost = 500;                       % [$/m2]
C_mem = m_cost*A_tot;               % [$] Membrane cost
C_v = 2000*N_units;                 % [$] Vessel cost
C_PV = 5926.13*(A_tot)^0.42;        % [$] Pipes and valves cost
C_IC = 1445.5*(A_tot)^0.66;         % [$] Instrumentation &
control cost
C_TF = 3047.21*(A_tot)^0.53;        % [$] Tanks and frames cost
C_MI = 7865.02*(A_tot)^0.57;        % [$] Miscellaneous cost
C_cc = 25000;                       % [$] Chemical cleaning
cost (practice)

Qr = pi*((di/2)^2)*v*n_channel;     % [m3/s] Recirculating
cross flow rate
t_down = cleaning_time;             % [s/cycle] Downtime
t_d = t_down/total_time;            % [-] Downtime fraction
Qf = Q_target/(1-t_d);              % [m3/s] Actual plant feed
flow rate

f = 23.5;                           % [-] Membrane friction
factor

```

```

    vel = Q_target/A; % [m/s] Convective velocity
    P_drop = 2*f*L*rho*(vel^2)/di; % [Pa] Pressure drop across
the module

    I = 3.32; % [-] Pump cost index ratio
    f1 = 1.5; % [-] Pump material
adjustment factor
    f2 = 1; % [-] Pump suction pressure
range adjustment factor
    L_pump = 1.4; % [-] Labor costs factor

    C_pf = I*f1*f2*L_pump*81.27*(Qf*(DP-P_drop/2))^0.39; % [$] Feed pump
cost
    C_pr = I*f1*f2*L_pump*81.27*((Qr+Qf*P_drop))^0.39; % [$]
Recirculating pump cost

    C_cap = C_mem + C_v + C_PV + C_IC + C_TF + C_MI + C_cc + C_pf + C_pr;
% [$] Capital cost

    A_15_7 = (1-1/((1+0.15)^7))/0.15; % Factor for costs
annualization

    C_cap_an = C_cap/A_15_7; % [$/year] Annualized

capital costs
    PLS = 10; % [years] Plant lifespan
    MLS = 10; % [years] Membrane lifespan
    Mr = PLS/MLS - 1; % Number of sets of
replacement membranes
    inter = 0.04; % [%/year] Annual interest
rate

C_r = Mr*A_tot*m_cost*(inter*((1+inter)^PLS)/(((1+inter)^PLS)-1));
eta = 0.8; % [-] Pump efficiency
W_pf = (DP-P_drop/2)*Qf/eta/1000*3600; % [kWh/year] Feed pump work
W_pr = P_drop*Qr/eta/1000*3600; % [kWh/year]
Recirculating pump work
    UEC = 0.1; % [$/kWh] Unit energy cost
    C_wpf = UEC*W_pf; % [$/year]
    C_wpr = UEC*W_pr; % [$/year]

    sal = 80000; % [$/person/year];
    N_lab = 3; % Number of personnel
    C_sal = N_lab*sal; % [$/year]

    C_maint = (1.5/100)*(C_cap-C_mem); % [$/year] Annual
maintenance costs

    C_chem = 25000; % [$/year]

    C_om = C_r + C_wpf + C_wpr + C_sal + C_maint + C_chem; % [$/year]
Operative costs

    C_total_year(i) = C_om+C_cap_an; % [$/year] Total costs per
year (for each triplet)
end

```

```
toc

%%
%Costruzione distrib.function
plot (C_total_year,tri_poss, 'x' )
x_mat=horzcat(C_total_year, tri_poss);
C_min=min(C_total_year);
C_max=max(C_total_year);
bin_width= (max(C_total_year)- min(C_total_year))/num;
bin_centers=linspace(C_min+0.5*bin_width,C_max-0.5*bin_width, num-1);
C_length=length(C_total_year);
bin_right=linspace(C_min,C_max, num-1);
x_mat_order=sortrows(x_mat);

for ii=1:num-1
    for jj=1:C_length
        if (x_mat(jj,1)>= (bin_centers(ii)-bin_width/2)) &&
(x_mat(jj,1)<= (bin_centers(ii)+bin_width/2))
            bin(jj,ii)=x_mat_order(jj,2);
        end
    end
end

for ii=1:num-1
    pi_bin_cost(ii)=max(bin(:,ii));
end
COSTO=linspace(4e5,C_max, 200);
for i=1:200
    if COSTO(i) <= C_min
        pi_COSTO(i) = 0;
    elseif COSTO(i) <= bin_right(1)
        pi_COSTO(i) = pi_bin_cost(1);
    elseif COSTO(i) <= bin_right(2)
        pi_COSTO(i) = pi_bin_cost(2);
    elseif COSTO(i) <= bin_right(3)
        pi_COSTO(i) = pi_bin_cost(3);
    else
        pi_COSTO(i) = 0;
    end
end

plot(COSTO,pi_COSTO)

xlabel('COSTO');
ylabel('\pi(COSTO)');
title ('costo totale');
```

Function Ultrafiltration_universal.m

Scope: contains the system of DAE of the modified Darcy Equation.

```

% Ultrafiltration at constant DP (transmembrane pressure)
% Ultrafiltration- Fedbatch operation + Shear induced diffusion and
Steady state

function dy = Ultrafiltration_universal(t,y)

global R_m DP mu Ra_ss Rp_ss b A alfa Cx_b_in k_m Cm

dy = zeros(4,1);                                %%% y1=C_b; y2=J; y3=m/A;
y4=V

R_a = Ra_ss*(1-exp(-b*t));                       % [1/m] Adsorption
resistance
R_p = Rp_ss*(1-exp(-b*t));                       % [1/m] Concentration
polarization resistance
R_c = y(3)*alfa;                                 % [1/m] Cake resistance

BM_mcells=(y(2)*y(1) - k_m*(Cm-y(1)));           % m_cake + shear induced
diff VINCOLO >=0
if BM_mcells<=0
    BM_mcells=0;
end

dy(1) = Cx_b_in/y(4)*y(2)*A;                    % [kg/m3] C_b    %%BM
FEDBATCH
dy(2) = y(2) - (DP./(mu*(R_m+R_a+R_p+R_c)));    % [m/s] J      AE!
dy(3) = BM_mcells;                              % [kg/s/m2]   m_cake/A
dy(4) = 0;                                       % ALE:        [m3]
Service volume =const

end

```


Appendix 3

Code for the regression of the kinetic parameters of a LHHW model in C++ language. The results are then compared with the least squares analysis on Matlab and plotted

1. Leastsquares17PModel4 (C++)
2. LHHW_17P_confidence_diss.m (MATLAB)
3. LHHW_17P_print_diss.m (MATLAB)

Function 1: Leastsquares17PModel4 (C++)

Scope: Performs the SSE minimization to provide the kinetic parameters of a LHHW model of the hydrogenation of muconic acid to adipic acid.

```
#define BZZ_COMPILER 3
#include "BzzMath.hpp"
#define SSE_STD

////////////////////////////////////////////////////////////////////////////////////////////////////////////////////////////////
////////////////////////////////////////////////////////////////////////////////////////////////////////////////////////////////
// GLOBAL VARIABLES

double ResMin(BzzVector &b); // Residues ycalc- yexp ->to be minimized
BzzMatrix ModelOdeMB(BzzVector &b, int &flag);
// Function for calculating the y calc to regress b parameters [n°models,
n°pt exp, parameters, time, exp points]
void MatBalModel4(BzzVector&y, double t, BzzVector &f); // mat bal function

BzzVector bOdeMB; // adaptive parameters
BzzVector tOdeMB; // t integration time points
int numModels = 1; // Number of models
int numX; // Nr columns input matrix
int numY; // Nr input variables
int numExperiments; // Nr experimental points
double T; // Temperature
int NumPar = 17; // Number of adaptive parameters in the model

double R = 8.3144; // Universal gas constant J/mol/K
BzzVector bGL(NumPar); // adaptive param of LHHW model, updated by
function ModelOdeMB
BzzMatrix X; // Input matrix acquired by file X.dat
BzzMatrix Y; // Input matrix acquired by file Y.dat
BzzMatrix Ycalc; // Calculated matrix by ModelOdeMB
BzzVector yexp;
FILE *resultati; // output file pointer
double RR; // RR relative residual, or normalized SSE
double SSE; // SSE sum of squared error
////////////////////////////////////////////////////////////////////////////////////////////////////////////////////////////////
////////////////////////////////////////////////////////////////////////////////////////////////////////////////////////////////

void main(void)
{
    bzzOpenMP = 0; // parallel computation deactivation
    bzzWarningWindow = 0; // warning deactivation
}
```

```

int maxIter = 10000;           // max iterations robust
BzzVector pOpt;

// print results
risultati = fopen("myresults.txt", "w");
fprintf(risultati, " %s\n ", "CALCOLO PARAMETRI CINETICI IDROGENAZIONE
ACIDO MUCONICO IN ACQUA");
fprintf(risultati, " %s\n ", "Modello a 17 parametri (serie 4HYDnodiss)
vin SMART, 2 run davvero");

printf(" %s\n ", "CALCOLO PARAMETRI CINETICI IDROGENAZIONE ACIDO MUCONICO
IN ACQUA");
printf(" %s\n ", "Modello a 17 parametri (serie 4HYDnodiss)  vin SMART,
2 run davvero");

//data acquisition
BzzMatrix inputX;
Load(&inputX, "Xinput.dat");
BzzMatrix inputY;

Load(&inputY, "Yinput.dat");
numExperiments = inputX.Rows(); // nr lines= nr experimental points
fprintf(risultati, "%s\t%i\n", "numero pti sperimentali",
numExperiments);
printf("%s\t\t%i\n\n", "numero pti sperimentali", numExperiments);
numY = inputY.Columns();
// Measured variables (they are 5: MucA, Hdioc cis, Hdioc trans, AdiA, Hydr)
numX = inputX.Columns();

// Measured variables in X (they are 7: Temperature, measured time, e y0)
BzzMatrix Xload(numExperiments, numX, 1, 1, inputX);
X = Xload;

BzzMatrix Yload(numExperiments, numY, 1, 1, inputY);
// Exp points matrix. numExp lines, numY columns, taken from position 1,1, of
input matrix inputY
Y = Yload;
Y.UseMatrixAsVector(&yexp); //vector experimental points
ChangeDimensions(numExperiments, &tOdeMB); //vector tOdeMB is resized so
that measure times correspond to the calculated times

for (int i; i <= numExperiments; i = i + 1)
{
    tOdeMB[i] = X[i][2];
}

BzzMinimizationRobust mr; // Class minimization robust

// 17 PARAMTETERS ++ CONSTRAINTS
BzzVector bL(NumPar, 0., 0., 0., 0., 0., 0., 2.5e4, 0., 2.5e4, 0., 0.,
0., 0., 0., 2.5e4, 0., 2.5e4);

```

```

    BzzVector bU(NumPar, 1.e6, 1.e6, 1.e6, 1.e6, 1.e6, 1.e6, 1.e6, 6.e4, 1.e6,
6.e4, 1.e6, 1.e6, 1.e6, 1.e6, 1.e6, 1.e6, 6.e4, 1.e6, 6.e4);
    BzzVector b0(NumPar, 49.439346, 0.434629, 109.909861,
0.000154, 533.932809, 0.259200, 25446.403051, 1.786284,
25069.625964, 13.748135, 11.788726, 94.644664, 55778.595363,
2.729225, 59999.836649, 1.730708, 25000.005689);

    //NO CONSTRAINTS
    //BzzVector bL(NumPar), bU(NumPar); // Search limits
    //BzzVector b0(NumPar);
    //b0 = 1.;
    //bU = 1.e6;
    //////////////////////////////////////
    // CALCULATION

//1 step
    printf("\n\n%-s\n", "PrimoStep...");
    mr(b0, ResMin, bL, bU); // initialize object mr [1attempt, fun, min and
max]
    mr(maxIter);
// Call
    mr.BzzPrint("Results 1");
    mr.GetSolution(&pOpt);

// 2 Step
    printf("\n\n%-s\n", "SecondoStep...");
    mr(pOpt, ResMin, bL, bU);
    mr(maxIter);
    mr.BzzPrint("Results 2");
    mr.GetSolution(&pOpt);

// 3 Step
    printf("\n\n%-s\n", "TerzoStep...");
    mr(pOpt, ResMin, bL, bU);
    mr(maxIter);
    mr.BzzPrint("Results 3");
    mr.GetSolution(&pOpt);

//4 Step
    printf("\n\n%-s\n", "QuartoStep...");
    mr(pOpt, ResMin, bL, bU);
    mr(maxIter);
    mr.BzzPrint("Results 4");
    mr.GetSolution(&pOpt);

//Plot screen
    pOpt.BzzPrint("\n\n\n\n%-s\n", "Parametri final:");
    printf("%s\t %f\n", "SSE", SSE);
// residues and par
    printf("%s\t %f\n", "RR%", RR*100.);
//plot to file myresults
    fprintf(risultati, "%s\t %f\n", "SSE", SSE);
    fprintf(risultati, "%s\t %f\n", "RR%", RR*100.);

```

```

    BzzMatrix rosematrice;
    rosematrice = Ycalc;
    int roserighe = rosematrice.Rows();
    int rosecolonne = rosematrice.Columns();
    int rosenmat, rosemmat;
    fprintf(risultati, "\n\n %s\t\n %i\t %i\n  ", "matrice Ycalc ",
roserighe, rosecolonne);
    for (int rosenmat = 1; rosenmat <= roserighe; rosenmat++)
    {
        for (int rosemmat = 1; rosemmat <= rosecolonne; rosemmat++)
        {
            fprintf(risultati, "%f\t",
rosematrice[rosenmat][rosemmat]);
        }
        fprintf(risultati, "\n\n");
    }

} //END MAIN

////////////////////////////////////
//////////////////////////////////////%
Residues function (Objective fun to be minimized)

double ResMin(BzzVector &b)
{
    int flag;
    Ycalc = ModelOdeMB(b, flag); // calculated points

    //Convergence check

    if (flag == 1)
    {
        bzzUnfeasible = 1;
        //printf("\n%-s\n", "cambiamo il giro...");

        return 0.;
    }
#ifdef SSE_STD
    BzzVector ycalc, diff, prod, prodnorm;
    Ycalc.UseMatrixAsVector(&ycalc); // big result matrix into vector
    diff = yexp - ycalc; // SSE difference
    ElementByElementProduct(diff, diff, &prod); // squared difference

    SSE = prod.GetSumElements(); // Sum of squared difference
#endif

#ifdef SSE_NORM
    //printf("%s\t %f\n", "RR", RR);
    BzzVector ycalc, diff, prod, prodnorm;
    Ycalc.UseMatrixAsVector(&ycalc);

    /

    diff = yexp - ycalc;
    int sz = diff.Size();
    BzzVector diffnorm(sz);

```

```

    for (int i = 1; i <= sz; i = i + 1)
    {
        diffnorm[i] = fabs(diff[i] / (yexp[i] + 10.e-5));
    }
    //system("pause");
    //ElementByElementProduct(diffnorm, diffnorm, &prodnorm);
    double RR0;
    SSE = diffnorm.GetSumElements();
    double szf = sz*1.;
    RR = RR0 / szf;
    #endif

    return (SSE);
}

%%%%%%%%%%%%%%%%%%%%%%%%%%%%%%%%%%%%%%%%%%%%%%%%%%%%%%%%%%%%%%%%%%%%%%%%%%%%%%%%%%%%%%%%%%%%%%%%%%%%%%%%%%%%%%%%%%%%%%%%%%%%%%%%%%%%%%%%%%%%%%%%%%%%%%
%%%%%%%%%%%%%%%%%%%%%%%%%%%%%%%%%%%%%%%%%%%%%%%%%%%%%%%%%%%%%%%%%%%%%%%%%%%%%%%%%%%%%%%%%%%%%%%%%%%%%%%%%%%%%%%%%%%%%%%%%%%%%%%%%%%%%%%%%%%%%%%%%%%%%%
Solution of the material balances (ODE integration)

BzzMatrix ModelOdeMB(BzzVector &b, int &flag)
// generates the calculated Ycalc values
{
    flag = 0;
    bGL = b;
    int i = 1;
    BzzMatrix y0m(numExperiments, numY, 1, 3, X);    // initial conditions
matrix
    BzzVector y0(numY);
                                                    // vector
initial conditions, correspond to the 3rd column of inpit matrix X
    BzzVector yMin(numY), yy(numY);                // min y=0.
Positive value constraint
    BzzMatrix Ycalcload(numExperiments, numY);
    fprintf(risultati, "%s\n\n", "valori parziali parametri");

    //17 PARAM    fprintf(risultati, " %s\t %f\t %f\t %f\t %f\t %f\t %f\t
%f\t %f\t %f\t %f\t %f\t %f\t %f\t %f\t %f\t %f\t %f\t %f\n ", "parametri regrediti",
bGL[1], bGL[2], bGL[3], bGL[4], bGL[5], (bGL[6]), bGL[7], (bGL[8]), bGL[9],
(bGL[10]), (bGL[11]), bGL[12], bGL[13], bGL[14], bGL[15], bGL[16], bGL[17]);

    // ODE SOLUTION
    BzzOdeStiff o;
    o.SetMinimumConstraints(&yMin); // Constraint y>=0

    for (i = 1; i <= numExperiments; i = i + 1)
    {
        y0 = y0m.GetRow(i);
        o.SetInitialConditions(y0, 0., MatBalModel14HYD);
        T = X[i][1]; // Temperature considered, updated on the global

```

```

        yy = o(tOdeMB[i]); // Integration: each step corresponds to the
experimental point. Integrates from 0 to tOdeMB[i]
        if (o.GetCalculationState() != 1 && o.GetCalculationState() != 2)
        {
            flag = 1; //If it does not converge
        }
        Ycalcload.SetRow(i, yy);
    }

    return (Ycalcload);
}

// Regression models

void MatBalModel14(BzzVector&y, double t, BzzVector &f) //LHHW with H2
dissociation ed R_h13
{
    // Model: 17 parameters
    // Idrogenazione irreversibile muconico solo a intermedio trans,
equilibrio isomerizzazione trans cis, idrogenazione irreversibile del trans ad
adipico
    // Le costanti sono LHHW CON formulazione Arrhenius
    // Dissociazione idrogeno esplicito
    // Si idrogena anche int CIS

    bOdeMB = bGL;

    double k333_h02 = bOdeMB[6];
    double Ea333_h02 = bOdeMB[7];
    double k333_h23 = bOdeMB[8];
    double Ea333_h23 = bOdeMB[9];
    double k333_i12 = bOdeMB[10];
    double k333_i21 = bOdeMB[11];
    double Ea333_i12 = bOdeMB[12];
    double Ea333_i21 = bOdeMB[13];
    double k333_h13 = bOdeMB[14];
    double Ea333_h13 = bOdeMB[15];
    double k333_h01 = bOdeMB[16];
    double Ea333_h01 = bOdeMB[17];

    double n = 3.;
    double hydcon = bOdeMB[5] * y[5];
    double denexp1 = 1. + bOdeMB[1] * y[1] + bOdeMB[2] * y[2] + bOdeMB[3] *
y[3] + bOdeMB[4] * y[4] + pow(hydcon, 0.5); //Adsorptions (denominator)

    double R_h02 = exp(k333_h02 - Ea333_h02 / R*(1. / T - 1. / 333.)) * y[1]
* y[5] / pow(denexp1, n);

    double R_h23 = exp(k333_h23 - Ea333_h23 / R*(1. / T - 1. / 333.)) * y[3]
* y[5] / pow(denexp1, n); // Hydrog ttMA to tHDA
    double R_i12 = -exp(k333_i12 - Ea333_i12 / R*(1. / T - 1. / 333.)) * y[2]
/ pow(denexp1, n) + exp(k333_i21 - Ea333_i21 / R*(1. / T - 1. / 333.)) * y[3] /
pow(denexp1, n); // Isomer cHDA->tHDA
    double R_h13 = exp(k333_h13 - Ea333_h13 / R*(1. / T - 1. / 333.)) * y[2]
* y[5] / pow(denexp1, n); // Hydrog cHDA to AA

```

```

double R_h01 = exp(k333_h01 - Ea333_h01 / R*(1. / T - 1. / 333.)) * y[1]
* y[5] / pow(denexp1, n); // Hydrog ttMA to cHDA
f[1] = -R_h02 - R_h01; // tMA consumption
f[2] = +R_i12 - R_h13 + R_h01; // formation consumption cHDA
f[3] = R_h02 - R_h23 - R_i12; // formation consumption tHDA
f[4] = R_h23 + R_h13; // formation AA
f[5] = 0.; //Hydrogen constant composition
}

```

```

////////////////////////////////////
//////////////////////////////////// THE END //////////////////////////////////

```

Input files: Xinput.dat

24 7

323.15	0	6.96E-02	0.00E+00	0.00E+00	0.00E+00	2.73E-03
323.15	1200	6.96E-02	0.00E+00	0.00E+00	0.00E+00	2.73E-03
323.15	2400	6.96E-02	0.00E+00	0.00E+00	0.00E+00	2.73E-03
323.15	3600	6.96E-02	0.00E+00	0.00E+00	0.00E+00	2.73E-03
323.15	4500	6.96E-02	0.00E+00	0.00E+00	0.00E+00	2.73E-03
323.15	5400	6.96E-02	0.00E+00	0.00E+00	0.00E+00	2.73E-03
323.15	7200	6.96E-02	0.00E+00	0.00E+00	0.00E+00	2.73E-03
323.15	10800	6.96E-02	0.00E+00	0.00E+00	0.00E+00	2.73E-03
323.15	14400	6.96E-02	0.00E+00	0.00E+00	0.00E+00	2.73E-03
333.15	0	6.96E-02	0.00E+00	0.00E+00	0.00E+00	2.59E-03
333.15	1200	6.96E-02	0.00E+00	0.00E+00	0.00E+00	2.59E-03
333.15	1800	6.96E-02	0.00E+00	0.00E+00	0.00E+00	2.59E-03
333.15	2400	6.96E-02	0.00E+00	0.00E+00	0.00E+00	2.59E-03
333.15	3000	6.96E-02	0.00E+00	0.00E+00	0.00E+00	2.59E-03
333.15	4500	6.96E-02	0.00E+00	0.00E+00	0.00E+00	2.59E-03
333.15	6900	6.96E-02	0.00E+00	0.00E+00	0.00E+00	2.59E-03
333.15	9000	6.96E-02	0.00E+00	0.00E+00	0.00E+00	2.59E-03
343.15	0	6.96E-02	0.00E+00	0.00E+00	0.00E+00	2.47E-03
343.15	600	6.96E-02	0.00E+00	0.00E+00	0.00E+00	2.47E-03
343.15	1200	6.96E-02	0.00E+00	0.00E+00	0.00E+00	2.47E-03
343.15	2400	6.96E-02	0.00E+00	0.00E+00	0.00E+00	2.47E-03
343.15	3600	6.96E-02	0.00E+00	0.00E+00	0.00E+00	2.47E-03
343.15	6000	6.96E-02	0.00E+00	0.00E+00	0.00E+00	2.47E-03
343.15	7200	6.96E-02	0.00E+00	0.00E+00	0.00E+00	2.47E-03

Input files: Yinput.dat

24 5

6.96E-02	0.00E+00	0.00E+00	0.00E+00	2.73E-03
4.80E-02	1.47E-03	1.45E-02	5.69E-03	2.73E-03
3.55E-02	8.39E-04	1.82E-02	1.50E-02	2.73E-03
2.07E-02	1.46E-03	2.22E-02	2.52E-02	2.73E-03
7.56E-03	3.59E-03	2.96E-02	2.89E-02	2.73E-03
6.47E-04	3.53E-03	2.26E-02	4.28E-02	2.73E-03
0.00E+00	2.12E-03	8.51E-03	5.90E-02	2.73E-03
6.96E-05	0.00E+00	0.00E+00	6.95E-02	2.73E-03

0.00E+00	0.00E+00	0.00E+00	6.96E-02	2.73E-03
6.96E-02	0.00E+00	0.00E+00	0.00E+00	2.59E-03
4.35E-02	1.13E-03	1.63E-02	8.67E-03	2.59E-03
3.09E-02	1.83E-03	2.21E-02	1.48E-02	2.59E-03
2.29E-02	2.76E-03	2.10E-02	2.29E-02	2.59E-03
1.98E-02	2.82E-03	1.95E-02	2.75E-02	2.59E-03
7.66E-04	2.72E-03	1.48E-02	5.13E-02	2.59E-03
1.33E-03	0.00E+00	0.00E+00	7.00E-02	2.59E-03
0.00E+00	0.00E+00	0.00E+00	7.00E-02	2.59E-03
6.96E-02	0.00E+00	0.00E+00	0.00E+00	2.47E-03
4.85E-02	6.87E-04	8.05E-03	1.24E-02	2.47E-03
3.01E-02	3.32E-03	1.27E-02	2.34E-02	2.47E-03
1.10E-02	1.86E-03	1.82E-02	3.85E-02	2.47E-03
0.00E+00	0.00E+00	0.00E+00	6.96E-02	2.47E-03
0.00E+00	0.00E+00	0.00E+00	6.96E-02	2.47E-03
0.00E+00	0.00E+00	0.00E+00	6.96E-02	2.47E-03

Function 2: LHHW_17P_confidence_diss.m (MATLAB)

Scope: Performs the SSE minimization to provide the kinetic parameters of a LHHW model of the hydrogenation of muconic acid to adipic acid.

```
%algorithm to calculate 95% confidence intervals for the parameters
regressed with lsqnonlin
```

```
function nonlinmatlab
```

```
global Xinput Yexp;
```

```
%Predictor variables: time[s]; C_muc[mol/L]; C_cis[mol/L];
```

```
C_trans[mol/L]; C_adia[mol/L]; C_H2[mol/L];T[K];
```

```
Xinput=[0      6.96E-02    0.00E+00    0.00E+00    0.00E+00    2.73E-03
323.15
1200    6.96E-02    0.00E+00    0.00E+00    0.00E+00    2.73E-03
323.15
2400    6.96E-02    0.00E+00    0.00E+00    0.00E+00    2.73E-03
323.15
3600    6.96E-02    0.00E+00    0.00E+00    0.00E+00    2.73E-03
323.15
4500    6.96E-02    0.00E+00    0.00E+00    0.00E+00    2.73E-03
323.15
5400    6.96E-02    0.00E+00    0.00E+00    0.00E+00    2.73E-03
323.15
7200    6.96E-02    0.00E+00    0.00E+00    0.00E+00    2.73E-03
323.15
10800   6.96E-02    0.00E+00    0.00E+00    0.00E+00    2.73E-03
323.15
14400   6.96E-02    0.00E+00    0.00E+00    0.00E+00    2.73E-03
323.15
0       6.96E-02    0.00E+00    0.00E+00    0.00E+00    2.59E-03
333.15
1200    6.96E-02    0.00E+00    0.00E+00    0.00E+00    2.59E-03
333.15
1800    6.96E-02    0.00E+00    0.00E+00    0.00E+00    2.59E-03
333.15
2400    6.96E-02    0.00E+00    0.00E+00    0.00E+00    2.59E-03
333.15
3000    6.96E-02    0.00E+00    0.00E+00    0.00E+00    2.59E-03
333.15
4500    6.96E-02    0.00E+00    0.00E+00    0.00E+00    2.59E-03
333.15
6900    6.96E-02    0.00E+00    0.00E+00    0.00E+00    2.59E-03
333.15
9000    6.96E-02    0.00E+00    0.00E+00    0.00E+00    2.59E-03
333.15
0       6.96E-02    0.00E+00    0.00E+00    0.00E+00    2.47E-03
343.15
600     6.96E-02    0.00E+00    0.00E+00    0.00E+00    2.47E-03
343.15
1200    6.96E-02    0.00E+00    0.00E+00    0.00E+00    2.47E-03
343.15
2400    6.96E-02    0.00E+00    0.00E+00    0.00E+00    2.47E-03
343.15
3600    6.96E-02    0.00E+00    0.00E+00    0.00E+00    2.47E-03
343.15
```

```

343.15      6000      6.96E-02      0.00E+00      0.00E+00      0.00E+00      2.47E-03
343.15      7200      6.96E-02      0.00E+00      0.00E+00      0.00E+00      2.47E-03
343.15];

%Response values experimental: C_muc[mol/L]; C_cis[mol/L];
C_trans[mol/L]; C_adia[mol/L]; C_H2[mol/L]
Yexp=[6.96E-02  0.00E+00  0.00E+00  0.00E+00  2.73E-03
4.80E-02  1.47E-03  1.45E-02  5.69E-03  2.73E-03
3.55E-02  8.39E-04  1.82E-02  1.50E-02  2.73E-03
2.07E-02  1.46E-03  2.22E-02  2.52E-02  2.73E-03
7.56E-03  3.59E-03  2.96E-02  2.89E-02  2.73E-03
6.47E-04  3.53E-03  2.26E-02  4.28E-02  2.73E-03
0.00E+00  2.12E-03  8.51E-03  5.90E-02  2.73E-03
6.96E-05  0.00E+00  0.00E+00  6.95E-02  2.73E-03
0.00E+00  0.00E+00  0.00E+00  6.96E-02  2.73E-03
6.96E-02  0.00E+00  0.00E+00  0.00E+00  2.59E-03
4.35E-02  1.13E-03  1.63E-02  8.67E-03  2.59E-03
3.09E-02  1.83E-03  2.21E-02  1.48E-02  2.59E-03
2.29E-02  2.76E-03  2.10E-02  2.29E-02  2.59E-03
1.98E-02  2.82E-03  1.95E-02  2.75E-02  2.59E-03
7.66E-04  2.72E-03  1.48E-02  5.13E-02  2.59E-03
1.33E-03  0.00E+00  0.00E+00  7.00E-02  2.59E-03
0.00E+00  0.00E+00  0.00E+00  7.00E-02  2.59E-03
6.96E-02  0.00E+00  0.00E+00  0.00E+00  2.47E-03
4.85E-02  6.87E-04  8.05E-03  1.24E-02  2.47E-03
3.01E-02  3.32E-03  1.27E-02  2.34E-02  2.47E-03
1.10E-02  1.86E-03  1.82E-02  3.85E-02  2.47E-03
0.00E+00  0.00E+00  0.00E+00  6.96E-02  2.47E-03
0.00E+00  0.00E+00  0.00E+00  6.96E-02  2.47E-03
0.00E+00  0.00E+00  0.00E+00  6.96E-02  2.47E-03];

beta0=[ 14.945133  4859.685480  5.812822  65.303215  419.716329
4.722541  120000.000000  4.348464  29569.064584  2.979021
0.543381  40294.045485  116612.941311  8.631272  85886.851277
6.445348  77711.047153];
betaL=[ 1., 1., 1., 1., 1., 1.e-8,
1.e4, 1.e-8, 1.e4, 1.e-8, 1.e-8, 1.e3,
1.e3, 1.e-8, 1.e4, 1.e-8, 1.e4];
betaU=[ 1.e6, 1.e6, 1.e6, 1.e6, 1.e6, 1.e6, 1.2e5, 1.e6, 1.2e5, 1.e8,
1.e8, 1.e6, 1.e6, 1.e6, 1.2e5, 1.e6, 1.2e5];

options = optimoptions(@lsqnonlin,'TolX',1e-8);

[beta,resnorm,residual,exitflag,output,lambda,jacobian]=lsqnonlin(@fun,
beta0, betaL, betaU,options);
disp(beta);
ci = nlparci(beta,residual,'jacobian',jacobian)
beta=beta';
stdev=ci(:,2)-beta;

beta_out = sprintf('%0.6e\n',beta)
stdev_out=sprintf('%0.6e\n',stdev)
% Calculation least squares value
function yy=fun(beta)
global Xinput Yexp;

```

```

texp323=Xinput(1:9,1);
C0323=Xinput(1,2:6);

texp333=Xinput(10:17,1);
C0333=Xinput(10,2:6);

texp343=Xinput(18:24,1);
C0343=Xinput(18,2:6);

[tls323,Cl323] = ode23s(@BMDIFF323,texp323,C0323,[],beta);
[tls333,Cl333] = ode23s(@BMDIFF333,texp333,C0333,[],beta);
[tls343,Cl343] = ode23s(@BMDIFF343,texp343,C0343,[],beta);
Ycalc=[Cl323;Cl333;Cl343];
YVcalc=reshape(Ycalc, [],1);
YVexp=reshape(Yexp, [],1);
yy=YVcalc-YVexp;

%% ----- FUNCTION MATERIAL BAL 323K-----
function dy = BMDIFF323(t,C,par)
% C Cexp(1) muconic Cexp(2) intermediate cis; Cexp(3)intermediate
trans; Cexp(4) adipic; Cexp(5) hydrogen
T=323;
R=8.314;
k333_h02 = par(6); % par from 1 to 5 are LHHW adsorption constants
Ea333_h02 = par(7);
k333_h23 = par(8);
Ea333_h23 = par(9);
k333_i12 = par(10);
k333_i21 = par(11);
Ea333_i12 = par(12);
Ea333_i21 = par(13);
k333_h13=par(14);
Ea333_h13 = par(15);
k333_h01 = par(16);
Ea333_h01 = par(17);
denexp=(1+par(1)*C(1)+par(2)*C(2)+par(3)*C(3)+par(4)*C(4)+(par(5)*C(5))^
3;

R_h02 = exp(k333_h02 - Ea333_h02/R*(1/T-1/333))*C(1)*C(5)/denexp;
%trans int formation
R_h23 = exp(k333_h23 - Ea333_h23 / R*(1 / T - 1 / 333))*C(3)*C(5)/denexp;
%trans int hydrog to aa
R_i12= (-exp(k333_i12 - Ea333_i12 / R*(1 / T - 1 /
333))*C(2)+exp(k333_i21 - Ea333_i21 / R*(1 / T - 1 / 333))*C(3))/denexp;
%isomerization cis->trans (e contrario)
R_h13=exp(k333_h13 - Ea333_h13 / R*(1 / T - 1 / 333))*C(2)*C(5)/denexp;
%cis int hydrog to aa
R_h01= exp(k333_h01 - Ea333_h01/R*(1/T-1/333))*C(1)*C(5)/denexp;
%trans cis formation

dC(1) = -R_h02-R_h01; %BM ttMA
dC(2) = R_i12-R_h13+R_h01; %BM cHDA
dC(3) = R_h02-R_h23-R_i12; %BM tHDA
dC(4) = R_h23+R_h13; %BM AA
dC(5) = 0.; %BM Const H2

```

```

dy=dC';

%% ----- FUNCTION MATERIAL BAL 333K-----
function dy = BMDIFF333(t,C,par)
% C Cexp(1) muconic Cexp(2) intermediate cis; Cexp(3)intermediate
trans; Cexp(4) adipic; Cexp(5) hydrogen
T=333;
R=8.314;
k333_h02 = par(6);
Ea333_h02 = par(7);
k333_h23 = par(8);
Ea333_h23 = par(9);
k333_i12 = par(10);
k333_i21 = par(11);
Ea333_i12 = par(12);
Ea333_i21 = par(13);
k333_h13=par(14);
Ea333_h13 = par(15);
k333_h01 = par(16);
Ea333_h01 = par(17);
denexp=(1+par(1)*C(1)+par(2)*C(2)+par(3)*C(3)+par(4)*C(4)+(par(5)*C(5))^3;

R_h02 =exp(k333_h02 - Ea333_h02/R*(1/T-1/333))*C(1)*C(5)/denexp;
%trans int formation
R_h23 =exp(k333_h23 - Ea333_h23 / R*(1 / T - 1 / 333))*C(3)*C(5)/denexp;
%trans int hydrog to aa
R_i12= (-exp(k333_i12 - Ea333_i12 / R*(1 / T - 1 /
333))*C(2)+exp(k333_i21 - Ea333_i21 / R*(1 / T - 1 / 333))*C(3))/denexp;
%isomerization cis->trans (e contrario)
R_h13=exp(k333_h13 - Ea333_h13 / R*(1 / T - 1 / 333))*C(2)*C(5)/denexp;
%cis int hydrog to aa
R_h01= exp(k333_h01 - Ea333_h01/R*(1/T-1/333))*C(1)*C(5)/denexp;
%trans cis formation

dC(1) = -R_h02-R_h01; %BM ttMA
dC(2) = R_i12-R_h13+R_h01; %BM cHDA
dC(3) = R_h02-R_h23-R_i12; %BM tHDA
dC(4) = R_h23+R_h13; %BM AA
dC(5) = 0.; %BM Const H2
dy=dC';

%% ----- FUNCTION MATERIAL BAL 343K-----
function dy = BMDIFF343(t,C,par)
T=343;
R=8.314;
k333_h02 = par(6); % par da 1 a 5 sono le costanti di
adsorbimento secondo LHHW
Ea333_h02 = par(7);
k333_h23 = par(8);
Ea333_h23 = par(9);
k333_i12 = par(10);
k333_i21 = par(11);
Ea333_i12 = par(12);
Ea333_i21 = par(13);
k333_h13=par(14);
Ea333_h13 = par(15);
k333_h01 = par(16);
Ea333_h01 = par(17);

```

```
denexp=(1+par(1)*C(1)+par(2)*C(2)+par(3)*C(3)+par(4)*C(4)+(par(5)*C(5))^3;

R_h02 =exp(k333_h02 - Ea333_h02/R*(1/T-1/333))*C(1)*C(5)/denexp;
%trans int formation
R_h23 =exp(k333_h23 - Ea333_h23 / R*(1 / T - 1 / 333))*C(3)*C(5)/denexp;
%trans int hydrog to aa
R_i12= (-exp(k333_i12 - Ea333_i12 / R*(1 / T - 1 / 333))*C(2)+exp(k333_i21 - Ea333_i21 / R*(1 / T - 1 / 333))*C(3))/denexp;
%isomerization cis->trans (e contrario)
R_h13=exp(k333_h13 - Ea333_h13 / R*(1 / T - 1 / 333))*C(2)*C(5)/denexp;
%cis int hydrog to aa
R_h01= exp(k333_h01 - Ea333_h01/R*(1/T-1/333))*C(1)*C(5)/denexp;
%trans cis formation

dC(1) = -R_h02-R_h01;           %BM ttMA
dC(2) = R_i12-R_h13+R_h01;     %BM cHDA
dC(3) = R_h02-R_h23-R_i12;     %BM tHDA
dC(4) = R_h23+R_h13;           %BM AA
dC(5) = 0.;                    %BM Const H2
dy=dC';
```

Function 3: LHHW_17P_print_diss.m (MATLAB)

Scope: Calculates the concentration profiles of the species and plots them against the experimental values, given the regressed model parameters.

```

%% PRINTING TOOL
%% REFERRED TO LHHW 17P

function fitDIFF

    close all          % per chiudere eventuali finestre di grafici
    clear all
    clc
    global npoint;

    %%% Temperature 323
    input='input_int';          % opens input dfile
    C0323=xlsread(input,3,'B2:F2'); % conc matrix col1 ttMA, col2
    cHDA, col3 tHDA, col4 AA, col 5 H2
    npoint=xlsread(input,3,'A20'); % nr exp points
    rM=xlsread(input,3,'A2:F10'); % matrice input (grezza)
    Cexp323=rM(1:npoint,2:end); % matrice concentrazione
    specie col1 muconico, col2 intermedio cis, col3 intermedio trans, col4
    adipico, col 5 hydr
    texp323 =rM(1:npoint,1); % vettore dei tempi
    sperimentali
    Cexp_muc323=[texp323, Cexp323(1:npoint,1)];
    Cexp_cis323=[texp323, Cexp323(1:npoint,2)];
    Cexp_trans323=[texp323, Cexp323(1:npoint,3)];
    Cexp_aad323=[texp323, Cexp323(1:npoint,4)];

    %%% Temperature 333
    C0333=xlsread(input,4,'B2:F2'); % conc matrix col1 ttMA, col2
    cHDA, col3 tHDA, col4 AA, col 5 H2
    npoint=xlsread(input,4,'A20'); % nr exp points
    rM=xlsread(input,4,'A2:F9'); % matrice input (grezza)
    Cexp333=rM(1:npoint,2:end); % matrice concentrazione
    specie col1 muconico, col2 intermedio cis, col3 intermedio trans, col4
    adipico, col 5 hydr
    texp333 =rM(1:npoint,1); % vettore dei tempi
    sperimentali
    Cexp_muc333=[texp333, Cexp333(1:npoint,1)];
    Cexp_cis333=[texp333, Cexp333(1:npoint,2)];
    Cexp_trans333=[texp333, Cexp333(1:npoint,3)];
    Cexp_aad333=[texp333, Cexp333(1:npoint,4)];

    %%% Temperature 343
    C0343=xlsread(input,5,'B2:F2'); % initial conc ttMA, cHDA, tHDA, AA, H2
    npoint=xlsread(input,5,'A20'); % nr exp points
    rM=xlsread(input,5,'A2:F8'); % matrice input (grezza)
    Cexp343=rM(1:npoint,2:end); % conc matrix col1 ttMA, col2 cHDA,
    col3 tHDA, col4 AA, col 5 H2
    texp343 =rM(1:npoint,1); % exp times
    Cexp_muc343=[texp343, Cexp343(1:npoint,1)];
    Cexp_cis343=[texp343, Cexp343(1:npoint,2)];
    Cexp_trans343=[texp343, Cexp343(1:npoint,3)];
    Cexp_aad343=[texp343, Cexp343(1:npoint,4)];

    % Insert final parameters

```

```

par=[14.945133 4859.685480 5.812822 65.303215 419.716329
4.722541 120000.000000 4.348464 29569.064584 2.979021
0.543381 40294.045485 116612.941311 8.631272 85886.851277
6.445348 77711.047153];

tsmooth323=[0:60:14400];
tsmooth333=[0:60:9000];
tsmooth343=[0:60:7200];
[tg323,Ctg323] = ode23s(@BMDIFF323,tsmooth323,C0323,[],par);
[tg333,Ctg333] = ode23s(@BMDIFF333,tsmooth333,C0333,[],par);
[tg343,Ctg343] = ode23s(@BMDIFF343,tsmooth343,C0343,[],par);

% LEAST SQUARE CALC
[tls323,Cls323] = ode23s(@BMDIFF323,texp323,C0323,[],par);
[tls333,Cls333] = ode23s(@BMDIFF333,texp333,C0333,[],par);
[tls343,Cls343] = ode23s(@BMDIFF343,texp343,C0343,[],par);

ClscalC=[reshape(Cls323(:,1:4),
numel(Cls323(:,1:4)),1);reshape(Cls333(:,1:4),
numel(Cls333(:,1:4)),1);reshape(Cls343(:,1:4),
numel(Cls343(:,1:4)),1)];
Clsexp=[Cexp_muc323(:,2);Cexp_cis323(:,2);Cexp_trans323(:,2);Cexp_aad323(
(:,2);Cexp_muc333(:,2);Cexp_cis333(:,2);Cexp_trans333(:,2);Cexp_aad333(:,2
);Cexp_muc343(:,2);Cexp_cis343(:,2);Cexp_trans343(:,2);Cexp_aad343(:,2);
];
SSE = sum((ClscalC-Clsexp).^2);
disp('SSE');
disp(SSE);
RR= (1-SSE/sum((Clsexp-mean(Clsexp)).^2))
disp('RR');
disp(RR);

%PLOT
figure
plot (ClscalC, Clsexp, 'x', [0:0.000001:0.07],[0:0.000001:0.07], '-')

figure (1)

plot(Cexp_muc323(:,1),Cexp_muc323(:,2), 'ob',
Cexp_cis323(:,1),Cexp_cis323(:,2), 'g',
Cexp_trans323(:,1),Cexp_trans323(:,2), 'xr',
Cexp_aad323(:,1),Cexp_aad323(:,2), 'c', tg323,Ctg323(:,1), 'b',
tg323,Ctg323(:,2), 'g', tg323,Ctg323(:,3), 'r', tg323,Ctg323(:,4), 'c',
tg323,zeros(size(tg323)));
title('Temperature 323K')
xlabel('time [s]'),ylabel('C(t) [moli/L]');
legend('muconic exp','intermediate cis exp', 'intermediate trans
exp','adipic exp','muconic calc','intermediate cis calc','intermediate
trans calc', 'adipic calc' );

figure (2)
plot(Cexp_muc333(:,1),Cexp_muc333(:,2), 'ob',
Cexp_cis333(:,1),Cexp_cis333(:,2), 'g',
Cexp_trans333(:,1),Cexp_trans333(:,2), 'xr',
Cexp_aad333(:,1),Cexp_aad333(:,2), 'c', tg333,Ctg333(:,1), 'b',

```

```

tg333,Ctg333(:,2),'g', tg333,Ctg333(:,3),'r', tg333,Ctg333(:,4),'c',
tg333,zeros(size(tg333)));
title( 'Temperature 333K')
xlabel('time [s]'),ylabel('C(t) [moli/L]');
legend('muconic exp','intermediate cis exp', 'intermediate trans
exp','adipic exp','muconic calc','intermediate cis calc','intermediate
trans calc', 'adipic calc' );

```

```

figure (3)
plot(Cexp_muc343(:,1),Cexp_muc343(:,2),'ob',
Cexp_cis343(:,1),Cexp_cis343(:,2),'+g',
Cexp_trans343(:,1),Cexp_trans343(:,2),'xr',
Cexp_aad343(:,1),Cexp_aad343(:,2),'*c', tg343,Ctg343(:,1),'b',
tg343,Ctg343(:,2),'g', tg343,Ctg343(:,3),'r', tg343,Ctg343(:,4),'c',
tg343,zeros(size(tg343)));
title('Temperature 343K')
xlabel('time [s]'),ylabel('C(t) [moli/L]');
legend('muconic exp','intermediate cis exp', 'intermediate trans
exp','adipic exp','muconic calc','intermediate cis calc','intermediate
trans calc', 'adipic calc' );

```

```

figure (4)
subplot(2,2,1);
plot(Cexp_muc323(:,1),Cexp_muc323(:,2),'ob',
Cexp_cis323(:,1),Cexp_cis323(:,2),'+g',
Cexp_trans323(:,1),Cexp_trans323(:,2),'xr',
Cexp_aad323(:,1),Cexp_aad323(:,2),'*c', tg323,Ctg323(:,1),'b',
tg323,Ctg323(:,2),'g', tg323,Ctg323(:,3),'r', tg323,Ctg323(:,4),'c',
tg323,zeros(size(tg323)));
axis([0 12000 0 0.08 ])
title('Temperature 323 K')
xlabel('time [s]'),ylabel('C(t) [mol/L]');

```

```

subplot(2,2,2);
plot(Cexp_muc333(:,1),Cexp_muc333(:,2),'ob',
Cexp_cis333(:,1),Cexp_cis333(:,2),'+g',
Cexp_trans333(:,1),Cexp_trans333(:,2),'xr',
Cexp_aad333(:,1),Cexp_aad333(:,2),'*c', tg333,Ctg333(:,1),'b',
tg333,Ctg333(:,2),'g', tg333,Ctg333(:,3),'r', tg333,Ctg333(:,4),'c',
tg333,zeros(size(tg333)));
axis([ 0 8000 0 0.08])
title( 'Temperature 333 K')
xlabel('time [s]'),ylabel('C(t) [mol/L]');

```

```

subplot(2,2,3);
plot(Cexp_muc343(:,1),Cexp_muc343(:,2),'ob',
Cexp_cis343(:,1),Cexp_cis343(:,2),'+g',
Cexp_trans343(:,1),Cexp_trans343(:,2),'xr',
Cexp_aad343(:,1),Cexp_aad343(:,2),'*c', tg343,Ctg343(:,1),'b',
tg343,Ctg343(:,2),'g', tg343,Ctg343(:,3),'r', tg343,Ctg343(:,4),'c',
tg343,zeros(size(tg343)));
axis([ 0 6000 0 0.08])
title('Temperature 343 K')
xlabel('time [s]'),ylabel('C(t) [mol/L]');
legend('ttMA exp','chDA exp', 'tHDA exp', 'AA exp', 'ttMA calc', 'chDA
calc', 'tHDA calc', 'AA calc' );

```

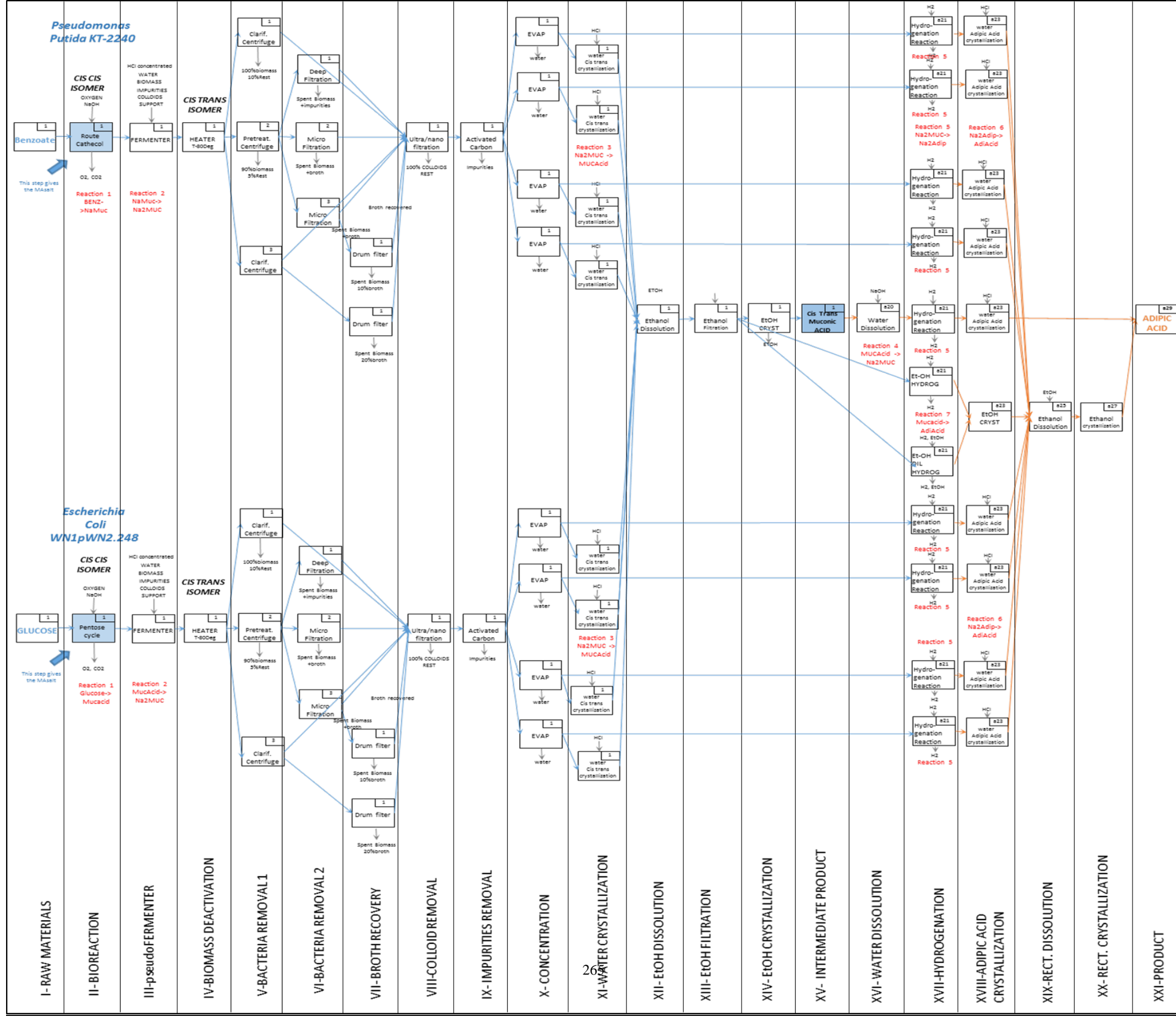


```
subplot(2,2,4);
plot (Clscal, Clsexp, 'x', [0:0.000001:0.07],[0:0.000001:0.07], '-' )
axis([0 0.07 0 0.07])
title('Dispersion')
xlabel('Calculated [mol/L]'),ylabel('Experimental [mol/L]');

figure (5)
plot (Clscal, Clsexp, 'x', [0:0.000001:0.07],[0:0.000001:0.07], '-' )
```

Appendix 4

The actual superstructure represented in Super-O and solved by GAMS routine can be visualized in a bigger format. It is therefore included as a A3 independent page.



The end